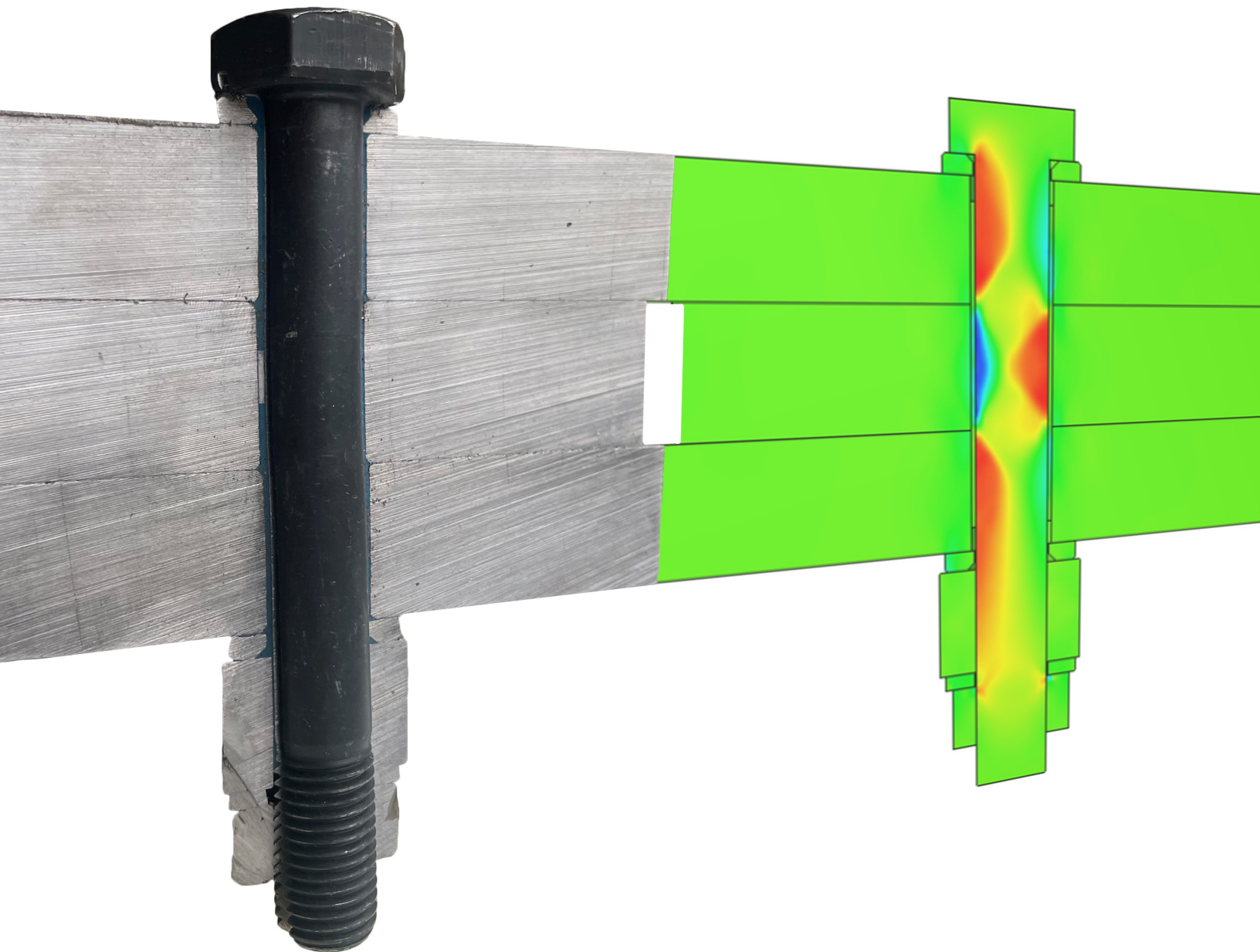


MSc Thesis:  
The resistance of a slip-critical steel-to-steel  
connection including preloading and/or injection



**MSc Thesis:**  
**The resistance of a slip-critical steel-to-steel  
connection including preloading and/or injection**

by

Ivo Derks

November 28, 2023

to obtain the degree of  
MSc Civil Engineering  
at the Delft University of Technology

to be defended on  
the 6<sup>th</sup> of December at 11:00h

Studentnumber: 5410673  
Project duration: February 2023 - December 2023  
Thesis supervisors: ir. P. de Vries (TU Delft)  
dr. ir. M. Nijgh (Rijkswaterstaat)  
Thesis committee: Prof. dr. M. Veljkovic (chair, TU Delft)  
dr. ir. S. van Es (TNO)  
Prof. dr. ir. B. Sluys (TU Delft)



# MSc Thesis:

## The resistance of a slip-critical steel-to-steel connection including preloading and/or injection

by

Ivo Derks

November 28, 2023

### Abstract

Both preloaded and injected bolted connections are commonly used in steel bridges in The Netherlands. Where preloaded bolted connections are already used for a longer time, the injection of bolt holes is a method used from the 1970s onwards. Injection of bolts became a good alternative for the replacement of riveted connections. This injection increases the slip resistance of the connection by filling the clearance between the bolt and the plate. Combining both methods increases the slip resistance of a bolted connection and is therefore even more beneficial.

According to the standard NEN-EN1993-1-8 [17], it is safe to assume that the resistance of a preloaded and injected bolted connection is equal to the sum of the two individual obtained resistances from preloading and injection. The aim of this research is to validate this statement and thus investigate the resistance of a slip-critical steel-to-steel connection including preloading and/or injection.

The study addresses this manner through both experiments and numerical analysis, addressing all three types of connections. In addition, this potential of summation is considered for two different levels of preloading, implementing plastic and elastic preload preloading. These levels of preloading were considered for two reasons, embodying different applications and identifying the effect of the preload force on the resistance. Each experiment is based on a short-term testing method that is in compliance with the described method of the EN1090-2. These resistances are verified by a numerical analysis with the goal of gaining more insight into the behaviour of the connection and validation of the obtained results.

From both experimental and numerical results, it is concluded that a summation of the individual resistances overestimates the actual resistance of a preloaded and injected bolted connection when measuring at the edge of the plates. This overestimation is similar for both preload levels.

Based on these results, it is concluded that it is unsafe to assume that the resistance of a preloaded and injected bolted connection is equal to the sum of the individual resistances obtained from preloading and injection. However, this conclusion might change if a different criterion for measuring relative displacements at specific locations is implemented.

The resistance of a connection is defined at a fixed magnitude of relative displacement measured at the edge of the plate, assuming that this is representing the displacement of the bolt. However, it turned out that the assumed limit displacement of 0.15mm did not result in the same displacement at the bolt(group) for all connections due to the amount of preload force and the geometry of the plates. Therefore, it is recommended to investigate the sensibility of the measured displacements for different geometries of and preload levels in the connection.

**Keywords:** Preloaded and injected bolted connection - Shear connection - Slip resistance

## Preface

This research started in February 2023 with the goal to obtain the Master's degree in Civil Engineering at the Delft University of Technology. This research investigated the resistance of preloaded and/or injected bolted connections. The results are based on both experimental and numerical analyses. The funder of this project is the Dutch Ministry of Infrastructure.

I would like to thank Rijkswaterstaat (Dutch Ministry of Infrastructure), TNO and the TU Delft for giving me the opportunity, responsibility and trust to manage and perform this research. It has been a challenging but unforgettable process. Especially the possibility of performing experiments in this research is something I am grateful for. Therefore, since all experiments have been performed with the guidance and help of laboratory staff, I would like to thank F.J.P. Schilperoort and J. Hermsen for helping me out during this experimental phase.

In special, I want to express my gratitude towards all committee members: dr. ir. Martin Nijgh (Rijkswaterstaat), dr. ir. Sjors van Es (TNO), ir. Peter de Vries (TU Delft), prof. dr. Milan Veljkovic (TU Delft) and Prof. dr. ir. Bert Sluys (TU Delft) for their investment in the process of this research. All meetings, both plenary and individual, were of great value. These moments of discussion were of significant importance for the quality of this research. Besides the committee members, also the colleagues of both Rijkswaterstaat and TNO were eager to help me with the challenges I faced during the process.

Last, I would like to thank my girlfriend Yinte, my parents and my friends for all the support they gave me. Thank you!

*Ivo Derks*  
*2023, December*

# Contents

|          |   |           |
|----------|---|-----------|
| <b>1</b> | <b>Introduction</b>   | <b>1</b>  |
| 1.1      | Research' objective   | 3         |
| 1.2      | Research questions  | 3         |
| 1.3      | Methodology   | 4         |
| 1.4      | Outline   | 4         |
| <b>2</b> | <b>State of the art</b>   | <b>5</b>  |
| 2.1      | Preloaded bolted connections  | 5         |
| 2.1.1    | Installation procedure of preloaded bolted connections  | 7         |
| 2.2      | Injected bolted connections   | 10        |
| 2.2.1    | Installation of injected bolted connections   | 11        |
| 2.3      | Preloaded and injected bolted connections   | 12        |
| 2.3.1    | Installation of preloaded and injected bolted connections                                       | 12        |
| 2.4      | Design resistance according to Eurocode   | 13        |
| 2.4.1    | Resistance of shear connections   | 13        |
| 2.4.2    | Preloaded bolted connections  | 14        |
| 2.4.3    | Injected bolted connections   | 16        |
| 2.4.4    | Preloaded and injected bolted connections   | 17        |
| 2.5      | Literature study  | 18        |
| 2.5.1    | Preloaded bolted connections  | 18        |
| 2.5.2    | Injected bolted connections   | 20        |
| 2.5.2.1  | Material properties of the resin  | 23        |
| 2.5.3    | Preloaded and injected bolted connections   | 26        |
| 2.5.4    | Friction coefficient  | 28        |
| 2.5.4.1  | Experimental procedure for determination of friction coefficients according to the NEN-EN1090-2 | 31        |
| 2.5.4.2  | Experimental procedure for determination of the resin's bearing resistance                      | 35        |
| <b>3</b> | <b>Experimental research</b>  | <b>36</b> |
| 3.1      | Experimental method   | 36        |
| 3.2      | Experimental setup  | 36        |
| 3.3      | Experimental parameters   | 41        |
| 3.4      | Material properties   | 42        |
| 3.4.1    | Bolt  | 42        |
| 3.4.2    | Resin   | 43        |
| 3.5      | Data extraction   | 44        |
| 3.5.1    | Mounting of strain gauges   | 44        |
| 3.5.2    | Calibration of bolts  | 45        |
| 3.6      | Installation procedure  | 47        |
| 3.6.1    | Combined method for preloading  | 47        |
| 3.6.2    | Specimen configuration  | 49        |
| 3.7      | Results - Experimental resistance of each connection  | 55        |
| 3.7.1    | Serie 1: Preloaded bolted connections (PBC)   | 55        |
| 3.7.2    | Serie 2: Injected bolted connections (IBC)  | 61        |
| 3.7.3    | Serie 3: Preloaded and injected bolted connections (PIBC)                                       | 66        |
| 3.8      | Analysis of experimental results  | 70        |
| 3.8.1    | Slip-resistance of preloaded connection   | 70        |
| 3.8.2    | Friction coefficient  | 71        |
| 3.8.3    | Bearing resistance of the resin   | 72        |
| 3.8.4    | Alignment of specimen   | 73        |
| 3.8.5    | Change in preload/axial force during experiment   | 74        |
| 3.8.6    | Averaged stiffness  | 76        |
| 3.8.6.1  | Preloaded bolted connection (PBC)   | 77        |

|          |   |            |
|----------|---|------------|
| 3.8.6.2  | Injected bolted connection (IBC)  | 79         |
| 3.8.6.3  | Preloaded and injected bolted connection (PIBC)                                     | 80         |
| 3.8.6.4  | Comparison of stiffnesses   | 81         |
| 3.8.7    | Summation of individual resistances   | 82         |
| 3.8.7.1  | According to the NEN-EN1993-1-8   | 82         |
| 3.8.7.2  | Nominal resistances   | 82         |
| 3.8.7.3  | Scenario - summation during entire experiment                                       | 85         |
| <b>4</b> | <b>Numerical verification</b>   | <b>88</b>  |
| 4.1      | Introduction  | 88         |
| 4.2      | Design  | 89         |
| 4.2.1    | Geometry  | 89         |
| 4.2.2    | Material properties   | 90         |
| 4.2.3    | Boundary conditions   | 91         |
| 4.2.3.1  | At both ends of the specimen  | 91         |
| 4.2.3.2  | Top and bottom of the spacer  | 91         |
| 4.2.4    | Loading steps   | 92         |
| 4.2.4.1  | Calibration   | 92         |
| 4.2.4.2  | Preloading  | 93         |
| 4.2.4.3  | Excitation  | 95         |
| 4.2.4.4  | Amplitude   | 95         |
| 4.2.5    | Mesh  | 97         |
| 4.2.6    | Mass scaling  | 98         |
| 4.2.7    | Contact interactions  | 98         |
| 4.2.7.1  | Contact with resin  | 99         |
| 4.3      | Results - Numerical resistance of each connection                                   | 100        |
| 4.3.1    | Preloaded bolted connections (PBC)  | 100        |
| 4.3.2    | Injected bolted connections (IBC)   | 101        |
| 4.3.3    | Preloaded and injected bolted connections (PIBC)                                    | 102        |
| 4.3.4    | Summation of individual resistances   | 103        |
| 4.3.4.1  | According to the NEN-EN1993-1-8   | 103        |
| 4.3.4.2  | Scenario - summation during entire experiment                                       | 104        |
| 4.4      | Results - Friction coefficient  | 106        |
| <b>5</b> | <b>Additional research: Lowered preloading force</b>                                | <b>109</b> |
| 5.1      | Application   | 109        |
| 5.2      | Modified method   | 110        |
| 5.3      | Results - Experimental resistance of each connection                                | 110        |
| 5.3.1    | Serie 4: Preloaded bolted connections (PBC)   | 110        |
| 5.3.2    | Serie 5: Preloaded and injected bolted connections (PIBC)                           | 114        |
| 5.4      | Analysis of experimental results (Lowered preloading force)                         | 117        |
| 5.4.1    | Slip-resistance of preloaded connection   | 117        |
| 5.4.2    | Friction coefficient  | 117        |
| 5.4.3    | Alignment of specimens  | 118        |
| 5.4.4    | Stiffness   | 118        |
| 5.4.4.1  | Preloaded bolted connection (PBC)   | 118        |
| 5.4.4.2  | Preloaded and injected bolted connection (PIBC)                                     | 120        |
| 5.4.4.3  | Comparison of stiffnesses (both $F_{p,C}=140\text{kN}$ and $F_{p,C}=100\text{kN}$ ) | 121        |
| 5.4.5    | Summation of individual resistances   | 122        |
| 5.4.5.1  | According to NEN-EN1993-1-8   | 122        |
| 5.4.5.2  | Scenario - summation during entire experiment                                       | 125        |

|          |  |            |
|----------|--|------------|
| <b>6</b> | <b>Discussion</b>  | <b>127</b> |
| 6.1      | Injection of specimens . . . . .   | 127        |
| 6.2      | Numerical modelling of resin . . . . .   | 128        |
| 6.2.1    | Decreased height of resin . . . . .  | 128        |
| 6.2.2    | Decreased mesh size of the resin . . . . .   | 130        |
| 6.3      | Preloading of the bolts by Combined method . . . . .                                     | 132        |
| 6.4      | Friction coefficient . . . . .   | 133        |
| 6.5      | Location of output versus obtained resistance . . . . .                                  | 135        |
| 6.5.1    | Relation to the determined stiffness . . . . .   | 135        |
| 6.5.2    | Relation to potential summation of individual resistances . . . . .                      | 137        |
| <b>7</b> | <b>Conclusion and recommendations</b>  | <b>141</b> |
| 7.1      | Conclusion . . . . .   | 141        |
| 7.2      | Recommendations . . . . .  | 143        |
| <b>A</b> | <b>Measuring coating</b>   | <b>149</b> |
| <b>B</b> | <b>Installation and calibration of strain gauges</b>                                     | <b>152</b> |
| B.1      | Installation . . . . .   | 152        |
| B.1.1    | Influential parameters . . . . .   | 153        |
| B.2      | Calibration . . . . .  | 153        |
| <b>C</b> | <b>Experimental results -</b>  |            |
|          | <b>Load displacement</b>   | <b>155</b> |
| C.1      | Serie 1 - Preloaded bolted connection (PBCs) . . . . .                                   | 155        |
| C.2      | Serie 2 - Injected bolted connection (IBCs) . . . . .                                    | 157        |
| C.3      | Serie 3 - Preloaded and injected bolted connection (PIBCs) . . . . .                     | 159        |
| C.4      | Serie 4 - Lowered $F_{p,C}$ - Preloaded bolted connection (PBCs) . . . . .               | 162        |
| C.5      | Serie 5 - Lowered $F_{p,C}$ - Preloaded and injected bolted connection (PIBCs) . . . . . | 163        |
| <b>D</b> | <b>Experimental results -</b>  |            |
|          | <b>Change in axial force</b>   | <b>165</b> |
| D.1      | Serie 1 - Preloaded bolted connection (PBCs) . . . . .                                   | 166        |
| D.2      | Serie 2 - Injected bolted connection (IBCs) . . . . .                                    | 167        |
| D.3      | Serie 3 - Preloaded and injected bolted connection (PIBCs) . . . . .                     | 168        |
| D.4      | Serie 4 - Lowered $F_{p,C}$ - Preloaded bolted connection (PBCs) . . . . .               | 169        |
| D.5      | Serie 5 - Lowered $F_{p,C}$ - Preloaded and injected bolted connection (PIBCs) . . . . . | 170        |
| <b>E</b> | <b>Stiffness parameters</b>  | <b>171</b> |
| <b>F</b> | <b>ABAQUS - Material properties</b>  | <b>174</b> |
| <b>G</b> | <b>ABAQUS - Effect of interface conditions IBC</b>                                       | <b>176</b> |
| <b>H</b> | <b>ABAQUS - Stiffness</b>  | <b>177</b> |
| H.1      | Modelling interaction properties . . . . .   | 178        |
| H.2      | Location of output . . . . .   | 179        |
| <b>I</b> | <b>Results Tribometer</b>  | <b>180</b> |

# List of Figures

|    |   |    |
|----|---|----|
| 1  | Double-lapped joint used for a splice connection [55]   | 2  |
| 2  | Schematic cross-sectional view of a preloaded bolted connection   | 5  |
| 3  | Schematic view of the difference between clamping length and gripping length obtained from NEN-EN1090-2 [46]  | 6  |
| 4  | Special components used for the assemblies of HRC-method and DTI-washer   | 7  |
| 5  | Preload force in the bolt during the implementation of rotation of the nut [25]   | 8  |
| 6  | Procedure of tightening the bolt by a certain angle, where in this case the bolt head is rotated by 120 degrees instead of the nut. The angle depends on the thickness of the clamping package  | 9  |
| 7  | Schematic cross-sectional view of an injected bolted connection   | 10 |
| 8  | Two allowed cross-sections for the use of injection. Last section shows the groove for the air to escape [15]   | 10 |
| 9  | Required tool for injecting the resin into the clearing of the connection   | 11 |
| 10 | Applied two-component-resin with at the back the RenGelSW404 and in front the hardener RenHY2404  | 11 |
| 11 | Schematic cross-sectional view of a preloaded and injected bolted connection  | 12 |
| 12 | Prescribed $k_s$ -factors related to type of bolt hole clearances according to NEN-EN1993-1-8 [17]  | 14 |
| 13 | Prescribed friction coefficients related to the type of interface according to EN1993-1-8 [17]  | 15 |
| 14 | Assumed $\beta$ and $t_{b,resin}$ per plate thickness ratio (Table 3.5 NEN-EN1993-1-8:2011 [17])  | 16 |
| 15 | Cross-sectional view of an injected bolted connection indicating the effective thickness of the resin according to the NEN-EN1993-1-8 [17].   | 17 |
| 16 | Distribution of introduced compressive stresses by preloading of the bolt [43]  | 19 |
| 17 | Determined slip factor for several test applications [59]   | 19 |
| 18 | Four different geometry layouts used by Bouwman for his investigation to the (bearing) resistance of an injected bolted connection [10]   | 20 |
| 19 | Effect on the bearing resistance of the resin by different plate thickness configurations, investigated by Bouwman [10]. On the horizontal axis the plate thickness ratio and on the vertical axis the bearing strength of the resin in $\text{kgf/cm}^2$ ( $\approx 0.1\text{MPa}$ ) | 21 |
| 20 | Strength of resin SW404+HY2404 [27]   | 22 |
| 21 | Compressive strength of enclosed concrete according to the NEN-EN1992-1-1 [20]  | 24 |
| 22 | Linear Drucker-Prager model yield surface and flow in the p-t plane [70]  | 24 |
| 23 | Governing resistances for the serviceability limit state for each thickness of the middle plate. Where the thickness of the side plate is 75% of the middle plate [23]. Assuming that summation of slip resistance by preloading and bearing resistance of the resin is allowed       | 26 |
| 24 | Comparison of results for different type of connections [30]  | 27 |
| 25 | Increasement of the tangential force due to a change in geometry of the slider [7]  | 29 |
| 26 | Two types of hysteresis obtained from friction test. Where both the Coulomb (dotted) and Non-Coulomb (continuous) friction is shown [42]  | 30 |
| 27 | Three different definitions of the slip resistance ( $F_{si}$ ) including prescribed graphs expected as output for the slip test [15] [65]. On the horizontal axis, the relative displacement at CBG in mm is shown. The vertical axis represents the applied force                   | 32 |
| 28 | Standard layout for obtaining friction coefficients for M16-bolts according to NEN-EN1090-2 [15]  | 33 |
| 29 | Applied layout for all specimens with two M16 bolts, including an overview of the locations for the LVDTs (M1-M8)   | 38 |
| 30 | Different views of the used M16 bolt assembly of class 10.9   | 39 |
| 31 | Entire framework designed for this current research. The red part is the specimen that is tested during each experiment (see Figure 29). Only the two bolts in the red specimen are preloaded. The other connection are bearing connections   | 40 |
| 32 | Two different tensile tests for a 10.9 M16 HV bolt  | 42 |

|    |   |    |
|----|---|----|
| 33 | Prescribed mixture properties of a resin made by RenGel SW404 and hardener Ren HY2404 [13] . . . . .  | 43 |
| 34 | Cross-section of the connection including the location of the inserted strain gauge . . . . .   | 44 |
| 35 | M16 bolts after installation of the strain gauges . . . . .   | 45 |
| 36 | Connector at the end of the bolt. Where one end of the connector is soldered to the tips of the strain gauge . . . . .  | 46 |
| 37 | Overview of experimental results when preloading bolts according to the combined method with friction factor determined by individual tests according to NEN-EN1090-2 . . . . .   | 48 |
| 38 | Four different shear planes are characterized by the colour orange, purple, green and blue . . . . .  | 50 |
| 39 | Different overviews for the predefined locations when determining the applied coating thickness . . . . .   | 51 |
| 40 | Possible outcomes according to the ASTM after investigation of the cured primer by the MEK-test [4] . . . . .   | 52 |
| 41 | Two types of degradation of the final applied primer after 50 rubs. Bottom and top path relates to the dry and moist cotton buds respectively . . . . .   | 52 |
| 42 | Difference in measured thickness between coated and uncoated surface areas per plates after recoating . . . . .   | 53 |
| 43 | Distribution of different measured coating thicknesses for the recoated surfaces . . . . .  | 54 |
| 44 | Distribution of average coating thickness per plate at a single shear plane . . . . .   | 54 |
| 45 | Results of all specimens when preloaded. This graph gives the relation between the displacement at CBG and the applied force in the connection. The faded graphs represent the results obtained from the initial coating, whereas the others are related to the final applied coating . . . . .   | 56 |
| 46 | Damage on the shear planes of the preloaded bolted connection after the experiment (Specimen R) . . . . .   | 57 |
| 47 | Decrease of the available preload force in each bolt during the experiment (PBC) . . . . .  | 58 |
| 48 | Local axis of the bolted connection. From left to right: local axis coordination, rotation around Y-axis, rotation around Z-axis . . . . .  | 59 |
| 49 | Alignment of the PBC concerning misalignment around Y-axis . . . . .  | 59 |
| 50 | Alignment of the PBC concerning misalignment around Z-axis . . . . .  | 60 |
| 51 | Results of all specimens when preloaded. This graph gives the relation between the displacement at CBG and the applied force in the connection . . . . .  | 62 |
| 52 | Cross-sectional view of a tested IBC . . . . .  | 63 |
| 53 | Increase of the axial force in each bolt during the experiment (IBC) . . . . .  | 64 |
| 54 | Alignment of the IBC concerning misalignment around Y-axis . . . . .  | 65 |
| 55 | Alignment of the IBC concerning misalignment around Z-axis . . . . .  | 65 |
| 56 | Results of all specimens for a preloaded and injected bolted connection. This graph gives the relation between the displacement at CBG and the applied force in the connection . . . . .  | 67 |
| 57 | Decrease of the available preload force in each bolt during the experiment (PIBC) . . . . .   | 68 |
| 58 | Alignment of the PIBC concerning misalignment around Y-axis . . . . .   | 69 |
| 59 | Alignment of the PIBC concerning misalignment around Z-axis . . . . .   | 70 |
| 60 | Decay in preload force at certain displacements of CBG for the two different types of connections: PBC (continuous) and PIBC (dotted) . . . . .   | 74 |
| 61 | Decay in preload force at certain displacements of CBG of the two different types of connections: PBC and PIBC compared with the applied force. The transparent graphs indicate the applied force whereas the bright lines represent the available preload force. In addition, the continuous lines are the preloaded bolted connections while the dotted graphs indicate the preloaded and injected bolted connections . . . . . | 75 |
| 62 | The two implemented regions where the stiffness is determined . . . . .   | 76 |
| 63 | PBC - Curve-fit for obtaining the stiffness of each bolt . . . . .  | 77 |
| 64 | Force-displacement results within the region of 0.003 up to 0.012mm displacement at CBG. Both results from this research and output of SIROCO are used [59] . . . . .   | 78 |
| 65 | IBC: Curve-fit of the load-displacement curve for the injected bolted connection . . . . .  | 79 |
| 66 | PIBC - Slope 1: Curve-fit of the load-displacement curve for a preloaded and injected connection within the range 0.003 to 0.012mm . . . . .  | 80 |

|    |  |     |
|----|--|-----|
| 67 | PIBC - Slope 2: Curve-fit of the load-displacement curve for a preloaded and injected connection within the range 0.12 to 0.21mm . . . . .   | 81  |
| 68 | Scenario 1: Average obtained resistances per type of connection, preloaded, injected and both preloaded and injected. Transparent areas show the range of experimental results for each tested connection . . . . .  | 86  |
| 69 | Scenario 2: Average obtained resistances per type of connection, preloaded, injected and both preloaded and injected. Transparent areas show the range of experimental results for each tested connection . . . . .  | 87  |
| 70 | Different perspectives of the ABAQUS model . . . . .   | 89  |
| 71 | Expansion of the spacer in U2-direction (Y-direction), after the preloading load step including both top (left) and bottom (right) view of the spacer . . . . .  | 95  |
| 72 | Implementation of the Smooth Step amplitude for load introduction in ABAQUS and its comparison with the tabular linear increase . . . . .  | 96  |
| 73 | Mesh pattern of both side- and middle-plates. The closer to the bolt hole, the smaller the mesh size (up to 0.5mm) . . . . .   | 97  |
| 74 | Assumed internal shear failure of resin (Nijgh [50]) . . . . .   | 99  |
| 75 | Preloading only: Numerical result of the load-displacement graph including the comparison with the experimental results . . . . .  | 100 |
| 76 | Injection only: Numerical result of the load-displacement graph including the comparison with the experimental results . . . . .   | 101 |
| 77 | Preloading and injection: Numerical result of the load-displacement graph including the comparison with the experimental results . . . . .   | 102 |
| 78 | Overview of the load-displacement behaviour of different types of connections allowing a decrease in slip resistance and including averaged experimental results and numerical results. Transparent areas show the range of experimental results for each tested connection . . . . .    | 104 |
| 79 | Overview of the load-displacement behaviour of different types of connections disallowing a decrease in slip resistance and including averaged experimental results and numerical results. Transparent areas show the range of experimental results for each tested connection . . . . . | 105 |
| 80 | Cross-sectional view of one of the two shear planes in the numerical model showing the stresses in vertical direction S22. The visible stresses are within the compressive stress range of 15 to 85MPa . . . . .   | 106 |
| 81 | Damaged specimen (II) after performing the tribometer test . . . . .   | 107 |
| 82 | Results of the Tribometer test using two Ethyl-Zinc-Silicate coatings. The adopted frequency and amplitude are 0.1Hz and 0.6mm respectively . . . . .  | 108 |
| 83 | Lowered $F_{p,C}$ - Load-displacement graph for a preloaded connection. The applied preload force $F_{p,C}$ is 100kN average . . . . .   | 111 |
| 84 | Lowered $F_{p,C}$ - Decrease of the available preload force in each bolt during the experiment (PIBC) . . . . .  | 112 |
| 85 | Lowered $F_{p,C}$ - Alignment of the PBC concerning misalignment around Y-axis . . . . .   | 113 |
| 86 | Lowered $F_{p,C}$ - Alignment of the PBC concerning misalignment around Z-axis . . . . .   | 113 |
| 87 | Lowered $F_{p,C}$ - Load-displacement graph for a preloaded and injected connection. The applied preload force $F_{p,C}$ is 100kN . . . . .  | 114 |
| 88 | Lowered $F_{p,C}$ - Decrease of the available preload force in each bolt during the experiment (PIBC) . . . . .  | 115 |
| 89 | Lowered $F_{p,C}$ - Alignment of the PIBC concerning misalignment around Y-axis . . . . .  | 116 |
| 90 | Lowered $F_{p,C}$ - Alignment of the PIBC concerning misalignment around Z-axis . . . . .  | 116 |
| 91 | Lowered preloading - PBC - Slope 1: Curve-fit of the load-displacement curve for a preloaded connection within the range 0.003 to 0.012mm . . . . .  | 119 |
| 92 | Lowered preloading - PBC - Slope 2: Curve-fit of the load-displacement curve for a preloaded connection within the range 0.12 to 0.21mm . . . . .  | 119 |
| 93 | Lowered preloading - PIBC - Slope 1: Curve-fit of the load-displacement curve for a preloaded and injected connection within the range 0.003 to 0.012mm . . . . .  | 120 |
| 94 | Lowered preloading - PIBC - Slope 2: Optimisation of the load-displacement curve for a preloaded and injected connection within the range 0.12 to 0.21mm . . . . .   | 121 |

|     |   |     |
|-----|---|-----|
| 95  | Overview of load-displacement difference between implement and $F_{p,C}$ of 140kN (Magenta) and 100kN (Light blue) including an indication of averaged displacement at which maximum resistance for preloading only is obtained . . . . .   | 123 |
| 96  | Contribution of the individual resistances to the combined resistance of a preloaded and injected bolted connection (PIBC) for two considered preload levels (140kN and 100kN). The contribution of bearing is determined by the difference between the total resistance and the slip-resistance . . . . .  | 124 |
| 97  | Lowered $F_{pc}$ : Overview of the load-displacement behaviour of different types of connections allowing a decrease in slip resistance and including averaged experimental results and numerical results. Transparent areas show the range of experimental results for each tested connection . . . . .    | 125 |
| 98  | Lowered $F_{pc}$ : Overview of the load-displacement behaviour of different types of connections disallowing a decrease in slip resistance and including averaged experimental results and numerical results. Transparent areas show the range of experimental results for each tested connection . . . . . | 126 |
| 99  | Cross-sectional cut of one of the injected bolted connections . . . . .   | 128 |
| 100 | The implemented reduced height of the resin. The left figure indicates the fully injected resin that is modelled to the washer (applied to IBC). The right figure shows the reduced height of the resin to prevent additional stresses by preloading (applied to PIBC) . . . .                              | 129 |
| 101 | IBC - Load-displacement of the two different geometries of the resin. Fully injected and reduced height of 5mm (see Figure 100) . . . . .   | 129 |
| 102 | Two additional considered mesh sizes. The top indicates a mesh size of 0.25mm in the through-thickness direction and the bottom figure shows a size of 0.15mm in the through-thickness direction . . . . .  | 130 |
| 103 | The load-displacement behaviour of three different implemented mesh sizes. Including offset of the lower mesh sizes by -0.01mm displacement at CBG . . . . .  | 131 |
| 104 | The consequence of applying a 25% less torque within the first step of the combined method to the preload force in the bolt after completion of this method. The unprocessed graph is obtained from the NEN-EN14339-2 [14] . . . . .  | 132 |
| 105 | Assumption in considered preload and applied force in time between calculation of the actual and initial friction coefficient . . . . .   | 133 |
| 106 | Design of the connection including components required for mounting and monitoring the displacement at CBG . . . . .  | 135 |
| 107 | Displacement along the width of the plate at CBG for two load steps: $F=45kN$ and $F=120kN$ including the difference in displacement. Implemented preload force is 140kN  | 136 |
| 108 | Displacement along the width of the plate at CBG and shear plane for two load steps: $F=45kN$ and $F=120kN$ including the difference in displacement. Implemented preload force is 140kN . . . . .  | 137 |
| 109 | Two considered nodes at the bearing side of the connection for the investigation of the displacement and stresses along the height of the clamping package . . . . .  | 138 |
| 110 | The effective difference in thickness ( $\Delta L$ ) of the resin measured at the two considered positions as shown in Figure 109 . . . . .   | 138 |
| 111 | The acting stresses along the height of the clamping package measured at the two considered positions as shown in Figure 109 . . . . .  | 139 |
| 112 | The total slip at the CBG along the entire width of the package . . . . .   | 140 |
| 113 | Difference in measured thickness between coated and uncoated surface areas . . . . .  | 149 |
| 114 | Distribution of different measured coating thicknesses for the initial coating . . . . .  | 150 |
| 115 | Different outcomes after the MEK-test: (a) initial coating (b) final coating . . . . .  | 151 |
| 116 | Quarter bridge with a 3-wire configuration (3 lead wires) . . . . .   | 153 |
| 117 | Initial setup for calibration and the accompanying load introduction . . . . .  | 154 |
| 118 | PBC - Load-displacement graph of specimen P . . . . .   | 155 |
| 119 | PBC - Load-displacement graph of specimen Q . . . . .   | 156 |
| 120 | PBC - Load-displacement graph of specimen R . . . . .   | 156 |
| 121 | IBC - Load-displacement graph of specimen K . . . . .   | 157 |
| 122 | IBC - Load-displacement graph of specimen L . . . . .   | 157 |
| 123 | IBC - Load-displacement graph of specimen M . . . . .   | 158 |

|     |  |     |
|-----|--|-----|
| 124 | IBC - Load-displacement graph of specimen N . . . . .  | 158 |
| 125 | IBC - Load-displacement graph of specimen O . . . . .  | 159 |
| 126 | PIBC - Load-displacement graph of specimen F . . . . .   | 159 |
| 127 | PIBC - Load-displacement graph of specimen G . . . . .   | 160 |
| 128 | PIBC - Load-displacement graph of specimen H . . . . .   | 160 |
| 129 | PIBC - Load-displacement graph of specimen I . . . . .   | 161 |
| 130 | PIBC - Load-displacement graph of specimen J . . . . .   | 161 |
| 131 | Lowered $F_{p,C}$ - PBC - Load-displacement graph of specimen A . . . . .  | 162 |
| 132 | Lowered $F_{p,C}$ - PBC - Load-displacement graph of specimen B . . . . .  | 162 |
| 133 | Lowered $F_{p,C}$ - PBC - Load-displacement graph of specimen AA . . . . .   | 163 |
| 134 | Lowered $F_{p,C}$ - PIBC - Load-displacement graph of specimen C . . . . .   | 163 |
| 135 | Lowered $F_{p,C}$ - PIBC - Load-displacement graph of specimen D . . . . .   | 164 |
| 136 | Lowered $F_{p,C}$ - PIBC - Load-displacement graph of specimen E . . . . .   | 164 |
| 137 | PBC - Decay of preload force until $U_{CBG}=0.2\text{mm}$ . . . . .  | 166 |
| 138 | PBC - Decay of preload force until $U_{CBG}=1.75\text{mm}$ . . . . .   | 166 |
| 139 | IBC - Increase in axial force until $U_{CBG}=0.2\text{mm}$ . . . . .   | 167 |
| 140 | IBC - Increase in axial force until $U_{CBG}=1.5\text{mm}$ . . . . .   | 167 |
| 141 | PIBC - Decay of preload force until $U_{CBG}=0.2\text{mm}$ . . . . .   | 168 |
| 142 | PIBC - Decay of preload force until $U_{CBG}=0.5\text{mm}$ . . . . .   | 168 |
| 143 | Lowered $F_{p,C}$ - PBC - Decay of preload force until $U_{CBG}=0.15\text{mm}$ . . . . .   | 169 |
| 144 | Lowered $F_{p,C}$ - PBC - Decay of preload force until $U_{CBG}=1.75\text{mm}$ . . . . .   | 169 |
| 145 | Lowered $F_{p,C}$ - PIBC - Decay of preload force until $U_{CBG}=0.2\text{mm}$ . . . . .   | 170 |
| 146 | Lowered $F_{p,C}$ - PIBC - Decay of preload force until $U_{CBG}=0.5\text{mm}$ . . . . .   | 170 |
| 147 | IBC: Numerical results before including rigid interaction at the interface of the resin<br>with the steel plates . . . . .   | 176 |
| 148 | Overview of the load-displacement behaviour of a preloaded bolted connection. Trans-<br>parent graphs indicate obtained results from experiments whereas the other represents<br>numerical results assuming different interaction properties . . . . . | 178 |
| 149 | Load displacement graphs based on three output locations . . . . .   | 179 |
| 150 | Results of the Tribometer test, where the frequency is 0.1Hz and amplitude is 0.6mm . . . . .  | 180 |
| 151 | Results of the Tribometer test, where the frequency is 0.1Hz and amplitude is 0.35mm . . . . .   | 181 |
| 152 | Results of the Tribometer test, where the frequency is 0.1Hz and amplitude is 0.6mm . . . . .  | 181 |

# List of Tables

|    |   |     |
|----|---|-----|
| 1  | Requirement for Category B and C according to NEN-EN1993-1-8:2011 [17] and prNEN-EN1993-1-8:2021 [16]   | 13  |
| 2  | Summary of the bearing strength of the resin (SW404 + HY(2)404)   | 23  |
| 3  | Slip factor per applied coating, preload force and clamping length [59]   | 28  |
| 4  | Methodology of test series  | 36  |
| 5  | Overview of material and geometric properties of the components within the bolt assembly  | 38  |
| 6  | Properties of the strain gauge BTMC-3-D20-006LE [12]  | 44  |
| 7  | Result of the required torque for applying 75% of the preload force in the bolt ( $F_{pc} = 0.7 \cdot f_{ub} \cdot A_s$ )   | 47  |
| 8  | Results of the combined method where the preload force ( $F_{pc}$ ) is given after each step  | 49  |
| 9  | Overview of nominal and actual initial preload force in all bolts for Serie 1 (preloading only) including the difference in percentage concerning the nominal preload force   | 55  |
| 10 | Obtained resistances from experiments when applying preloading including comparison with average obtained resistance  | 57  |
| 11 | Obtained resistances from experiments when applying injection, including comparison with average obtained resistance  | 63  |
| 12 | Overview of nominal and actual initial preload force in all bolts for Serie 3 (injection and preloading)  | 66  |
| 13 | Obtained resistances from experiments when applying both injection and preloading   | 68  |
| 14 | Determined friction coefficient for each bolt and difference to the nominal friction coefficient of 0.4 [15]  | 71  |
| 15 | Obtained stiffnesses of three different types of preloaded connections. Where series 1 and 2 are adopted from the SIROCO research [59].   | 78  |
| 16 | Overview of obtained stiffnesses and resistances  | 81  |
| 17 | Results for obtained resistances per series   | 82  |
| 18 | Obtained resistances from experiments when applying only preloading including comparison with average and the obtained resistance of the standard NEN-EN1993-1-8 excluding partial factors and implementing the actual applied preload force of 140kN | 83  |
| 19 | Obtained resistances from experiments when applying injection   | 83  |
| 20 | Obtained resistances from experiments when applying both injection and preloading   | 84  |
| 21 | Comparison of obtained experimental resistances for three different types of connections and the related nominal resistance including partial factors. Both bearing strength of the resin of 187MPa and 112MPa are taken into consideration           | 84  |
| 22 | Properties for two different boundary conditions  | 91  |
| 23 | Applied boundary conditions on the top and bottom surfaces of the spacer. This boundary condition is only activated in the preloading load step   | 91  |
| 24 | Overview of the duration and sequence of the different load steps   | 92  |
| 25 | Numerical results of preloaded connection including comparison with obtained results from experiments   | 100 |
| 26 | Numerical results of injected connection including comparison with obtained results from experiments  | 101 |
| 27 | Numerical results of preloaded and injected connection including comparison with obtained results from experiments  | 102 |
| 28 | Results for obtained resistances per series including comparison of experimental and numerical results  | 103 |
| 29 | Test matrix for the Tribometer test   | 107 |
| 30 | Methodology of test series for lowered preloading force   | 110 |
| 31 | Overview of aimed and actual initial preload force in all bolts (lowered preloading only)   | 110 |
| 32 | Obtained resistances from experiments when applying a lowered preloading force only   | 111 |
| 33 | Overview of aimed and actual initial preload force in all bolts for Serie (preloading only)   | 114 |
| 34 | Obtained resistances from experiments when applying both injection and preloading   | 115 |
| 35 | Determined friction coefficient for each bolt   | 117 |

|    |   |     |
|----|---|-----|
| 36 | Overview of obtained stiffnesses for each slope, each type of connection and each implemented preload force $F_{p,C}$ . . . . .   | 121 |
| 37 | Results for obtained resistances per series. Two series are compared, namely including an $F_{p,C}$ of 140kN and 100kN for the first and second column respectively . . . . . | 122 |
| 38 | Stiffness of three different types of connections within the range of 0.12 to 0.21mm displacement at CBG (slope 2) . . . . .  | 123 |
| 39 | Lowered $F_{pc}$ : Experimental and numerical results of the obtained resistances for the three different connections including summation . . . . .                           | 125 |
| 40 | Determined friction coefficient for each bolt and difference to the nominal friction coefficient of 0.4 [15] . . . . .  | 134 |
| 41 | Determined friction coefficient for each bolt and difference between two methods (based on initial and actual preload force) . . . . .  | 134 |
| 42 | Results for the calibration procedure of one bolt . . . . .   | 154 |
| 43 | Preloading only - Slope 1 - Optimisation parameters of each bolt to determine the trajectory . . . . .  | 171 |
| 44 | Preloading only - Slope 2 - Optimisation parameters of each bolt to determine the trajectory . . . . .  | 171 |
| 45 | Injection only - Slope 1 - Optimisation parameters of each bolt to determine the trajectory   | 171 |
| 46 | Injection only - Slope 2 - Optimisation parameters of each bolt to determine the trajectory   | 172 |
| 47 | Preloading and injection - Slope 1 - Optimisation parameters of each bolt to determine the trajectory . . . . .   | 172 |
| 48 | Preloading and injection - Slope 2 - Optimisation parameters of each bolt to determine the trajectory . . . . .   | 172 |
| 49 | Lowered $F_{pc}$ - Preloading only - Slope 1 - Optimisation parameters of each bolt to determine the trajectory . . . . .   | 173 |
| 50 | Lowered $F_{pc}$ - Preloading only - Slope 2 - Optimisation parameters of each bolt to determine the trajectory . . . . .   | 173 |
| 51 | Lowered $F_{pc}$ - Preloading and injection - Slope 1 - Optimisation parameters of each bolt to determine the trajectory . . . . .  | 173 |
| 52 | Lowered $F_{pc}$ - Preloading and injection - Slope 2 - Optimisation parameters of each bolt to determine the trajectory . . . . .  | 173 |
| 53 | Implemented material properties for the bolt, washer and nut in ABAQUS . . . . .  | 174 |
| 54 | Implemented material properties for the plates . . . . .  | 174 |
| 55 | Implemented material properties for the spacer (including thermal expansion coefficient   | 175 |
| 56 | Implemented material properties for the resin (SW404+HY2404) . . . . .  | 175 |

# Abbreviations and symbols

## Abbreviations

| Abbreviation | Description                                      |
|--------------|--|
| ASTM         | American society for testing materials           |
| BC           | Boundary condition                               |
| CBG          | Center bolt group                                |
| CHS          | Circular hollow section                          |
| COF          | Coefficient of friction                          |
| DOF          | Degree of freedom                                |
| DTI          | Direction tension indicator                      |
| EC3          | Eurocode 3 (1993 series)                         |
| ECCS         | European convention for constructional steelwork |
| EZS          | Ethyl-Zinc-Silicate                              |
| FEA          | Finite element analysis                          |
| GC           | General contact (ABAQUS)                         |
| HRC          | High resistance calibrated                       |
| HV           | Vickers Hardness (Pyramid number)                |
| IBC          | Injected bolted connection                       |
| LT           | Long-term  |
| LVDT         | Linear variable differential transformer         |
| MEK          | Methyl Ethyl Ketone                              |
| PBC          | Preloaded bolted connection                      |
| PIBC         | Preloaded and injected bolted connection         |
| ROK          | Richtlijn ontwerp kunstwerken                    |
| SLS          | Serviceability limit state                       |
| ST           | Short-term                                       |
| STS          | Surface-to-surface (ABAQUS)                      |
| TCB          | Tension controlled bolt                          |
| ULS          | Ultimate limit state                             |

## Symbols

| Parameter                         | Description   | Unit      |
|-----------------------------------|---|-----------|
| $\alpha_b$                        | Factor for geometry of plate in parallel direction to loading direction and ductility | [-]       |
| $\alpha(\vartheta, f_b)$          | Thermal coefficient at reference temperature  | [1/°C]    |
| $\alpha(\vartheta^I, f_b^I)$      | Thermal coefficient at lowered or elevated temperature                                | [1/°C]    |
| $\alpha$                          | Angle of load transfer  | [degrees] |
| $\beta$                           | Factor related to the plate thickness ratio of the side and middle plate              | [-]       |
| $\beta$                           | Friction angle of material  | [degrees] |
| $\Delta L_{\text{bolt,required}}$ | Required change of length to obtain a certain preload force                           | [mm]      |
| $\Delta L_{\text{plates}}$        | Contraction of the clamping package   | [mm]      |
| $\Delta L_{\text{spacer,FEA}}$    | Elongation of the spacer in the numerical analysis                                    | [mm]      |
| $\Delta L_{\text{spacer}}$        | Elongation of the spacer  | [mm]      |
| $\sigma_{\text{bolt}}$            | Stress at the cross-section of the bolt   | [MPa]     |
| $\Delta T$                        | Change in temperature   | [°C]      |
| $\gamma_{M2}$                     | Partial safety factor   | [-]       |
| $\gamma_{M3}$                     | Partial safety factor   | [-]       |
| $\gamma_{M4}$                     | Partial safety factor   | [-]       |
| $\gamma$                          | Ratio between bolt diameter and diameter of bolt head                                 | [-]       |

| Parameter                            | Description   | Unit                   |
|--------------------------------------|---|------------------------|
| $\mu_{\text{actual}}$                | Friction coefficient based on actual preload force at slip            | [-]                    |
| $\mu_{\text{init,mean}}$             | Mean friction coefficient implementing initial preload force          | [-]                    |
| $\mu_{\text{nom}}$                   | Friction coefficient based on nominal preload force                   | [-]                    |
| $\mu$                                | Friction coefficient at interface                                     | [-]                    |
| $\rho$                               | Density of the material   | [ton/mm <sup>3</sup> ] |
| $\sigma_b(\vartheta)$                | Bearing stress along the perimeter at an angle $\vartheta$            | [MPa]                  |
| $\vartheta$                          | Temperature at point of interest                                      | [C] or [K]             |
| $\vartheta$                          | Angle   | [degrees]              |
| $\varepsilon_{\text{th}}$            | Strains from varying temperature                                      | [mm/mm]                |
| $A_{\text{bolt,net}}$                | Cross-sectional area of the bolt at the threads                       | [mm <sup>2</sup> ]     |
| $A_s$                                | Net cross-sectional area of the bolt                                  | [mm <sup>2</sup> ]     |
| $c$                                  | Wave speed  | [m/s]                  |
| $d_0$                                | Bolt hole diameter  | [mm]                   |
| $D_0$                                | Available width of the connection to transfer the preloading force    | [mm]                   |
| $d$                                  | Bolt diameter   | [mm]                   |
| $d$                                  | Cohesion of material  | [-]                    |
| $E$                                  | Young's modulus   | [MPa]                  |
| $F_{b,Rd}$                           | Design bearing resistance   | [kN]                   |
| $F_{b,resin,Rd}$                     | Design bearing resistance of the resin                                | [kN]                   |
| $F_{b,resin}$                        | Bearing resistance of the resin                                       | [kN]                   |
| $f_{b,resin}$                        | Bearing strength of the resin   | [MPa]                  |
| $F_{\text{max}}$                     | Maximum applied force in the experiment                               | [kN]                   |
| $F_N$                                | Normal force  | [kN]                   |
| $F_{p,C,\text{init}}$                | Initial preload force   | [kN]                   |
| $F_{p,C,\text{nom}}$                 | Nominal preload force   | [kN]                   |
| $F_{p,C,\text{slip}}$                | Acting preload force at maximum slip resistance                       | [kN]                   |
| $F_{p,C}$                            | Preload force in the bolt   | [kN]                   |
| $F_{Rd,\text{preloading+injection}}$ | Design resistance of a preloaded and injected bolted connection       | [kN]                   |
| $F_{s,i}$                            | Maximum applied force until a displacement at CBG of 0.15mm           | [kN]                   |
| $F_{s,Rd,\text{ser}}$                | Design slip resistance at serviceability limit state                  | [kN]                   |
| $F_{s,Rd}$                           | Design slip resistance at ultimate limit state                        | [kN]                   |
| $F_S$                                | Friction resistance   | [kN]                   |
| $f_u$                                | Nominal ultimate strength of the steel plates                         | [MPa]                  |
| $f_{ub}$                             | Nominal ultimate design strength of the bolt                          | [MPa]                  |
| $F_{v,Ed}$                           | Acting design force in the connection                                 | [kN]                   |
| $F_{v,Rd}$                           | Design shear resistance per shear plane                               | [kN]                   |
| $f_{yb}$                             | Nominal yield strength of the bolt                                    | [MPa]                  |
| $h$                                  | Height of the CHS   | [mm]                   |
| $k_1$                                | Factor considering the location and geometry of the bolted connection | [-]                    |
| $k_s$                                | Takes into account the clearance around the bolt                      | [mm <sup>2</sup> ]     |
| $k_t$                                | Factor related to loading duration (long-term/ short-term)            | [-]                    |
| $l$                                  | Total thickness of the clamping package                               | [mm]                   |
| $l_{\text{bolt}}$                    | Length of the bolt  | [mm]                   |
| $M_{r,\text{test}}$                  | Determine required torque by experiment                               | [Nm]                   |
| $M_{\text{req}}$                     | Required torque   | [Nm]                   |
| $m$                                  | Difference between normal and oversized bolt holes                    | [mm]                   |

| <b>Parameter</b>     | <b>Description</b>  | <b>Unit</b>       |
|----------------------|---|-------------------|
| $N_{\text{net,Rd}}$  | Design netto cross-sectional resistance at location of the bolt row | [kN]              |
| $n$                  | amount of shear planes  | [pcs.]            |
| $P_{\text{max}}$     | Maximum acting stress   | [MPa]             |
| $p$                  | Hydrostatic stress  | [MPa]             |
| $R_a$                | Average height of the profile                                       | [ $\mu\text{m}$ ] |
| $R_q$                | Root mean square roughness  | [ $\mu\text{m}$ ] |
| $R_z$                | Ten-point height  | [ $\mu\text{m}$ ] |
| $t_{\text{b,resin}}$ | Effective thickness of the resin                                    | [mm]              |
| $t_1$                | Thickness of middle plate   | [mm]              |
| $t_2$                | Thickness of cover plate  | [mm]              |
| $t$                  | Thickness of considered plate                                       | [mm]              |
| $t$                  | Wall thickness of the CHS   | [mm]              |
| $t$                  | Deviatoric stress   | [MPa]             |
| $u$                  | Displacement of the bolt in bearing direction                       | [mm]              |
| $u_{\text{CBG}}$     | Relative displacement of CBG  | [mm]              |

# 1

## Introduction

Bolted connections are commonly used in structures worldwide, serving as a means to mount components together. The term “bolted connection” itself, denotes a mechanical fastening method with the use of bolts. Such linkages are adopted into various kinds of geometries. For example, bolt clearance size and shape can vary, but also initial conditions can be implemented to improve resistance. Besides these geometry specifications, the loading direction determines the design of a connection. The current version of the NEN-EN1993-1-8:2011 [17] classifies bolted connections into categories where the force is in the longitudinal (tension) or transverse (shear) direction of the bolt. Within this research, the focus is laid on the latter solely.

Within a non-preloaded bolted shear connection, the force is transferred by contact of the plates with the bolt. In this case, the bearing of the plates and the shear resistance of the bolt are decisive. However, force transfer is only activated if the bolt clearance has been overcome. Otherwise, bearing is not enabled and no force is transferred through the bolt.

The solution to prevent or minimize the occurring displacement in such connections is the slip-resistant connections. An advantage of a slip-resistant connection is that it is not required to initiate significant slip for activation of its resistance. Therefore, this methodology is implemented into structures that contain serviceability requirements and/or are sensitive to fatigue, due to significant fluctuations in stresses by variable loads. Namely, if a structure consists of large spans and relatively many connections, then this slip may introduce large deformations which in the end may exceed these serviceability requirements. However, the amount of connections can often not be reduced due to logistical practicalities. Besides the deformation limit, a slip-resistant connection decreases the stress range in bolts which is favourable for its durability.

The development of a slip-resistant bolted connection is in practice mostly enabled through two methods:

1. Slip-resistance through preloading;
2. Slip-resistance through injection.

In the case of a preloaded bolted connection (PBC), an external clamping force is applied which is created by a tensile force within the bolt. This tensile force is the result of a rotation of the nut that clamps the package together. The reaction is a compressive normal force between the components of the package. In a non-preloaded shear connection, the force must be transferred by the plates and bolts (connection of Category A). However, if the bolt is installed ideally, the bolt is not bearing against an adjacent member and therefore not able to transfer a force (Category B and C). Clamping of the steel plates results in a frictional resistance. This resistance enables the transfer of the load until any load increment exceeds the resistance. Surpassing this resistance will result in slip of the connection.

Besides preloading of bolts, injection of the clearance between the bolt and the edge of the bolt hole is an option to generate slip-resistant connections. Injected bolted connections (IBC) gained popularity as a replacement for riveted connections, particularly in repairs from the 1970s [28]. Filling the voids of bolt clearances with a two-component resin increases the resistance of the individual fasteners against slip. Since the bolt can not manoeuvre freely in the bolt hole, slip is prevented until a certain limit. In this scenario, the acting force may not exceed the bearing resistance of the resin ( $F_{b,resin}$ ). In The Netherlands, repairing road and railway bridges with injected bolted connections has even become a standard practice [27].

As both approaches have their own advantages, a combination of both might result in increased resistance. Even though this resistance has only been scientifically investigated once by Gresnigt et al. [30], examples can already be seen in practice, for instance by the renovation of the Suurhoffbridge [58].

According to the NEN-EN1993-1-8, it is safe to sum the two individual resistances such that it represents the resistance of a preloaded and injected bolted connection [17]. However, it is doubted whether this summation is reliable and overestimation is expected. These doubts especially arose after the initial results of the research of Gresnigt and Beg [29], see Subsection 2.5.3. Therefore, this research aims to investigate the relation of these factors with respect to the resistance of a preloaded and injected bolted connection. Bridging this emerging knowledge gap can result in more reliable regulations regarding the use and nominal resistance of preloaded injected connections.

The goal of this research is to investigate the behaviour of a double-lapped joint under a combination of preloading and injection when subjected to a tensile force. Compared to a single-lapped joint, a double-lapped is significantly more common within connections. Namely, single-lapped joints introduce eccentricities that create unfavourable internal bending moments. In bridges, splice connections are often used to connect members. These splices are realised by side-plates on both sides to prevent such unfavourable eccentricities, see Figure 1. Due to this common application, this research focuses on the double-lapped connection.



**Figure 1:** Double-lapped joint used for a splice connection [55]

## 1.1 Research' objective

Since there is a knowledge gap and large interest in the total resistance of an injected and preloaded connection and how calculations of these resistances are currently approached, the goal of this research is stated as follows:

### Goal of the research

Determine the contribution of preloading and injection to the combined resistance of a preloaded injected double-lapped bolted connection. In addition, give insight into these contributions through computational analysis.

According to the Eurocode 3 (EC3) part NEN-EN1993-1-8:2011, the resistance of the preloaded and injected connection is equal to the sum of the two individual components. However, it is questioned whether this is correct. Besides the verification of the slip-resistance created by a preload force and the bearing resistance from the resin, additional checks have to be executed to make sure that no other failure mechanisms are governing. Both experiments and numerical analysis will be executed to answer the problem statement.

After this research, the knowledge gap can, hopefully, be bridged which may result in more reliable regulations regarding the use of preloaded injected connections.

## 1.2 Research questions

To guide and substantiate the process of achieving this goal, several research questions are created. By resolving these subquestions, the main question will be addressed in an all-encompassing and structured manner. The subquestions are formulated as follows:

1. What are the individual resistances of a preloaded and injected bolted connection?
2. What is the resistance of a preloaded and injected bolted connection?
3. What is the behaviour in the contribution of the two individual resistances in a preloaded and injected bolted connection?
4. What is the influence of the measuring methodology on the resistance of a preloaded and/or injected bolted connection?

The first two subquestions are related to the combined relationship between preloading and injection. It can be questioned at what point during an increase in applied force the two components play a role. In the build-up, the frictional force will most likely take into account all applied forces. After a certain point, this slip resistance is exceeded whereby bearing of the resin is activated more significantly. However, since the resistance is determined at a certain measured displacement from 0 to 0.15mm at CBG, the relation between the applied force at failure and slip resistance is important.

## 1.3 Methodology

Achieving the objective of this research will be done through a process which is divided into three main phases. The first phase, state of the art, relates to gathering information on the current point of knowledge. This involves a study of the current regulations on how certain connections are calculated and what the requirements are for investigating different types of connections. In addition, available literature will be collected to gather information from other researchers that extend the knowledge of the behaviour of connections, material properties etc.

After this study on the state of the art, experiments will be executed. This includes the preparation of specimens, including design. Since the objective will mostly be based on experimental results, the methodology of this research is quantitative.

In the end, the experimental results will be used to verify a numerical analysis. After verification, this numerical analysis will give insight into the behaviour of the connection when exerted by a loading.

## 1.4 Outline

This report consists of seven chapters. In each of them, a specific topic is elaborated contributing to the goal of this research. The corresponding chapters are summated in the following list, including a brief explanation of the contents.

### **Chapter 2: State of the art**

First, a brief introduction is given about the two types of connections (PBC and IBC). Each of these parts includes specifications of the required components and the method of installation. Whereafter the design resistances according to the standard are mentioned and explained. In the following part, the available literature is elaborated and combined.

### **Chapter 3: Experimental research**

In this third chapter, the experimental research is explained. The preparation of the specimens, the geometry and test-matrices are shown. To evaluate the quality of the specimens, an additional investigation is executed. Furthermore, the material properties and calibration factors of the bolts are determined.

After this preparation, the results of all three types of connections are elaborated. In addition to resistances, the bearing strength, friction coefficients and stiffnesses of various slopes are determined. With these properties, possible summation is investigated.

### **Chapter 4: Numerical verification**

After the experimental results are obtained and explained, the numerical model is used to verify experimental results. First modelling properties, such as geometry, boundary conditions, loadings step and interactions are explained. Whereafter the results obtained from the numerical analyses are compared with the those obtained from the experiments.

### **Chapter 5: Additional research: Lowered preloading force**

One of the subquestions of this research relates to the effect of the preload force on the resistance of a preloaded and injected bolted connection. In this part, both experimental and numerical results are given.

### **Chapter 6: Discussion**

In this chapter, all procedures and results are discussed. These discussions relate to obtained doubts and pitfalls within the process. In addition, the applicability of the results are discussed.

### **Chapters 7 and 8: Conclusion and recommendations**

The final chapter of the main part of this report consists of the conclusion and recommendations. Within the conclusion, the obtained results and answers to the subquestions and main research question are elaborated. From these findings, the recommendations are enumerated. These recommendations relate to the findings of this research and potential follow-up research.

# 2

## State of the art

Within this chapter, the state of the art is elaborated. This consists of an introduction to the different types of connections (preloaded and injected bolted connections). On top of that, the methodology of the current design resistance according to the Eurocode is explained. Whereafter a literature study is introduced that elaborates on obtained information regarding specific topics related to both types of connections.

### 2.1 Preloaded bolted connections

A preloaded bolted connection is a connection wherein the initial phase of mounting consists of applying an axial force in the bolt. This so-called clamping force creates a frictional resistance at the shear planes. [Figure 2](#) visualises the cross-section of such a connection. Also, the force introduction is shown whereas the red arrows at the shear planes indicate the clamping force ( $F_{p,c}$ ).

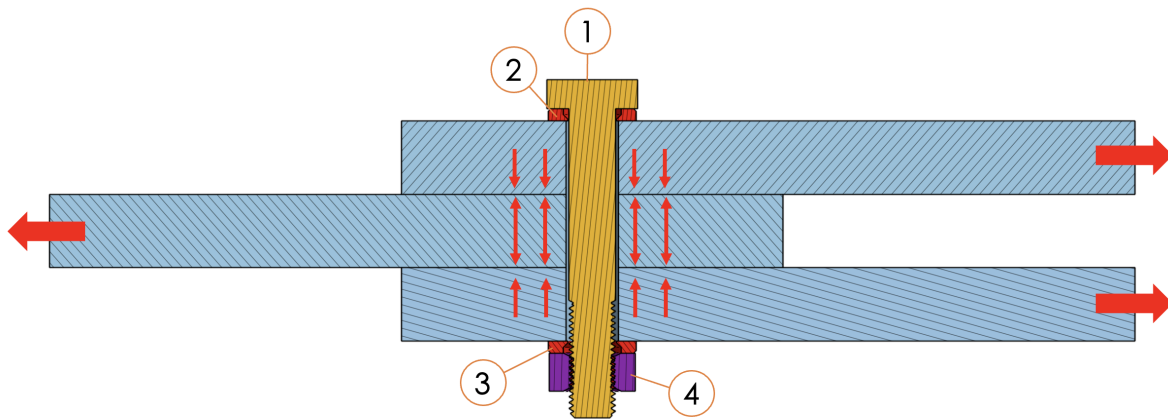


**Figure 2:** Schematic cross-sectional view of a preloaded bolted connection

As can be seen in the figure above, a bolt assembly used for preloaded connections consists of four components:

1. Bolt, consisting of one of the required classes;
2. Washer (top);
3. Washer (bottom);
4. Nut.

All mentioned components are not made out of regular steel (S235 or S355). According to NEN-EN 1993-1-8:2011, the material for preloading bolts is required to be of class 8.8 or 10.9 [17]. These values refer to the yielding and ultimate strength of the steel. In addition to the material class of the bolt, the geometry plays a significant role, especially in the failure mode. In the NEN-14399-2, two different types of preloading bolts are specified, namely HV and HR bolts [14]. The dissimilarities between those are in particular the geometry of the threads in combination with nut assembly, which results in different failure mechanisms.

Since the amount of preload force, compared to the contact area between the bolthead or nut and washer is relatively large, a higher hardness of the washer is required. Therefore prescribed washers must satisfy a hardness range between 300 and 370HV (NEN-EN 14399-6). This value of HV refers to the Vickers Pyramid Number (HV) [39].

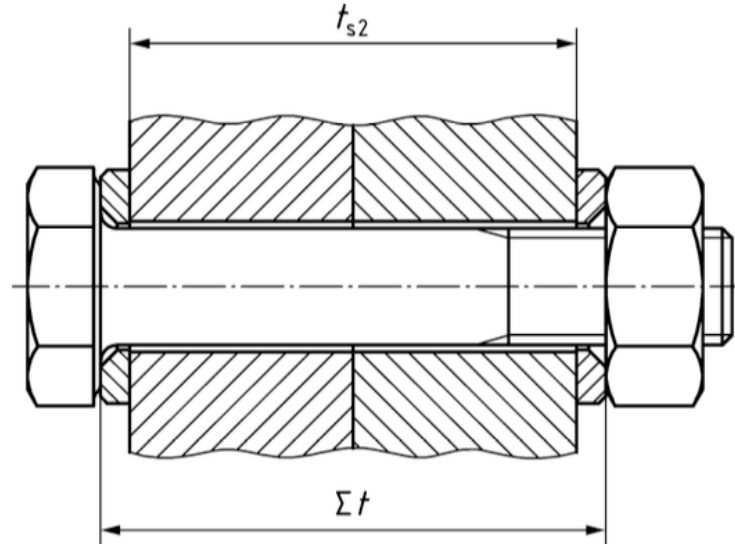


**Figure 3:** Schematic view of the difference between clamping length and gripping length obtained from NEN-EN1090-2 [46]

When designing a connection, that is in accordance with the NEN-EN14399-4:2015 [14], i.e. HV-bolts, the bolt has both a net- and gross-section. In other words, such bolts are not fully threaded, see Figure 3. When choosing a specific length of the bolt, both clamping and gripping lengths must be satisfied according to Table A.1 and A.2 of the NEN-EN14399-4:2015 [14]. Where clamping length refers to the thickness of the package including washers.

### 2.1.1 Installation procedure of preloaded bolted connections

Installing preloaded bolts can in practice be done through several methods. However, all prescribed methods result in different outcomes in preload force [6]. Within the literature, it is mentioned that, for example, speed, coating thickness, installation method and clamping thickness affect the preload force over time [2][41][48].

The following enumeration resembles different preloading methods to insert a preloading force. However, only the ones stated in **bold** are allowed according to the NEN-EN1090-2 [15].

1. **Torque method**;
2. Turn of the nut method (not allowed for solely application according to NEN-EN1090-2);
3. **Combined method**;
4. **HRC method**;
5. **Direction tension indicator (DTI) method**.

From these methods, both HRC and DTI use special components for assembly. The HRC method implements a special assembly whereby a specifically designed component will break after the application of a certain torque, see [Figure 4a](#). The DTI method uses a washer with protrusions as visualised in [Figure 4b](#). These protrusions will yield and deform after an applied load in the bolt. This indicates that the prescribed load is achieved. Nevertheless, due to their absence in allowable assemblies for preloading set by Rijkswaterstaat, these applications are not adopted into this research [61].



(a) Tension controlled bolt (HRC) [66]



(b) Washer used for the DTI preloading method where the eight protrusions are included [38]

**Figure 4:** Special components used for the assemblies of HRC-method and DTI-washer

Considering the torque method, applying torque to a clamping package creates a normal force in the bolt due to the elongation of the bolt. The amount of axial force that will be exerted, relates to the amount of friction acting in the package. Significant friction between the nut and the threads reduces the axial force after the application of a prescribed torque.

Rotation of the nut increases the elongation of the bolt due to the stiffness of the clamping package. This is implemented in the turn of the nut method. The increment in axial force in the bolt relates to the angle of rotation of the nut. A pitfall of this method is, in special, imperfections in the package. As mentioned, an axial force builds up in case of acting stiffness. However, if plates have significant imperfections in flatness, no axial force will appear in the bolt. Therefore, an axial force in the bolt will only be created if plates are in contact with each other. This is also indicated in Figure 5. This figure shows that a preload force in the bolt will only arise if the clamping package is in contact at each intermediate interface.

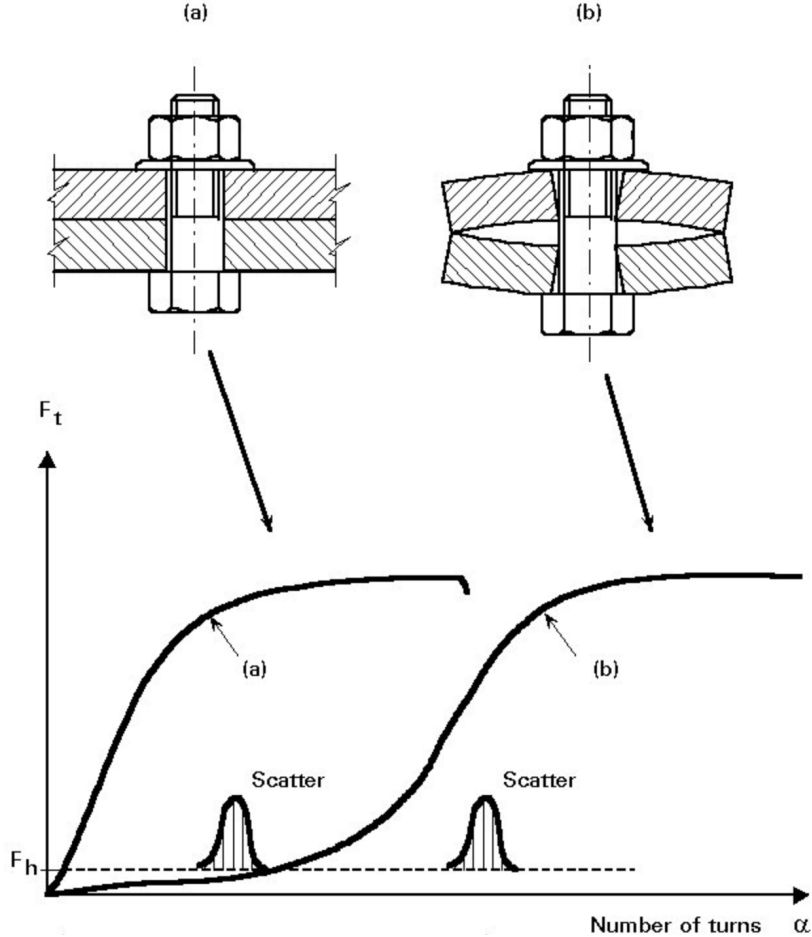


**Figure 5:** Preload force in the bolt during the implementation of rotation of the nut [25]

The combined method is composed of both the torque and turn of the nut method. This gathers the advantageous characteristics of both methods. This application consists of two steps with a prescribed and irreplaceable order. First, a torque has to be applied to the assembly to make sure that plates do make contact with each other. Thereafter, the nut must be rotated with a prescribed angle. This angle is with respect to the bolt, otherwise, no tightening occurs. Both torque and angle relate to the properties of the entire connection.

According to regulations set by Rijkswaterstaat, for the allowed bolt assembly the tightening procedure has to be determined when one of the following criterion is valid [61]:

- Every day when preload bolts are installed;
- When a new batch of bolts is being used.

As mentioned, the second step of the combined method consists of a rotation of the bolt with a certain angle depending on the thickness of the clamping package. [Figure 6](#) indicates the applied and required amount of such rotation.



**Figure 6:** Procedure of tightening the bolt by a certain angle, where in this case the bolt head is rotated by 120 degrees instead of the nut. The angle depends on the thickness of the clamping package

In cases where the diameter of the bolt is relatively small, it is possible to apply a certain (nominal) torque with a regular wrench. However, if the bolt size increases, and thereby also the nominal preload force, applying the required torque may require a hydraulic wrench. Within each different spectrum of torques, a different instrument is recommended due to its precision [40].

## 2.2 Injected bolted connections

An injected bolted connection is a connection where the clearance around the bolt is filled after assembly. A two-component resin is injected into this bolt clearance such that the connection contains resistance against slip. Since one product of this two-component resin is a hardener, the resistance increased after a certain curing period.

Figure 7 shows a schematic cross-sectional view of an injected bolted connection. In contrast to the preloading bolts, it is not mandatory to have a minimum material class for the bolts. However, an injected bolted connection has a requirement for the applied bolt. Figure 7 indicates this requirement of an available injection channel in the bolt head. Figure 7 indicates this requirement of an available injection channel in the bolt head. This channel makes it possible to inject the resin after installation and eventual tightening of the bolt.

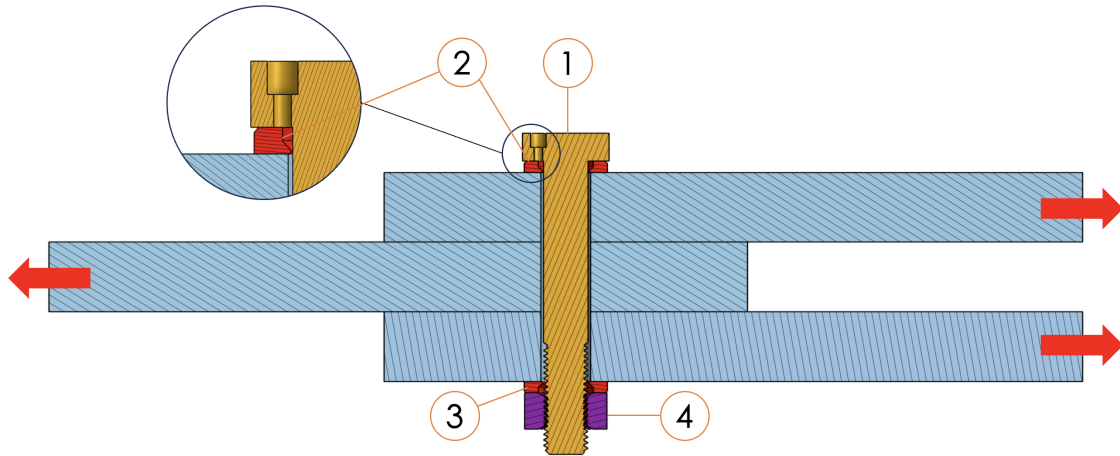


Figure 7: Schematic cross-sectional view of an injected bolted connection

During injection, air needs to be able to escape the bolt clearance. The bottom washer enables this since it contains an air escape groove on the top of the washer, see Figure 8. It is important that this groove's face is directed towards the nut. This increases the reliability that the entire clearance is filled with the resin and that the resin can escape.

Therefore, assembling an injected bolted connection requires the following different components:

1. Bolt, including injection channel;
2. Washer, including chamber;
3. Washer, including chamber and air escaping channel;
4. Nut.

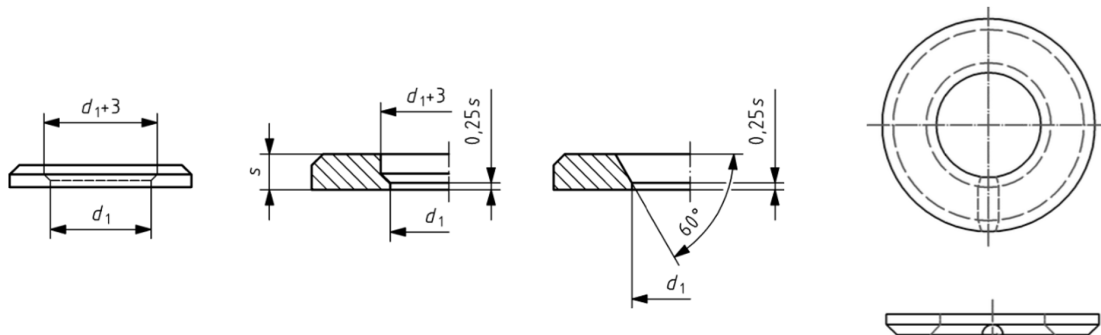


Figure 8: Two allowed cross-sections for the use of injection. Last section shows the groove for the air to escape [15]

### 2.2.1 Installation of injected bolted connections

As mentioned, injection of the bolt clearance is allowed after assembling and mounting the (preloaded) bolts. To inject the resin, an injection gun is required. This gun is a general sealing- or chalk gun, see [Figure 9](#). As resin, a predefined two-component resin is compulsory. These components are the two types of resins, of which one is the hardener. Both are stored separately, see [Figure 10](#). On the market, several different combinations of epoxies and hardeners are available. However, in this research context, the utilisation of preloaded and injected bolted connections is related to structures owned by Rijkswaterstaat. According to clause ROK-0372 within the "Richtlijn Ontwerp Kunstwerken" (ROK), the use of RenGel SW404 in combination with Ren HY2404 (hardener) is mandatory [61]. This mixture can be used up to 15 minutes after completing and must rest for at least 8h [13]. This ROK is a Rijkswaterstaat-owned document that comments on formulations and applications from the Eurocode and states additional requirements.



**Figure 9:** Required tool for injecting the resin into the clearing of the connection



**Figure 10:** Applied two-component-resin with at the back the RenGelSW404 and in front the hardener RenHY2404

## 2.3 Preloaded and injected bolted connections

Besides the preloaded or injected bolted connections, the standard NEN-EN1993-1-8 allows the combination of these two types. This results in a preloaded and injected bolted connection. In [Figure 11](#), a schematic cross-section is visualised where it can be seen that both preloading and injection are combined.

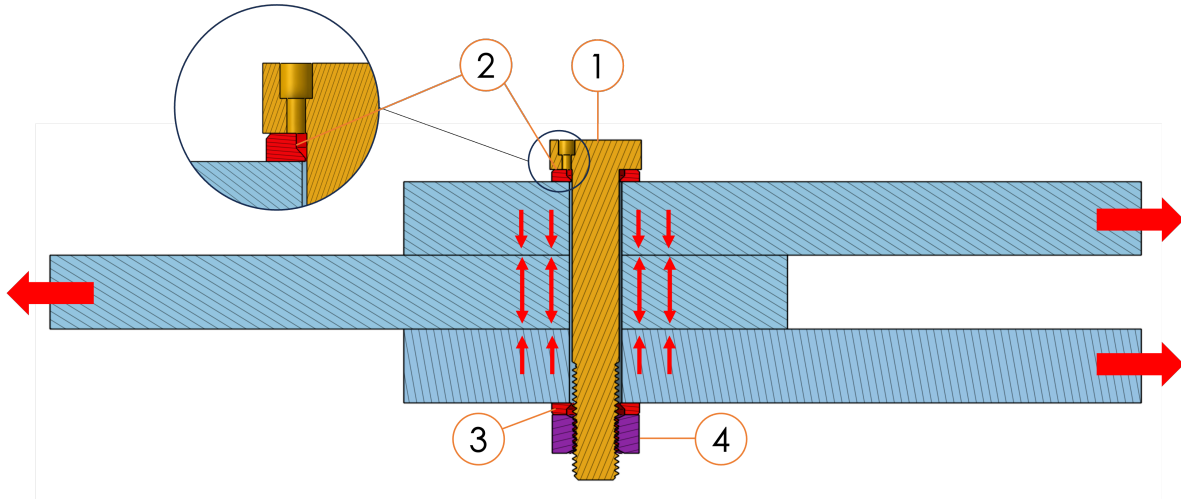


**Figure 11:** Schematic cross-sectional view of a preloaded and injected bolted connection

For such type of connections, special washers, nut and bolt is required to allow both the application of preloading and injection. Therefore, the assembly of a preloaded and injected bolted consists of the following components:

1. Bolt, including injection channel and consisting of one of the required classes;
2. Washer, including chamber;
3. Washer, including chamber and air escaping channel;
4. Nut.

### 2.3.1 Installation of preloaded and injected bolted connections

When constructing a preloaded and injected bolted connection, installation contains a specific sequence that is also mentioned by the NEN-EN1090-2:2018 [15]. It is stated that the initial step is to apply a preload to all bolts. After completion, all bolts are allowed to be injected. However, after all bolts are injected, it is not allowed to apply an additional preload. In case a bolt is preloaded after injection, the resin will be damaged.

## 2.4 Design resistance according to Eurocode

Designing connections in steel structures is handled in part 1993-1-8 of the Eurocode. NEN-EN1993-1-8:2011 prescribes methods on how to calculate the resistances of different types of connections. Within the NEN-EN1993-1-8, distinguishment is made between two types: shear and tension connections [17]. In this research, the focus is put on slip behaviour and therefore shear connections are considered only. In Table 1 an overview is shown of several criteria decisive for the design resistance of a slip-critical connection. However, as this research investigates the reliability of summation of the individual resistances of preloaded and injection as (governing) resistance, the question arises if this prescribed scenario is allowable.

### 2.4.1 Resistance of shear connections

A bolted connection in shear implies that the direction of the bolt is perpendicular to the loading direction. In contrast, a tensile connection has a loading direction similar to the direction of the bolt. As connections of categories B and C are slip-resistant in Serviceability limit state (SLS) and Ultimate limit state (ULS) respectively, preloading (or injection) of bolts is a prerequisite for fulfilling this requirement.

When designing a connection according to the NEN-EN1993-1-8:2011 [17], requirements primarily depend on the category of the connection. Associated conditions are shown in Table 1. Within this table, both current requirements from NEN-EN1993-1-8:2011 and the 2021 draft of the revised prNEN-EN1993-1-8:2021 [16] are given.

**Table 1:** Requirement for Category B and C according to NEN-EN1993-1-8:2011 [17] and prNEN-EN1993-1-8:2021 [16]

| Category | EN1993-1-8:2011                                   | prEN1993-1-9:2021                         |
|----------|---|---|
| B        | $F_{v,Ed,ser} \leq F_{s,Rd,ser} + F_{b,Rd,resin}$ | $F_{v,Ed} \leq F_{s,Rd} + F_{b,Rd,resin}$ |
|          | $F_{v,Ed} \leq F_{b,Rd}$                          | $F_{v,Ed} \leq F_{v,Rd}$                  |
|          | $\sum F_{v,Ed} \leq N_{net,Rd}$                   | $F_{v,Ed} \leq F_{b,Rd}$                  |
|          | $F_{v,Ed} \leq F_{v,Rd}$                          | $\sum F_{v,Ed} \leq N_{net,Rd}$           |
| C        | $F_{v,Ed} \leq F_{s,Rd} + F_{b,Rd,resin}$         | $F_{v,Ed} \leq F_{s,Rd} + F_{b,Rd,resin}$ |
|          | $F_{v,Ed} \leq F_{b,Rd}$                          | $F_{v,Ed} \leq F_{v,Rd}$                  |
|          | $\sum F_{v,Ed} \leq N_{net,Rd}$                   | $\sum F_{v,Ed} \leq N_{net,Rd}$           |
|          | $F_{v,Ed} \leq F_{v,Rd}$                          |   |

Table 1, indicates the requirements set by two versions of the EN1993-1-8. Of this, the following factors are important:

1.  $F_{v,Ed}$ : Acting design force in the connection;
2.  $F_{s,Rd}$ : Slip resistance at ultimate limit state;
3.  $F_{s,Rd,ser}$ : Slip resistance at serviceability limit state;
4.  $F_{b,Rd,resin}$ : Design bearing resistance of the resin;
5.  $F_{v,Rd}$ : Design shear resistance per shear plane;
6.  $N_{net,Rd}$ : Design netto cross-sectional resistance at location of the bolt row.

The main difference between the current version [17] and the draft of 2021 [16] is that the current version takes into account the possible failure due to the bearing of the steel plates. Whereas the draft of 2021 neglects this possibility.

## 2.4.2 Preloaded bolted connections

In the case where a single bolt is preloaded according to the prescribed methods of NEN-EN1090-2, the assumed preload force in the bolt is known as given in [Equation 1](#) [15].

$$F_{p,C} = 0.7 \cdot f_{ub} \cdot A_s \quad (1)$$

With:

$$\begin{aligned} F_{p,C} &= \text{preload force [N]}; \\ f_{ub} &= \text{nominal ultimate design strength of the bolt [MPa]}; \\ A_s &= \text{net cross-sectional area of the bolt [mm}^2\text{]}. \end{aligned}$$

For the assumed preload force in the bolt, the ultimate strength of the bolt ( $f_{ub}$ ) is multiplied by the cross-sectional area at the location of the threads, also called the net cross-sectional area ( $A_s$ ). When tightening a bolt according to one of the prescribed methods by EN1090-2, it is sufficiently reliable that the bolt is stressed to a level of 70% of  $f_{ub}$ .

This preloading force in the bolt is the vertical component that compresses the clamping package together. A compressive reaction force within the plates directs into a friction force, due to a surface roughness, which is activated at the shear planes of the package. According to NEN-EN1993-1-8:2011, this relation between the nominal preload and design slip resistance ( $F_{s,Rd}$ ) is shown in [Equation 2](#).

$$F_{s,Rd} = \frac{k_s \cdot n \cdot \mu}{\gamma_{M3}} \cdot F_{p,C} \quad (2)$$

With:

$$\begin{aligned} F_{s,Rd} &= \text{design slip resistance [kN]}; \\ k_s &= \text{takes into account the clearance around the bolt [-]}; \\ n &= \text{number of shear planes [pcs.]}; \\ \mu &= \text{friction coefficient at interface between steel plates [-]}; \\ F_{p,C} &= \text{nominal preload force [kN]}; \\ \gamma_{M3} &= \text{partial safety factor [-]}. \end{aligned}$$

Of the equation shown above, important parameters, besides the number of shear planes and the implemented partial safety factor of 1.25 (valid for The Netherlands), are  $k_s$  and  $\mu$ . According to table 3.6 of NEN-EN1993-1-8:2011, the former, factor  $k_s$ , is dependent on the applied bolt clearances [17]. Distinguishment can be made between normal holes, oversized holes and slotted holes. For normal clearances, this factor is 1.0, whereas this factor will decrease for larger clearances, see [Equation 3](#) and [Figure 12](#). However, this dependence on the type of bolt holes is not taken into consideration in this research.

$$k_s = 1.0 - 0.1 \cdot m \quad (3)$$

| Description   | $k_s$ |
|---|-------|
| Bolts in normal holes.  | 1,0   |
| Bolts in either oversized holes or short slotted holes with the axis of the slot perpendicular to the direction of load transfer. | 0,85  |
| Bolts in long slotted holes with the axis of the slot perpendicular to the direction of load transfer.                            | 0,7   |
| Bolts in short slotted holes with the axis of the slot parallel to the direction of load transfer.                                | 0,76  |
| Bolts in long slotted holes with the axis of the slot parallel to the direction of load transfer.                                 | 0,63  |

**Figure 12:** Prescribed  $k_s$ -factors related to type of bolt hole clearances according to NEN-EN1993-1-8 [17]

The latter, factor  $\mu$ , is called the friction coefficient. A friction coefficient considers the relation between the normal and friction force of two specific surfaces. The higher this friction coefficient is, the higher the slip resistance of the connection. However, the NEN-EN1993-1-8 states that the friction coefficient is the relation between the initial preload force, which is the preload force at the start of the experiment after initial losses, and the maximum applied force within the displacement range at CBG of 0 to 0.15mm. In this same NEN-EN1993-1-8:2011, a table as shown in Figure 13 is given that defines friction coefficients per type of used surface based on the last mentioned methodology [17]. In total four different types of surface combinations are considered and labeled A to D with coefficients varying from 0.5 to 0.2 respectively. Regardless of what the design preload force in a connection is, shown factors must be considered if experimental proof is not conducted.

| Class of friction surfaces (see 1.2.7 Reference Standard: Group 7) | Slip factor $\mu$ |
|--|-------------------|
| A  | 0,5               |
| B  | 0,4               |
| C  | 0,3               |
| D  | 0,2               |

**NOTE 1:** The requirements for testing and inspection are given in 1.2.7 Reference Standards: Group 7.

**NOTE 2:** The classification of any other surface treatment should be based on test specimens representative of the surfaces used in the structure using the procedure set out in 1.2.7 Reference Standards: Group 7.

**NOTE 3:** The definitions of the class of friction surface are given in 1.2.7 Reference Standards: Group 7.

**NOTE 4:** With painted surface treatments a loss of pre-load may occur over time.

**Figure 13:** Prescribed friction coefficients related to the type of interface according to EN1993-1-8 [17]

### 2.4.3 Injected bolted connections

The second scenario is where individual bolts are injected by a two-component resin. Injecting a resin in the cavity of the bolthole increases the slip resistance [17]. However, the NEN-EN1993-1-8 states that the application of a resin does not directly imply that the connection is considered to be slip-resistant. Category A connections also allow the implementation of a resin. Even if a Category A connection is referred to as a “bearing connection” instead of “slip-resistant”.

One of the failure mechanisms listed by the NEN-EN1993-1-8 is the bearing of adjacent material [17]. In this case, bearing occurs in the resin and must therefore be implemented into possible governing resistances. According to the Eurocode, this resistance of the resin is determined by Equation 4.

$$F_{b,Rd,resin} = \frac{k_t \cdot k_s \cdot d \cdot t_{b,resin} \cdot \beta \cdot f_{b,resin}}{\gamma_{M4}} \quad (4)$$

With:

- $k_t$  = related to the duration of the loading within the limit state [-];
- $k_s$  = takes into account the clearance around the bolt [-];
- $d$  = diameter of the bolt [mm];
- $t_{b,resin}$  = effective thickness of the resin, see Figure 14 [mm];
- $\beta$  = factor related to the plate thickness ratio of the side and middle plate [-];
- $f_{b,resin}$  = bearing strength of the resin [MPa];
- $\gamma_{M4}$  = partial safety factor (=1.0 in The Netherlands) [-].

The  $k_t$  factor is related to the duration of the loading. There are two main different checks to be performed for such connection, namely a serviceability limit state (SLS) and ultimate limit state (ULS) check. This factor  $k_t$  is known to be 1.0 and 1.2 for both cases respectively. Since these two scenarios have different loading combinations (including partial factors), governing loads are different. For the case of the ultimate limit state, the loading combination is focussed on ultimate loads which are acting in extreme scenarios that do not occur often. While the serviceability limit state focuses on combinations that are acting more frequently. Therefore, this factor is lower for the serviceability limit state than for the ultimate limit state. The  $\gamma_{M4}$  parameter is a considered partial safety factor. This factor contains a different value for each country. In the Netherlands, this factor is 1.0.

Another important parameter is  $\beta$ . This  $\beta$ -factor takes into account the ratio of the main plate and the side plates. In the next section, Section 2.5, the relation between bearing strength and length of the bolt is considered by introducing additional literature regarding this topic. In Figure 14, the assumed values for  $\beta$  are shown which are stated by the NEN-EN1993-1-8:2011 [17].

| $t_1 / t_2$             | $\beta$                   | $t_{b,resin}$      |
|-------------------------|---------------------------|--------------------|
| $\geq 2,0$              | 1,0                       | $2 t_2 \leq 1,5 d$ |
| $1,0 < t_1 / t_2 < 2,0$ | $1,66 - 0,33 (t_1 / t_2)$ | $t_1 \leq 1,5 d$   |
| $\leq 1,0$              | 1,33                      | $t_1 \leq 1,5 d$   |

**Figure 14:** Assumed  $\beta$  and  $t_{b,resin}$  per plate thickness ratio (Table 3.5 NEN-EN1993-1-8:2011 [17])

It is important to note that the Eurocode states that the total thickness, which is taken into consideration for the bearing resistance of the resin ( $t_{b,resin}$ ), may not exceed three times the nominal bolt diameter for double-lapped joints. Exceedance of this value will be limited by three times  $d$  (1.5 times  $d$  per shear plane). By the considered height, it means that the resistance against bearing is determined by taking into consideration a certain height of the available thickness. However, this length is related to the thicknesses of all plates, and especially their ratios. Since the middle plate takes one-half of this thickness, the value is divided by two. This explains the assumed value for  $t_{b,resin}$ , which is also indicated in [Figure 15](#).

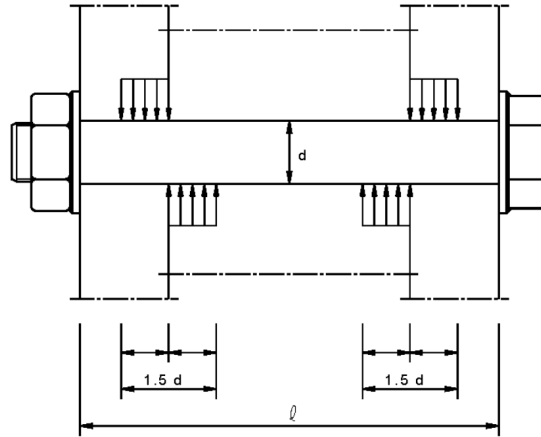


**Figure 15:** Cross-sectional view of an injected bolted connection indicating the effective thickness of the resin according to the NEN-EN1993-1-8 [17].

#### 2.4.4 Preloaded and injected bolted connections

*Paragraph 3.6.2.2 of NEN-EN1993-1-8:2011 states that for a preloaded and injected bolted connection the resistance is equal to the summation of the obtained individual resistances from injection and preloading.*

This implies that acting force may not exceed the summation of the resistances obtained from preloading ( $F_{s,Rd}$ ) and bearing strength of the resin ( $F_{b,resin,Rd}$ ).

## 2.5 Literature study

As mentioned in the introduction, the use of preloading and injection of bolts is a phenomenon which has been used in practice for a relatively short period compared to other types of connecting methods. Especially injection, injection of the bolt clearance started to replace riveted connections from the 80s [28]. Riveted connections are based on a perfect fit principle such that the shaft of the rivet itself is equal to the hole's when neglecting the shrinkage of the rivet by the decrease in temperature since riveted connections are installed with a high temperature. However, after renovation, it is only possible to reassemble a new connection when using fitting bolts, which is not a cost-effective method. For this problem, the injection bolt was developed to solve this problem and prevent the structure from slipping [29].

The other option for making a (new) connection slip-resistant is acknowledged to be by preloading bolts. As mentioned earlier in this report, preloading a connection increases the frictional resistance which prevents displacement of the bolts and thus slip-resistant. However, using a preloaded bolted connection as a replacement for the riveted connection is not recommended since the quality of the contact area can be poor. In addition, the surface can not be investigated or improved since the replacement of the riveted connection is done bolt-by-bolt. This lower quality affects the slip-resistance and is therefore not recommended.

To gain more insight into the design and behaviour of such connections, a literature study is performed which acts as a fundament for achieving this research's objective. Within the next paragraphs, information is explained elaborately to, for instance, prove the state of the art.

### 2.5.1 Preloaded bolted connections

Preloading of bolts creates a frictional force within a package that increases the resistance against slip. This resistance, which can be used in a connection, depends on many dependent variables, such as the clamping thickness, roughness of the bolt and nut, and the roughness of the plate's interface. According to the NEN-EN1993-1-8:2011, this preload force is determined by Equation 1. This preloading force is confirmed to be a safe estimation. According to Berenbak and Bijlaard, the probability of exceeding this 70% mark when using the combined method is 100% [6]. They expect that if the combined method for installation is used, a preload force of 90%, instead of 70% is more likely to be accurate. Besides the combined method, the torque method is an option to preload bolts. However, applying this method involves uncertainty in the procedure. If extraordinary friction exists between, for instance, bolt and nut, a significant amount of the applied torque disappears in bridging this region instead of extending the bolt itself. This is also the reason why the factor of 70% is involved. To minimize such uncertainties, the combined method is recommended to preload bolts. The Dutch Ministry of Infrastructure, Rijkswaterstaat, obliges this method to preload bolts [61].

This preloading force will decay over time. Especially in the first 15 minutes, a preloading loss of 6% for a connection containing an Ethyl Zinc Silicate [69][65]. In addition to the coating and its thickness, aspects such as the preparation of the surface and the preload force itself influence this percentage. This percentage may even increase when the  $l/d$  ratio decreases. According to Ness and Donohue, one of their three mentioned benefits of a larger  $l/d$  ratio is the decrease in preloading loss due to the proportion of embedment loss of the plates with respect to the length of the bolt [47]. The other two are related to resistance against self-loosening and reduced risk of fatigue failure. Nevertheless, such aspects as the  $l/d$  ratio are not taken into consideration by the Eurocode when calculating the nominal slip-resistance of a preloaded bolted connection. In addition to the positive effect of the  $l/d$  ratio on the preload loss, it also influences the effective force which creates the slipping resistance. Research done by Nassar and Abboud (2009) states that the thickness of the package determines the preloading loss [43]. This loss is related to the stiffnesses of the plates, bolt, and the area whereover the load, introduced by the bolt head and nut, is spread. In Figure 16, the distribution of the force and acting stresses over the distance from the bolt is visualised. Since the preload force determines the slip resistance of the connection, a large  $l/d$  ratio is preferable, due to such potential losses. In the next paragraph, Subsection 2.5.2 and in Figure 14, the importance of the  $l/d$  ratio for injected bolted connections is elaborated. However, the positive effect of this  $l/d$ -ratio for injection bolts is limited and therefore not infinitely.

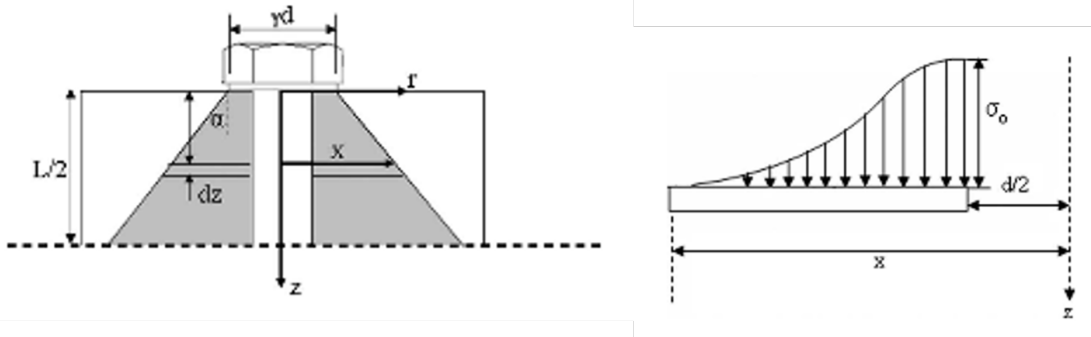


Figure 16: Distribution of introduced compressive stresses by preloading of the bolt [43]

Within the literature, preloaded bolted connections are investigated by many researchers. However, the specific application of an Ethyl-Zinc Silicate coating is rare. In one of the chapters in the SIROCO program, a European investigation of the execution and reliability of slip resistance connections, preloaded bolted connections are investigated. The goal of this part is to investigate the effect of the preload force and clamping thickness on the slip-factor, thus resistance according to the NEN-EN1993-1-8. Figure 17 [17].

| specimen batch                              | surface treatment / Rz <sup>2)</sup> | film thickness (average) | $\Sigma t$ | bolt class | $F_{p,C}$ | number of test results (n) | slip factor $\mu_{act,mean}$ <sup>3)</sup> | slip factor $\mu_{init,mean}$ <sup>4)</sup> | ratio $\mu_{init,mean}$ at $\Sigma t=152$ vs $\Sigma t=48$ mm | ratio $\mu_{init,mean}$ at $F_{p,C}=138$ vs $F_{p,C}=172$ kN |
|---|--------------------------------------|--------------------------|------------|------------|-----------|----------------------------|--|---|---|--|
|   | [ $\mu\text{m}$ ]                    | [ $\mu\text{m}$ ]        | [mm]       |            | [kN]      |                            | [-]  | [-]   | [-]   | [-]  |
| <b>Grit blasted surfaces (GB)</b>           |                                      |                          |            |            |           |                            |  |   |   |  |
| wp1.2                                       | Sa 1) 2½ / 80                        | -                        | 152        | HV10.9     | 172       | 6                          | 0,84                                       | 0,79  | 1,14  | 1,05   |
|   |                                      |                          | 48         |            |           | 4                          | 0,81                                       | 0,69  |   |  |
|   |                                      |                          | 48         | HR10.9     |           | 2                          | 0,80                                       | 0,70  |   |  |
|   |                                      |                          |            | HR 8.8     |           | 4                          | 0,85                                       | 0,74  |   |  |
| <b>Alkali-zinc silicate coating (ASiZn)</b> |                                      |                          |            |            |           |                            |  |   |   |  |
| wp1.2                                       | Sa 2½ / 80                           | 62                       | 152        | HV10.9     | 172       | 24                         | 0,76                                       | 0,72  | 1,07  | 1,06   |
| wp2.1                                       | Sa 2½ / 84                           | 55                       | 48         | HR10.9     |           | 8                          | 0,78                                       | 0,69  |   |  |
|   |                                      |                          |            | HR 8.8     | 138       | 8                          | 0,84                                       | 0,73  |   |  |
| <b>Zinc spray metalized coating (ZnSM)</b>  |                                      |                          |            |            |           |                            |  |   |   |  |
| wp1.2                                       | Sa 3 / 104                           | 140                      | 152        | HV10.9     | 172       | 6                          | 0,83                                       | 0,79  | 1,08  | 1,21   |
|   |                                      |                          | 48         |            |           | 4                          | 0,82                                       | 0,73  |   |  |
| wp2.1                                       | Sa 3 / 100                           | 165                      | 48         | HR10.9     |           | 8                          | 0,73                                       | 0,65  |   |  |
|   |                                      |                          |            | HR 8.8     |           | 138                        | 8  | 0,91  | 0,79  |  |

<sup>1)</sup> Sa: surface preparation grade | <sup>2)</sup> Rz: roughness steel surface | <sup>3)</sup>  $\mu_{ini,mean}$ : slip factor (mean values) considering the initial preload when the tests started | <sup>4)</sup>  $\mu_{act,mean}$ : slip factor (mean values) considering the actual preload at slip

Figure 17: Determined slip factor for several test applications [59]

Within this figure, the initial preload force ( $F_{p,C}$ ) and friction coefficients are shown. Since only the initial and not actual preload force is given, the resistance ( $F_{s,i}$ ) can only be determined by the related friction coefficient ( $\mu_{init,mean}$ ). This is valid since the determination of this friction coefficient is based on the linear relation between the normal and friction force. In Subsection 2.5.4, an elaboration is given on the influence of the friction coefficient on the resistance.

In another chapter of the SIROCO research, a full Ethyl-Zinc coating system is investigated. This coating system consisted of the following structure [64]:

1. 50 $\mu\text{m}$  Interzinc 22 (ESI primer);
2. 30 $\mu\text{m}$  Intergard 269 (EP coupling agent);
3. 50 $\mu\text{m}$  Interzinc 22 (EP intermediate);
4. 50 $\mu\text{m}$  Interzinc 22 (coat PUR top coat);

Each connection consisted of 2x M20 bolts with a preload force of 172kN. The geometry of each specimen is in line with Annex G of the NEN-EN1090-2 [15]. In total three different tests were performed. Each of them contained the described coating. However, one of the batches was an old batch. In addition, one of the other series was conditioned for three weeks instead of one week like the other specimens.

From each of these series, the average friction coefficient was 0.52 for short-term tests. For the extended creep test, the obtained friction coefficient is 0.42.

### 2.5.2 Injected bolted connections

In Subsection 2.4.3, formulas for the bearing resistance of a resin-injected bolted connection are given. In 1974, Bouwman investigated this influence of plate thicknesses on the bearing resistance of an injected bolted connection [10]. In his research, four different configurations of plate layouts were tested, see Figure 18.

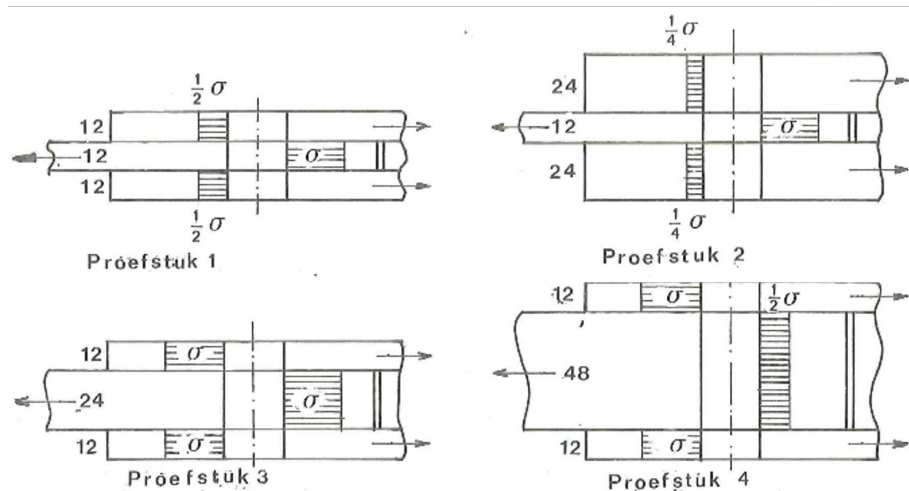


**Figure 18:** Four different geometry layouts used by Bouwman for his investigation to the (bearing) resistance of an injected bolted connection [10]

From this figure, it can be concluded that for layouts 1 and 2, the middle plate is the governing plate. While for layout 4, the side plate is governing. From specimen 3, the result pointed out that the side plate determined the resistance, even since the longitudinal stresses in all plates were identical. All specimen types were tested two times of which one test failed within specimen type 1.

From the results obtained from this research, the graph visualised in Figure 19 is given. Within this figure, the side plates are meant by “stukplaat” and the middle plate is referred to as “hoofdplaat”. It is assumed that the side plate is governing with a ratio of up to 0.5. Until this ratio, the stresses in the side plates are higher than in the main plates. Between 0.5 and 1, there is a linear increase since relatively thick side plates increase the resistance. In addition, Bouwman indicates that the resistance of “Prøefstuk 3” and “Prøefstuk 4” are similar to each other, while the stresses in the middle plate are twice as small. For this, Bouwman suggests two possible reasons. The first reason is that since the stresses in the side plates are high, the displacements in these plates may become governing from an early stage onwards. The second reason for this similar difference is that besides the thickness-ratio, the absolute thickness of each plate plays a role [10].

As mentioned, Bouwman concludes that there is a relation between the thickness ratio of the side and middle plates. To take this effect on the bearing resistance into account the  $\beta$ -factor is introduced. This factor can vary from 1 up to 1.33 depending on the ratio of the plate thicknesses. This is also shown in Figure 14. In case the thickness ratio is 1.0 and the thickness of each plate is 12mm, the longitudinal stress in the middle plate is twice as much as the stresses in the side plates. When the thickness of the middle plate is increased to 24mm, a higher absolute resistance is obtained since stresses are reduced. However, from this investigation, it turned out that until a displacement of 0.3mm, this resistance is not twice as much. It turned out that the obtained stresses are 33% higher in the first case than for the second case where the side plates have an equal thickness as the middle plate. This results in a 33% increase of the bearing strength ( $f_{b,resin}$ ) when reducing the ratio of the middle plate over the side plates. This is considered by this  $\beta$ -factor of maximum 1.33.

Besides the influence of the plate thickness ratio on the bearing strength of the resin, the plate thickness itself is also of importance. As Bouwman indicates, “Proefstuk 3” and “Proefstuk 4” have similar resistances, while the average stresses in the middle plates are halved. As Koper shows in his research, stress concentration occurs around the shear planes [37]. This is also adopted in the NEN-EN1993-1-8, where the length whereover a resin can act is limited by  $1.5d$  since larger dimensions result in significant non-uniformity of the stress distribution in the resin over the length [17]. Therefore not the entire length may be taken into consideration, see Figure 15.

However, these test results of Bouwman are obtained by performing the described specimens two times each. In other words, a total of eight tests have been performed. Therefore, it can be questioned whether or not these tests cover all possible geometries.

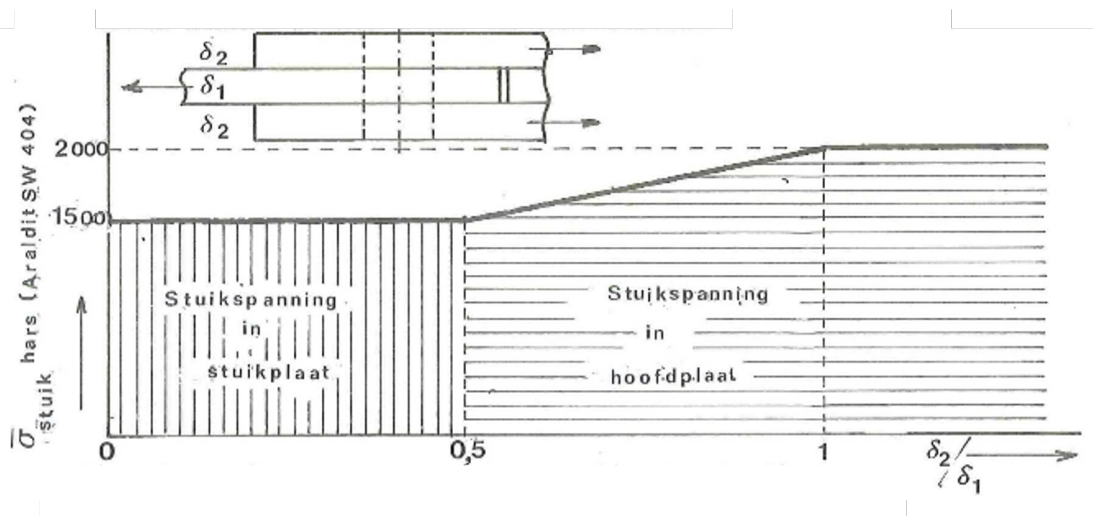


**Figure 19:** Effect on the bearing resistance of the resin by different plate thickness configurations, investigated by Bouwman [10]. On the horizontal axis the plate thickness ratio and on the vertical axis the bearing strength of the resin in  $\text{kgf/cm}^2$  ( $\approx 0.1\text{MPa}$ )

The result of this research is later used as the foundation of the resistance of injected connections within the NEN-EN1993-1-8 [17]. It can however be questioned whether this is safe since the research of Bouwman is based on 4 different configurations with two tests each. Within Bouwman’s research, the resin type Araldite SW404 in combination with HY404 hardener is used. Nowadays, this type of resin is prohibited for usage since the HY404 hardener appeared to be toxic [28]. However, assuming this type of hardener, Bouwman concluded that the bearing strength of the resin varies between 150 and 200 MPa. For the HY2404 hardener, which is nowadays more commonly used, such strength may differ and could influence the overall behaviour of the connection.

When investigating the behaviour of injected (and preloaded) connections, the importance of bearing strength and stiffness is significant. Especially since the code allows direct summation of strengths. In addition to the exclamation is the ambiguity of bearing strengths of two-epoxy-resins.

After 1974, many tests were performed at the TU-Delft laboratory which resulted in similar strengths properties as Bouwman's [10] [11]. The ECCS publication of 1994 (No.79) states that the best resin tested by the TU-Delft has a bearing strength of 150MPa for long-term usage [23] [11]. Nevertheless, in a published report from 1996, this same strength is determined to be 130MPa [28]. Gresnigt stated that creep tests of SW404-HY2404 resins allow bearing strengths of 130MPa. It is unfortunately not known how many tests have been executed and how these tests are executed to determine this value of the bearing strength. However, the noted difference is that the different (non-toxic) hardener HY2404 instead of HY404 is used.

A couple of years later, in 2000, the same researcher, Gresnigt, performed another study about the material properties of the two-component resin. From these tests, a significantly increased bearing strength is determined. Gresnigt states that a safe assumable strength of 175 or even 200 MPa can be used, instead of the initial 130MPa, see Figure 20. Where it can be questioned what the effect of measured location is on the resistance. In the experiment where the 130MPa is determined, it is unknown how displacements were monitored. For the other case, displacements are measured at the end of the plate in line with the force.

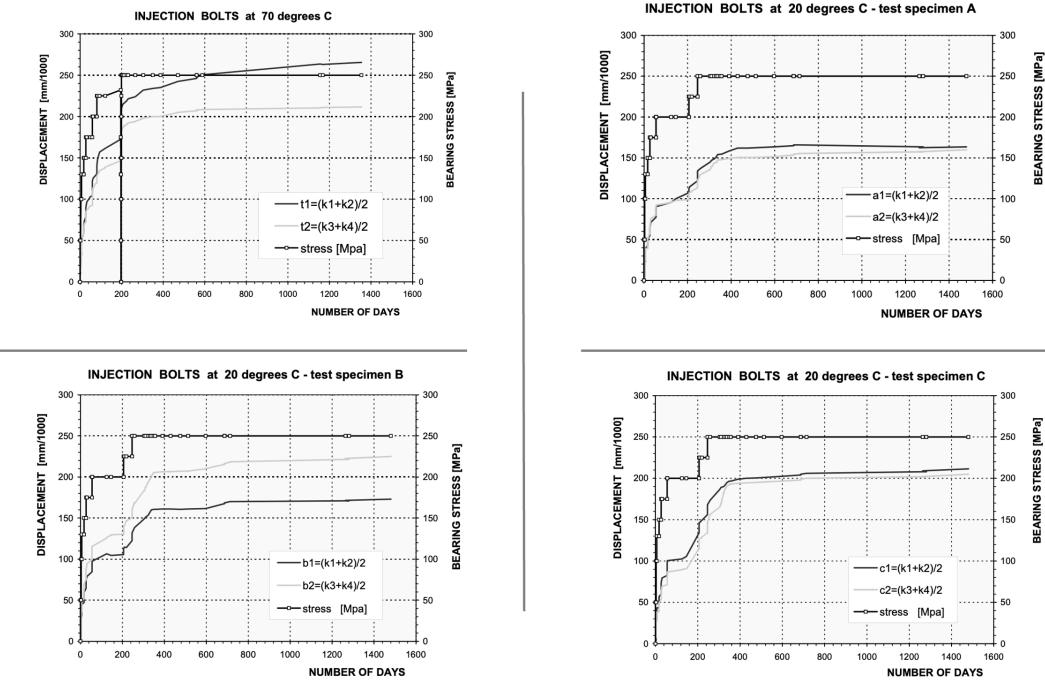


Figure 20: Strength of resin SW404+HY2404 [27]

The results, shown in Figure 20, are obtained from creep tests at both 20 and 70 degrees. From these tests, the acting bearing stresses are determined. This bearing stress is the applied force divided by the contact area. That is the width of the bolt times the thickness of the middle plate. It can be seen that the temperature has a moderate influence on this bearing strength [27]. Nevertheless, implementing such material properties directly into the current test setup may lead to incorrect results since these properties are all based on creep (long-term) tests. Therefore the research of Gresnigt and Beg plays a significant role. Gresnigt and Beg performed additional research regarding five different types of tests, namely standard bearing tests, monotonic long- and short-term tests, a cyclic test and long-duration creep test [29][30]. From these tests, the short-duration cyclic tests obtained a bearing strength of the resin of 200MPa. These tests are performed in Ljubljana, Slovenia. At the same time, tests of injected bolted connections were executed in The Netherlands.

Within the latter, the obtained resistance is implemented into the project of extension Railway Station Amsterdam Central. These connections contained of 2x M27 bolts whereby the bolts are installed manually to mimic execution procedures in practice. The obtained result is an allowable bearing stress of 284MPa. Afterwards it was decided to limit bearing strengths to 200 and 280MPa for long- and short-term duration respectively. However, since the installation procedures involved manual handling, the location of the bolt with respect to the clearance is at random. This may affect the bearing resistance of the bolt both positively and negatively.

The most recent research regarding injected bolted connections was performed by Ungermann and Kröger. The goal of their research was, similar to this research, to investigate the potential summation of connections using preloading and injection solely. In their short-term test, the bearing strength of the resin SW404+HY2404 turned out to be approximately 211MPa [67]. This is determined by the exerted force on the specimens, divided by the width of the bolt times the plate thickness.

In [Table 2](#), an overview is given of the determined resin properties of the last decades. Distinguishment is made between the type of bearing strengths (Long-term and Short-term) and the method of determination of this bearing strength of the resin.

**Table 2:** Summary of the bearing strength of the resin (SW404 + HY(2)404)

| Bearing strength               | Resin          | Criterion                             | Published | Cite     |
|--------------------------------|----------------|---------------------------------------|-----------|----------|
| 150MPa                         | SW404 + HY404  | 0.3mm slip                            | 1974      | [10]     |
| 150MPa (LT)                    | SW404 + HY404  | Creep tests (0.3mm slip)              | 1989      | [11]     |
| 150MPa (LT)                    | SW404 + HY404  |                                       | 1994      | [23]     |
| 130MPa (LT)                    | SW404 + HY2404 | <i>UNKOWN</i>                         | 1996      | [28]     |
| 175-200MPa (LT)                | SW404 + HY2404 | Creep tests                           | 2000      | [27]     |
| 200MPa (LT) and<br>280MPa (ST) | SW404 + HY2404 | Cyclic, Short-term<br>and Long-term * | 2012      | [29][30] |
| 211MPa (ST)                    | SW404 + HY2404 | 0.15mm slip                           | 2023      | [67]     |

ST = Short-term

LT = Long-term

\* = random location of bolt with respect to bolt hole

### 2.5.2.1 Material properties of the resin

Material characteristics and properties of the resin are dependent on the environment of the application and the direction of placement. For instance, for anisotropic materials and components, properties are different in each direction. Properties for various resins are investigated in the available literature. Nijgh and Xin investigated the computational homogenization simulation of the RenGel SW404 with hardener HY2404 [71]. This research brought to life the material behaviour under certain conditions. Within this research, distinguishment is made between confined and unconfined conditions. Within concrete structures, the degree of confinement is taken into consideration since it influences the compressive strength of concrete. A confined situation is an environment that supports a compressed member by lateral pressure. This lateral pressure increases the compressibility of a component. The principle of enclosure is also adopted into the NEN-EN1992-1-1[20], a code including guidelines from concrete structures, see [Figure 21](#). In addition to this confinement, they considered resins with steel shots as well. Nevertheless, the latter is not taken into consideration since that option is left out of this scope.

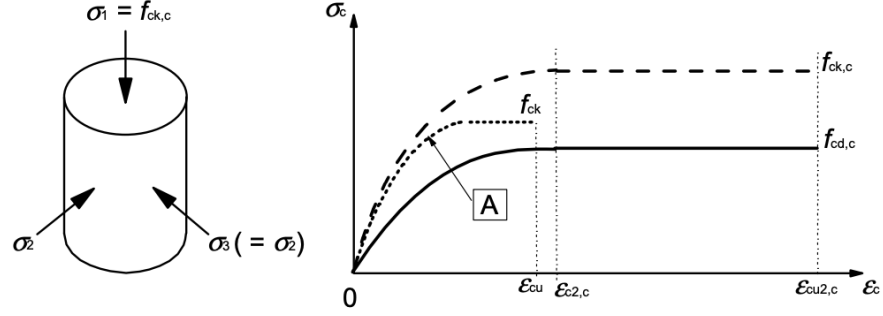


**Figure 21:** Compressive strength of enclosed concrete according to the NEN-EN1992-1-1 [20]

Two of the assumptions made in this research are that a resin behaves isotropically and that the plastic behaviour is governed by the linear Drucker-Prager model. Such a model takes into account the multi-direction behaviour of volumes while being loaded. For this, a Drucker-Prager model is often used, especially in Soil Mechanics [60]. This principle of Drucker-Prager is formulated by Equation 5 and visualised by Figure 22.

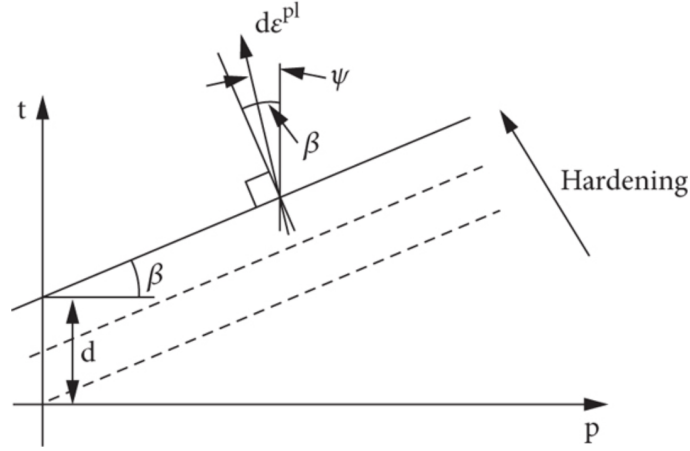


**Figure 22:** Linear Drucker-Prager model yield surface and flow in the p-t plane [70]

$$F = t - p \cdot \tan \beta - d = 0 \quad (5)$$

With:

- $t$  = Deviatoric stress;
- $p$  = Hydrostatic stress;
- $\beta$  = Friction angle of material;
- $d$  = Cohesion of material.

Obtaining the parameters for the Drucker-Prager model requires experimental results. The research of Nijgh and Xin investigated these parameters of the associated model based on unconfined conditions. These characteristics were found by analyzing results from the Mohr-Coulomb failure model, which is characterized by Equation 6.

$$\tau = c + \sigma \cdot \sin \varphi \quad (6)$$

When identifying the Mohr-Coulomb criterion, a linear function can be drawn according to [Equation 6](#). However, when substituting [Equation 5](#) into Mohr-Coulomb, two different approaches can be assumed: Associated flow and Non-dilatant flow. Between these two phenomena, differences can be seen in the behaviour while exerted to a shear force. When a shearing force is exerted on a volume, the strength depends on two factors, the internal friction and the degree of dilatancy. The latter relates to the amount of energy required to overcome the effect of interlocking between particles [32]. If dilatancy does not occur in volumes, the volume is assumed to be non-dilatant ( $\psi = 0$ ). This parameter  $\psi$  relates to the angle of plastic flow potential, see [Equation 7](#). When this factor for dilatancy is zero, then the plastic flow is independent of the hydrostatic stress. However, in the case of the assumed associated flow, dilatancy occurs and therefore the plastic flow is dependent on the hydrostatic stresses. This can also be seen in [Figure 22](#).

$$G = t - p \cdot \tan \psi \tag{7}$$

Given these statements, a resin is injected into the bolt clearance. It can be said that the bolt, and so resin, behaves in a confined environment since expansion in a transverse direction is not possible. However, in confined conditions, the total volume of the chamber and the volume of the substance will be equal. Nevertheless, in the current setup, it will not be correct to assume that the environment acts as a fully confined condition.

### 2.5.3 Preloaded and injected bolted connections

Application of injection and preloading into a connection is nowadays often done in The Netherlands. Especially since the NEN-EN1993-1-8 allows summation of obtained individual resistances from preloading and injection [17]. From this increase in resistance, fewer bolts are required for a certain connection which may reduce costs. In 1994, the European Convention for Constructional Steelwork (ECCS) already introduced examples of how to calculate preloaded and injected connections, based on investigations of Gresnigt and Bouwman and many others [29][10]. Their outcome is the graph shown in Figure 23. Within this figure, all relevant failure modes are shown and based on design values.

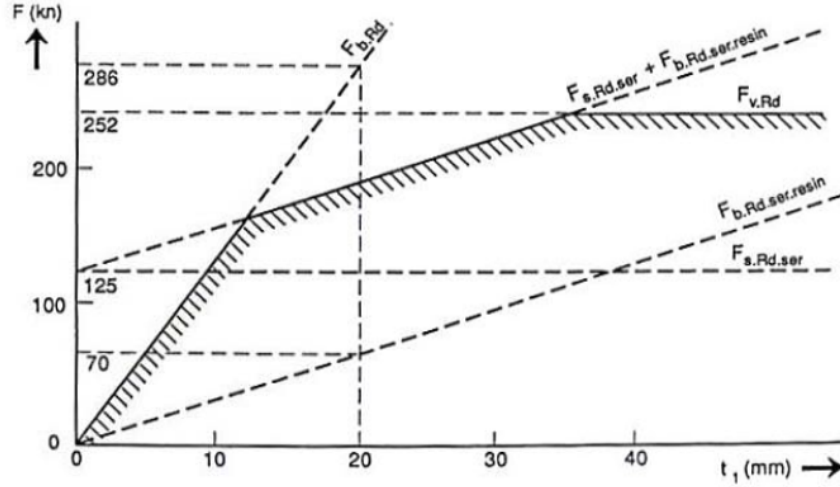


**Figure 23:** Governing resistances for the serviceability limit state for each thickness of the middle plate. Where the thickness of the side plate is 75% of the middle plate [23]. Assuming that summation of slip resistance by preloading and bearing resistance of the resin is allowed

The related characteristics of the figure above are as follows:

1. The ratio of plate thickness is 3:4 ( $t_2 = 3/4 t_1$ ). This results in a  $\beta$ -factor of 1.17;
2. The connection consists of one M20 bolt of grade 10.9 in combination with nominal clearance;
3. The assumed friction coefficient is 0.4.

From this figure, it can be seen that for example, the bearing resistance of the steel plate is governing until a certain plate thickness. The prEN1993-1-8 indicates that the bearing resistance does not have to be checked in slip-resistance connections (Category B and C) [16]. It is thought that this check does not have to be performed since the stiffness created by friction is significantly larger than the bearing stiffness and therefore not activated. After approximately 12mm, a different failure mode is governing, namely, the mode where the bearing resistance of the resin plus the slip resistance, created by the preloading force, is governing. From a plate thickness of 35mm onwards, the shear resistance of the bolt determines the resistance of the connection. One can argue this statement, however in practice, it is possible that the bolt immediately bears against the adjacent steel plate and while brittle failure of the connection has to be prevented. Thus, the shear resistance of the bolt must be taken into consideration.

From this same document, it is concluded that the analogy of this principle is in fact based on research results shown in Figure 19 by Bouwman in 1974 [10]. Two years before this research, also done by Bouwman [9], he investigated the fatigue behaviour of injected-preloaded-bolted connections including the case study of a railway bridge near Culemborg, The Netherlands. These test series show that the fatigue strength of preloaded-injected connections is significantly higher than in connections realised by fitted preloaded bolts. To implement this outcome in the current project, parameters are required which are unfortunately not given by the released document. In this research performed by Bouwman, a coating of 50  $\mu\text{m}$  is applied with a brush. The unanswered question is which type of coating is applied and how precisely a coating can be applied in such a way. Important to mention is that the coating thickness plays a crucial role in relation to the slip resistance and the applied normal force (by preloading). This namely affects the assumed friction coefficient (short-term) and the preloading loss (long-term). The friction coefficients, which were tested in this research by Bouwman, are between 0.05 and 0.1. These are significantly lower than the current codes prescribe, namely between 0.2 and 0.5.

Another research, performed by Kluwen in 1982, established the difficulty and simultaneously the importance of a well-applied coating [35]. He investigated the long-term behaviour of preloaded injection bolts. Tests were performed until specimens had a displacement of more than 300 $\mu\text{m}$  (=0.3mm). From these tests, the friction coefficient, for specimens which are coated by Ethyl Zinc Silicate, resulted to be 0.2. This coefficient is however calculated from tests where both injection and preloading are used. This implies that the bearing strength of the resin had to be deducted from the maximal exerted force. Where the bearing strength of the resin was assumed to be 200MPa. From a previously mentioned research, by Gresnigt et al. a bearing strength of 280MPa could be used safely, keeping the random positioning of the bolts in mind [29]. If the same resin is used, the calculated force created by friction reduces. Which subsequently reduces the calculated friction coefficient. Due to these uncertainties, a good estimation of the friction coefficient can not be concluded.

In 2012, Gresnigt, Beg and Bijlaard published their results on the behaviour of monotonic long- and short-term double-lapped bolted connections. They investigated three different connections: preloading only, injection only and the application of both preloading and injection. For this experiment, each specimen's geometry is in line with the NEN-EN1090-2 [15]. For post-processing of these results, a resin with a long-term bearing strength of 200MPa was assumed. From the test performed in Ljubljana, Slovenia, it was concluded that the summation of preloading and injection does not give similar results to the combined tested resistance [30]. In Figure 24, the average results per type of connection are shown.

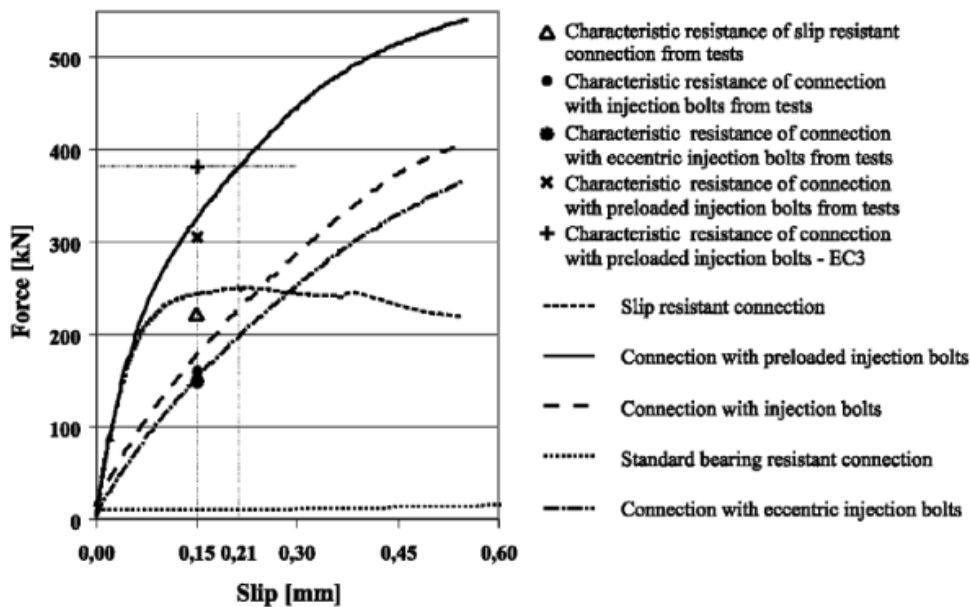


Figure 24: Comparison of results for different type of connections [30]

### 2.5.4 Friction coefficient

A preloaded connection prevents exceeding the slip criteria due to its clamping force. Slip is in this case prevented if the resistance is larger than the acting force. Such resistance is obtained by the clamping force perpendicular to the shear plane. These forces, resistance and clamping force, are related to each other by a factor called the friction coefficient ( $\mu$ ), by Amonton and Coulomb stated as the formulation shown in Equation 8 [62].

$$F_S = F_N \cdot \mu \quad (8)$$

In 1699, Amonton discovered two phenomena whereof he concluded two laws, which are cited as follows by Blau [8]:

1. The friction force ( $F_S$ ) is directly proportional to the applied load ( $F_N$ );
2. The friction force ( $F_S$ ) is independent of the apparent area of contact.

This first law implies that the written formula Equation 8 is correctly prescribed since the area is not involved in this equation. However, it can be wondered whether or not the constant  $\mu$  is dependent on, for instance, time, displacement and material properties. According to Blau [7] there are many factors which practice involvement in the friction coefficient. Such as contact geometry, applied normal forces and temperature. Implementing this into this research, it can be questioned whether these parameters are constant or not. Often, it is generalised that the friction coefficient is proportional to the roughness of a shear plane. However, it is analyzed that a higher roughness does not immediately increase its coefficient of friction (COF). Khaday et al. investigated this relation between surface roughness and COF for stone and ceramic floors [34]. Based on his conclusion no linear relation exists. For his research, he suggests a relation including third-order components. This same research confirms that a rougher surface does not directly imply a higher coefficient of friction. Whether this applies to the applied coating is yet unknown. However, it opens up the possibility that it can not be assumed that higher roughnesses involve higher COFs. When measuring the surface roughness, the primer/coating is sprayed onto the surface where contact will take place. This roughness decreases if the preload force increases due to local compression of the layer. In the research from SIROCO, this relation between the preload force and slip factor is investigated [59]. From this research, it is concluded that there is indeed a positive effect on the friction coefficient when decreasing the preload force. In Table 3, the conclusion from this research is given. Two different scenarios are elaborated for three different types of coatings. The first scenario relates to the effect of the thickness of the clamping package on the COF. The other scenario visualises the effect of the applied preload force on the COF. From these two cases, it was concluded that both a thicker clamping package and lower preload force increase the friction coefficient.

**Table 3:** Slip factor per applied coating, preload force and clamping length [59]

| Ratio of COF                 | t = 152mm | t = 48mm | F <sub>p,C</sub> = 138kN | F <sub>p,C</sub> = 172kN |
|------------------------------|-----------|----------|--------------------------|--------------------------|
| Grit blasted surface         | 1.14      | 1        | 1.05                     | 1                        |
| Alkali-zinc silicate coating | 1.07      | 1        | 1.06                     | 1                        |
| Zinc spray metalized coating | 1.08      | 1        | 1.21                     | 1                        |

In [Subsection 2.5.1](#), it is mentioned that according to Ness and Donohue, one advantage of a larger  $l/d$ -ratio is the decrease in the preload loss [47]. This can also be confirmed by [Figure 17](#) since the difference of the friction coefficient based on the actual and initial preload force is less when using a larger  $l/d$ -ratio. An additional advantage is the distribution of stresses. In the case of a larger clamping thickness, the preload force is distributed over a larger area such that local stresses are reduced. This reduction will probably decrease the degree of damage to the coating. Therefore, a higher friction coefficient is obtained (see [Table 3](#)).

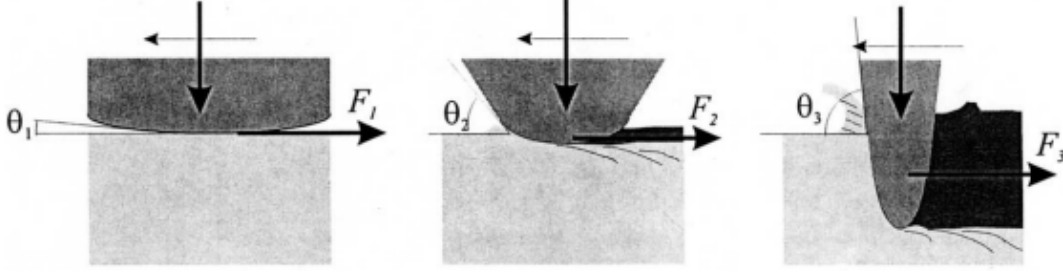


**Figure 25:** Increase of the tangential force due to a change in geometry of the slider [7]

However, it can be argued that an increase in the COF, when applying a higher preload, is the result of the roughness at the surface interaction. According to Blau the shape of the slider geometry, as indicated in [Figure 25](#), affects the tangential force with the same normal force due to the ductile behaviour of the mother material [7]. This slider can also indicate the roughness of the surface. Since the mother (base) material may act more ductile, a larger contact surface occurs. The contact area in the normal direction to the slider increases the resistance and thus friction. However, this surface does not transfer force by a shear force but by normal force instead which affects the friction coefficient. If the surface already contains a rough profile, friction has already accumulated. This roughness is expressed with the parameter  $R$  for profiles and  $S$  for surfaces. The most widely used parameters for roughness characterisation are  $R_a$ ,  $R_q$  and  $R_z$  [26].

- $R_a$  = average height of the profile;
- $R_q$  = root mean square roughness;
- $R_z$  = ten-point height.

The average height ( $R_a$ ) is the line where the area of the peaks and valleys are equal to each other. This parameter gives a general description of the roughness. Nevertheless, it is not influenced by small changes in profile. Root mean square ( $R_q$ ) refers to the standard deviation of the roughness. The last parameter is the ten-point height ( $R_z$ ) which tells something about the difference in height of the five highest peaks and five lowest valleys.

$$R_a = \frac{1}{l} \int_0^l |y(x)| dx \quad (9)$$

$$R_q = \sqrt{\frac{1}{l} \int_0^l (y(x))^2 dx} \quad (10)$$

$$R_z = \frac{1}{n} \left[ \sum_{i=1}^n p_i - \sum_{i=1}^n v_i \right] \quad (11)$$

Besides the R-values, it is also possible to investigate the S-values. The difference between these two parameters is that R represents a line roughness. While the S-parameter relates to surface roughness. Identifying the R- or S-parameters is done by measuring in one line or surface area respectively. In the case of line roughness, Mitutoyo SurfTest SJ-210 uses a needle over a length of 4.5mm. From this profile, it calculates the described parameters above. However, the outcome of these values differs from the surface roughness. Differences occur since the surface roughness uses an entire 3D space to determine the roughness while the profile roughness is determined on one line (2D). Therefore peaks are assumed to occur over the entire width. While surface roughness creates cone-shaped roughness. The result is that the factors for surfaces are often higher than for profiles.

Within customized steel surfaces, the average surface height ( $S_a$ ) is commonly used as identification of the surface roughness. For a surface preparation of the application of a coating, the requirement is that this area must be sandblasted to remove particles or any single initiation of corrosion. In the ISO8501-1:2007, preparation specifications are given which have to be fulfilled before applying the coating [44]. For most surface preparations,  $S_a$  2.5 is prescribed, where a value of  $80\ \mu\text{m}$  is assumed for  $R_z$  [65]. In addition to these specifications, the manufacturer of the coating requires a surface roughness. For the Interzinc22, a surface profile of 40-75 microns is recommended [33].

When looking into the friction coefficient, Amonton and Coulomb suggest a linear relation between the normal and shear force. However, it can be questioned whether this is representative of all surfaces and conditions. When two sliding surfaces are compressed, the friction force must be overcome for slip to occur. If the required force after setting in motion of the sliding surface is less than initially needed, the kinetic friction coefficient is lower than the static friction coefficient. In this case, the required shear force differed over the entire displacement amplitude. This effect can be seen by the hysteresis obtained from such a test, an example is given in Figure 26 [42].

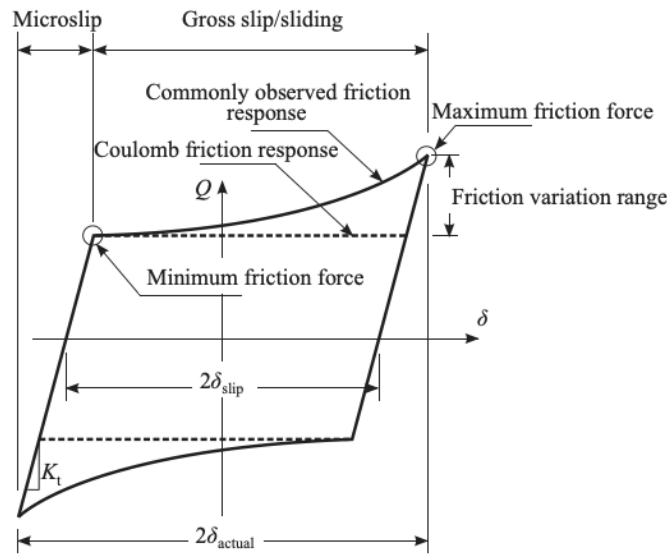


**Figure 26:** Two types of hysteresis obtained from friction test. Where both the Coulomb (dotted) and Non-Coulomb (continuous) friction is shown [42]

In Figure 26, two different types of hysteresis are shown, namely the Coulomb and the Non-Coulomb. In the Non-Coulomb behaviour, non-linearity is obtained. In addition to these two graphs, distinction can be made between the static (peak) and kinetic (plateau) friction coefficients. If the implemented displacement amplitude within a test is large enough, a horizontal plateau will be visible. In addition, the peak shows the static friction coefficient. The identification of both coefficients can be done by the use of a Tribometer. Within such a test, two sliding blocks are pressed on top of each other by a normal force ( $F_N$ ). During the experiment, these blocks will be pushed back and forth for a certain time interval. Monitoring of the required shear force to push and pull the specimens is used for the formulation of the friction coefficients. Such a test indicates the behaviour of a surface interaction and whether a slip-resistance can be maintained after microslip.

#### 2.5.4.1 Experimental procedure for determination of friction coefficients according to the NEN-EN1090-2

In general, the resistance of a connection is related to the dimensions of the connection. To open up abilities for comparing results between studies, a general layout is designed and given in the NEN-EN1090-2 section G1 [15]. Therefore, a mandatory geometry is designed for experiments involving the goal of obtaining friction coefficients. In Figure 28, an overview is shown of this prescribed geometry. Of this design, some important characteristics are that on both sides of the connection two M16 bolts are mounted to an 80mm wide plate with two cover plates. Where the middle plate is 16mm and the side plates are 8mm. Besides this design for M16 bolts, another option is the use of two M20 bolts. The latter implements different geometries. However, the ratio of the thickness of the side and middle plates remains 1:2. Therefore stresses are still expected to be equal over all plates. For the application of M20 bolts, the middle plate has a thickness of 20mm instead of 16mm.

To measure the relative displacement of the plates, a mandatory amount of locations are prescribed to install the instruments. A total of 8 measuring points are assumed to be sufficient. A remark to this is that the ROK prohibits the determination of a friction coefficient by Annex G. Within calculations a standard value must be acknowledged in accordance with Table 17 of NEN-EN 1993-1-8, also see Figure 13.

Annex G of the NEN-EN1090-2 distinguishes two methods, namely short-term and extensive creep test procedures [15] (long-term). This research focuses on the short-term slip test procedure only. Justifying a reliable conclusion of the friction coefficient requires a full analysis of both methods. For the short-term phase, at least five specimens must be tested where the relative displacement of the bolt group is measured at all indicated points are shown in Figure 28. For the long-term (creep) test, this is only one specimen.

In addition to the methodology of testing and required locations, the relation between displacement and applied force needs to be monitored. When post-processing the result of a single connection, the output of the displacement measured at the central bolt group (CBG) is important for the determination of the friction coefficient. One can suspect three types of graphs in this described plot (Figure 27). Within this overview, the X-axis represents the displacement at the centre of the bolt group (mm). While the Y-axis is the applied force. This displacement at the centre of the bolt group is determined by averaging the monitored displacement at the four locations on each side of the connection.

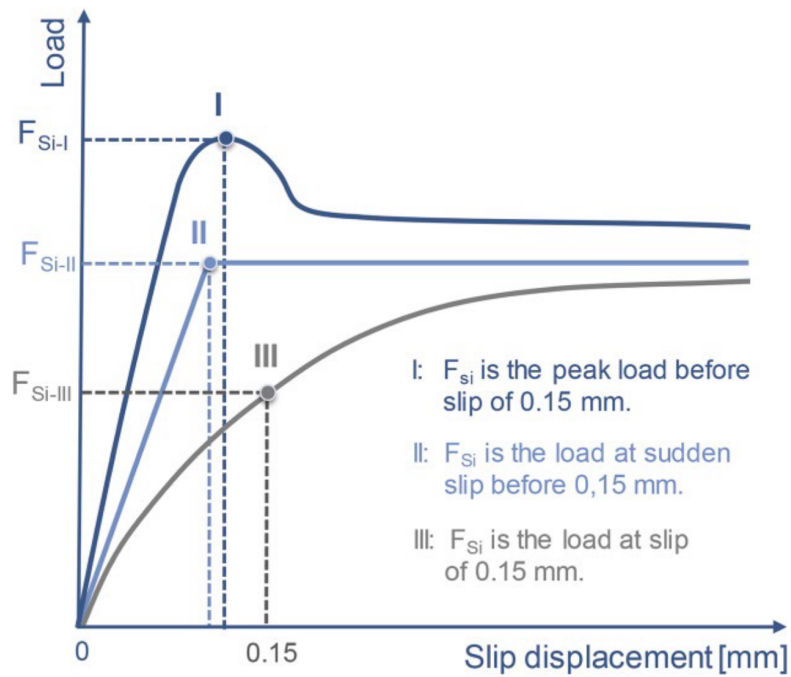


**Figure 27:** Three different definitions of the slip resistance ( $F_{si}$ ) including prescribed graphs expected as output for the slip test [15] [65]. On the horizontal axis, the relative displacement at CBG in mm is shown. The vertical axis represents the applied force

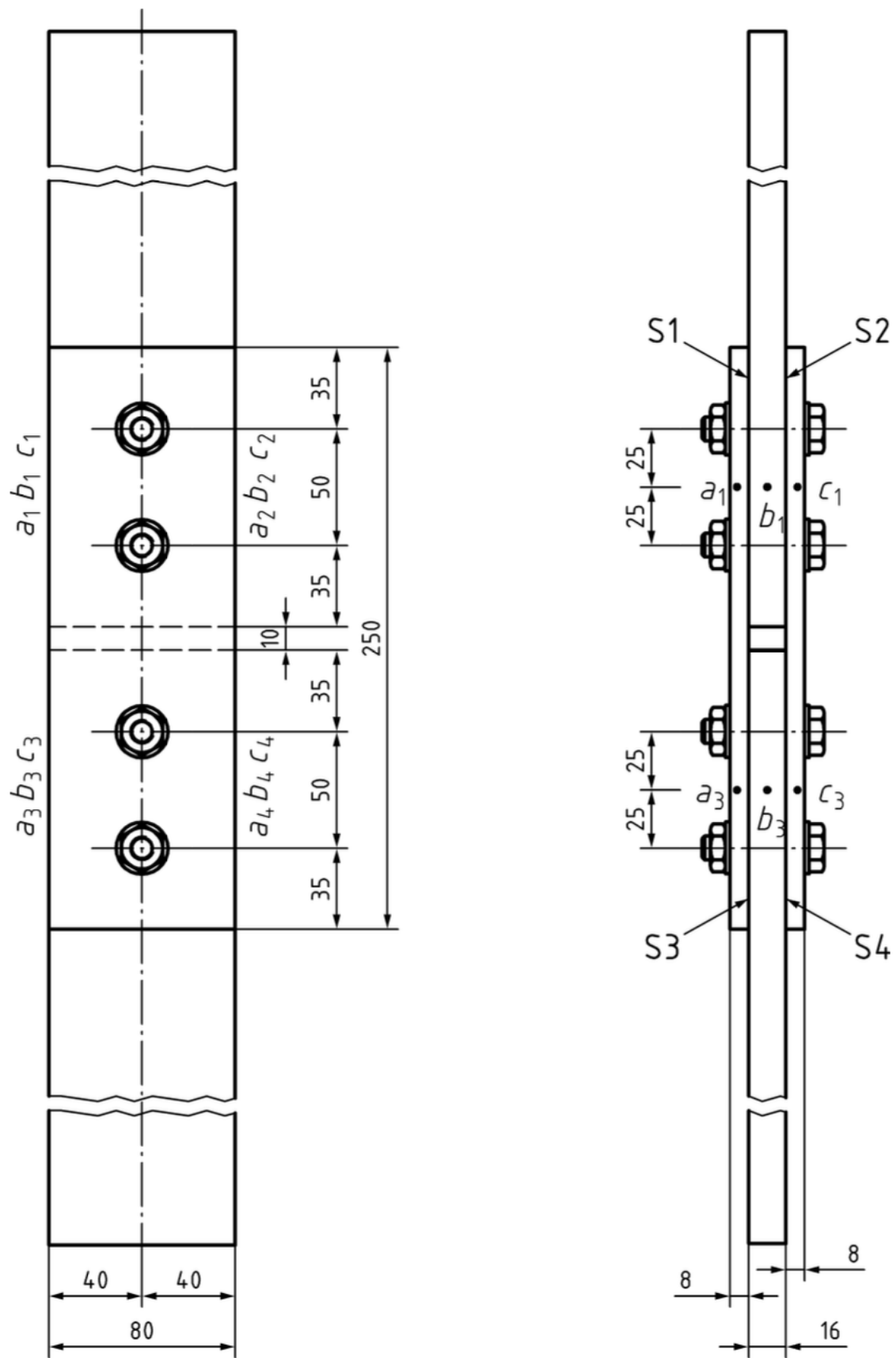


Figure 28: Standard layout for obtaining friction coefficients for M16-bolts according to NEN-EN1090-2 [15]

It is assumed that the friction coefficient is the relationship between the normal force and the maximum applied force in the shear connection. In [Equation 8](#), a generalised formula is given for the relation between those forces. Physically, this generalisation is valid for an interface of two bodies. From this point of view, the NEN-EN1090-2 expands the formulation to a connection including two bolts. Where each bolt is preloaded ( $F_{p,C,i}$ ). In addition, it is assumed by the NEN-EN1090-2, that each bolt contains the same preload force ( $F_{p,C}$ ). Besides the change from one to two “interfaces”, this formula is adopted at a double-lapped connection. Therefore, each bolt has two shear planes. Combining the amount of bolts and shear planes, a total of four interfaces occur. Still assuming that the preload force is equal over all bolts, the NEN-EN1090-2 determines the friction coefficient by the formula as shown in [Equation 12](#).

$$\mu_i = \frac{F_{Si}}{4 \cdot F_{p,C}} \quad (12)$$

With:

$$\begin{aligned} \mu_i &= \text{friction coefficient of connection } i \text{ [-]}; \\ F_{Si} &= \text{slip resistance until 0.15mm [kN]}; \\ F_{p,C} &= \text{preload force [kN]}; \end{aligned}$$

The applied force ( $F_{Si}$ ) relates to the applied force within the experiment. Over the displacement trajectory, this force will increase and can be expected to decrease, see [Figure 27](#). To limit allowable deformations, the region wherein the friction coefficient is determined runs from 0.00mm to a relative displacement of the CBG of 0.15mm. Within this equation stated above, the applied shear force ( $F_{Si}$ ) is the maximum force that occurred within this range.

In the calculation of the friction coefficient, there are several options that can be implemented which are all based on different definitions of  $F_{p,C}$ . Especially since the compared force (applied and preload) do not have to act at the same time. Therefore, the maximum slip force ( $F_{Si}$ ) can occur at a displacement of 0.05mm ( $t_1$ ) while the preload force is measured at a displacement of 0.0mm ( $t_0$ ). In addition, as preload force a nominal value is assumed. For example, for a 10.9 M16 bolt, this force will be 110kN after the substitution of corresponding values into [Equation 1](#). However, according to Berenbak, the chance of exceeding this value is 100% which overestimates the friction coefficient for such a connection [\[6\]](#). Therefore the actual preload force is most likely to be higher than this nominal value which reduces the calculated COF according to [Equation 12](#). In this current research, three different values of  $F_{p,C}$  can be implemented, since the initial applied preload force is not equal to the nominal preload force. In addition, the third different preload force is the measured preload force at that time where the maximum force is subjected to connection. These criteria are also investigated by De Vries and Berger [\[69\]](#):

1. Slip factor based on the initial preload force ( $F_{p,C,initial}$ );
2. Slip factor based on the actual preload force at slip ( $F_{p,C,slip}$ ).

In the research of De Vries and Berger, the applied and nominal preload forces are similar and therefore no significant differences are obtained [\[69\]](#). Nevertheless, for this current research, the two scenarios will be taken into consideration to investigate effects and behaviour.

#### 2.5.4.2 Experimental procedure for determination of the resin's bearing resistance

From the described situation, bearing of the bolt against the steel plate is not expected. However, in the situation where a two-component resin is injected, the bearing of the bolt occurs at the interface to the resin instead of the steel plate. One can question the degree of the non-uniform distribution of the stresses along the perimeter of the bolt since plastification of the resin may occur. This affects the (non-)linearity of the stress distribution. If there is a neat interface between the bolt and an infinite stiff plate, stresses are distributed equally. This implies that the value of stiffness (Young's Modulus) affects the bearing at the contact area of a cylinder (bolt) and cylindrical groove (bolt hole) [5].

In the Dutch National Annex of the NEN-EN 1993-1-8:2011/NB a standard procedure is given on how to determine the bearing resistance of a resin [18]. The assumed layout is similar to the setup shown in Figure 28 given in Annex G of the NEN-EN1090-2[15]. Within the procedure for the bearing resistance, long-term tests are part of the operational method. Three specimens (six connections) are subjected to creep which determines the resistance. During the assembly of the specimens, all bolts are installed first. When tightening the bolts, the applied torque may not exceed 30Nm. Such a limit on the applied torque is introduced to prevent impact on the resistance created by an increased stiffness from preloading. The implemented bearing resistance of the resin is determined by applying a constant force over time, equal to or larger than the value of the expected force that will be exerted on the connection. The resistance is approved if all specimens have a CBG displacement of less than 0.3mm within the reference period. The displacements of the specimens are measured at both ends of the plates. This is not the same location as prescribed in NEN-EN1090-2, where the displacement of CBG is measured at the edges of the plates. From this procedure, it is however still unknown how the bearing resistance of the resin is determined. If the displacement of 0.3mm is not exceeded, it implies that the connection is accepted. However, the only way the bearing resistance of the resin is determined is by decomposing the equation of the NEN-EN1993-1-8, where this strength is one of the input parameters.

# 3

## Experimental research

### 3.1 Experimental method

From the state of the art including the literature review, doubts arise about the actual resistance of a preloaded and injected bolted connection (see [Subsection 2.5.3](#)). To investigate and bridge this gap, an experimental research is designed. The goal of this research is to investigate the potential allowable summation of individual resistances. Such that this summed resistance represents the resistance of a preloaded and injected bolted connection. Performing such analyses requires determining the resistance of connections with preloading or injection only. This results in a total of three different setups, namely preloading only, injection only and combining preloading and injection. [Table 4](#) shows the different procedures with their specifications of what type of reinforcing method is implemented.

**Table 4:** Methodology of test series

| Test | Preloading | Injection | Nr. of connections |
|------|------------|-----------|--------------------|
| 1    | Yes ✓      | No ✗      | 10                 |
| 2    | No ✗       | Yes ✓     | 10                 |
| 3    | Yes ✓      | Yes ✓     | 10                 |

### 3.2 Experimental setup

[Paragraph 2.5.4.1](#) explained the prescribed procedure for obtaining friction coefficients in bolted connections. In many cases of experimental research available in the literature, the M20 setup is applied. Nevertheless, due to the limitations of available testing rigs, it was not possible to assume this geometry. Test series 1 and 2 (preloading (PBC) and injection (IBC) solely, see [Table 4](#)) are expected to obtain a resistance less than the capacity of the testing rig. However, when combining resistance, the expectation is that the total resistance of the standard layout of the NEN-EN1090-2, as indicated in [Figure 30a](#), exceeds the capacity of the testing rig [[15](#)]. Therefore a different design is assumed, see [Figure 29](#).

In this research, the preferred proportion of individual resistance to the combined resistance is that a relatively large percentage of this combined resistance consists of bearing resistance of the resin. According to the formulation from the NEN-EN1993-1-8, the full capacity of an injected connection is utilised when the middle plate has an equal thickness to one individual side plate, see also [Figure 19](#). On top of that, the zone that contributes to this resistance is limited by 1.5 times the diameter of the bolt. In addition, other failure mechanisms have been determined. Where the geometry is chosen such that the interaction of failure mechanisms to influence measured displacements is minimised. Therefore, the absolute thickness is based on intermediate checks such that no other failure mechanisms are governing. The ratio as mentioned above is implemented as follow-up. In the case of the standard layout, both requirements are not satisfied. Therefore one bolt M16 is applied in combination with a thickness larger than 24mm. This 24mm is the minimum thickness required to satisfy the second statement.

Since standardised thicknesses are implemented in daily projects and are more available, 25mm is the applied thickness for all plates. Therefore, the stresses in the cover plates are 50% lower compared to the stresses in the main plates.

However, applying the geometry described above to the analogy of Annex G to use two bolts, exceeds the capacity of this testing rig. Therefore, only one bolt is implemented into the design, see [Figure 29](#).

Since only one bolt is implemented, an additional degree of freedom became unrestrained within the connection, namely a rotation around the longitudinal axis of the bolt. Comparing this to the standardised design, one can see that each side consists of two bolts. As a result, rotations are more “restrained” since the capacity and thus resistance is twice as large. However, when preloaded, this degree of freedom (DOF) will be affected by a resistance created by a rotational friction force at the shear planes. In a perfect straight specimen, the applied force is assumed to be in line with the frictional force. Despite this, if the specimen is not perfectly straight, under an angle, the applied force initially straightens the specimen which damages the coating and may affect the obtained experimental results. Therefore, for practical applications such misalignments are limited by the NEN-EN1090-2 [15].

Besides the number of bolts, the assembly differs from the standard layout. Within this research, one assembly consists of a bolt, two washers, including a chamber, a spacer, a plain washer and a nut. An overview of this assembly is shown in [Figure 30](#), whereas [Table 5](#) gives the characteristics of these components. The two washers, including chambers, are required to satisfy the flow of resin through the clearance between the bolt and the bolt hole. After the outlet washer, a spacer is mounted. From the bottom of the bolt, a strain gauge is installed inside the shaft of the bolt. This strain gauge of type BTMC-3-D20-006LE, see [Section 3.5](#), monitors the axial force in the bolt throughout the entire experiment by measuring strains. These strains might be affected by the shearing behaviour of the bolt near the shear planes. After installation, the strain gauge is located at a depth of 50mm from the bottom of the bolt. If the clamping package consists of the two washers and the three plates only, then this strain gauge is located close to the shear plane which affects monitored results. Therefore, the clamping package is enlarged to secure a neutral zone at which the axial force in the bolt measures reliable forces. Normally, strain gauges are installed at the bolt head. The consequence is that this spacer should be mounted at this side of the connection if the strain gauge is installed at the head of the bolt. However, this is not an option. The main reason is that if the spacer is located near the bolt head, one of the shear planes is positioned at the cross-section of the threads. Therefore, the spacer is located at the bottom of the bolt after the outlet of the resin.

A plain washer is located after the spacer to prevent torsional behaviour in the spacer during preloading. As mentioned, the height of the spacer is significant and therefore won't behave as a rigid body when exerted by a normal and rotational force from preloading. The last component of the entire assembly is the nut, required for the application of the axial force. In the next section, [Section 3.4](#), the characteristic of an HV bolt assembly is elaborated by example of experimental results.

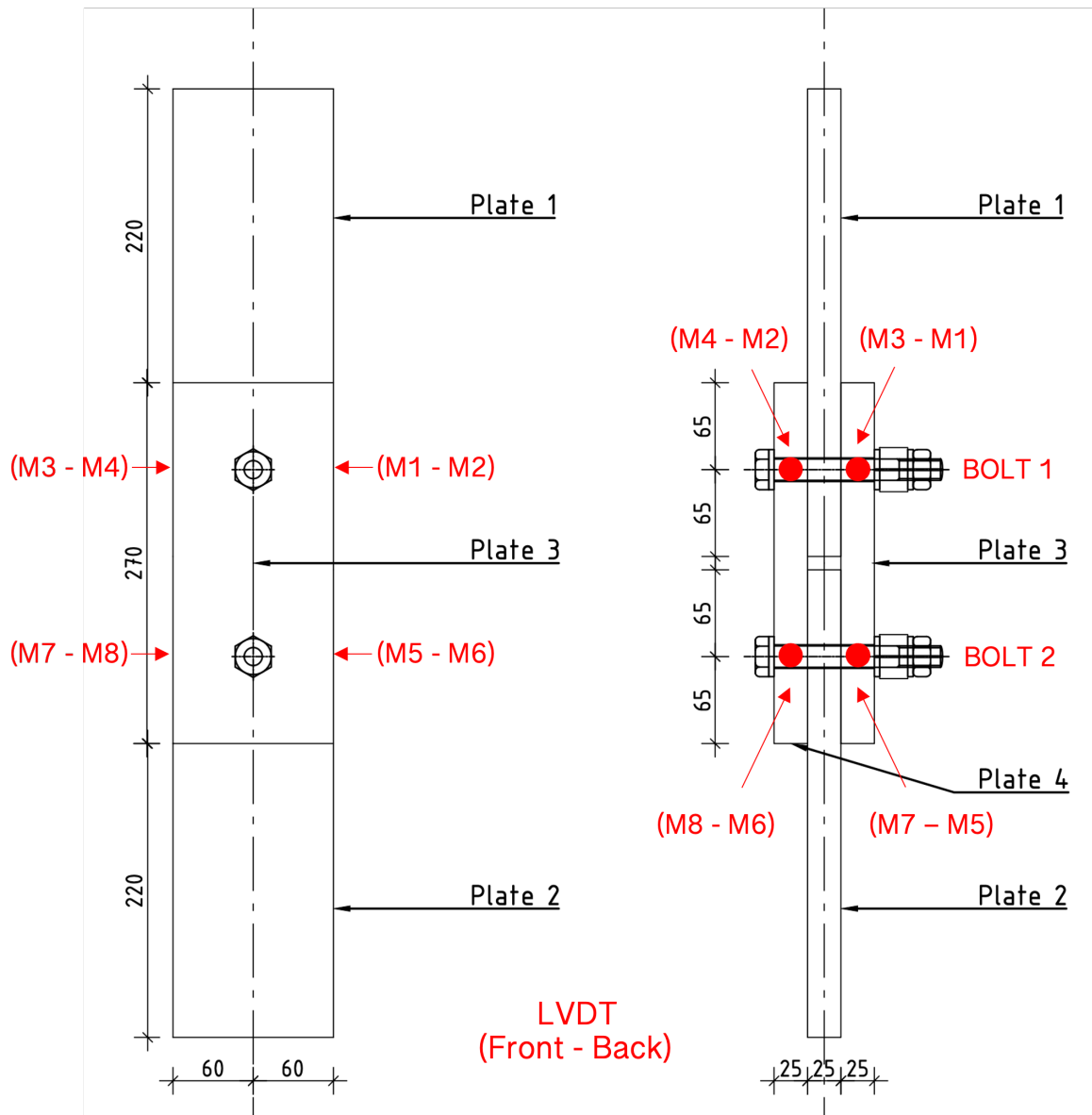


**Figure 29:** Applied layout for all specimens with two M16 bolts, including an overview of the locations for the LVDTs (M1-M8)

**Table 5:** Overview of material and geometric properties of the components within the bolt assembly

| Component                 | Class   | Height [mm] | Code          |
|---------------------------|---------|-------------|---------------|
| M16                       | HV 10.9 | 130         | NEN-EN14339-4 |
| M16 Nut                   | HV      | 13          | NEN-EN14339-4 |
| M16 Washer (with chamber) | 300HV   | 4           | NEN-EN14399-6 |
| M16 Washer (plain)        | 300HV   | 3           | ISO7089       |
| Spacer                    | S355    | 22          | -             |

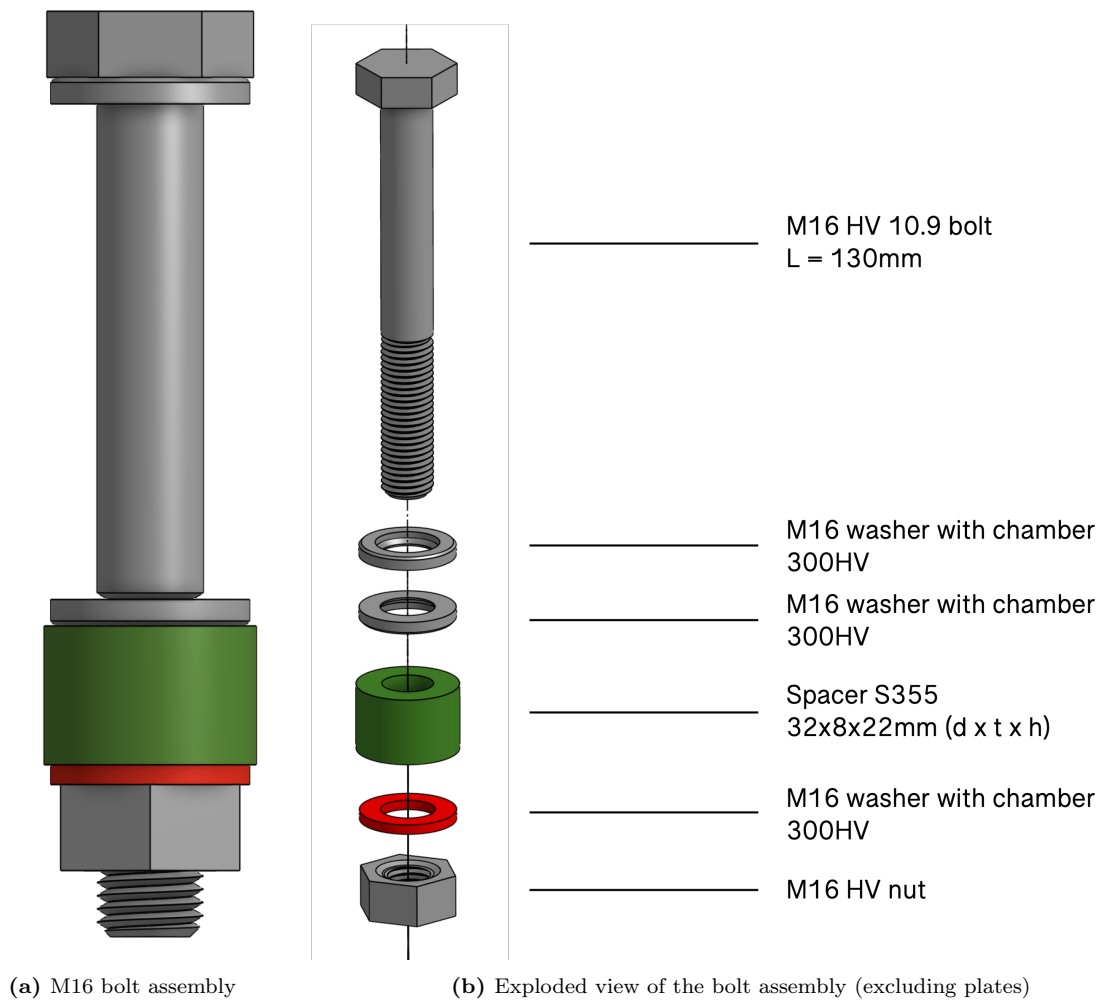


**Figure 30:** Different views of the used M16 bolt assembly of class 10.9

In addition to this assumed layout of the specimens, a framework is designed (see [Figure 31](#)). The width of the tested plates is 25mm. However, the maximum width allowed in the available clamping jaws is 20mm. To prevent excessive work to grind both ends of each single specimen to 20mm, the framework solves this problem. By the application of this frame, grinding of the plates has to take place only twice. Another advantage of the framework is that each experiment takes less time since the clamping jaws do not have to be opened after each experiment.

To install each individual specimen in the framework, two additional connections are designed on each side. The first connection consists of one M27 bolt, while the other connections contain two M20 bolts. All additional connections are installed by tightening the bolts hand-tight. During the analysis of the results, the effect of tightening these bolts by hand is elaborated in [Section 3.8](#) and [Subsection 5.4.1](#).

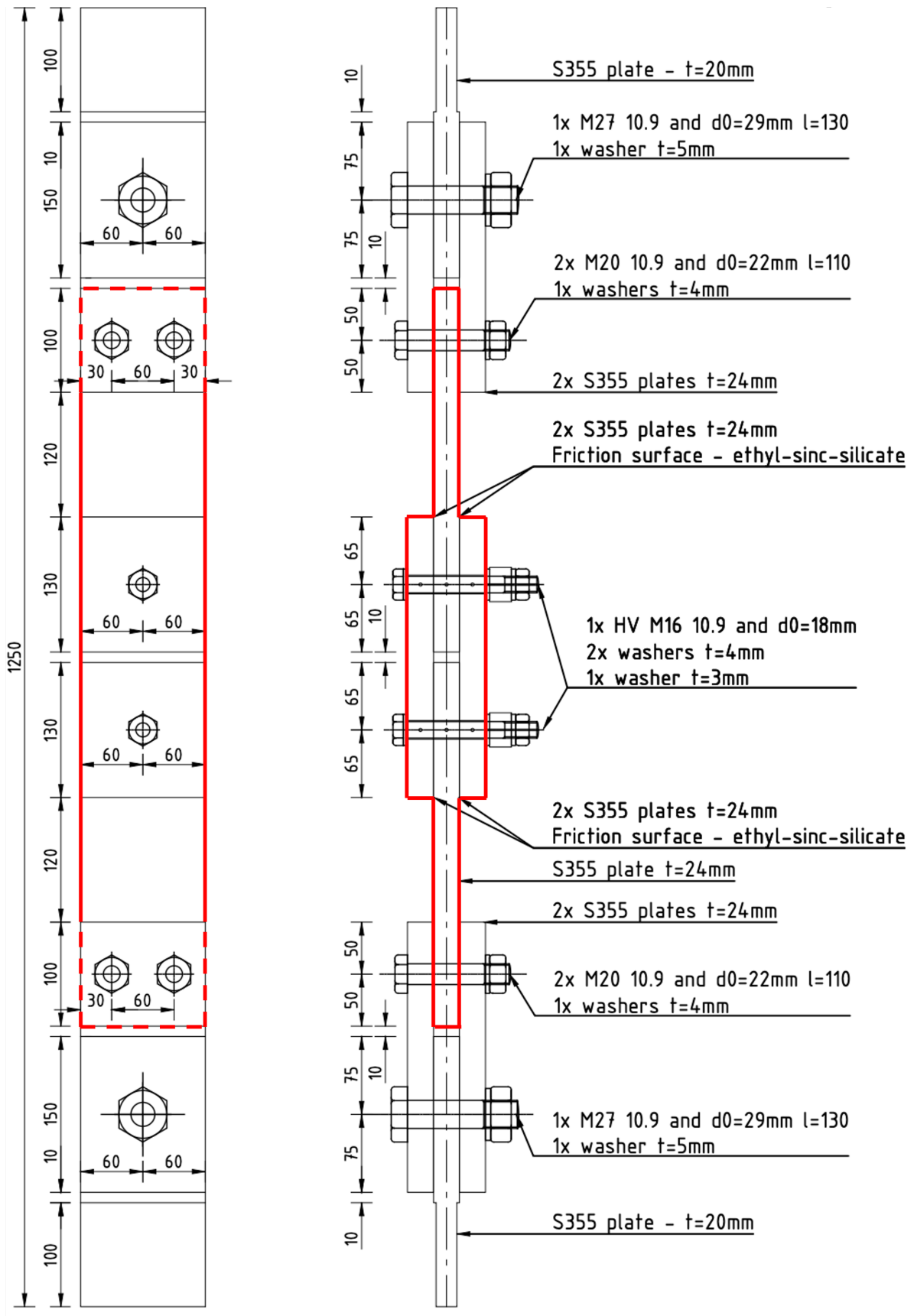


**Figure 31:** Entire framework designed for this current research. The red part is the specimen that is tested during each experiment (see Figure 29). Only the two bolts in the red specimen are preloaded. The other connections are bearing connections

### 3.3 Experimental parameters

Achieving the goal of the experimental research requires monitoring of several parameters necessary for the investigation of the resistance and behaviour of connections. The following list indicates the recorded variables during the experiments.

- **Force in testing rig:** this force is limited by the capacity of the testing rig of 500kN. Since the test is displacement-controlled, the force is able to decrease. This force is equal to the applied force transferred by the connection.;
- **Displacement of testing rig:** the displacement of the testing rig covers all displacements from expansion, slip and shearing. This parameter is monitored but not required for the displacement of the CBG.;
- **Normal force in bolts:** over all types of tests, the axial force in the bolt is monitored. Especially for the initial phase, measuring the axial force in the bolt is required since an equal initial axial force is preferred to be applied to all bolts. Investigating all experiments requires identical initial conditions such as this axial force. This can only be achieved when the axial force is measured. Injected bolted connections do not implement a preload force. Nevertheless, this axial force is still measured to investigate the possible occurrence due to bending. During the experiment, the bending of the bolt is expected due to the transfer of shear force. This bending involves an elongation of the bolt which subsequently results in an axial force of the bolt.;
- **Displacement of individual LVDTs:** in total 8 individual LVDTs (Linear Variable Differential Transformer) are used to measure the displacement, see [Figure 29](#). An LVDT is used to monitor a displacement between two components. The capacity of the used LVDT is 2mm. Since a double-lapped connection is implemented ([Figure 29](#)) combinations will be made to investigate the displacement of the CBG. Each side of the connections contains four LVDTs which will be averaged to find the displacement of the centre bolt group.;
- **Temperature:** the environmental temperature affects the resistance of the electrical circuits. A change in temperature results in a change of resistance of an electrical wire. Since the forces measured by the LVDTs are determined by a differential in voltage, unreliable forces can be measured since the temperature affects the resistance, thus the amount of voltage. Therefore, the temperature is measured in case significant changes in temperature occur over all tests.;
- **Humidity:** besides the surrounding temperature, humidity plays a role in the behaviour of these circuits. Therefore, the humidity is also monitored.

Averaging the displacement of all LVDTs related to a certain bolt group is required for the determination of the resistance. This methodology is in accordance with EN1090-2, Annex G [15]. Within this procedure of Annex G, it is stated that for short-term experiments, the limitation of allowed displacement is 0.15mm for preloaded bolted connections [15]. In the case of investigating the long-term behaviour, such as creep, a displacement of 0.30mm is used. For experimenting with injected bolted connections, no displacement criterion is specified. Nevertheless, the NEN-EN1993-1-8/NB gives a prescribed layout required to determine the bearing strength of the resin [16]. In this experimental procedure, a creep displacement of 0.3mm is stated. This is in line with the long-term displacement of a preloaded bolted connection. However, a short-term resistance of the bearing strength is not prescribed by the Dutch Annex of the NEN-EN1993-1-8.

Besides the prescribed limitation of displacements until a resistance is determined also a maximum duration is mentioned. According to the NEN-EN1090-2, the prescribed duration of a short-term experiment is ten to fifteen minutes [15]. Since the range of resistances of all series is different, it is unfortunately not possible to fulfil the requirements of the NEN-EN1090-2. It is in this research preferred that the velocity of the loading is equal rather than the time of the experiment. Therefore, only the actuator speed is equal for each type of connection. For this, a load increase of 0.001 mm/s is programmed.

### 3.4 Material properties

When verifying and comparing the results of both experiments and numerical analyses, material properties must be obtained. This chapter gives an overview, including elaboration, of the assumed or determined properties of the components. These properties are obtained by literature or by performing experiments.

Within the experiments, three main components are procured. Namely, the two-component resin, the bolt assembly and the steel plates including coating. Since the geometry of the plates is chosen such that failure of the steel plates is not expected, these material properties are not investigated. For further research, nominal values for the steel plates are assumed if required.

#### 3.4.1 Bolt

The bolt assembly consists of the following components: bolt, nut and two types of washers. Since the bolts are being preloaded, only classes 8.8 and 10.9 are qualified for usage according to EN14399-4 [21]. Within this research, bolts of class 10.9 HV are implemented. Where the HV type of bolts are mandatory to use in steel structures managed by Rijkswaterstaat since this type of bolt consists of a ductile failure mechanism [61]. Keeping the ability of identical initial situations, all tests are executed with the same products from the same batch. In this way, different failure modes or intrusion of phenomena by material properties can be excluded.

Tensile tests are executed on the bolt assembly to obtain associated material properties. These tests are performed five times on different bolts. The results obtained from these experiments are shown in Figure 32. From this figure, two different kinds of graphs are visualised. The first two bolts in green and red (Bolt 1 and Bolt 2) have failed at the interface of the threads between the bolt and nut. The other bolts show another behaviour since these bolts have failed at the net-section of the bolt. Where the failure is abrupt and does not increase after initial failure.

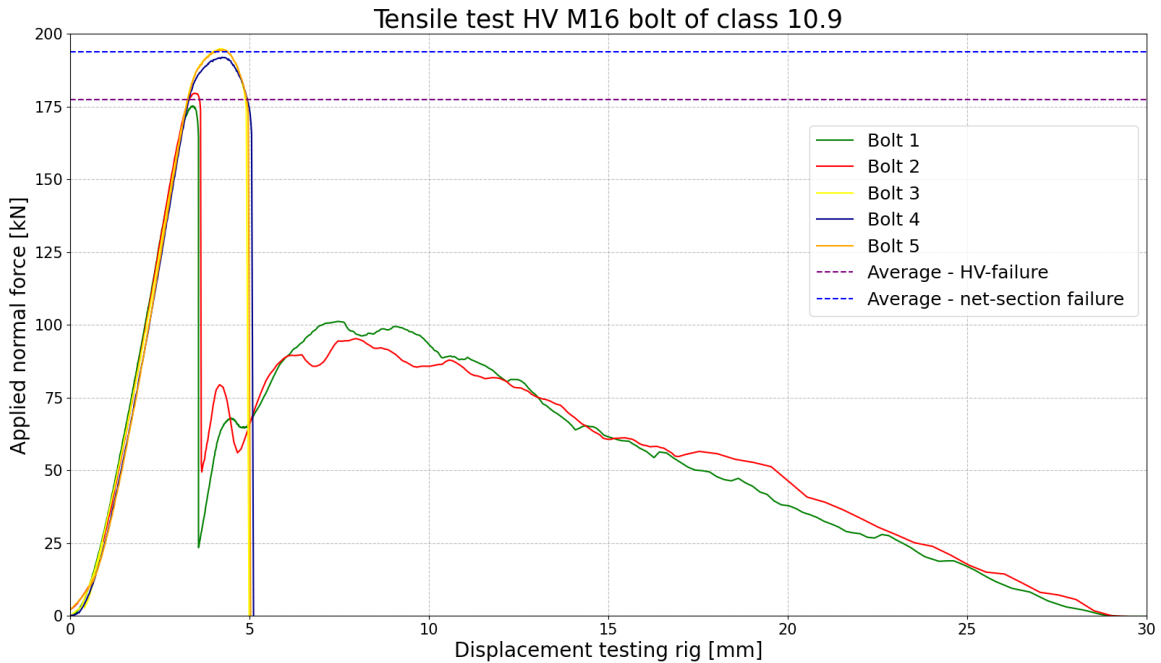


Figure 32: Two different tensile tests for a 10.9 M16 HV bolt

From the figure above, two resistances can be obtained, namely 177.43kN and 193.48kN for the purple and blue dotted lines respectively. The latter is used for obtaining the ultimate strength property of the bolts produced from the same batch. According to this tensile failure of approximately 194kN, the ultimate strength ( $f_{u,bolt}$ ) of the bolt appeared to be around 1232MPa.

$$\sigma_{bolt} = \frac{F_{normal}}{A_{bolt,net}}$$

$$\sigma_{bolt} = f_{u,bolt} = \frac{193.48 \cdot 1000}{157} = \mathbf{1232MPa}$$

In the equation above, the net area of failure ( $A_{bolt,net}$ ) is located just above the first thread. The area of this cross-section is 157 square millimetres. Within the bolts used for the tensile test, no strain gauges were installed and therefore the loss in area due to drilling does not have to be taken into consideration.

### 3.4.2 Resin

The other component required for numerical verification is the injected resin. For all injections, the same resin is used. This mixture consists of two components, namely the epoxy resin itself and a hardener. In this research, the resin RenGel SW404 and hardener RenHY2404 are used, see [Figure 10](#). According to the supplier Huntsman, the desired mixture properties can be achieved by the shown proportions in [Figure 33](#).

| Mix ratio                  | Parts by weight |     |
|----------------------------|-----------------|-----|
| RenGel <sup>®</sup> SW 404 | 100             | 100 |
| Ren <sup>®</sup> HY 2404   | 10              | -   |
| Ren <sup>®</sup> HY 5159   | -               | 8   |

**Figure 33:** Prescribed mixture properties of a resin made by RenGel SW404 and hardener Ren HY2404 [13]

The mechanical properties allocated to the modelled resin are in line with acquired literature elaborated in [Paragraph 2.5.2.1](#). From this available information, it is concluded that the unconfined condition in combination with associative flow properties is modelled. Since the Drucker-Prager modelling and Young's Modulus involve strength behaviour, no bearing strength of the resin was required. However, in the results of this report, the bearing strength is determined by dividing the applied force by the available area.

## 3.5 Data extraction

### 3.5.1 Mounting of strain gauges

To measure the axial force in the bolt, strain gauges have been installed. These gauges are required to obtain monitoring values of the axial force in the bolt. In this research, BTMC-3-D20-006LE gauges are implemented to determine the normal force within the bolt precisely. Table 6 presents characteristics of this type of strain gauge [12].

**Table 6:** Properties of the strain gauge BTMC-3-D20-006LE [12]

| Type                       | <i>BTMC-3-D20-006LE</i> |
|----------------------------|-------------------------|
| Length strain gauge (mm)   | 50                      |
| Gauge length (mm)          | 3                       |
| Gauge center position (mm) | 10                      |
| Backing diameter (mm)      | 1.9                     |
| Resistance ( $\Omega$ )    | 120                     |
| Hole diameter (mm)         | 2.0                     |

As indicated in the table, the required specifications for the drilled hole are a length of 50mm and a diameter of 2.0mm, as illustrated in Figure 34. The gauge, that measures the strains, is located 10mm from the tip of the instrument and is 3mm long. It is made up of electrical wires with one input and one output, forming a closed and serial circuit. To ensure accurate strain measurements, the gauge is attached to the bolt by a recommended and prescribed adhesive. The gauges are supplied with a general-purpose CN adhesive. This adhesive is a single-component cyanoacrylate (CN). Cyanoacrylates are known as strong and fast-acting adhesives which polymerize rapidly when exposed to moisture [51]. This is automatically the pitfall since bolt holes contain moisture due to rinsing. Rinsing of the holes is required to clean the grime of drilling of the holes. Figure 35 shows the bolts after cleaning of the bolt holes and installation of the strain gauges.

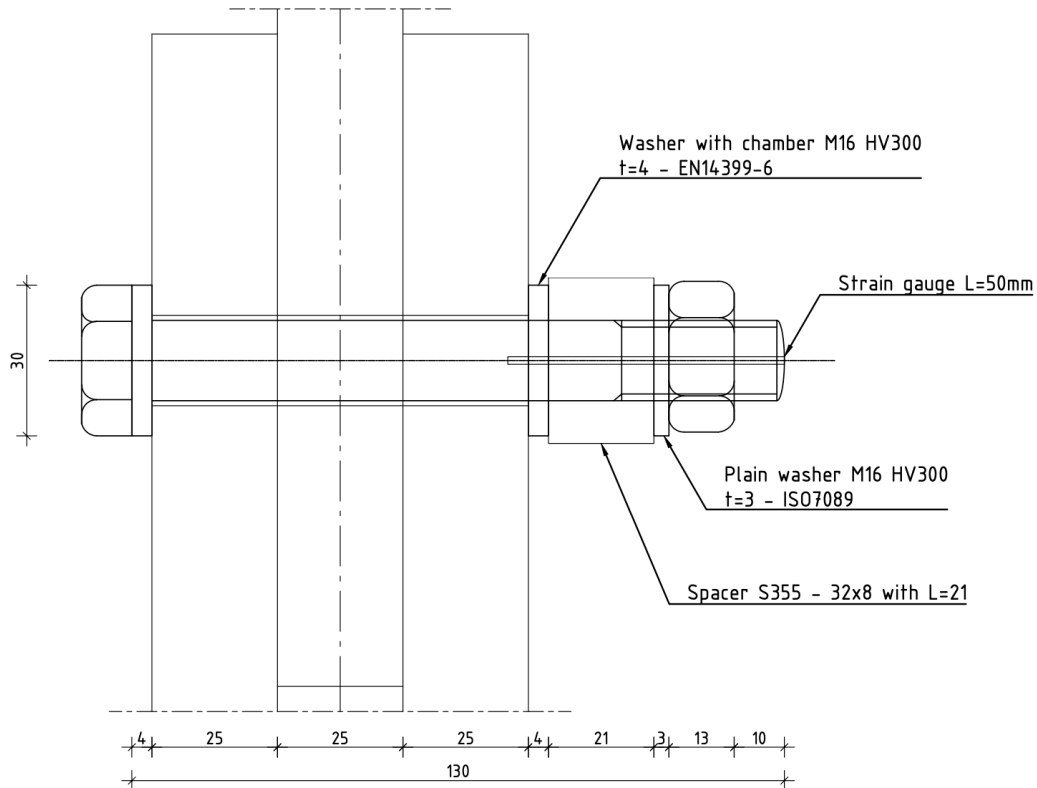


**Figure 34:** Cross-section of the connection including the location of the inserted strain gauge

Figure 35 shows that at the top of the bolts, two wires extend. These wire ends are soldered to cables, which in turn are connected to an amplifier. This amplifier records the voltage that surpasses the circuit. Measured voltages are required for determining the normal force. When a strain gauge is exerted to a force, the length of the gauge's patch either increases or decreases, depending on the direction of loading. This change in length leads to a change in resistance. Within a serial circuit, the amperage remains constant along its path, while the voltage is affected by this change. This phenomenon is consistent with the relation between amperage, voltage and resistance (ohm). Therefore, when a force is applied, a difference in voltage is measured. To convert the voltage difference into a force, all individual bolts are calibrated. This procedure is elaborated in [Subsection 3.5.2](#).



**Figure 35:** M16 bolts after installation of the strain gauges

### 3.5.2 Calibration of bolts

To derive the magnitude of axial force in the bolt, the relation between the difference in normal force and voltage must be determined. This relation is a conversion factor that is assumed to be a constant. To determine this factor, each bolt has been exerted by a normal force with a stepwise build-up. First, the bolt is installed in the testing rig whereafter a normal force of 110kN is applied and released gradually before calibration. This applied force is approximately 75% of the yielding limit at the net-section ( $157\text{mm}^2$ ). After this release, again, a normal force of 110kN is applied to start the calibration. However, after each 10kN both normal force and voltage are monitored. Completion of this prescribed sequence results in thirteen data points including the normal force and voltage. Since this ratio of voltage and normal force is affected by the location of the bolt with respect to the bolt hole, the sequence is executed twice. Since the obtained difference of the conversion factor between the two tests is neglectable, it is assumed that determining this factor based on two tests is sufficient.

Each strain gauge is inserted under different conditions, such as temperature, humidity, angle of gauge and amount of adhesive. In addition, each channel at the amplifier is connected and soldered differently. Due to these aspects, each individual bolt is calibrated according to the prescribed process in combination with an associated channel. Such a connection with the channel is visualised by [Figure 36](#). In the following enumeration, this procedure is mentioned briefly.

1. Install the entire bolt assembly in the instrument in the testing rig.;
2. First increase the tensile force to 110kN.;
3. Release axial force gradually (set to 0kN).;
4. Increase the load in steps of 10kN to 110kN. Whereafter each step, both voltage and axial force are noted (start and ending at 0kN). This results in 13 data points per calibration.;

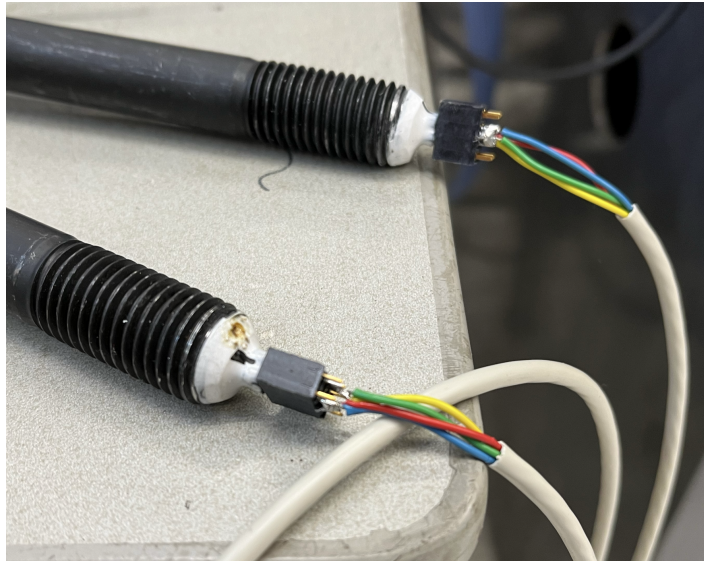


**Figure 36:** Connector at the end of the bolt. Where one end of the connector is soldered to the tips of the strain gauge

The first increment to 110kN without intermediate steps is performed such that all components have already been elongated once. This force of 110kN is carefully chosen since the calibration must remain within the elastic region due to both the conversion factor (linear) and unwanted plastification within the bolt. The calibration of the bolts is performed in the testing rig where the bolt is elongated. This elongation results in an axial force that is required at each intermediate step. Initially, a different calibration method is applied. However, this resulted in damage to the bolts. In [Section B.2](#), this calibration procedure is elaborated. In addition to this, an example of the calibration output is shown.

## 3.6 Installation procedure

### 3.6.1 Combined method for preloading

Subsection 2.1.1 discussed four allowed installation methods of preloading bolts according to the NEN-EN1993-1-8. In The Netherlands, the owner and responsible party of most of the steel bridges is Rijkswaterstaat. In extension to the regulations set by the Eurocodes, Rijkswaterstaat made adjustments to those regulations and combined them in the ROK (richtlijn ontwerp kunstwerken). Within this guideline, clause ROK-0198 states that of the four mentioned methods, only the combined method is allowed for tightening preloading bolts. One can say that this adjustment is due to the high reliability, which is also in line with the result of Berenbak [6], see Section 2.5. Since this specific preloading procedure is obliged to be used in structures owned by Rijkswaterstaat, this application is considered in this research.

In the first step of the combined method, a specific torque is applied to the assembly. The value of the torque is dependent on the friction activated during tightening, such as friction between the nut, bolt, washer and plate. The angle of rotation depends on the ratio of the clamping package and the bolt diameter. Since a specific rotation results in a pre-known elongation of the bolt, if the stiffness of the clamping package is infinitely high. According to the predefined angles, the applied angle increases by an increasing thickness of the package [15].

NEN-EN1090-2 Table 20 states that for an M16 bolt, the nominal required torque of step 1 is 165Nm. The angle for tightening is 120 degrees for the implemented clamping thickness. However, of these two steps, the torque can also be determined by experiments. As already described in Section 2.5, each bolt set has to be calibrated. This calibration determines the magnitude of torque required for a specific application, taking into consideration aspects such as friction between nut and bolt and thickness of the clamping package. Due to this obliged implementation, the same procedure has been followed as practice.

The **implemented** procedure for the determination of the required torque is as follows. First, five bolts were exerted to a tensile force of 82.5kN, which is 75% of the preload force ( $0.75F_{p,C} = 0.75 \cdot 0.7 \cdot f_{ub} \cdot A_s$ ). Achieving this preload force in the bolt requires a specific torque. For all tests, this necessary torque is registered. Table 7 gives an overview of the applied preload force and the mandatory torque per assembly.

**Table 7:** Result of the required torque for applying 75% of the preload force in the bolt ( $F_{pc} = 0.7 \cdot f_{ub} \cdot A_s$ )

| Test | Preload force 75% $F_{pc}$ [kN] | Required torque $M_{req}$ [Nm] |
|------|---------------------------------|--------------------------------|
| 1    | 82.5                            | 205                            |
| 2    | 82.5                            | 195                            |
| 3    | 82.5                            | 170                            |
| 4    | 82.5                            | 185                            |
| 5    | 82.5                            | 165                            |

From these values, the variation, which is the difference between the maximum and minimum value divided by the average, is lower than the limit of acceptance according to the NEN-EN1090-2 (known as  $e_m$ ). In this case, the variation is 0.217 whilst results are not reliable anymore from a variation of 0.350 onwards. This value is related to the amount of executed tests, namely five. A note to these torques is that all values are rounded to the nearest 5 Nm. According to the NEN-EN1090-2 the critical torque obtained from testing ( $M_{r,test}$  of method K2) is 185 Nm. This value is obtained by the average of the maximum (=205Nm) and minimum (=165Nm) values.

Within the **implemented** procedure of the combined method, the applied torque of the first step is 75 % of this  $M_{r,test}$  (=140Nm). However, this 75% must only be taken into consideration when using the formulas stated in the NEN-EN1090-2 for  $M_{r,1}$  and  $M_{r,2}$  and not for  $M_{r,test}$ . In Section 6.3, the consequence of this wrongly implemented procedure is discussed.

During preloading of the bolts by the combined method, the axial force within the bolt is monitored continuously. An overview of the preload force over time is shown in [Figure 37](#). A total of 8 bolts have been tested whereby one of them has failed (see bolt 4). After the first attempt of this bolt (bolt 4a), a failure within the strain gauge was expected. Repetition of the procedure resulted in another unexpected result (bolt 4b) which confirmed the presumed failure in the strain gauge. Therefore, the results of bolt 4 are not included in the further process.

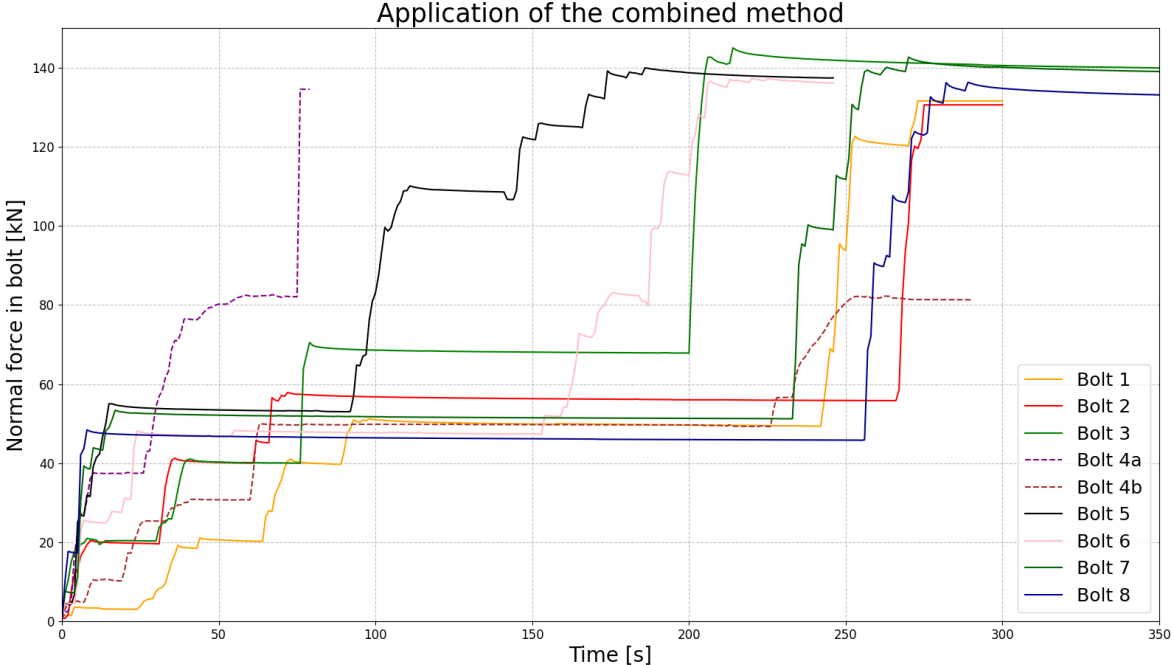


**Figure 37:** Overview of experimental results when preloading bolts according to the combined method with friction factor determined by individual tests according to NEN-EN1090-2

[Figure 37](#) describes the axial force in the bolt monitored by the strain gauge during the entire preloading procedure. To distinguish the axial force after each step of the combined method, a table is constructed where these values are given, see [Table 8](#). From these results, it can be concluded that after the application of the combined method, all bolts contain a preload force significantly larger than nominally assumed. Of these outcomes, the average preload force after completion of the entire procedure is 133.8kN. This value has a variation of less than 3% (see [Table 8](#)). While after step 1, this variation of results is even larger than 10%. Since the average value and standard deviation are known for each step, the statistical results can be derived.

**Table 8:** Results of the combined method where the preload force ( $F_{pc}$ ) is given after each step

|                          | <b>Step 1: Torque [kN]</b> | <b>Step 2: Turn the nut [kN]</b> |
|--------------------------|----------------------------|----------------------------------|
| Bolt 1                   | 50.4                       | 131.6                            |
| Bolt 2                   | 56.4                       | 130.6                            |
| Bolt 3                   | 40.2                       | 138.9                            |
| Bolt 4a                  | 37.5*                      | 134.5*                           |
| Bolt 4b                  | 30.7*                      | 82.4*                            |
| Bolt 5                   | 53.3                       | 137.4                            |
| Bolt 6                   | 47.1                       | 136.1                            |
| Bolt 7                   | 52.3                       | 133.9                            |
| Bolt 8                   | 46.8                       | 128.0                            |
| Average                  | 49.5                       | 133.8                            |
| Standard deviation       | 5.322                      | 3.628                            |
| Coefficient of variation | 10.7 %                     | 2.7 %                            |

\* = not considered due to failure of strain gauge

### 3.6.2 Specimen configuration

One individual specimen consists of four shear planes. Each bolt within this specimen contains two of these shear planes. In [Figure 38](#) a cross-sectional view is shown with the four different shear planes. These can be identified by four different colours, orange, purple, green and blue. The frictional characteristics of these shear planes are expected to be one of the decisive parameters of the slip resistance. In [Subsection 2.5.4](#) it is mentioned that the slip resistance of a connection depends on the friction of that surface and its applied normal force. With the result that a plane with more friction contains a higher resistance. In practice, a coating is often applied on surfaces to increase durability and sustainability [\[54\]](#). However, such coatings decrease the friction between materials. This is also in line with the NEN-EN1993-1-8 since uncoated planes contain the highest coefficients of 0.5. In practice, coatings are therefore implemented to increase their durability to prevent internal corrosion. According to the ROK, one and only one specific type of coating is prescribed and allowed for usage, namely, Ethyl-Zinc-Silicate [\[61\]](#).

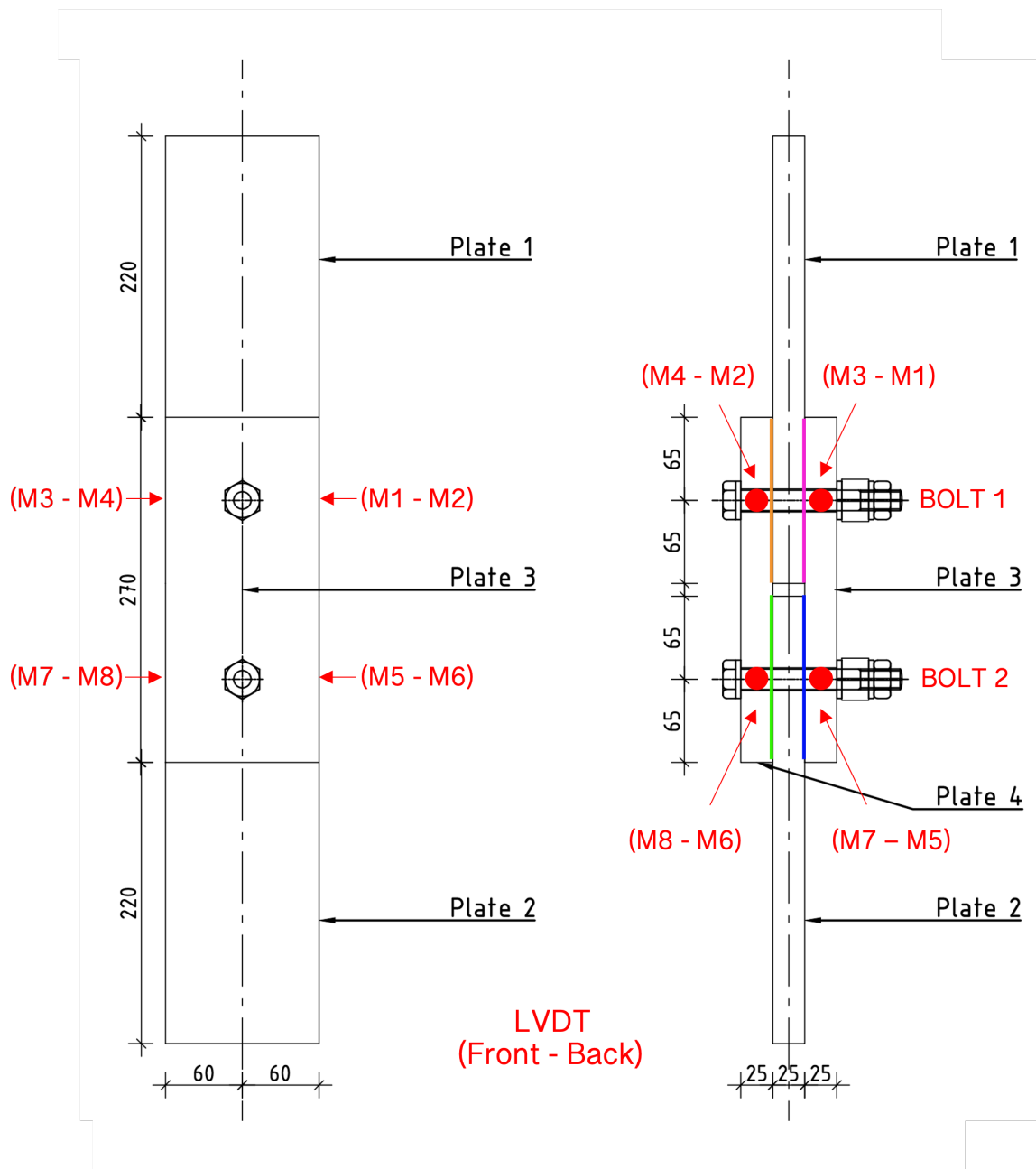
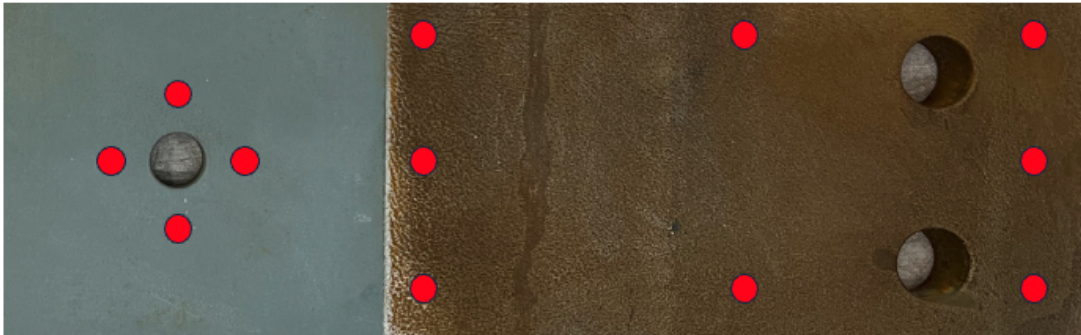


**Figure 38:** Four different shear planes are characterized by the colour orange, purple, green and blue

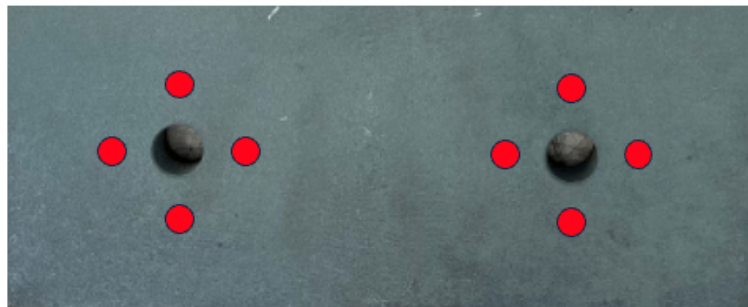
### Coating - Ethyl-Zinc-Silicate

Ethyl-Zinc-Silicate (EZS) is a coating that at first is applied to protect the steel member in aggressive corrosive environments. In general, a total of up to 4 different layers are applied on top of each other to secure the sustainability of the steel member and connection over its lifetime. However, Rijkswaterstaat prescribes that at the shear planes, only the primer made of EZS can be applied. All other layers will namely decrease the frictional resistance of the shear planes significantly. In addition to the limited number of coatings, there is also a prescribed thickness of the applied coating. The ROK states that the thickness of such layers in slip-resistant connection may not exceed the prescribed layer thickness. In this case, the Ethyl-Zinc-Silicate of Zandleven coatings is implemented [54]. According to their datasheet, the recommended thickness is 50-75  $\mu\text{m}$ . Therefore, the aimed applied coating thickness is 60  $\mu\text{m}$ .

The application of coatings by contractors remains a non-automated process. Within this process, curing of the coating is important for the quality of the layer. Since the thickness and roughness of the coating play an important role in the frictional behaviour, the thickness of the coating is measured. These measurements are executed over all plates at specific and fixed locations. To measure the coating, the Elcometer 456C is utilised [24]. This instrument is calibrated according to the prescription. This defined calibration relates to the expected coating thickness. Identifying the coating thickness is performed according to the following procedure. First, the coated locations are measured. Next are the locations which are positioned at the uncoated parts, see Figure 39a. Since the uncoated parts are also blasted by sand, the shown value of thickness will not be equal to zero. Therefore the measured thicknesses at the locations of the coating have to be subtracted from these values to determine the genuine coating thickness. For the cover plates, the uncoated locations are on the other side of the plate since only one side is covered by the EZS, see Figure 39b.



(a) Overview of predefined locations to determine the coating thickness of the middle plates (4 at coated and 8 at uncoated)



(b) Overview of predefined locations to determine the coating thickness of the cover plates (4 at coated area per bolt)

**Figure 39:** Different overviews for the predefined locations when determining the applied coating thickness

After procurement of the conserved plates, all measurements were executed immediately to investigate the quality of the EZS application. First, this measured thickness is evaluated to see if the preferred thickness of 60 microns is achieved. After investigating the quality of and experimenting with the first two connections, it turned out that this initial coating was not applied and cured correctly. Both the applied thickness and curing method were not adopted correctly. Therefore, the plates were recoated. In [Appendix A](#) of the appendix, the results and procedure are elaborated.

To qualify a coating for acceptability, a standardised MEK-test is implemented and investigated [68, 4]. A MEK-test consists of a two-step procedure where the coating is investigated by the use of Methyl Ethyl Ketone (MEK), also known as butanone. Butanone is a ketone, just like acetone. This chemical is acknowledged to be dangerous. MEK is in the chemistry written as  $C_4H_8O$ . The American Society for Testing Materials (ASTM) adopted this procedure into their national code when investigating inorganic Ethyl zinc-rich primers [4]. This procedure of testing consists of seven subjacent procedures to diagnose the quality of the primer. At first, a specific area of 150 by 25 mm must be designated. Whereafter a cloth, or in this case a cotton bud, is dripped into the MEK. This bud must be wiped back and forth at an angle of 45 degrees with 50 repetitions. During this step, degradation of the primer can be observed gradually. The amount of degradation depends on the level of curing. After rubbing the primer with a moist cotton bud, the same step must be followed but with a dry cotton bud instead. According to this procedure described by Valinsab, all resistances can be rated from 0 to 5. [Figure 40](#) shows each rating including their descriptions. The pitfall of such quantification is that it might be too subjective.

| Resistance Rating | Description  |
|-------------------|--|
| 5                 | No effect on surface; no zinc on cloth after 50 double rubs                                  |
| 4                 | Burnished appearance in rubbed area; slight amount of zinc on cloth after 50 double rubs     |
| 3                 | Some marring and apparent depression of the film after 50 double rubs                        |
| 2                 | Heavy marring; obvious depression in the film after 50 double rubs                           |
| 1                 | Heavy depression in the film but no actual penetration to the substrate after 50 double rubs |
| 0                 | Penetration to the substrate in 50 double rubs or less                                       |

**Figure 40:** Possible outcomes according to the ASTM after investigation of the cured primer by the MEK-test [4]

Nevertheless, this prescribed procedure by the ASTM [68, 4] is still adopted into this research. This application is executed to gain perception about the quality of the coating. After completion of this procedure by rubbing the different surfaces, the outcome of the coating is shown in [Figure 41](#).

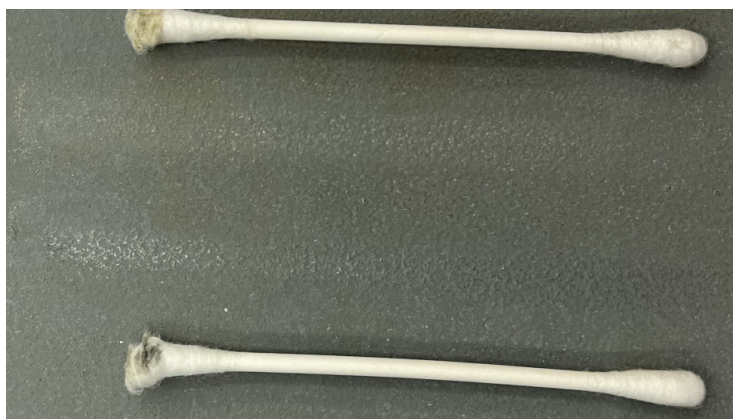


**Figure 41:** Two types of degradation of the final applied primer after 50 rubs. Bottom and top path relates to the dry and moist cotton buds respectively

From Figure 41 two paths can be identified. The bottom path is the results of the MEK-test after being scrapped 50 times by a dry cotton bud. The top path is the damaged path after rubbing with a moist bud. From these two paths, it is assumed that the resistance rating of the coating is two or three (Figure 40). As mentioned before, rating the coating is subjective.

Besides the quality of the coating, the thickness is accepted since there is no more clear division visible between the middle and cover plates anymore, see Figure 42. From this figure, the difference can be observed between the thickness before and after coating for both the initial primer (blue and green) and the final primer (red and yellow). In addition, the average thickness has an improved correspondence with the ordered 60 microns.

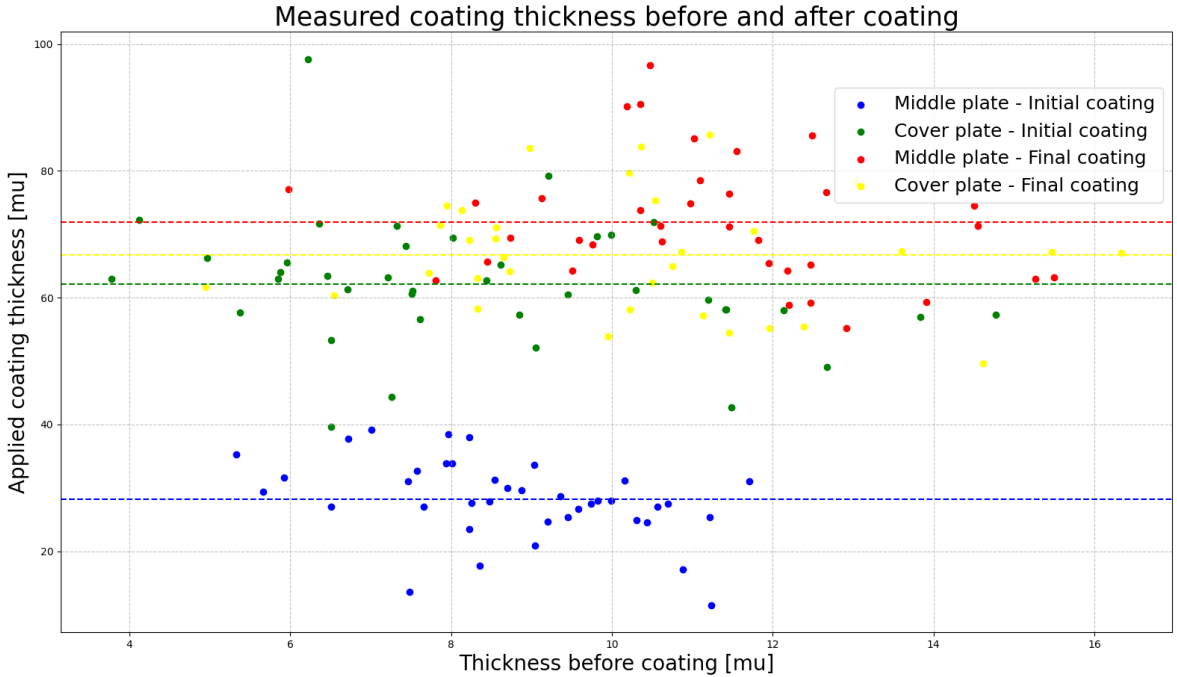


**Figure 42:** Difference in measured thickness between coated and uncoated surface areas per plates after recoating

When applying a division of all measurements per shear plane by individual locations, the results from Figure 43 are secured. Within this data, all single thicknesses are rounded to the nearest  $0.5\mu\text{m}$  and summed for each possible outcome of thickness. Comparing this outcome with the initially applied coating thickness as visualised in Figure 114, there has been a significant improvement. However, for the final plates, the uncoated surfaces do have a higher deviation than the initial. It is expected that this deviation is the result of the corrosion that arose during the storage of the plates at the paint shop.

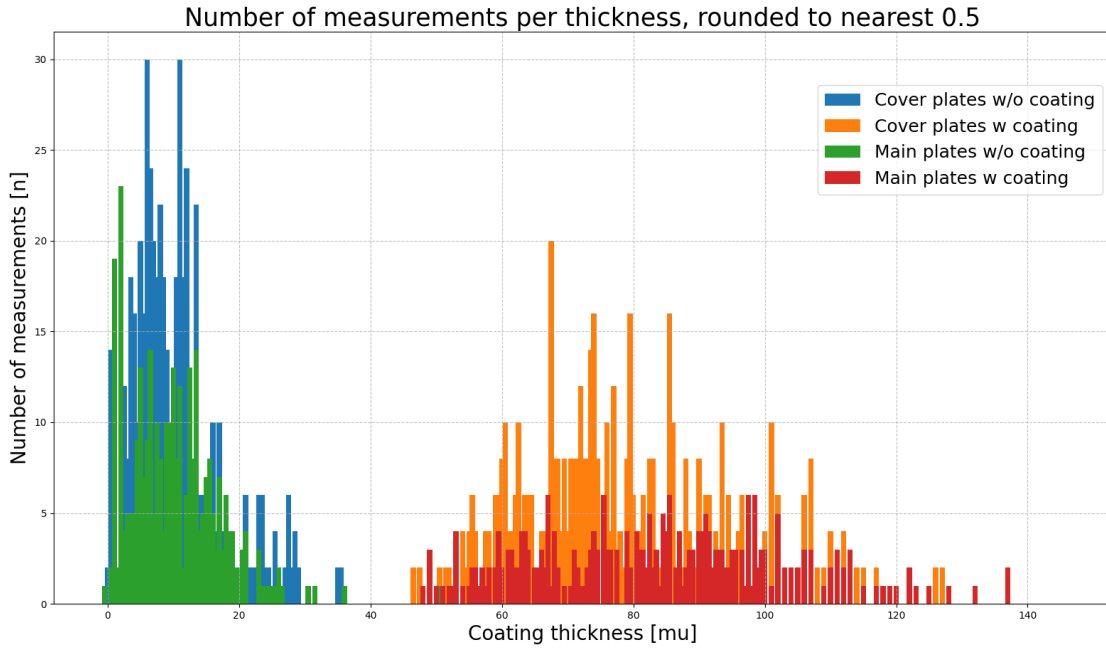


**Figure 43:** Distribution of different measured coating thicknesses for the recoated surfaces

Figure 43 concludes that the applied coating thickness is expected to be similar between the cover and main plates. When assembling the specimens, both the cover and main plates contribute to the combined coating thickness at the shear plane. Since the thickness of the coating may affect the frictional behaviour at these planes, specific combinations are made such that outliers in thickness are prevented. Figure 44 shows the average coating thickness of a single plate at each shear plane. If the coating thickness of the cover and main plate is 120 and 40 μm, then after assembly, the average coating thickness of each plate is accounted as 80 μm. The values are shown in this figure. In total 72 occurrences are registered. Since each specimen consists of 4 shear planes, a total of 18 specimens are taken into consideration. Two specimens are missing since these are used with the initial applied coating.

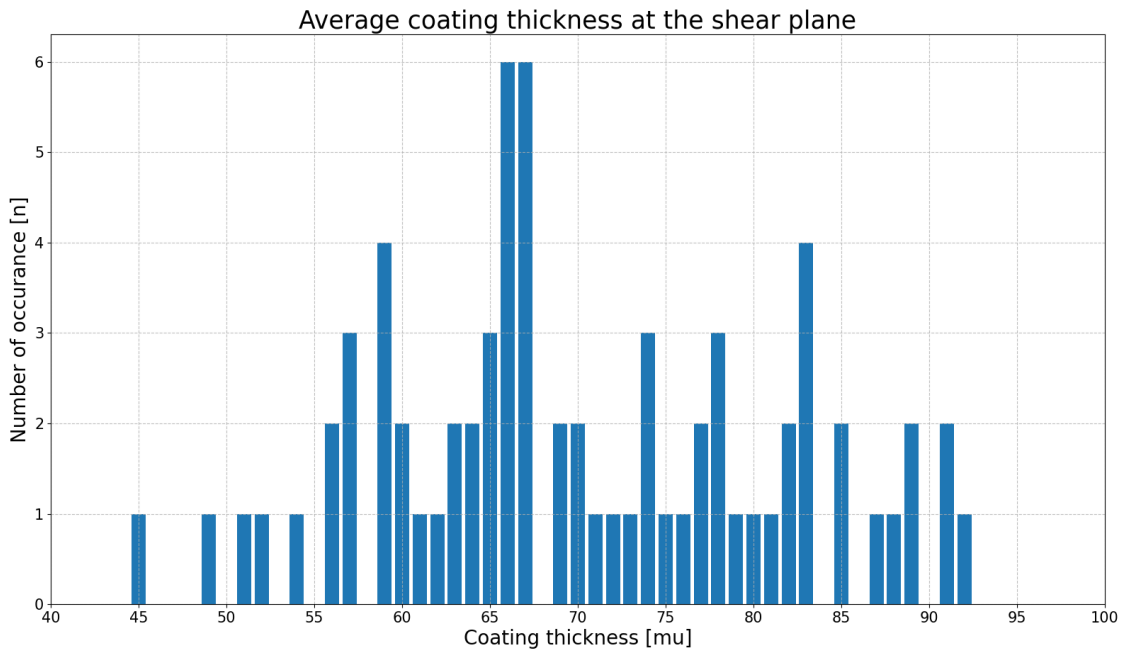


**Figure 44:** Distribution of average coating thickness per plate at a single shear plane

### 3.7 Results - Experimental resistance of each connection

Within this section of the report, the experimental results are elaborated on. In total, three different series are dealt with: preloading only, injection only and connections consisting of both preloading and injection. These are in line with the stated methodology in Table 4. Each series contains five specimens with two separate connections (ten connections in total). Within this connection, only one single bolt is located. Therefore the legend will refer to the characterisation of specimen (A, B, C etc.) including the number of the bolt (1 or 2). Where “Bolt 1” and “Bolt 2” refer to the upper and lower connection respectively.

This section consists of a total of three subsections. These sections are related to each type of connection (preloading only, injection only and both preloading and injection). In the subsection of preloading only, the friction coefficient is calculated. For the part regarding injection only, the bearing strength of the resin is determined. For all types of connections, the stiffness in two different regions is elaborated. This stiffness is determined with the goal of comparing the stiffness of each connection in the specific regions.

#### 3.7.1 Serie 1: Preloaded bolted connections (PBC)

Within the first performed series, only a preload force is applied. The preloading procedure is performed such that the most significant relaxation losses occur before the experiment starts. This is done by preloading at least 3 hours upfront. In this way, the decay after the start is expected to be minimized. This axial force in the bolt is preferred to be 140kN for all bolts, as this was the outcome of the combined method (see Table 8). However, a small but neglectable deviation arose over the initial preload forces with respect to this 140kN. This variation arose since a manual preloading application was performed. Table 9 shows the arising values of available preload force.

**Table 9:** Overview of nominal and actual initial preload force in all bolts for Serie 1 (preloading only) including the difference in percentage concerning the nominal preload force

|         | $F_{p,C,nom}$ [kN] | $F_{p,C,init}$ [kN] |
|---------|--------------------|---------------------|
| P1      | 110                | 140.49 (+28%)       |
| P2      | 110                | 137.83 (+25%)       |
| Q1      | 110                | 140.24 (+27%)       |
| Q2      | 110                | 138.39 (+26%)       |
| R1      | 110                | 138.74 (+26%)       |
| R2      | 110                | 138.97 (+26%)       |
| S1      | 110                | 139.61 (+27%)       |
| S2      | 110                | 139.61 (+27%)       |
| T1      | 110                | 138.38 (+26%)       |
| T1      | 110                | 138.75 (+26%)       |
| Average |                    | 139.20 (+26%)       |

The overview of results from all tests is shown in Figure 45. This overview shows the relation between the CBG displacement and the applied force of each bolt during the experiment. The vertical dotted line represents the limit of displacement at CBG of 0.15mm, which is stated by the NEN-EN1090-2 [15]. In addition to this line, four graphs are shown more transparently. These first two specimens were tested with the initial coating consisting of bad quality. Since this coating has changed, due to a different curing procedure, these results are **left out of scope**. However, within graphs, these outcomes are still visualised with a more transparent colour. This automatically implies that the clear graphs indicate the results after recoating.

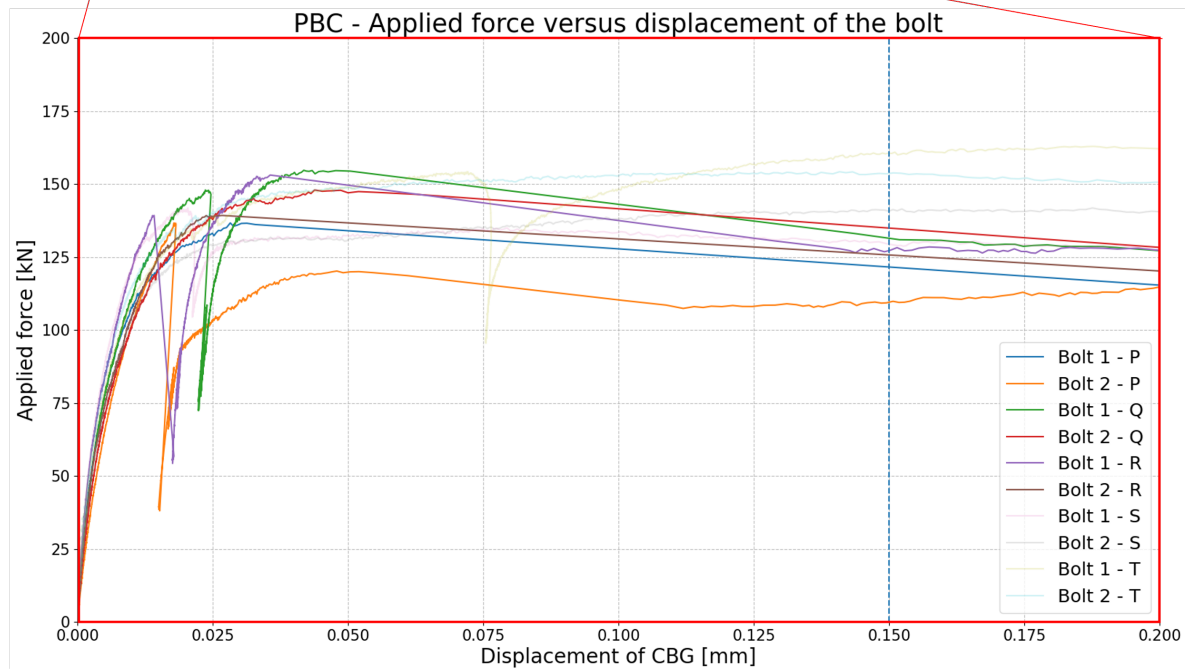
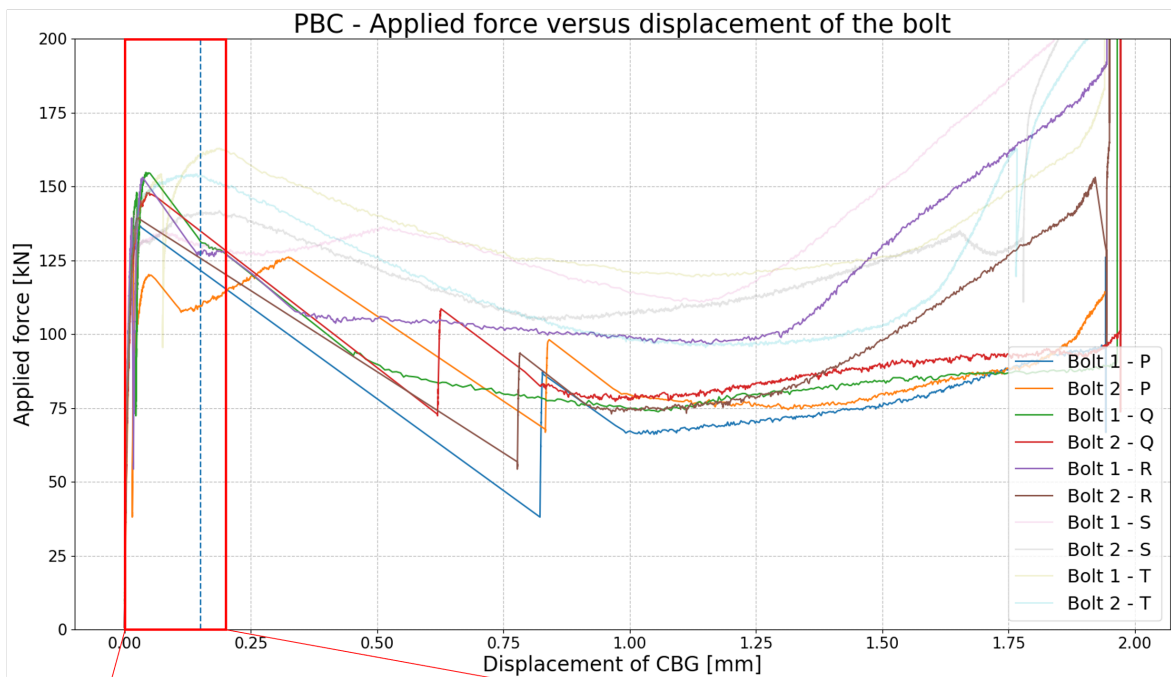


**Figure 45:** Results of all specimens when preloaded. This graph gives the relation between the displacement at CBG and the applied force in the connection. The faded graphs represent the results obtained from the initial coating, whereas the others are related to the final applied coating

When zooming in, into the region until nominal failure, the result is obtained as also shown in [Figure 45](#). According to the NEN-EN1090-2, the resistance of such connection is the largest applied force until a displacement of 0.15mm at the CBG ([blue dotted line](#)). In [Table 10](#), an overview is shown with the maximum applied force for each connection. From this table, it is concluded that the average resistance of a preloaded connection as designed in this research is 144.7 kN.

**Table 10:** Obtained resistances from experiments when applying preloading including comparison with average obtained resistance

|         | Resistance ( $F_{\max}$ ) [kN] | Diff. to average [kN] |
|---------|--------------------------------|-----------------------|
| P1      | 136.7                          | -8 (-6%)              |
| P2      | 136.7*                         | -8 (-6%)              |
| Q1      | 154.7                          | +10 (+7%)             |
| Q2      | 148.0                          | +3.2 (+2%)            |
| R1      | 153.1                          | +8.4 (+6%)            |
| R2      | 139.3                          | -5.5 (-4%)            |
| Average | 144.7                          | N/A                   |

\* = could not obtain initial resistance anymore after slip of the other connection

After disassembly of the specimens, the damage that occurred at the shear plane is clearly visible. This damage of the shear plane is shown in [Figure 46](#). On top of the shear planes, general damage over the entire surface is visible. This is initially not as expected. Since a preload force is implemented in this current research, the damage of the coating is more expected where the clamping stresses are acting. From this figure, one can say that the relatively large thickness of the plates creates a more uniform distribution of stresses and displacement.



**Figure 46:** Damage on the shear planes of the preloaded bolted connection after the experiment (Specimen R)

Besides the resistance of the connection during the experiment, the available preload force is monitored. This course over time is visualised in Figure 47. From this figure, it can be seen that there is a gradual decrease in available preload force in the bolt. After some displacement, approximately 0.030mm, a horizontal plateau can be identified. Since the horizontal axis represents the displacement at CBG, this plateau does not imply that no further decrease in preload force occurs. Due to abrupt and significant slip at CBG, the available preload force in the bolt shows this behaviour. The decay of preload force at larger displacements at CBG is elaborated in Subsection 3.8.5.

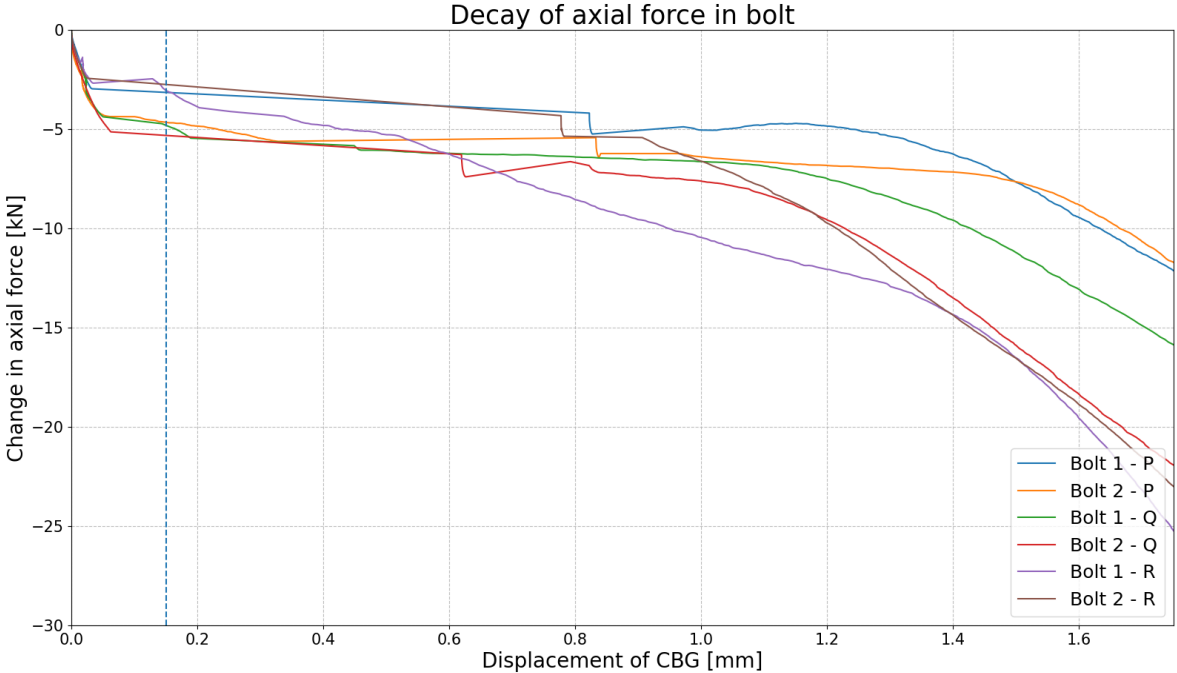
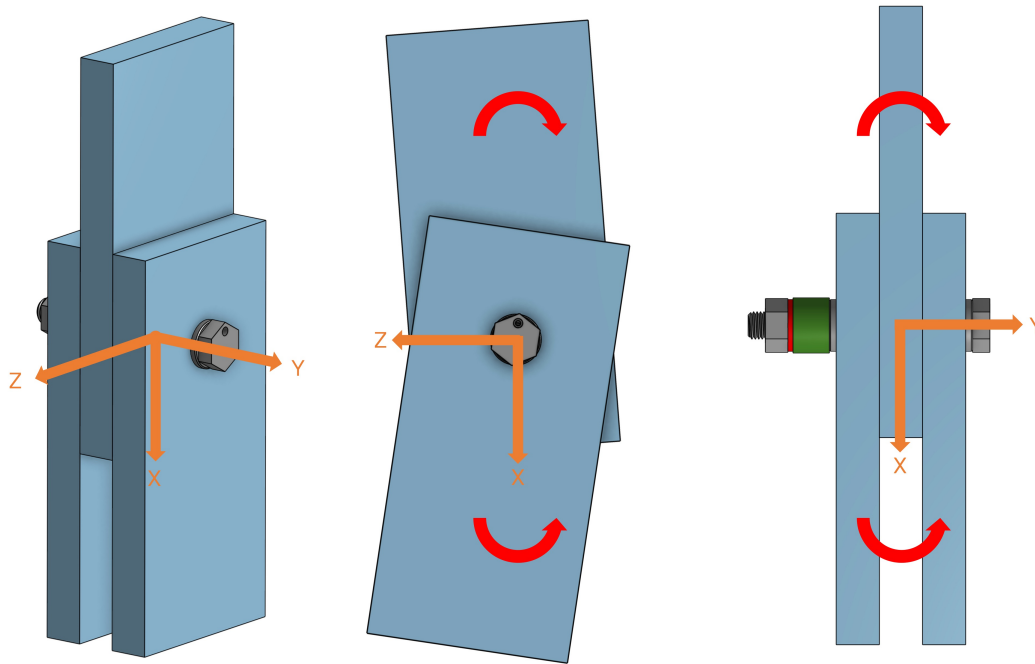


Figure 47: Decrease of the available preload force in each bolt during the experiment (PBC)

At the start of all experiments, the preload force in the bolt is aimed to be 140kN, see Table 9. When the maximum slip-resistance is obtained, the decrease of this preload force is approximately between 3 to 5kN (=2 to 4%). In addition, one can see that three graphs show unstable behaviour at approximately 0.02mm. This effect occurs due to the decrease in force within the connection since the other connection obtains abrupt slip. For larger displacements, the decrease of preload force increases per additional displacement. After 1.75mm displacement at CBG, the average change in axial force is below a decrease of 20kN (approx. -15%). In Appendix D the decrease in preload force of all experiments is visualised.

In the following graphs, the LVDT displacement is shown. These graphs show the displacement of two different but related LVDTs on both horizontal and vertical axes, the different axes are visualised in Figure 48. In this case, possible defects in alignment can be detected. In Subsection 3.8.4, the analysis of these results is elaborated. In Figure 49 and Figure 50 the displacement of pairs of LVDTs are visualised around two different axes. These different axes are the Y- and Z-axis, indicated in Figure 48.



**Figure 48:** Local axis of the bolted connection. From left to right: local axis coordination, rotation around Y-axis, rotation around Z-axis

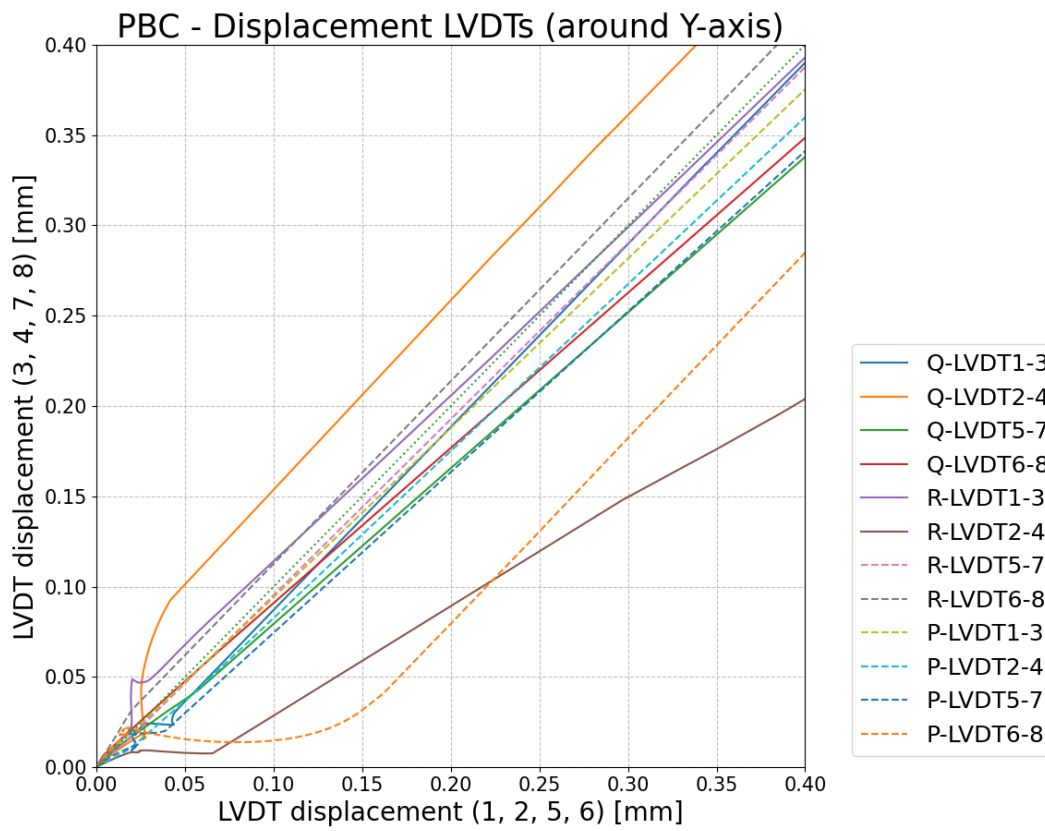


**Figure 49:** Alignment of the PBC concerning misalignment around Y-axis

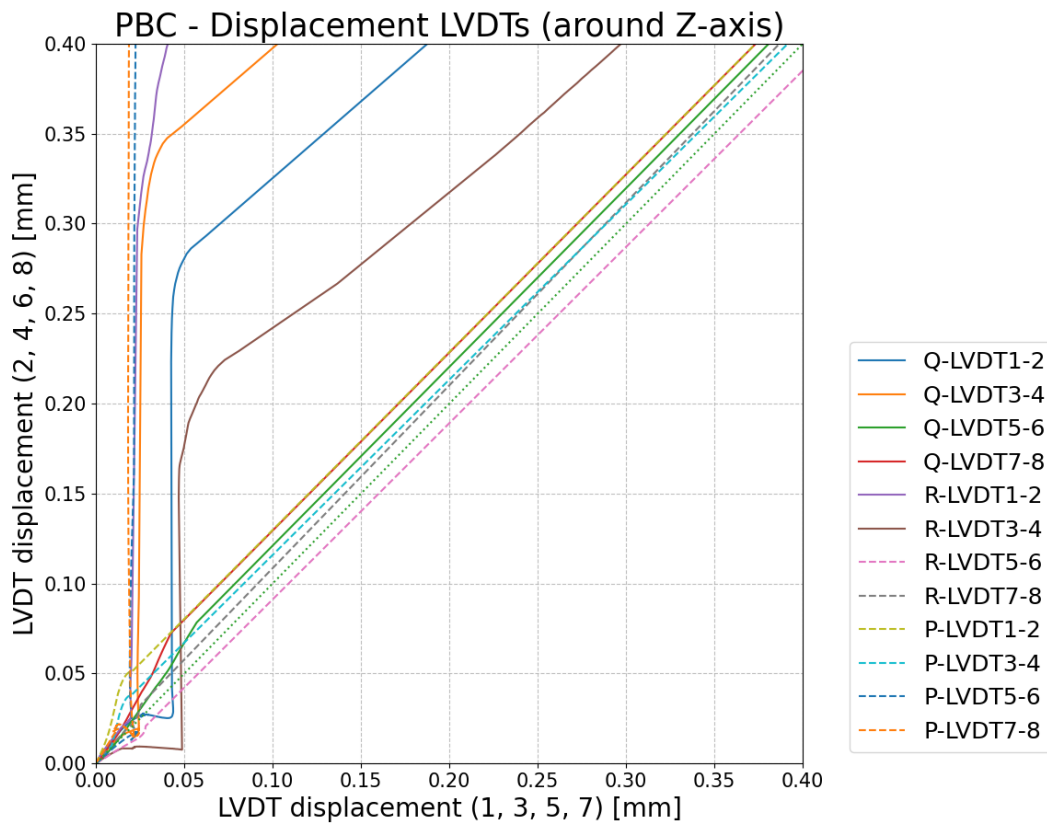


**Figure 50:** Alignment of the PBC concerning misalignment around Z-axis

### 3.7.2 Serie 2: Injected bolted connections (IBC)

The second series of this research involves the implementation of injection bolts. Injection of connection is done by the prescribed mixture of [Figure 33](#). After the curing period of the resin, each specimen is tested by the prescribed displacement of the piston of 0.001mm/s. The outcome of all experiments is shown in [Figure 51](#).

When zooming in on the region at which the resistance is determined a more linear behaviour is visualised, see [Figure 51](#). At the start of the experiments, a large variation in stiffness is obtained, in which some even include jumps. This difference occurred to overcome the stiffness by tightening the bolts. According to NEN-EN1090-2, the maximum applied torque to mount the connection is 30Nm[15]. Even this little torque creates a preloading force in the bolt. However, after some applied force, the bearing stiffness of the reading is almost linear.

Within this graph, the blue dotted line represents the limit criterion of the NEN-EN1090-2 [15] for a slip-critical preloaded connection which is in this research also implemented for an injected bolted connection. In this type of connection, in contrast with a preloaded connection, no abrupt slip occurred. This automatically implies that the maximum applied force in the connection is determined at a displacement of 0.15mm. This limit of displacement at CBG is assumed for the comparison with preloaded bolted connections. In addition, within the literature, this same value was implemented for short-term tests [67], while for long-term/creep tests this value is increased to 0.3mm.

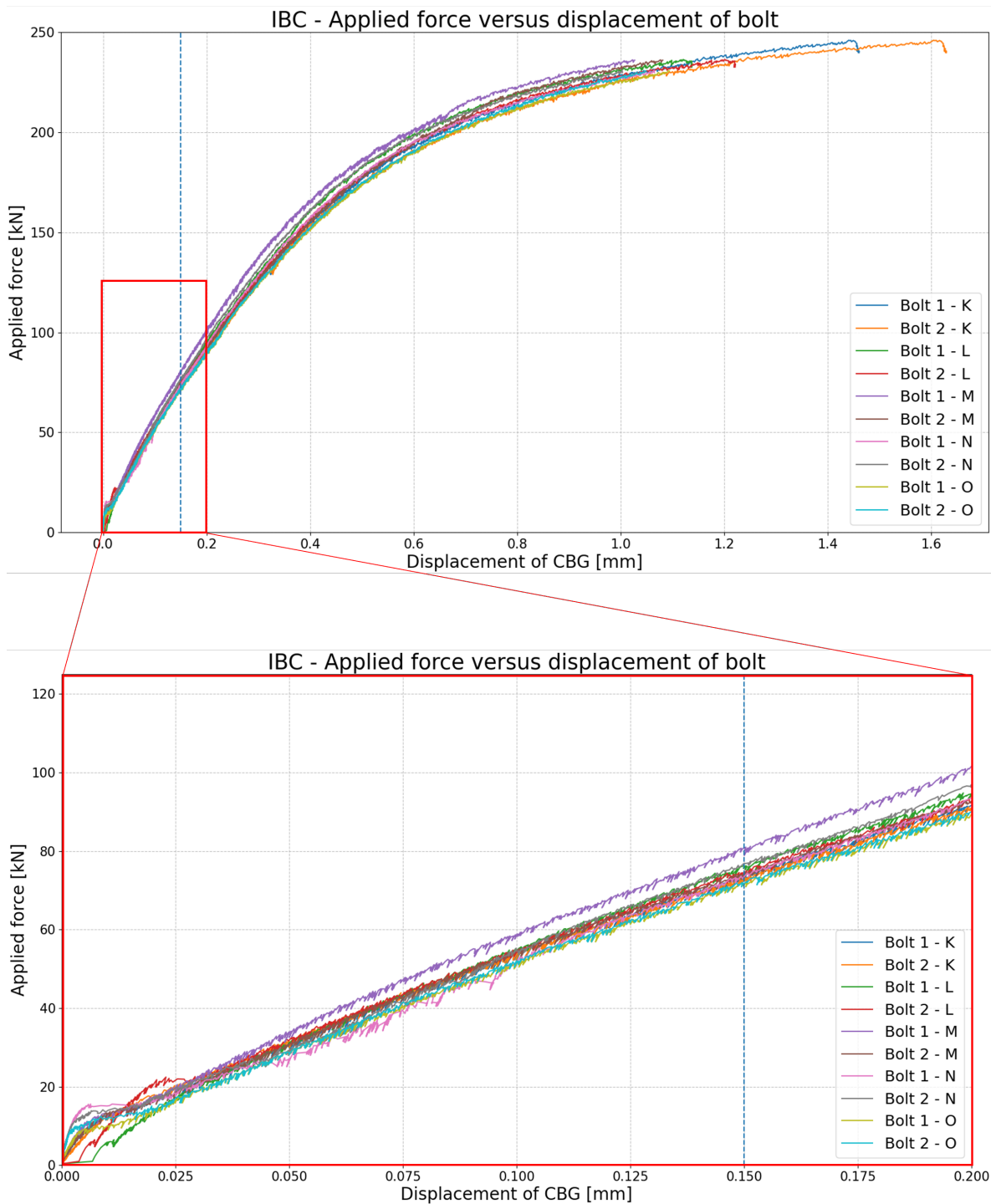


**Figure 51:** Results of all specimens when preloaded. This graph gives the relation between the displacement at CBG and the applied force in the connection

Of the obtained resistances at 0.15mm displacement from the graphs shown in [Figure 51](#) a coefficient of variation of 3.6 % is obtained. Implies that all results are close to each other and that the behaviour of these connections are similar. The average resistance of these tests is 74.7kN, see [Table 11](#). The outcome with the largest deviation is connection M1, with a difference of 6kN (8%). During the injection of bolts, three different mixtures had to be made. Therefore, a higher potential risk of obtaining various properties was introduced. Nevertheless, according to the results, these differences in properties were limited.

**Table 11:** Obtained resistances from experiments when applying injection, including comparison with average obtained resistance

|         | Resistance ( $F_{\max}$ ) [kN] | Diff. to average [kN] |
|---------|--------------------------------|-----------------------|
| K1      | 73.3                           | -1.4 (-2%)            |
| K2      | 73.1                           | -1.6 (-2%)            |
| L1      | 76.3                           | 1.6 (+2%)             |
| L2      | 74.5                           | -0.2 (0%)             |
| M1      | 80.7                           | 6.0 (+8%)             |
| M2      | 74.8                           | 0.1 (0%)              |
| N1      | 73.5                           | -1.2 (-2%)            |
| N2      | 76.8                           | 2 (+3%)               |
| O1      | 71.8                           | -2.8 (-4%)            |
| O2      | 72                             | -2.7 (-4%)            |
| Average | 74.7                           | N/A                   |

The resistance of an injected bolted connection is obtained by bearing of the resin itself. Since the injected resin fills the entire cavity around the bolt, the bolt is directly bearing against this resin. During the application of the external force, the resin is activated by internal compression such that the bolt will slightly bend. In [Figure 52](#) a cross-sectional view is shown of the connection after testing. From this figure, it can be seen that the bolt indeed bends slightly. In addition, the spacer inserted to center the bolt in the bolt hole can be seen clearly.



**Figure 52:** Cross-sectional view of a tested IBC

It can however be questioned what the amount of bending is at a measured displacement of 0.15mm at CBG. The experiment for IBC is aborted at a force of approximately 230kN which is significantly higher than the applied force at 0.15mm displacement. Bending of the bolt and the application of the external force introduces an increase in axial force in the bolt. This increase is shown in [Figure 53](#). At at displacement at CBG, the axial force in the bolt is on average 4kN. This axial force increases to 10 to 25kN at a displacement of 1.0mm (see [Appendix D](#)).

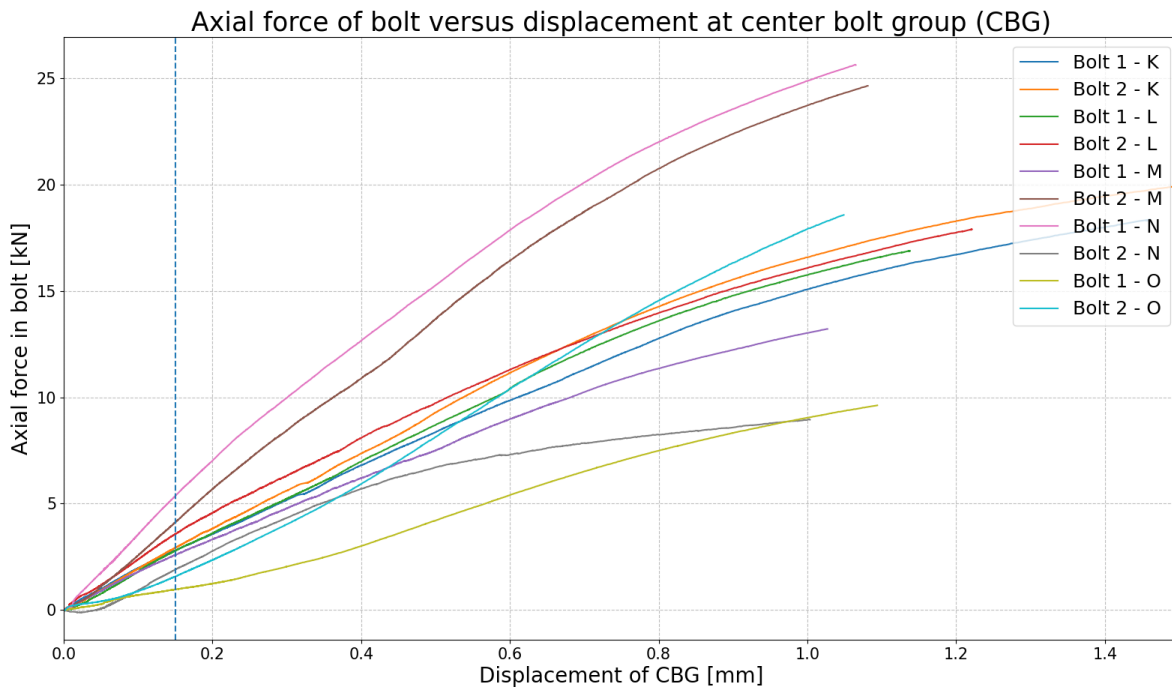


**Figure 53:** Increase of the axial force in each bolt during the experiment (IBC)

In [Figure 54](#) and [Figure 55](#) the displacement of pairs of LVDTs are visualised around two different axis. These represent misalignment around two different axes. From these graphs, it can be seen that the bolted injected connections are more sensible to displacements around the z-axis than around the y-axis. This is in contrast with the results of the preloaded bolted connections since for injected bolted connections, there is no clamping force that minimises rotations around the Y-axis. Around the Z-axis, the misalignment is lower since the resistance of an injected bolted connection is (almost) not affected by COF at the interface.

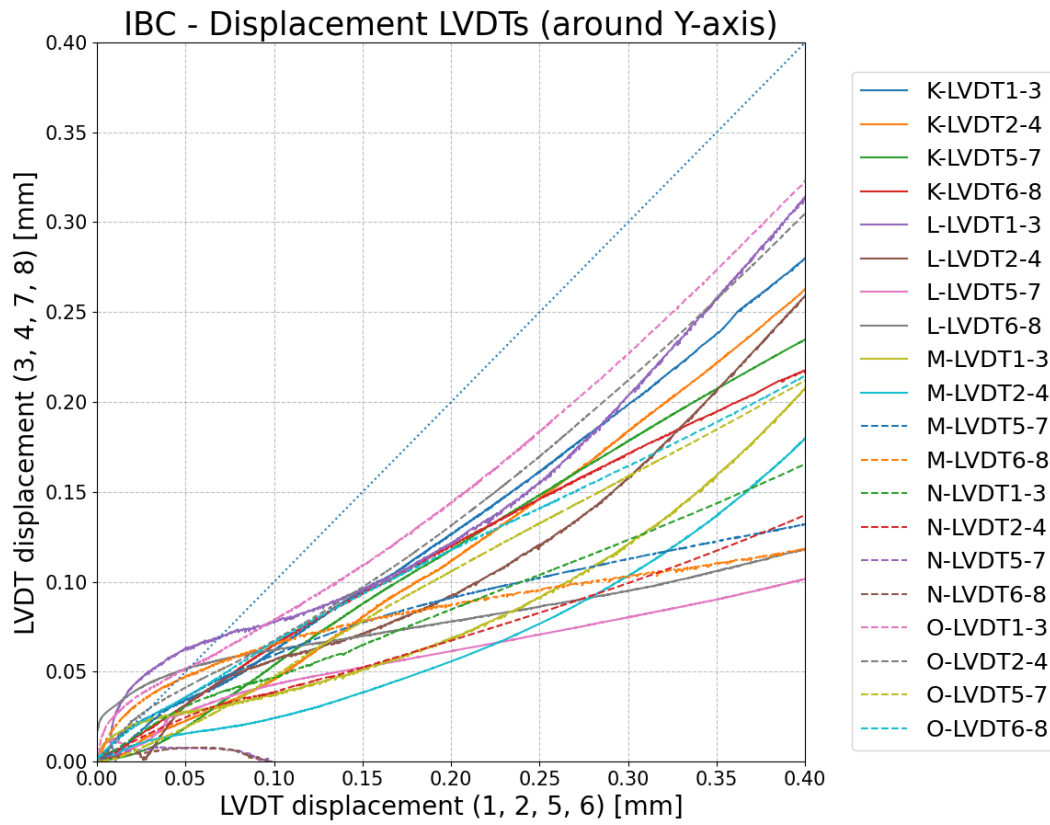


Figure 54: Alignment of the IBC concerning misalignment around Y-axis

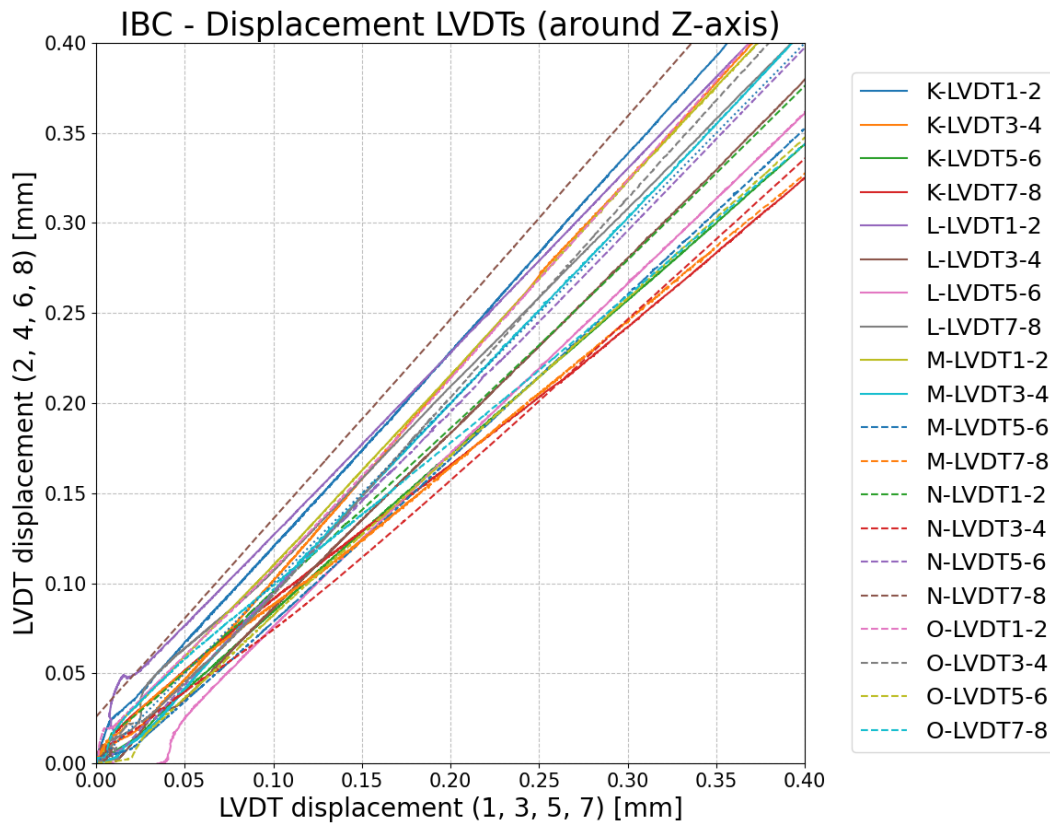


Figure 55: Alignment of the IBC concerning misalignment around Z-axis

### 3.7.3 Serie 3: Preloaded and injected bolted connections (PIBC)

The last series of the principal research is the preloaded and injected bolted connection. Within this series, all bolts are preloaded according to the combined method. [Table 12](#) shows both nominal and acting preload force in the force at the start of the experiment.

**Table 12:** Overview of nominal and actual initial preload force in all bolts for Serie 3 (injection and preloading)

|         | $F_{p,C,nom}$ [kN] | $F_{p,C,init}$ [kN] |
|---------|--------------------|---------------------|
| F1      | 110                | 142.13 (+29%)       |
| F2      | 110                | 137.99 (+25%)       |
| G1      | 110                | 139.19 (+27%)       |
| G2      | 110                | 139.56 (+27%)       |
| H1      | 110                | 138.57 (+26%)       |
| H2      | 110                | 139.16 (+27%)       |
| I1      | 110                | 139.40 (+27%)       |
| I2      | 110                | 137.64 (+25%)       |
| J1      | 110                | 137.64 (+25%)       |
| J1      | 110                | 138.45 (+26%)       |
| Average |                    | 138.97 (+26%)       |

[Figure 56](#) visualises an overview of the load-displacement of all monitored bolts of series 3. Two different behaviours are obtained from this graph. Whereas the first part, until an applied force of approximately 150kN consists of a significantly large proportion of stiffness obtained by preloading since the stiffness of the resin is small, see [Paragraph 3.8.6.3](#). After some point, the stiffness of the preloading decreases since its componential resistance is exceeded. From this point onwards, the stiffness behaviour relates to the acquired stiffness from injection bolts.

During the experiment, the same amount of displacement per time is assumed as in the previous tests. Within the PIBC, a limit force of 230kN is implemented since the bolt itself is expected to fail at the shear planes at an applied force of approximately 260kN. This value of 230kN is assumed to be on the safe side to prevent abrupt failure.

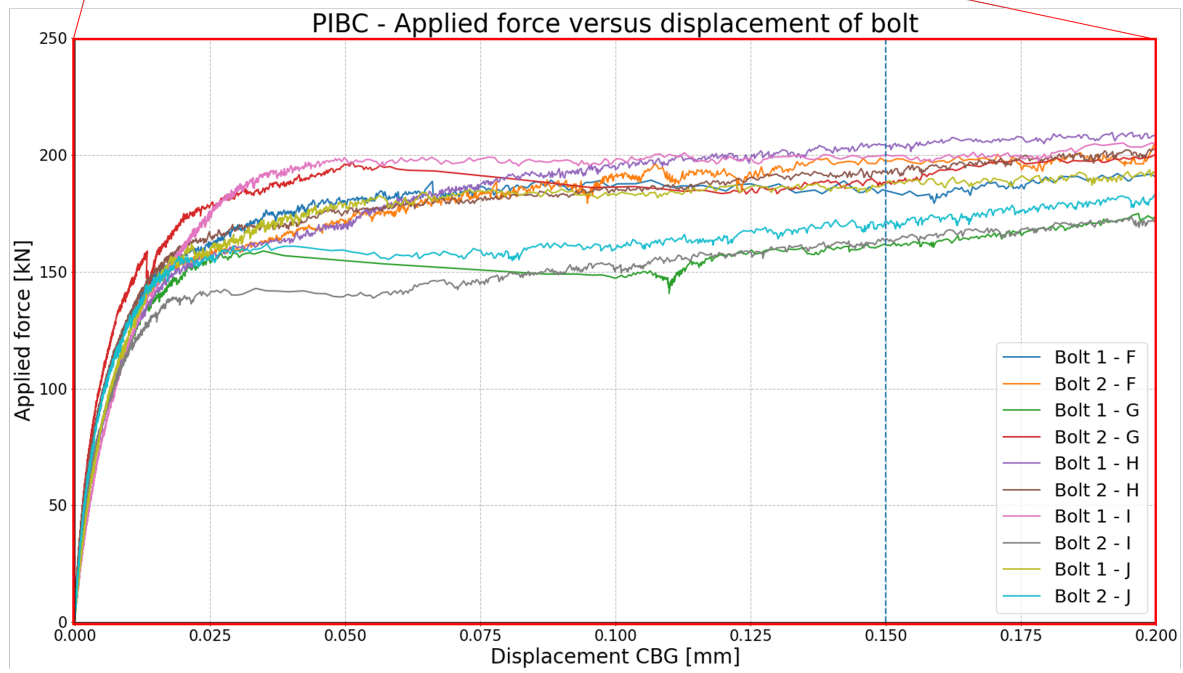
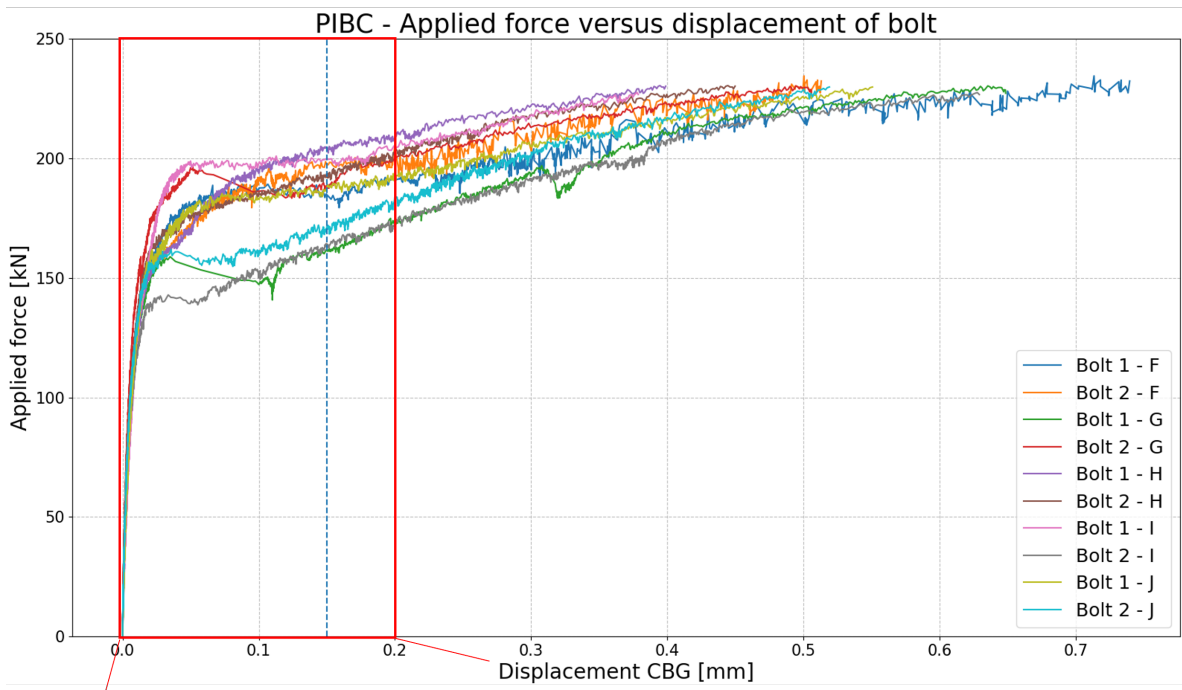


**Figure 56:** Results of all specimens for a preloaded and injected bolted connection. This graph gives the relation between the displacement at CBG and the applied force in the connection

In the figure [Figure 56](#), a more detailed view is given of the load-displacement curve until a displacement of 0.2mm at CBG. From this figure, it can be seen that for bolts G1(green), G2(red), I2(grey) and J2(cyan) limited slip occurs before the resin is activated properly. This is elaborated in [Subsection 3.8.1](#). For all other bolts, a smoother transition is observed.

To obtain the resistance of a preloaded and injected bolted connection, the same analogy of the previous connections is implemented. This resemblance is that the resistance from a connection is the maximum applied force until a displacement of 0.15mm. This limit is again visualised with the vertical blue dotted line. For all bolts, this is at the 0.15mm line, except bolt G2(red) which holds the maximum resistance at 0.050mm displacement. A summarisation of the results obtained from this series is given in [Table 13](#).

**Table 13:** Obtained resistances from experiments when applying both injection and preloading

|         | Resistance ( $F_{\max}$ ) [kN] | Diff. to average [kN] |
|---------|--------------------------------|-----------------------|
| F1      | 189.23                         | 2.1 (+1%)             |
| F2      | 198.67                         | 11.5 (+6%)            |
| G1      | 161.88                         | -25.3 (-14%)          |
| G2      | 196.98                         | 9.8 (+5%)             |
| H1      | 205.08                         | 17.9 (+10%)           |
| H2      | 194.22                         | 7.1 (+4%)             |
| I1      | 200.99                         | 13.8 (+7%)            |
| I2      | 164.35                         | -22.8 (-12%)          |
| J1      | 187.95                         | 0.8 (+0%)             |
| J2      | 172.21                         | -14.9 (-0.8%)         |
| Average | 187.2                          | N/A                   |

For a preloaded and injected bolted connection, this obtained resistance is achieved by both slip-resistance and bearing resistance. Since both resistance might affect each other, by for instance the preload force, the following graph is given. [Figure 57](#) visualises the decrease in available preload force in the bolt. The decay of the preload force compared for both PBC and PIBC is elaborated in [Subsection 3.8.5](#).

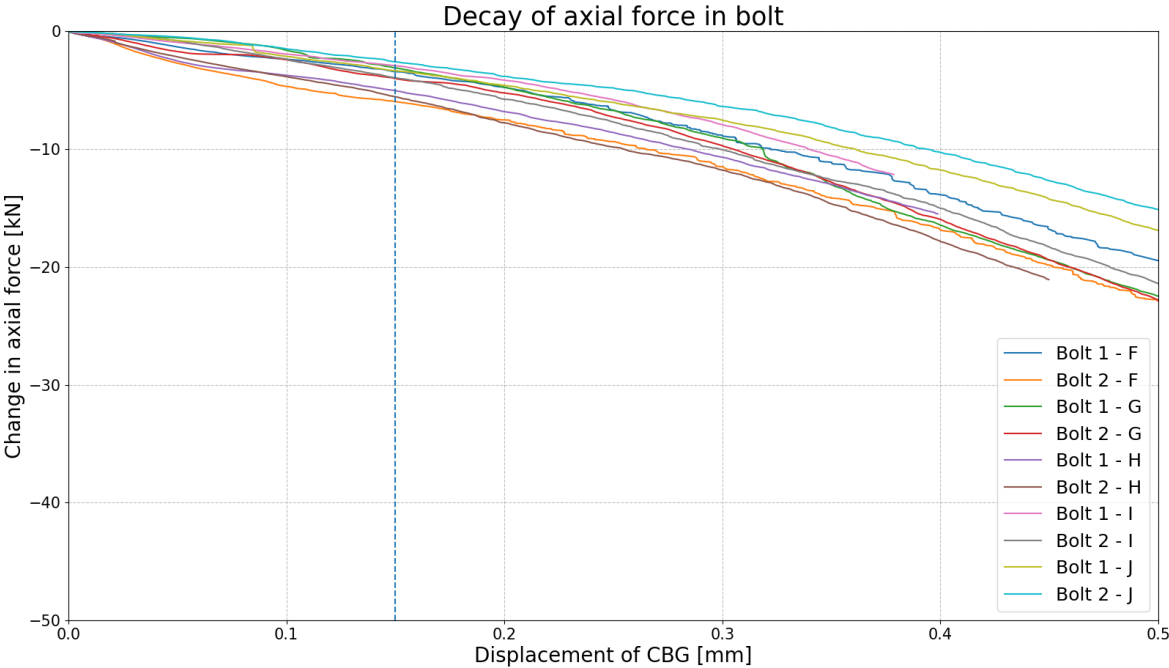


**Figure 57:** Decrease of the available preload force in each bolt during the experiment (PIBC)

From this graph, it can be seen that there is no abrupt decrease in preload force. At the displacement of 0.15mm at CBG, this decrease is approximately between 3 and 6kN. Compared to the preloaded bolted connections, this decrease was in between 3 and 5 at maximum slip-resistance. Therefore, the decay in preload force is similar for a preloaded injected bolted connection (PIBC) than for a preloaded bolted connection (PBC) (see [Subsection 3.8.5](#)).

In addition to the progression of the decay of the preload force, the alignment of the specimens is investigated. Similar to the other connections, two different LVDTs are plotted against each other. These two different LVDTs represent the possible rotation around the Y- and Z-axis, see [Figure 58](#) and [Figure 59](#).

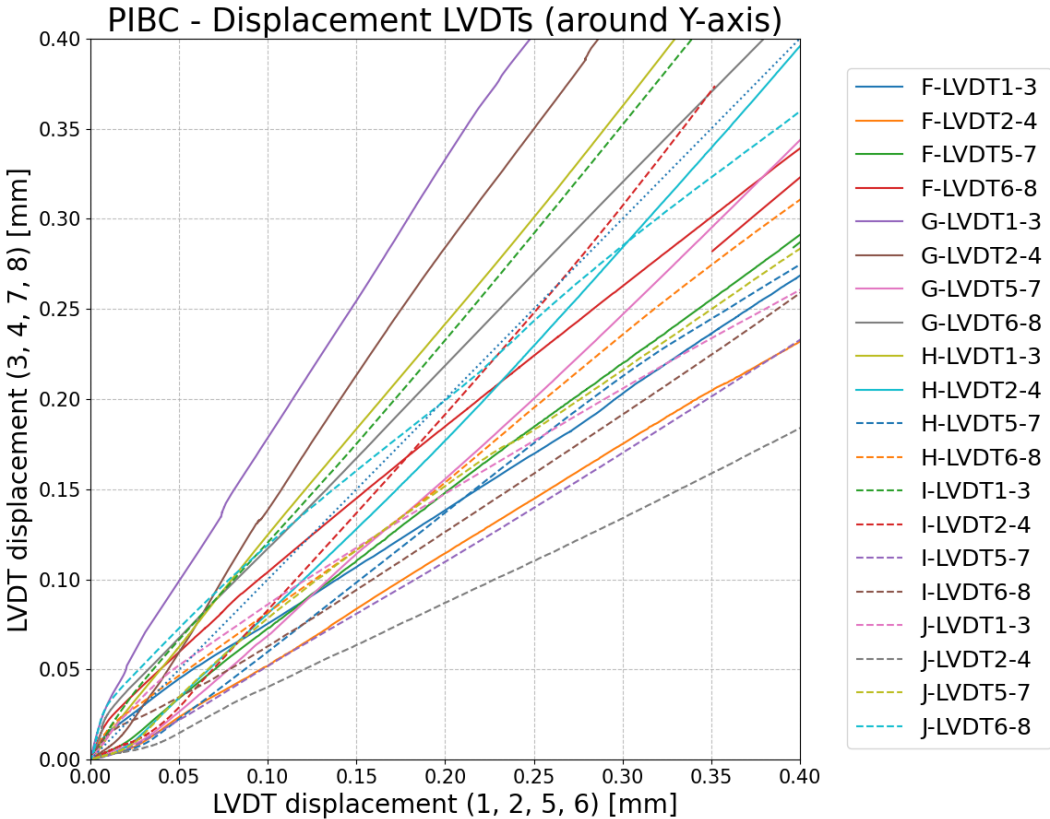


**Figure 58:** Alignment of the PIBC concerning misalignment around Y-axis

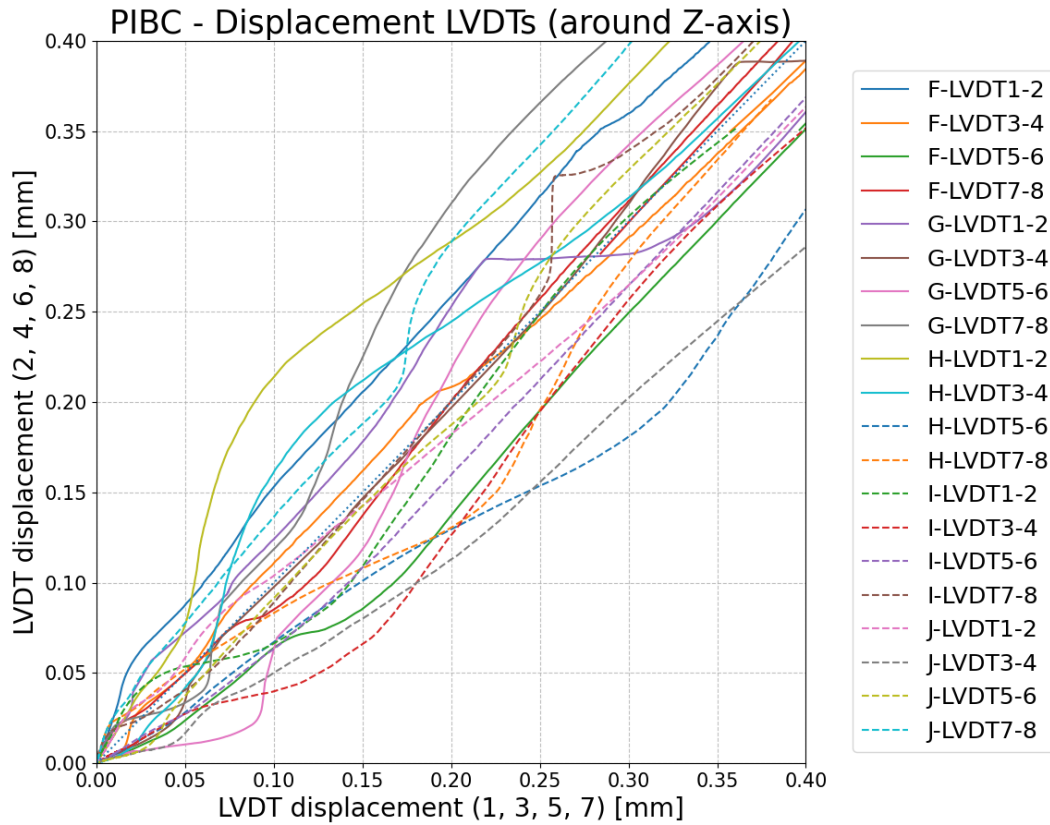


Figure 59: Alignment of the PIBC concerning misalignment around Z-axis

### 3.8 Analysis of experimental results

In this section of the report, the results obtained as presented from experiments are elaborated. This elaboration is divided into several subsections related to the specific analysis.

#### 3.8.1 Slip-resistance of preloaded connection

In [Subsection 3.7.1](#), the results are shown of the load-displacement behaviour of a preloaded bolted connection with an initial preload of 140kN. For all connections, it can be seen that when the maximum slip-resistance is reached, a significant drop of force occurs in combination with a large amount of immediate slip. In addition to this observation, one of the connections shows deviating results compared to the others, namely connection P2. Within this experiment, slip occurred first at bolt P1. Due to this slip, the applied force decreases until more friction is found or the bolt starts bearing. After this phase, the force started increasing again. However, this force never reached its initial resistance anymore since bolt P2 started slipping before reaching the resistance of 136.7kN again. This outcome is not as expected since the experiment is placed as a serial circuit whereby the same force passes all components. In this case, the connection with the least capacity is expected to fail first. This prescribed situation can also be seen in [Figure 45](#) where the orange line (bolt P2) never reaches the initial resistance of 136.7kN (at an approximated displacement of 0.02mm) within the specified displacement range from 0 to 0.15mm. If the preload force in this connection drops significantly before the second build-up, then the result is less unexpected. However, as [Figure 47](#) indicates for bolt P2, there is no significant drop in preload force observed. Therefore, it is assumed that this behaviour is not related to the preload force.

When comparing these results with the expected nominal outcome of the NEN-EN1993-1-8 (excluding partial safety factor), a clear difference can be observed [17]. The nominal slip-resistance of such a preloaded connection is 112kN when taking into consideration the actual applied preload force and excluding the partial safety factor. Compared to the obtained average resistance of 144.7kN, one can say that this difference is significant but also as expected since both the friction surface and tightening method exceed the nominal value tremendously. Therefore, this distinction is a result of the applied input parameters, see [Subsection 3.8.2](#) and [Section 6.4](#). Both the actual friction coefficient and implemented initial preload force are decisive for this difference. When comparing this outcome with the literature, Ungermann and Kröger investigated the combined resistance for non-preloaded and preloaded injected connections [67]. Their result is that the preloaded connection has a capacity of 357.7kN, which is approximately 35 percent higher than its nominal strength. Unfortunately, no applied preload force is mentioned. Since the current research involves the combined method as the basis of the tightening procedure, the consequence is a larger difference in obtained resistance.

### 3.8.2 Friction coefficient

From the obtained results of the preloaded bolted connection, it turned out that the resistance is more than 100% larger than the nominal assumed values. The first reason is the increase in initial preload force. Besides this reason, the actual friction coefficient plays an important role. In [Table 14](#) an overview is shown of the calculated friction coefficients. Within this equation, the actual initial preload force is assumed.

**Table 14:** Determined friction coefficient for each bolt and difference to the nominal friction coefficient of 0.4 [15]

|         | $F_{p,C,init}$ | $F_{max}$ | $\mu_{init}$ |
|---------|----------------|-----------|--------------|
| P1      | 140.5          | 136.7     | 0.49 (+22%)  |
| P2      | 137.8          | 136.7*    | 0.50 (+24%)  |
| Q1      | 140.2          | 154.7     | 0.55 (+38%)  |
| Q2      | 138.4          | 148.0     | 0.53 (+34%)  |
| R1      | 138.7          | 153.1     | 0.55 (+38%)  |
| R2      | 139            | 139.3     | 0.50 (+25%)  |
| Average | 139.1          | 144.7     | 0.52 (+30%)  |

\* = could not obtain initial resistance anymore after slip of the other connection

The average determined friction coefficient is 0.52. This value is 32% larger than the nominal value of 0.4 stated by the NEN-EN1993-1-8. Therefore it can be concluded that the assumed value of 0.4 by the NEN-EN1993-1-8 is conservative. However, one can doubt the formulation of the term friction coefficient for this situation. Since both implemented forces (preload force and slip-resistance) do not occur simultaneously, it is not correct to implement those within the same equation. Therefore, it is assumed that the factor  $\mu$  describes the relation between the slip-resistance and the initial preload force.

In [Section 6.4](#) a comparison is made **if** the term friction coefficient is implemented correctly, assuming **Coulomb** friction behaviour.

### 3.8.3 Bearing resistance of the resin

The NEN-EN1993-1-8/NB, prescribes a method to determine the bearing resistance of a resin experimentally [18]. However, this determination requires long-term tests which are not performed in this research. In addition, the equation of how the bearing strength ( $f_{b,resin}$ ) is determined is not given. In this paragraph, the bearing resistance is evaluated based on the applied force and area of loading and therefore short-term and by deriving the bearing strength of the equation of the NEN-EN1993-1-8. This results in the following three scenarios:

1. Scenario 1: Taking into consideration the governing thickness (middle plate) and the width of the bolt as available area and assuming uniform stress distribution of the resin;
2. Scenario 2: Taking into consideration the governing thickness (middle plate), whereby this thickness may not exceed  $1.5d$  (regulation of the NEN-EN1993-1-8) and the width of the bolt as available area and assuming uniform stress distribution of the resin;
3. Scenario 3: Taking the bearing strength of the resin as an unknown parameter in the formulation of the NEN-EN1993-1-8 (Equation 4) and using the average experimental resistance as the outcome of this formula to derive the bearing strength.

According to the requirements of the Eurocode, the area where the force is distributed, is the diameter of the bolt times the minimum thickness of the middle plate ( $=25\text{mm}$ ), two times the thickness of the side plates ( $=50\text{mm}$ ) or  $1.5$  times the diameter of the bolt ( $=24\text{mm}$ ). Since the NEN-EN1993-1-8 limits the effective thickness of the resin by  $1.5$  times the diameter of the bolt, both limited ( $=24\text{mm}$ , scenario 2) and unlimited ( $=25\text{mm}$ , scenario 1) are taken into consideration for comparison. The third scenario relates to the equation of the NEN-EN1993-1-8 without substitution of the bearing strength.

In the first scenario, where the bearing strength is determined by the thickness of the middle plate and the bolt, the bearing strength turned out to be  $187\text{MPa}$ . For the second scenario, the determined bearing strength of the resin was  $194\text{MPa}$ . Since the available area is limited for the latter case, the bearing strength is higher.

In the last scenario, the formulation of the NEN-EN1993-1-8 is adopted. In this case, all parameters are substituted by the acknowledged values:

- $k_t = 1.2$ ;
- $k_s = 1.0$ ;
- $d = 16\text{mm}$ ;
- $t_{b,resin} = 24\text{mm}$ ;
- $\beta = 1.33$ ;

After rewriting and substitution, the bearing strength according to this formulation is  $122\text{MPa}$ . In other words, if a bearing strength of  $122\text{MPa}$  is inserted in Equation 4, including all other parameters, the bearing resistance is equal to the average obtained resistance by experiments.

Ungermann et al. investigated the bearing resistance of the resin as well. From their experiments, the bearing resistance turned out to be  $211.7\text{MPa}$ . In this case, the made assumption is that the contributed area is the width of the bolt times the thickness of the middle plate [67]. However, this is allowed since geometry of the NEN-EN1090-2 is adopted in this research. Since both the diameter of the bolt and the thickness of the middle plate is  $20\text{mm}$ .

Within the scenario of an M20 bolt, including a plate thickness of  $20\text{mm}$  and a ratio of  $1:2$  with the side plates, the nominal bearing resistance is a bit larger than  $172\text{kN}$ . This is also in line with the obtained resistance of  $169.34\text{kN}$  by Ungermann et al. [67]. Looking into the formulation set by the Eurocode, the most important difference is the implementation of the  $\beta$ -factor. This factor is  $1.33$  ( $+33\%$ ) if the plate thickness ratio of the middle and side plate is  $1:1$ . Since this research's geometry satisfies this equation, a significant overestimation occurs. Therefore, one can doubt the implementation of the  $\beta$ -factor.

### 3.8.4 Alignment of specimen

For each connection, the alignment of the connection is given. This alignment is considered around two different axes. The local coordinate system assumed for each connection is visualised in [Figure 48](#). The x-axis is the longitudinal axis of the specimen. This is also the direction in which the external load is applied. The second axis, Y-axis, is the longitudinal axis of the bolt. Whereas the Z-axis is the transverse direction of the loading. The figures shown at each connection relate to a certain misalignment. Such misalignment may occur during, for instance, the installation of the specimen, force equilibrium inside the connection or resistance of the shear plane.

In the preloaded bolted connections, it turned out that there is almost no misalignment around the Y-axis since all lines are almost under an angle of 1:1. It is assumed that this is the result of two scenarios. The first relates to the perfect assembling of the specimen. The other scenario could be that the preload force clamps this rotational degree of freedom such that the connection will not be straightened. However, around the Z-axis, there is a significant difference between specimens. This may be due to the lower frictional resistance of the plane. For example, P-LVDT5-6 and P-LVDT7-8 show that LVDTs 6 and 8 (plane 4) show a significantly larger initial displacement than LVDTs 5 and 7 (plane 3). However, after some displacement of plane 4, the proportion in increase between both planes becomes equal (1:1). Therefore, this mostly affects the initial phase of the experiment.

For the injected bolted connection, a different result is obtained. These connections show more sensitivity to misalignment around the Y-axis instead of the Z-axis. Almost all specimens show more initial movement towards one side of the connection. Even one specimen N-LVDT5-7 and N-LVDT6-8 show negative displacements. This can only occur if rotation around the longitudinal axis of the bolt occurs (Y-axis). Since there is no clamping force, straightening of the specimens occurs almost immediately. However, it is expected that the interface of the resin and the plate includes a “sticking” behaviour. Due to this straightening and connection of the resin and the plate, the resin might undergo damage. This damage occurs by the torsional effects inside the resin.

From the experimental results it turned out that from both preloaded and injected connections, injected bolted connections are more sensitive to misalignment around the Y-axis. This is also expected since the preload prevents such rotations. However, this may be at the cost of slip-resistance capacity.

The last type of connection, the preloaded and injected bolted connection shows that there is one governing direction of misalignment around the Y-axis. Therefore, since all specimens are assembled in similar positions, one can say that the method of installation of the connections did not solely result in deviation of results. However, from these measured misalignments around the Y-axis, there is a significantly less tendency to follow the slope 1:1 compared to the previous results.

### 3.8.5 Change in preload/axial force during experiment

Two of the three connections (PBC and PIBC) have been preloaded before the start of each experiment. During the experiment, the preload force is expected to decay. In the results section of this report, the decay in preload force of each connection is already visualised by [Figure 47](#) and [Figure 57](#). However, it can be questioned what the relation of the type of connection is with the amount of decay in preload force. In [Figure 60](#), an overview is shown of this behaviour for the two considered preloaded connections (PBC and PIBC).

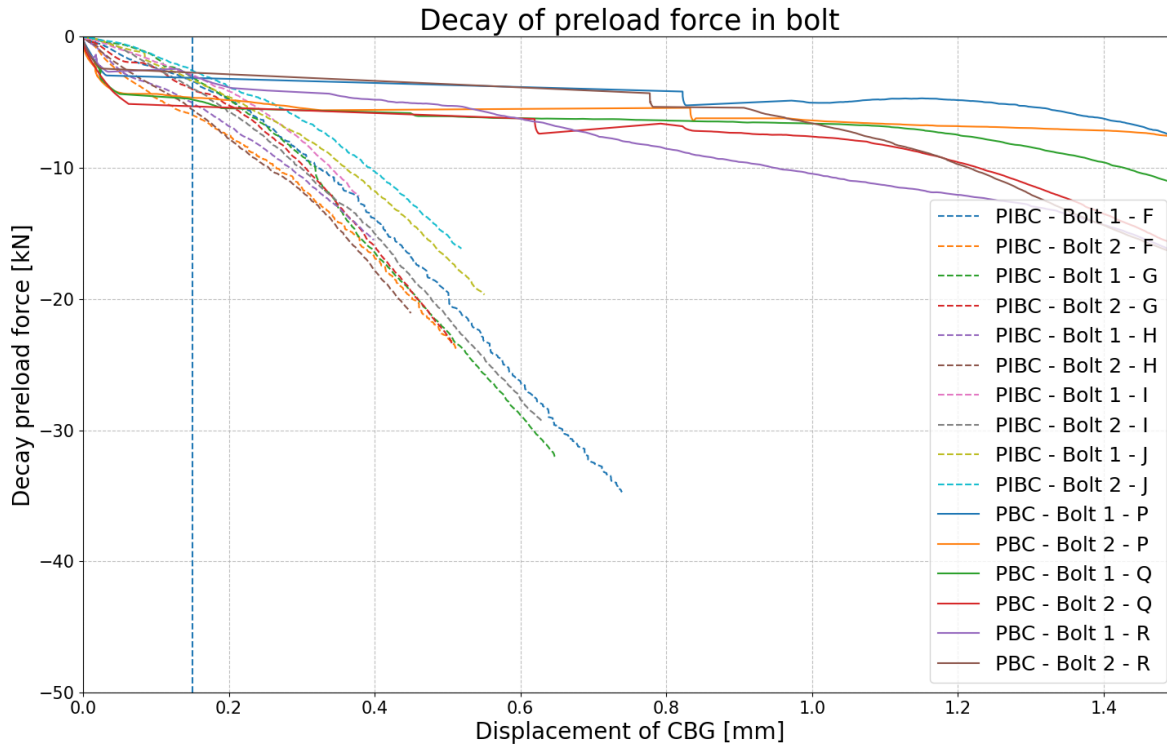


**Figure 60:** Decay in preload force at certain displacements of CBG for the two different types of connections: PBC (continuous) and PIBC (dotted)

From this figure, it can be seen that the loss in preload at the point of a displacement of 0.15mm is similar. Therefore, one can say that the contribution of the slip-resistance can be assumed to be similar for the two connections. However, when proceeding with the experiment and increasing the displacement at CBG, the preload force exponentially decreases for the preloaded and injected bolted connection while for the preloaded bolted connection, the decay in preload force is not found until the bolt is getting closer to the edge of the bolt hole (bearing). In other words, there is a significant decay in preload force expected when the bolt starts bearing against the resin of steel. Thus, there is an activated interaction of the normal (preload) force and the shear force.

In the NEN-EN1993-1-8, such interaction of the normal and shear force is already incorporated by the formulation as shown in [Equation 13](#)[17]. This equation shows that there is an interaction of tensile and shear components at a cross-section of a component. In other words, if the applied force (in shear) is increasing, from a certain point onwards, the tensile force vector must decrease to satisfy [Equation 13](#). This can only be achieved when the available preload force decreases.

$$1.0 \geq \frac{F_{t,Ed}}{1.4 \cdot F_{t,Rd}} + \frac{F_{v,Ed}}{F_{v,Rd}} \quad (13)$$

The amount of shear force acting in the bolt is similar to the force taken into consideration by bearing of the resin. For a preloaded and injected bolted connection, this is equal to the applied force subtracted by the slip-resistance of the preloaded connection. However, this slip-resistance is dependent on the available preload forces. In the case of acting shear force, the preload force drops significantly whereby the slip-resistance reduces. Therefore, there is an iterative dependency expected between these two parameters.

In [Figure 61](#), this behaviour is visualised by comparing the decay of the preload force with the applied force in the connection for both PBC and PIBC. It can be seen that for the PIBCs, bearing is increasingly more governing from an applied force of 150kN onwards. From this point, the decay in preload force becomes more significant.

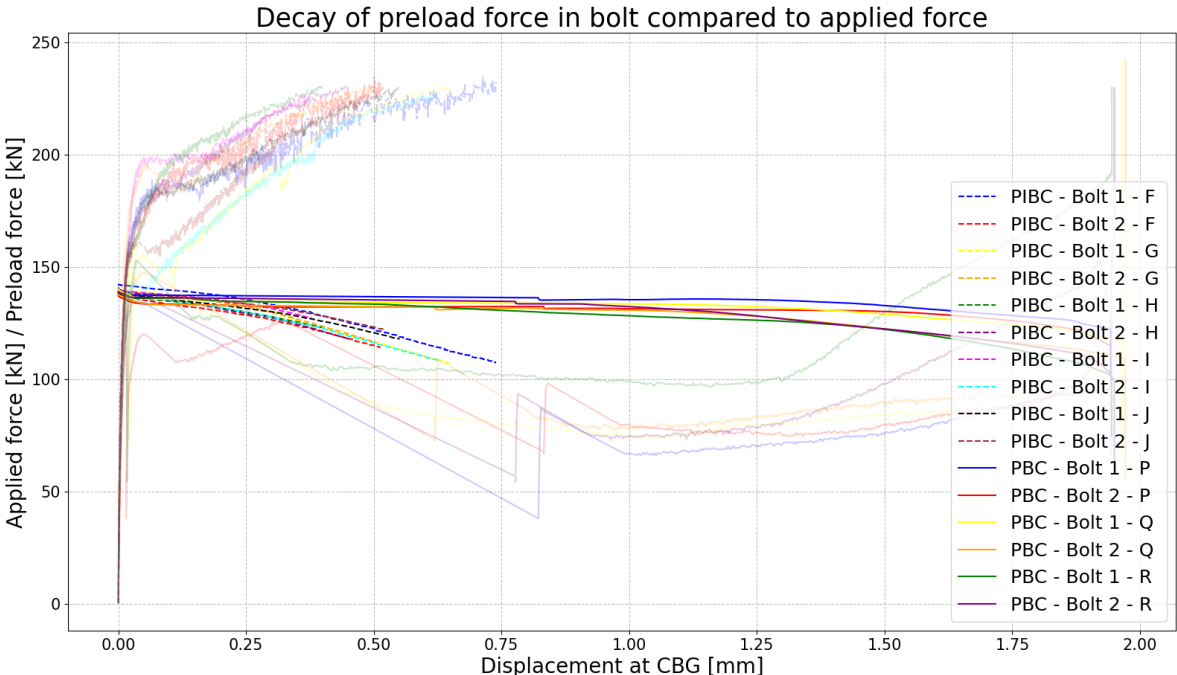


**Figure 61:** Decay in preload force at certain displacements of CBG of the two different types of connections: PBC and PIBC compared with the applied force. The transparent graphs indicate the applied force whereas the bright lines represent the available preload force. In addition, the continuous lines are the preloaded bolted connections while the dotted graphs indicate the preloaded and injected bolted connections

### 3.8.6 Averaged stiffness

In this section, the **average** stiffness of each type for two different displacement intervals is determined. The main goal of this research is to investigate if the summation of the individual resistance of preloading and injection is representative of the resistance of a preloaded injected bolted connection. Therefore, one can also question if this also implies that stiffnesses can be summed.

Two intervals are considered since it is assumed that two different types of regions occur within a preloaded connection: before and after the slip-resistance is exceeded (see Figure 62). For this first interval, it is assumed that the stiffness is most representative of a displacement at CBG from 0.003 up to 0.012mm. The start of the experiment is not representative of the stiffness. Therefore this region starts at 0.003mm instead of 0mm. The end point of this region is located at 0.012mm such that the significant decay of stiffness did not affect calculated stiffness. At a displacement of 0.02mm at CBG, it is observed that there is a change in stiffness for some of the connections. Therefore, the limit of 0.012mm was chosen. The second interval is located between the displacement at CBG of 0.12mm and 0.20mm. This region starts after a significant proportion of the release is slip-resistance has been overcome. This limit is set at a value of 0.20mm displacement at CBG since this region must be large enough and also representable for the resistance obtained at 0.15mm. Therefore, increasing this limit might reduce its reliability. However, it can be questioned whether or not these chosen areas are representative.

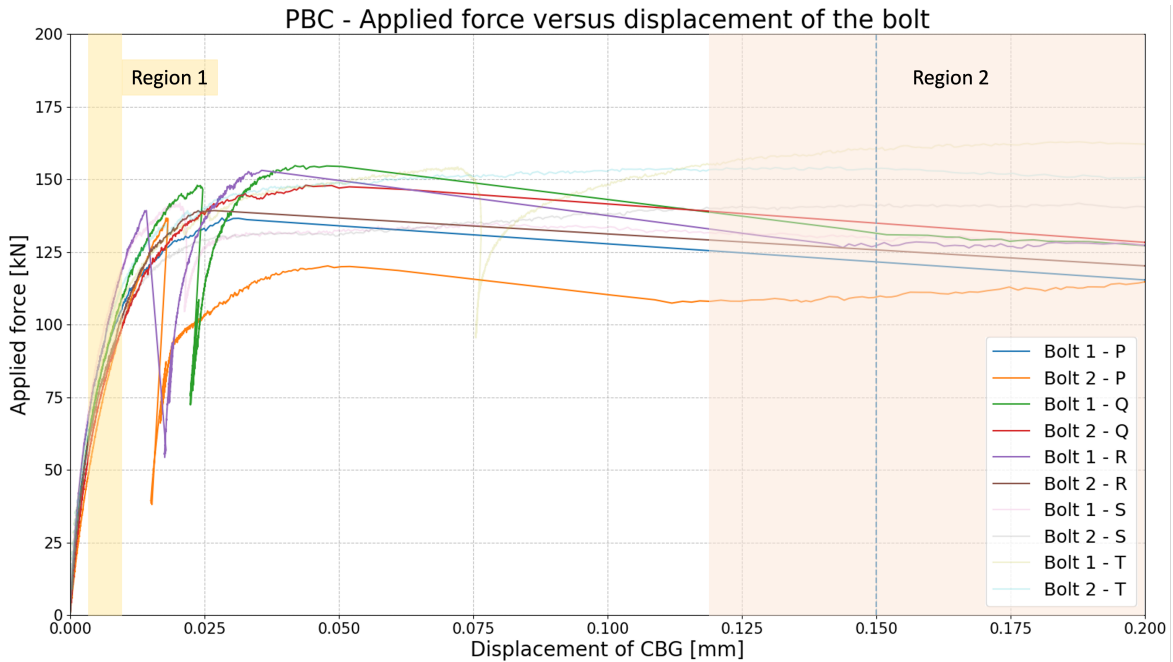


**Figure 62:** The two implemented regions where the stiffness is determined

From the obtained experimental data it turned out that the load-displacement is not continuously increasing over at least one axis. This is also visible in each individual graph that shows that the behaviour is not smooth. This made it more difficult to determine the slope of the curve with an interval. Therefore, an idealization method is implemented. This methodology consists of a formula that represents an individual experiment within a certain region in the best manner such that the  $R^2$  - value is approaching 1.0. This is done by curve-fitting each experiment by adopting exponential or quadratic equations. These equations are implemented since both preloaded and injected bolted connections show different behaviour of stiffness over displacement at CBG. In each following subsection, the adopted equation is formulated. From the result of this exponential or quadratic function, the stiffness is determined by a linear slope between the representative limits (0.003mm and 0.012mm or 0.12mm and 0.20mm). It must be kept in mind that determining the stiffness based on a curve-fit of a graph contains increased sensitivity. However, to include intermediate results between the first and last node of a region, that is used to determine the stiffness, the option of the curve-fit is assumed to be the best alternative.

### 3.8.6.1 Preloaded bolted connection (PBC)

For the preloaded bolted connection an exponential equation is implemented to curve-fit to the first slope. Equation 14 was the basis of this function wherein parameters A0 to A3 are determined by the curve-fit.

$$F_{\text{applied}} = A0 + A1 \cdot u_{\text{CBG}} - A2 \cdot \exp(-A3 \cdot u_{\text{CBG}}) \quad (14)$$

This exponential formula is adopted since it represents a more vertical slope with an increasing decay. Also known as an exponential curve with a negative increase. Since this curve is expected to decay, both A2 and A3 values are already assumed to be negative. Therefore these parameters are expected to be positive.

After perfecting this equation for each bolt, the subsequent parameters are acquired including their coefficient of determination ( $R^2$  - value). These are given in Table 43 (Appendix E) and visualised in Figure 63.

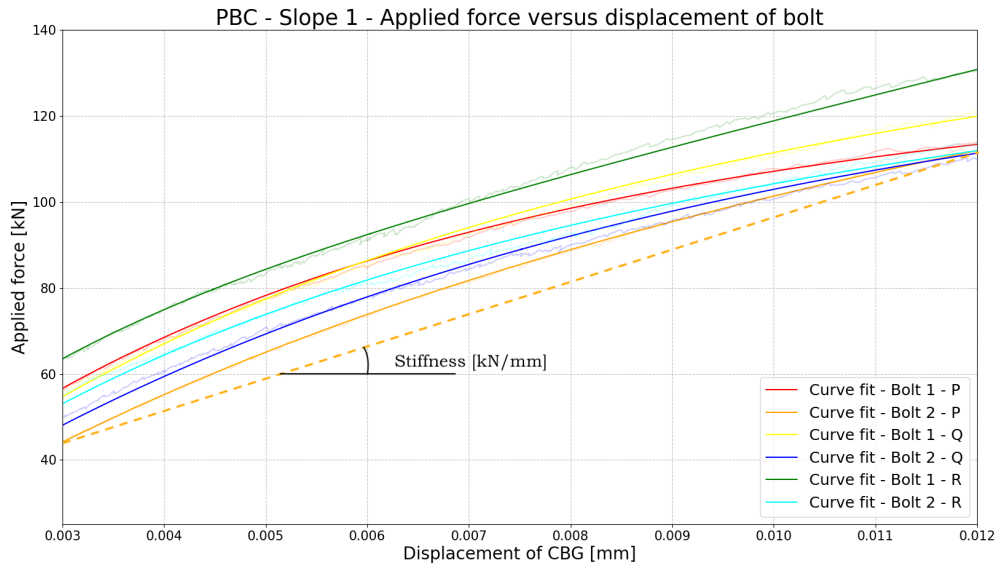


**Figure 63:** PBC - Curve-fit for obtaining the stiffness of each bolt

From this optimisation of the load-displacement curve, the **averaged** stiffness obtained from the experiments is approximately **7000 kN/mm**. However, a sidenote to this approach is that the stiffness at each region differs due to its exponential behaviour. When assuming a comparison within the same region, the stiffness from the SIROCO research is as follows [59]. Within this comparison, two series are considered. Both series adopt the prescribed design from Annex G of the EN1090-2. This design uses 2x M20 bolts. Compared to this research' design, only one M16 bolt is used per connection. By comparing the obtained stiffness in this region with the obtained stiffness from both SIROCO tests, insights can be gained into the affecting parameters on the stiffness of preloaded connections.

To compare the obtained stiffness with available literature, the stiffness within the specific region is determined for two other types of connections. Figure 64 shows the three described series. The red graphs are the results of this current research. The blue line represents series A of the SIROCO research. These lines are related to two M20 bolts with a preload force of 172kN. Within the connections are coating is applied which has a friction coefficient of 0.52. The other series (B), is shown by the orange lines. This serie differs from the previous since a lower friction coefficient is obtained, namely 0.25 instead of 0.52.

From the results shown in [Figure 64](#), the following is determined, see [Table 15](#). In the current research, the stiffness of a preloaded connection implementing a preload force of 140kN and a surface friction coefficient of 0.52, the stiffness in this specific region is **7000kN/mm**. In case the amount of bolts and their size increase from 1x M16 to 2x M20, the stiffness increases to **9750kN/mm**. Therefore, if the total normal force within a connection increases by 146 %, it does not imply that the stiffness increases with the same amount. In other words, from this, it can be stated that the stiffness of a connection is not solely affected by its normal force. Within the SIROCO project, two different surfaces are considered. The first, as described above, contains a friction coefficient of 0.52. Whereas the second results in a friction coefficient of 0.25. The stiffness of the latter within this prescribed region is **7400 kN/mm**. Therefore, besides the total preload force, the friction coefficient does not solely affect the stiffness.

**Table 15:** Obtained stiffnesses of three different types of preloaded connections. Where series 1 and 2 are adopted from the SIROCO research [\[59\]](#).

| Type of series   | Preloading force [kN] | Friction coefficient [-] | Stiffness [kN/mm] |
|------------------|-----------------------|--------------------------|-------------------|
| Current research | 140                   | 0.52                     | 7000              |
| Serie A: SIROCO  | 2x 172                | 0.52                     | 9750              |
| Serie B: SIROCO  | 2x 172                | 0.25                     | 7400              |

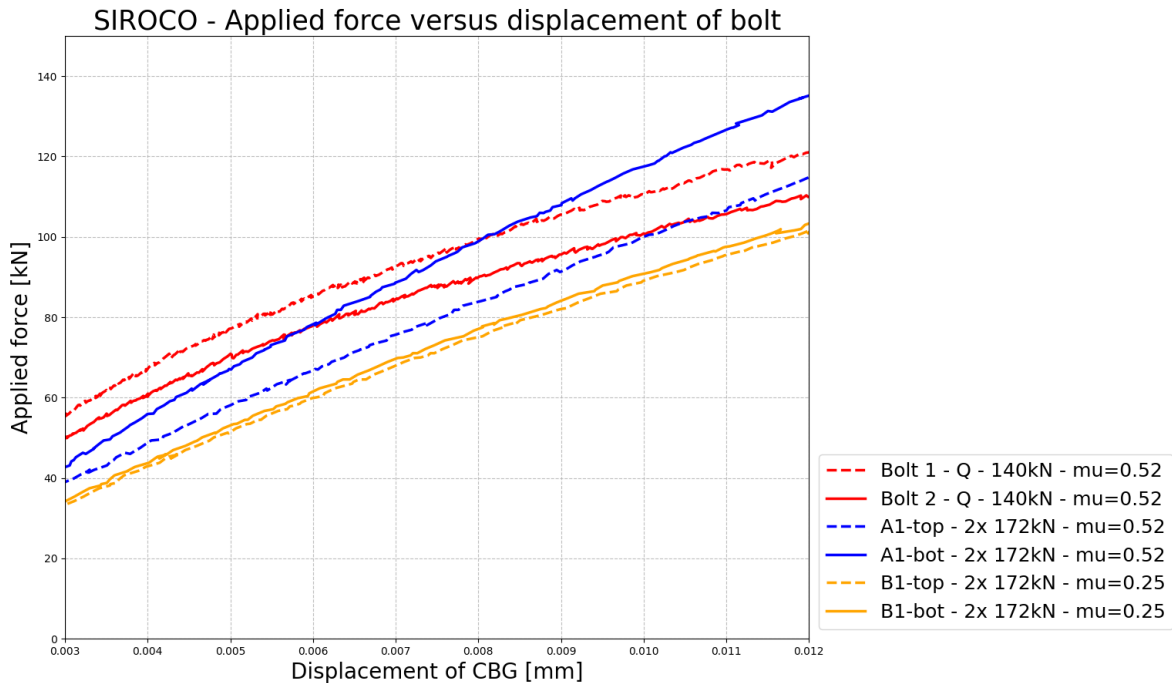


**Figure 64:** Force-displacement results within the region of 0.003 up to 0.012mm displacement at CBG. Both results from this research and output of SIROCO are used [\[59\]](#)

At a displacement of the CBG of 0.003mm, the results of the current research have a higher acting force. Therefore it can be said that until this point, the stiffness of this research' design is higher than the others. However, the resistance of this type of connection is the lowest. Namely approximately 140kN, compared to almost 340kN and 170kN for series 1 and 2 respectively. Therefore, it is expected that the surface conditions of the current research deteriorate during the experiment. This is also expected by the extreme non-linear behaviour of the load-displacement curve. In [Section 4.4](#) these statements are elaborated and discussed by experimental results.

Besides the investigation of the stiffness within this region, a different region (after slip) is considered. The additional area is considered for the comparison with preloaded and injected connections. The results for the curve-fitting procedure for this part are shown in [Table 44](#), see [Appendix E](#).

**3.8.6.2 Injected bolted connection (IBC)**

The stiffness of the resin is assumed to be a quadratic function with decreasing growth. However, in the initial phase, until 0.15mm, the stiffness is relatively stable and constant. This stiffness relates to the relative displacement at the center of the bolt group. Since the curve itself shows fluctuations, an curve-fitting is performed by Equation 15.

$$F_{\text{applied}} = B0 + B1 \cdot u_{\text{CBG}} - B2 \cdot u_{\text{CBG}}^2 \tag{15}$$

Curve-fitting the output of the experiments is done based on the displacement region of 0.03 to 0.12mm. The input parameters for this idealisation of the load-displacement curve for this injected bolted connection are shown in the appendix of this report (see Table 45 in Appendix E). From both Figure 65 and Table 45 the result is that the **average** obtained stiffness for an injection bolted connection with the applied geometry is **460 kN/mm**.

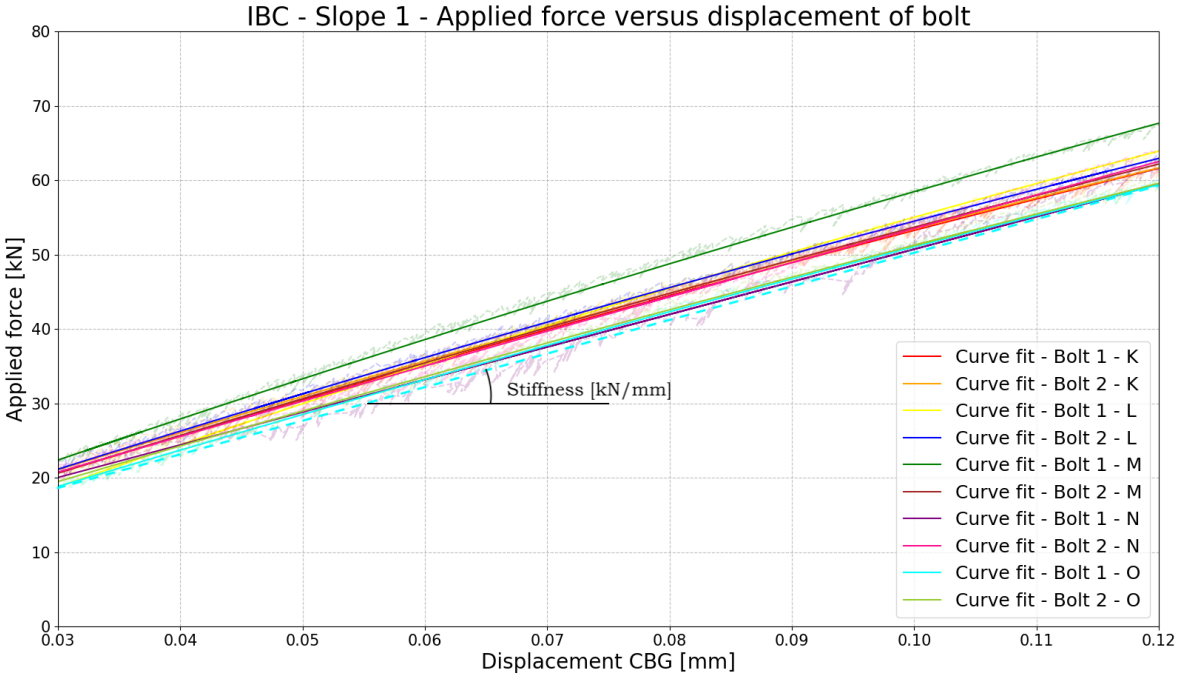


**Figure 65:** IBC: Curve-fit of the load-displacement curve for the injected bolted connection

### 3.8.6.3 Preloaded and injected bolted connection (PIBC)

To gain more insight into the build-up of the resistance of a preloaded injected connection, two regions are taken into consideration. These regions represent the stiffness of Zone 1 and Zone 2. Where zone 1 refers to the region from 0.003 to 0.012mm displacement at CBG. This zone is dominantly influenced by the stiffness of preloading. The latter zone, zone 2, represents the behaviour after the activation of the resin. For this stiffness, the region between 0.12 and 0.21mm at CBG is assumed.

As mentioned, Zone 1 is dominated by preloading. Therefore, for optimisation of the load-displacement curve, an identical equation is assumed for the series of preloading only. After the curve-fitting of each connection, the solution of all parameters is shown in Table 47. The corresponding curves are visualised in Figure 66.

$$F_{\text{applied}} = C0 + C1 \cdot u_{\text{CBG}} - C2 \cdot \exp(-C3 \cdot u_{\text{CBG}})$$

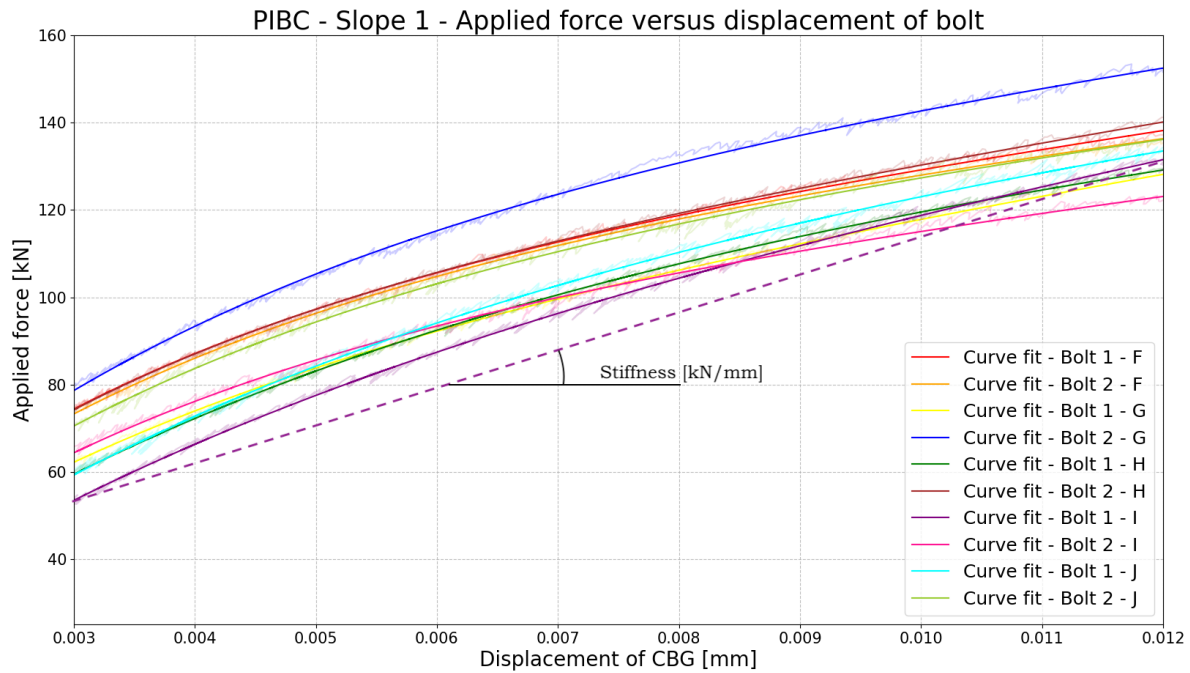


**Figure 66:** PIBC - Slope 1: Curve-fit of the load-displacement curve for a preloaded and injected connection within the range 0.003 to 0.012mm

Within the region of 0.003 to 0.012mm the average stiffness of all specimens turns out to be **7950kN/mm**. Compared to the stiffness of only applying a preload force, the stiffness of such a connection is more than 900kN/mm lower than the identified stiffness of both preloading and injection. It is most likely that the stiffness of the resin can be added since the resin is present. If the stiffness of the injected bolted connections will be added, then extrapolation is required. After extrapolation, this stiffness turns out to be approximately 460kN/mm. Adding this to 7000kN/mm gives a stiffness of approximately 7500kN/mm. The result is that the summation of stiffness from both preloading and injection is 450kN/mm lower than the obtained stiffness of a preloaded injected bolted connection. This is a difference of 6%.

For the second slope, the corresponding region follows the displacement from 0.12 to 0.21mm. According to the idealisation parameters, shown in Table 48 and Figure 67, the obtained stiffness is 150 kN/mm. When again adding the individual stiffnesses within this region of preloading and injection, the expected stiffness is 250kN/mm. Therefore, the experiments show a 40% lower stiffness than nominally expected. If the determined stiffness is compared to the stiffness of injection only of 350kN/mm, then a significant decrease is obtained. This decrease is the effect of the release of stiffness by preloading only. Figure 45 shows to release by a negative slope. From the literature, this significant negative slope is not expected [59] [29] [67]. One can say that such an effect can only appear if there is a significant reduction from the static to kinetic friction coefficient, when assuming that no significant difference in preload force occurs. If both coefficients are equal, the slope is expected to remain horizontal after achieving the maximum slip-resistance.

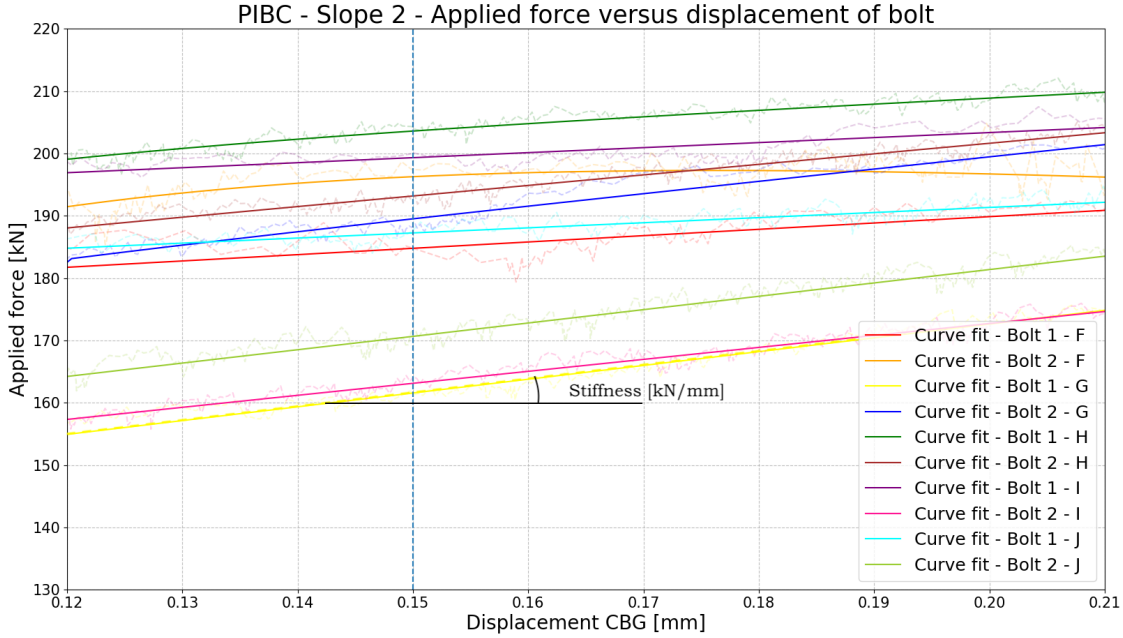


**Figure 67:** PIBC - Slope 2: Curve-fit of the load-displacement curve for a preloaded and injected connection within the range 0.12 to 0.21mm

### 3.8.6.4 Comparison of stiffnesses

From the obtained stiffnesses and resistance, the following conclusion can be drawn (Table 16). Based on the experimental results where the displacement of the CBG is measured at the edges of the plates, the stiffness of a preloaded and injected bolted connection is 7950 kN/mm. This is approximately 7 percent higher than the summation of the individual resistances. It is expected that this difference is related to the chosen region and the small amount of results. For the second slope, this difference in stiffness is 40 percent. Therefore one can say that summation of stiffnesses is not allowed. In addition, for the preloaded connection, there is a negative stiffness, since the abrupt increased slip involves a decrease in force. However, one can question if this reduction of maintained slip-resistance is also applicable to a preloaded and injected bolted connection. If this is not the case, the absolute percentage difference will even increase.

**Table 16:** Overview of obtained stiffnesses and resistances

| $F_{p,C} = 140\text{kN}$    |            |           |                      |      |
|-----------------------------|------------|-----------|----------------------|------|
|                             | Preloading | Injection | Preloading+Injection |      |
| Stiffness - slope 1 [kN/mm] | 7000       | 450       | 7950                 | 7%   |
| Stiffness - slope 2 [kN/mm] | -100       | 350       | 150                  | -40% |
| Resistance [kN]             | 144.7      | 74.7      | 187.2                | -15% |

### 3.8.7 Summation of individual resistances

Within this section, the validity of the summation of resistances is elaborated. First, the formulation of the NEN-EN1993-1-8 that allows summation of individual resistances of preloading and injection is considered [17].

Besides this, in total two different scenarios are considered. The first scenario relates to the **actual** experimental results. The second scenario contains **customised** results. This customisation relates to the preloaded bolted connection and therefore also to the calculated summation of preloading and injection. The goal of this scenario is to adapt the experimental results to the methodology of the NEN-EN1090-2 [15]. The NEN-EN1090-2 states that the resistance of a preloaded bolted connection is the maximum obtained resistance until a displacement of 0.15mm at CBG. Therefore, the assumption within this second scenario is that the experimental resistance can not decrease over time. In other words, once the maximum resistance until 0.15mm displacement at CBG is reached, it will not decrease.

#### 3.8.7.1 According to the NEN-EN1993-1-8

According to the formulation of the NEN-EN1993-1-8, it is allowed, thus considered safe, to assume that the resistance of the preloaded injected bolted connection is equal to the sum of the individual components, see Equation 16. Within this formula,  $F_{Rd,preloading+injection}$  refers to the nominal resistance of a preloaded and injection bolted connection.

$$F_{Rd,preloading+injection} = F_{s,Rd} + F_{b,Rd,resin} \quad (16)$$

Therefore, from this formula, it is expected that the outcome of the third series is equal to the sum of the acquired resistance from series 1 and 2. The table below (Table 17) shows that, based on these experiments, it is **unsafe** to allow summation of the individual resistances. It is unsafe since the outcome shows that the resistance from experiments is 15% lower than the summation of obtained resistances of both preloading and injected from experiments.

**Table 17:** Results for obtained resistances per series

| Type of series                    | Resistance [kN] | Resistance Acc. to Equation 16 [kN] |
|-----------------------------------|-----------------|-------------------------------------|
| Serie 1: Preloading only          | 144.7           | -                                   |
| Serie 2: Injection only           | 74.7            | -                                   |
| Serie 3: Preloading and injection | 187.2 (-15%)    | 219.4                               |

#### 3.8.7.2 Nominal resistances

From Table 17, it is obtained that the summation of resistances is not safe since the resistance is 15% lower than expected. Besides the experimentally obtained resistances, the nominal resistances are determined. Whereafter the individual resistances are summed and compared with the experimental results.

First, the preloaded bolted connection (PBC) is considered. In the calculation of the nominal resistances, nominal values are assumed. However, for the substituted preload force, the actual preload force is implemented. In addition, the partial safety factor is **not taken into consideration**. Based on these assumptions, the determined nominal resistance is 32.7kN lower than the experimental resistance (see Table 18). This increase of 29% is based on the increase in friction coefficient (see Table 14) and further discussed in Section 6.4.

**Table 18:** Obtained resistances from experiments when applying only preloading including comparison with average and the obtained resistance of the standard NEN-EN1993-1-8 excluding partial factors and implementing the actual applied preload force of 140kN

| PBC     | Resistance ( $F_{\max}$ ) [kN] | Diff. to nom. resistance [kN] |
|---------|--------------------------------|-------------------------------|
| P1      | 136.7                          | +24.7 (+22%)                  |
| P2      | 136.7*                         | +24.7 (+22%)                  |
| Q1      | 154.7                          | +42.7 (+38%)                  |
| Q2      | 148.0                          | +36.0 (+32%)                  |
| R1      | 153.1                          | +41.1 (+37%)                  |
| R2      | 139.3                          | +27.3 (+24%)                  |
| Average | 144.7                          | +32.7 (+29%)                  |

\* = could not obtain initial resistance anymore after slip of the other connection

The next considered connection is the injected bolted connection (IBC). In this analysis, two different bearing strength of the resin were already elaborated in [Subsection 3.8.3](#). Of these scenarios, two of them are considered again, namely the bearing strength of 187MPa and 122MPa. The latter is based on the derived formulation of the NEN-EN1993-1-8, therefore the difference to the experimental result is 0%. For the former case, when assuming a uniform stress distribution of the resin along the thickness of the plate and width of the bolt, the resistance is 40kN lower than obtained from experiments. These results are shown in [Table 19](#). In the literature, a safe short-term bearing resistance of the resin is assumed to be between 175 and 200MPa, for long-term, this value is 150MPa [29] [63]. Therefore one can say that one of the assumed values, 187MPa, is in line with the literature. However, it must be kept in mind that this is based on an incorrectly assumed uniform stress distribution in the resin. Substitution of this bearing strength in the formulation drawn by the NEN-EN1993-1-8, see [Equation 4](#), the resistance is expected to be 115kN. The evaluated resistance of this experiment is 40kN lower than the nominal resistance ( $F_{b,Rd,resin}$ ). This is a decrease of around 35 percent. However, as mentioned previously, it must be kept in mind that there is no equation given in the NEN-EN1993-1-8/NB to determine the bearing resistance of the resin.

**Table 19:** Obtained resistances from experiments when applying injection

| IBC     | Resistance ( $F_{\max}$ ) [kN] | Diff. to nom. resistance [kN] | Diff. to nom. resistance[kN]  |
|---------|--------------------------------|-------------------------------|-------------------------------|
|         |                                | $f_{b,resin} = 187\text{MPa}$ | $f_{b,resin} = 122\text{MPa}$ |
| K1      | 73.3                           | -41.3 (-36%)                  | -1.4 (-2%)                    |
| K2      | 73.1                           | -41.5 (-36%)                  | -1.6 (-2%)                    |
| L1      | 76.3                           | -38.3 (-33%)                  | 1.6 (2%)                      |
| L2      | 74.5                           | -40.1 (-35%)                  | -0.2 (0%)                     |
| M1      | 80.7                           | -33.9 (-30%)                  | 6 (8%)                        |
| M2      | 74.8                           | -39.8 (-35%)                  | 0.1 (0%)                      |
| N1      | 73.5                           | -41.1 (-36%)                  | -1.2 (-2%)                    |
| N2      | 76.8                           | -37.8 (-33%)                  | 2.1 (3%)                      |
| O1      | 71.8                           | -42.8 (-37%)                  | -2.9 (-4%)                    |
| O2      | 72                             | -42.6 (-37%)                  | -2.7 (-4%)                    |
| Average | 74.7                           | -39.9 (-35%)                  | -0.03 (0%)                    |

According to the NEN-EN1993-1-8 [17], the nominal resistance of a preloaded and injected bolted connection is equal to the summation of individual obtained resistances of preloading and injection. In [Table 20](#), an overview of results is shown where distinguishment is made between the maximum experimental resistance of the connection and the difference to the nominal resistance for both considered bearing strengths (excluding partial safety factors). For the determination of the slip-resistance, the actual preload force is implemented. These results are in line with the shown results in [Table 18](#).

In the case of an assumed bearing strength of 187MPa, the summation of individual resistances is 40kN higher than the obtained results from experiments. For the other scenario, where the nominal resistance is equal to the obtained resistance from experiments ( $f_{b,resin}=122\text{MPa}$ ), the summation is similar to the obtained experimental resistance with a difference of 0.16kN.

**Table 20:** Obtained resistances from experiments when applying both injection and preloading

| IBC     | Resistance ( $F_{max}$ ) [kN] | Diff. to nom. resistance [kN]<br>( $f_{b,resin} = 187\text{MPa}$ ) | Diff. to nom. resistance [kN]<br>( $f_{b,resin} = 122\text{MPa}$ ) |
|---------|-------------------------------|--|--|
| F1      | 189.3                         | -37.4 (-16%)   | +2.2 (1%)  |
| F2      | 198.7                         | -27.9 (-12%)   | +11.7 (6%)   |
| G1      | 161.9                         | -64.7 (-29%)   | -25.1 (-13%)   |
| G2      | 197.0                         | -29.6 (-13%)   | +10.0 (5%)   |
| H1      | 205.1                         | -21.5 (-9%)  | +18.1 (10%)  |
| H2      | 194.2                         | -32.4 (-14%)   | +7.2 (4%)  |
| I1      | 201.0                         | -25.6 (-11%)   | +14 (7%)   |
| I2      | 164.4                         | -62.2 (-27%)   | -22.6 (-12%)   |
| J1      | 188.0                         | -38.7 (-17%)   | +0.9 (1%)  |
| J2      | 172.2                         | -54.4 (-24%)   | -14.8 (-8%)  |
| Average | 187.2                         | -39.44 (-17%)  | 0.16 (0%)  |

From the three tables above (Table 18, Table 19 and Table 20), the resistances are summarised in Table 21. Based on the intermediate results, the obtained resistance of preloading exceeds the nominal resistance by 29%. While the injected connection falls short with 35% or is equal to the obtained resistance by experiments (0%). When adding the nominal resistance of the components and comparing them with the experimental result, the resistance of a preloading injected bolted connection is calculated to be 226.6 or 186.7kN (for  $f_{b,resin}=187$  or 122MPa respectively). The latter resistance is similar to the obtained resistance from experiments. However, this does not imply that summation is safe to assume. In this case, results are similar but as the intermediate resistances already indicate, there is a significant difference in resistance from preloading. Therefore, the obtained result is not in line with the methodology of summation and is not safe.

**Table 21:** Comparison of obtained experimental resistances for three different types of connections and the related nominal resistance including partial factors. Both bearing strength of the resin of 187MPa and 112MPa are taken into consideration

| Type of series                    | Resistance [kN]   | Nominal resistance [kN] |
|-----------------------------------|-------------------|-------------------------|
| Serie 1: Preloading only          | 144.7 (+29%)      | 112                     |
| Serie 2: Injection only           | 74.7 (-35% / 0%)  | 114.6 / 74.7            |
| Serie 3: Preloading and injection | 187.2 (-17% / 0%) | 226.6 / 186.7           |

### 3.8.7.3 Scenario - summation during entire experiment

From the elaborated results, it is shown that the summation of the individual resistances from preloading and injection does not result in the resistance obtained from preload and injected connections. This statement uses the criterion of adopting maximum resistances within a range of 0 to 0.15mm displacement at CBG. However, the maximum obtained resistance per type of connection does not per se act simultaneously and may therefore not be representative of the summation. For instance, the maximum resistance from a preload connection acts at a different displacement at CBG, than the maximum resistance of an injected connection. Another remark to this domain at which the resistance is determined is that the behaviour, thus resistance, of a single bolt may be different beyond this 0.15mm limit than within this range of 0.15mm displacement at CBG. Especially for larger bolt groups, this behaviour at a larger displacement is of importance since activation of, preferably, all bolts is required. Therefore, the focus is laid on resistances within a larger spectrum of displacement at CBG.

Within this section, this requirement that the resistance is determined within a specific range of displacement at CBG is released, thus relaxed. The goal is to investigate any possibility of summation of the individual components. Adding the resistances implies that it is assumed that all related resistances are active at the same displacement of the center bolt group. Since experimental results are used, all single experiments are used for averaging. The con of averaging is an already mentioned issue, namely that the peak of resistance does not have to occur at the same displacement. Since averaging is performed to the force at a certain displacement, the magnitude of force may be affected. This has to be kept in mind when adapting this section's results.

From the obtained load-displacement behaviour of the preloaded bolted connections, a reduction of the slip-resistance in combination with significant slip is observed. After exceedance of the maximum slip-resistance ( $F_{s,Rd}$ ), the resistance drops. Therefore, this maximum resistance can not be maintained. According to the NEN-EN1090-2, the resistance is the maximum value within a range until 0.15mm displacement at CBG. However, this force is significantly lower at 0.15mm than this maximum resistance. Nevertheless, the NEN-EN1090-2 does not penalise such a reduction in the slip-resistance. Therefore two scenarios are considered. The difference is related to this mentioned issue. The first scenario compares the **actual** resistance of each connection. While the second scenario **customises** the resistance of the preloaded bolted connection such that is in line with the assumption of the NEN-EN1090-2. This assumption is namely based on a resistance that does not decrease since the maximum resistance is assumed.

**Scenario 1: Actual experimental results**

The first considered scenario assumes actual obtained experimental results. Figure 68 shows different outputs, where the blue, orange and green lines represent the averaged monitoring results of the experiment. The red line is the calculated summation of the blue and orange lines at each specific displacement. If this red line is located above the green line, the summation is an overestimation of the resistance of the actual connection. Until an approximated displacement at the CBG of 0.05mm, the green line shows a higher resistance than the red line. However, it is not expected that in this phase summation is allowed since this region introduces the effect of slip occurrence at the other. In addition, this behaviour is most likely related to a lower difference of location where the maximum force is obtained than having a higher resistance.

From this graph (Figure 68), it can be concluded that, besides this initial displacement, the summation is not allowed for any amount of displacement.

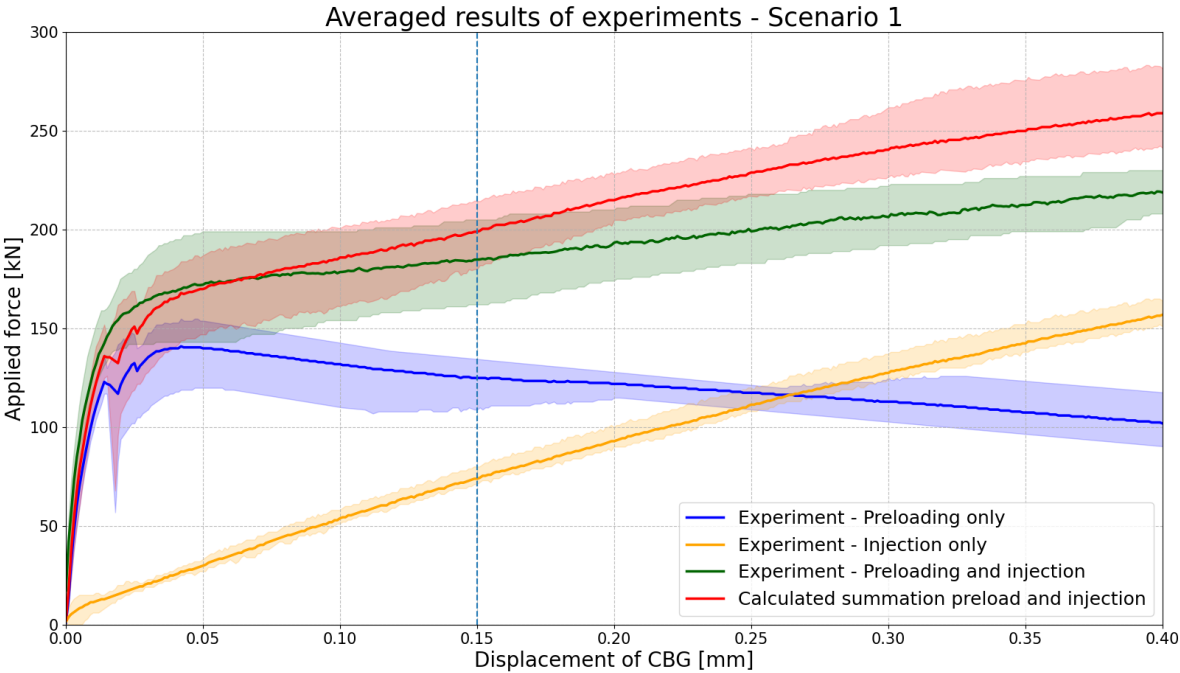


**Figure 68:** Scenario 1: Average obtained resistances per type of connection, preloaded, injected and both preloaded and injected. Transparent areas show the range of experimental results for each tested connection

**Scenario 2: Customised experimental results**

It is now assumed that the slip resistance will not decrease during the experiment. Therefore, once the maximum slip resistance is reached, it is maintained over the entire procedure. This assumption is based on the obstruction of slip by the resin in the preloaded and injected connections. Figure 69 identifies four graphs. Of these four graphs, only the blue and red line differs to Figure 68. The blue line, representing the preloaded connection, remains horizontal after reaching its maximum resistance. Therefore, the red line increases resistance compared to scenario 1. Both scenarios are however identical until this peak in resistance takes place.

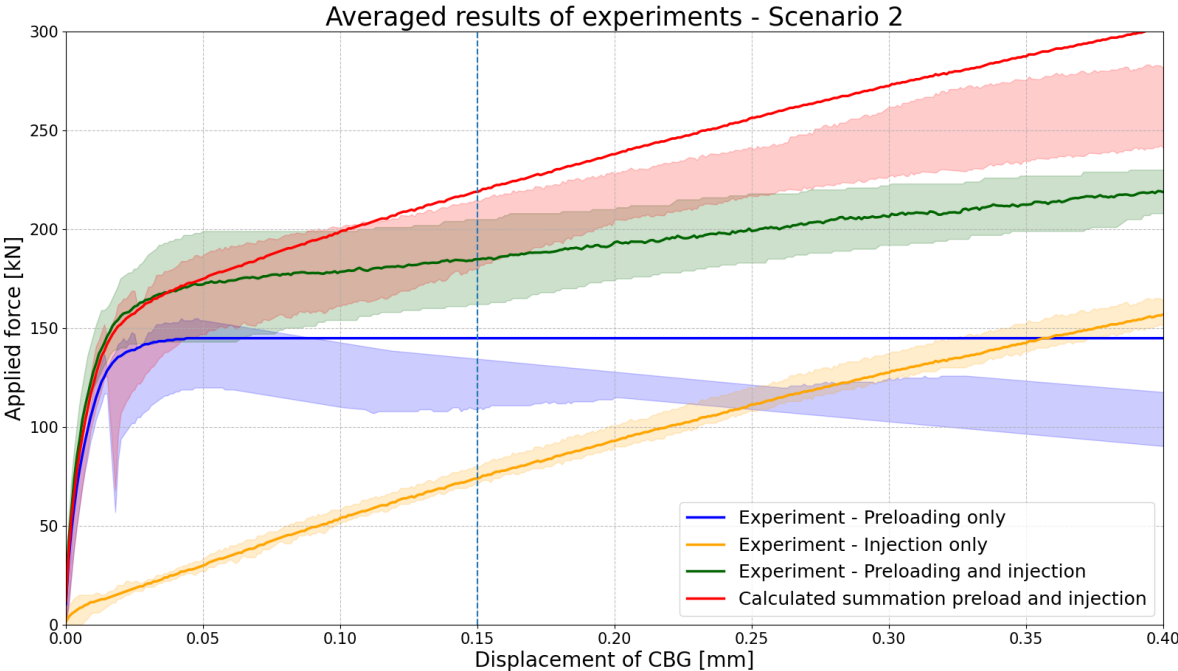


**Figure 69:** Scenario 2: Average obtained resistances per type of connection, preloaded, injected and both preloaded and injected. Transparent areas show the range of experimental results for each tested connection

# 4

## Numerical verification

### 4.1 Introduction

In this research, a numerical model is made iteratively to represent the experiments. This model aims to both verify the experimental outcomes and investigate the behaviour of the connection in depth. Implemented geometries and properties correspond with the values in experimental research, as elaborated in [Chapter 3](#). However, at some points, simplifications are made to reduce computational time where results are in agreement with the experimental results. These are elaborated throughout this chapter.

The goal of this analysis is to gain insight into the behaviour of the connection and verify experimental results. In total three different models are analysed:

- Model 1: Preloaded bolted connection (PBC);
- Model 2: Injected bolted connection (IBC);
- Model 3: Preloaded and injected bolted connections (PIBC);

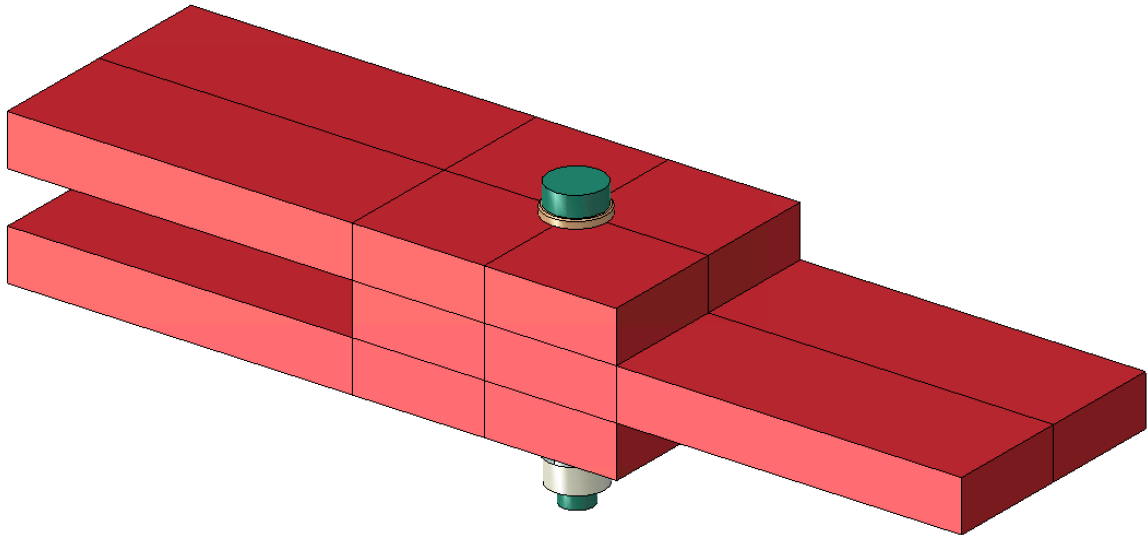
During the process, the model is validated with experimental results and optimisation took place to mimic reality and expectations. To achieve this goal, the software of the Dassault Systems company named ABAQUS/Explicit 2021 is used. The explicit version of ABAQUS is required due to the limitations of the standard version. In the following sections, assumptions are elaborated more extensively.

## 4.2 Design

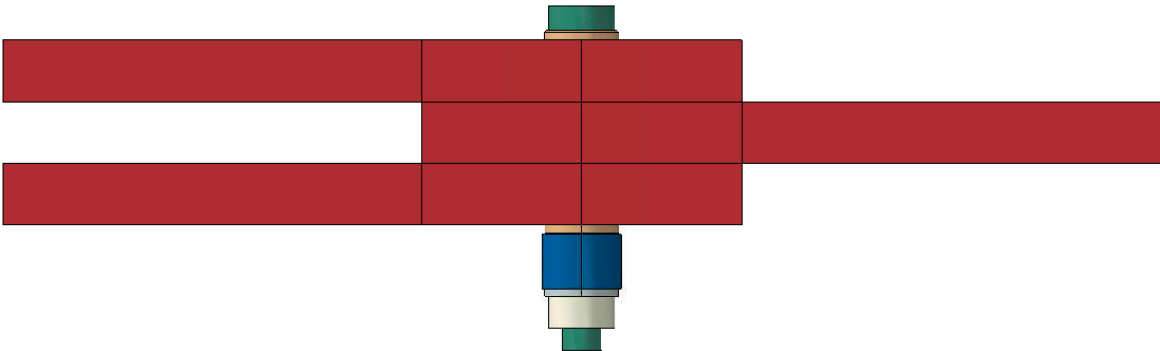
### 4.2.1 Geometry

In each experiment, one specimen is tested. This specimen consists of two connections, containing one M16 bolt each. As this setup is symmetrical, the numerical model only considers one connection, as visualised in [Figure 70a](#) and [Figure 70b](#). This simplification of the specimen is assumed since a difference within the symmetrical part is not expected.

To connect the plates, an M16 bolt is modelled. This assembly consists of the same components as the experimental setup, namely: a bolt, two chamfered washers, one spacer, a plain washer and a nut. Whereby both nut and bolt are modelled without threads to reduce computational time. Also, the local behaviour of the nut-bolt interaction is not expected to influence the results. The dimensions of the components within the assembly are in accordance with the specified dimensions in [Figure 30](#).



(a) 3D-view of the numerical model



(b) Side-view of the considered numerical model.

**Figure 70:** Different perspectives of the ABAQUS model

### 4.2.2 Material properties

Within the ABAQUS model, material properties are adopted from both literature and experimental results. To start with the steel middle and side plates. One of the requirements of the plates' geometry is that these may not influence the experimental results by for instance bearing deformations. Particular failure mechanisms are elaborated such that with nominal values for S355 steel, influence can safely be disregarded. In addition, experiments to obtain material properties for steel are not executed. Therefore, nominal values are assumed within the model. In total three aspects are taken into consideration: density, elasticity and plasticity. As a density, the value of  $7.85\text{E-}09$  is assumed. As Young's modulus,  $210.000\text{MPa}$  was adopted with a Poisson ratio of  $0.3$ . For plasticity, a bi-linear behaviour is assumed where plastic strains start arising at a stress of  $355\text{MPa}$ . The rupture of the steel will take place at a stress level of  $490\text{MPa}$  with a strain of  $0.2$ .

In the stage of preloading, the spacer is subjected to an elevated temperature. The expansion effect of this temperature increase with respect to its volume depends on the thermal coefficient in each of the three directions (x, y and z, see [Paragraph 4.2.4.2](#)). Since expansion with a rising temperature is restricted in the preferred direction only, all other directions are excluded due to an applied thermal coefficient of zero for those directions. In the longitudinal axis of the bolt, a thermal coefficient of  $0.001$  is inserted. This coefficient is not the actual thermal expansion coefficient of steel, but an assumed value instead since only the coefficient between elevation in temperature and this ratio is important, see [Paragraph 4.2.4.2](#). Besides these additional material properties, the spacer does not involve different characteristics in addition to those described above for the steel plates.

For the bolt assembly (including nut and washers), density, elastic and plastic properties are implemented. The bolt has an increased yielding strength of  $900\text{MPa}$  and an ultimate strength of  $1232\text{MPa}$ . The latter value is based on the experiments as shown in [Figure 32](#). Since the preloading of the bolt is applied by expanding an external component, no additional properties are involved.

The resin properties are based on the available literature. In one of the most recent documents, which includes numerical analyses, the adopted parameters are reported [\[49\]](#). In [Paragraph 2.5.2.1](#), the background of these values is elaborated. Within the numerical model, the resin has a Young's Modulus of  $5640\text{MPa}$  and a Poisson factor of  $0.315$  [\[49\]](#). The density of the resin is set at a value of  $1.8\text{E-}06$  [\[49\]](#). Besides these parameters, the Drucker-Prager model and its hardening characteristics are taken into consideration. These are given in [Appendix F](#) [\[49\]](#). The values above are related to the associated and unconfined properties of the resin. The associated parameters are assumed due to a significantly lower chance of divergence. Whereas the unconfined properties are assumed since it is expected that implementing confined conditions overestimates the behaviour. In addition, the bolt is enclosed by the resin which is enclosed by the plate. Therefore one can consider the resin to be positioned in a confined condition. Assuming confined properties will therefore overestimate transverse support. This results in the choice to implement unconfined conditions.

### 4.2.3 Boundary conditions

In the numerical model, the boundary conditions are applied for two main reasons. Firstly, these conditions are used at both ends of the model such that the loading can be applied. Secondly, where required, additional boundary conditions are applied within certain loading steps to improve the behaviour of the model and thus reliability.

#### 4.2.3.1 At both ends of the specimen

To take the effect of symmetry into account, specific conditions are applied. In addition to these properties, the Poisson effect at the end is neglected, since the “encastre” conditions are applied. In other words, all displacements and rotations are restrained at both ends of the specimen. In [Table 22](#), the properties of the two possible assumptions are shown. Of these options, the encastre is implemented.

**Table 22:** Properties for two different boundary conditions

| Name              | U1 | U2 | U3 | R1 | R2 | R3 |
|-------------------|----|----|----|----|----|----|
| <i>X-symmetry</i> | 0  | -  | -  | -  | 0  | 0  |
| <i>Encastre</i>   | 0  | 0  | 0  | 0  | 0  | 0  |

#### 4.2.3.2 Top and bottom of the spacer

Within the experiments, a spacer is adopted into the bolt assembly to create a neutral zone for the strain gauges. Besides this, the spacer has another advantage. Within the numerical analysis, the spacer is used to apply the preloading force in the bolt assembly. [Paragraph 4.2.4.2](#) elaborates this procedure of preloading.

However, during the verification of the model, it turned out that the spacer was moving horizontally in the longitudinal direction of the specimen during the preloading phase. Even since this had a minimal effect on the results, additional boundary conditions are applied at the top and bottom of the spacer during the preloading load step only. After completion of this phase, the applied boundary conditions are deactivated. In [Table 23](#), the boundary conditions for both the top and bottom surfaces of the spacer are shown.

**Table 23:** Applied boundary conditions on the top and bottom surfaces of the spacer. This boundary condition is only activated in the preloading load step

| Name               | U1 | U2 | U3 | R1 | R2 | R3 |
|--------------------|----|----|----|----|----|----|
| <i>BC - Spacer</i> | -  | 0  | 0  | -  | -  | -  |

#### 4.2.4 Loading steps

Within ABAQUS, performing analyses requires the programming of the loading sequence. Adding loading steps provides availability for different stages of procedures. In the applications of preloading only and both preloading and injection, activating a normal force in the bolt is required before excitation. The first load step is called the “initial phase” where the model is produced. The goal of the second step is to apply a small load such that parts are already connected. The following step relates to the application of the preload force. Whereby the third loading step is to activate the displacement by the testing rig. [Table 24](#) shows the duration of different load steps. In the series where the bolts are only injected, the second load step (preloading) is suppressed.

**Table 24:** Overview of the duration and sequence of the different load steps

|                     | $t_{\text{start}}$ [s] | $t_{\text{end}}$ [s] | <b>Duration</b> [s] |
|---------------------|------------------------|----------------------|---------------------|
| <i>Initial step</i> | 0                      | 0                    | -                   |
| <i>Calibration</i>  | 0                      | 1                    | 1                   |
| <i>Preloading</i>   | 1                      | 4                    | 3                   |
| <i>Excitation</i>   | 4                      | 12                   | 8                   |

##### 4.2.4.1 Calibration

Calibration is implemented during the optimisation of the model. The goal is to let the meshes of plate, resin and bolt already make contact with each other by a small amount of bearing before the actual experiment starts. In this way, the connection of meshes, which initiates additional and overestimated displacements, does not have to find equilibrium during the excitation phase. The bearing of these associated parts is activated by applying a displacement of 0.02mm. Since the reaction force of this displacement is just above 4kN, the goal is expected to be achieved. Whereby assumed is that no negative effects to the meshes are involved.

#### 4.2.4.2 Preloading

Two of the investigated models require an applied preloading force. In the ABAQUS/Standard application, a pre-programmed function called “Bolt load” is available to apply axial forces in cross-sections to mimic the preloaded force. However, this command is implementable in the standard version only whilst ABAQUS/Explicit is adopted in this numerical analysis due to the complexity of the model. Therefore, the following alternative methods for preloading of bolts are explored:

1. External force;
2. Elongation of any member of the bolt assembly (except bolt) by temperature;
3. Contraction of the bolt itself by temperature;

The application of an external force is not an option since the combination of tensile stresses in the bolt and clamping of the package can not be created by an external force since the nut and bolt are rigidly connected. Therefore, approaches two and three are considered. Qin et al use a differential of temperature within members to create axial loads [56]. Their goal was to apply a clamping force in a band joint. This clamping force was introduced by an elevating temperature when assuming a positive thermal coefficient ( $\alpha_t$ ). Because of this thermal coefficient, the volume starts expanding which clamps intermediate components. The result is that the stresses in bolts change when subjected to different temperatures [31].

Within ABAQUS/Explicit, the arising strains obtained from in- or decreasing temperatures are determined by Equation 17.

$$\varepsilon_{th} = \alpha(\vartheta, f_b)(\vartheta - \vartheta^0) - \alpha(\vartheta^I, f_b^I)(\vartheta^I - \vartheta^0) \quad (17)$$

With:

$$\begin{aligned} \varepsilon_{th} &= \text{Strains from varying temperature [-]} \\ \alpha(\vartheta, f_b) &= \text{Thermal coefficient at reference temperature [1/Celsius] or [1/K]} \\ \alpha(\vartheta^I, f_b^I) &= \text{Thermal coefficient at lowered or elevated temperature [1/Celsius] or [1/K]} \\ \vartheta &= \text{Temperature at point of interest [Celsius] or [K]} \end{aligned}$$

The main assumption made in this current research is that there is a maintained linear relationship between temperature and strains. Therefore, Equation 17 can be simplified as Equation 18.

$$\varepsilon_{th} = \alpha \cdot (T - T_0) \quad (18)$$

In practice, these strains are the result of preloading of the bolt. Therefore, the strains obtained from a difference in temperature and obtained from preloading can be equated as Equation 19 [56]. This is valid for a rigid member without any change in geometry and with constant material properties.

$$F = \alpha_t \cdot E \cdot A \cdot \Delta T \quad (19)$$

After verification of both methods for shrinkage of the bolt and expansion of the spacer, the preload force is introduced by the latter. Even since bolt properties and behaviour are not influenced by the decrease in temperature, it is not favourable to apply temperature loadings to the bolt.

To apply a preloading force in the bolt, the spacer increases in length when the internal temperature increases. This relationship of expansion and temperature increase is given by Equation 17. Since the initial preload force in all specimens is approximately 140 kN, the spacers must introduce an expansion which results in this preload force.

If it is assumed that the stiffness of the clamping package is infinitely large, the elongation of the spacer is equal to the elongation of the bolt. However, due to this impaired stiffness of the clamping package, the expansion of the spacer is larger than the required value for introducing a normal force in the bolt of 140 kN only. To combine the required elongation, [Equation 20](#) is used:

$$\Delta L_{\text{spacer}} = \Delta L_{\text{bolt,required}} + \Delta L_{\text{plates}} \quad (20)$$

The first parameter is the required elongation of the bolt to create a preload force of 140kN. Assumed is that the elongation is only initiated over the distance of the bottom of the bolt head until the top of the nut. This length is 108mm. The diameter of the bolt is 16mm over this entire length since threads are not modelled. Therefore, to create a preload force of 140 kN, the elongation of the bolt is 0.358mm:

$$\Delta L_{\text{bolt,required}} = \frac{F_{p,C}L}{EA} = \frac{140000 \cdot 108}{210000 \cdot 201} = 0.358\text{mm}$$

The stiffness of the clamping package primarily depends on the stiffness created by the plates. Some of this expansion created by the spacer affects the contraction of the plates. The amount of contraction can be determined by [Equation 21](#), investigated by Nassar [43].

$$\Delta L_{\text{plates}} = \frac{2F_{p,C}}{\pi E \tan \alpha} \left[ \frac{1}{d} \left[ \left( \frac{\gamma + 3}{D_0 + 3d} \right) \left( \frac{D_0 - d}{\gamma - 1} \right) \right] + \frac{4(L \tan \alpha - D_0 + \gamma d)}{(D_0 + 3d)(D_0 - d)} \right] \quad (21)$$

With:

|           |   |   |   |         |
|-----------|---|---|---|---------|
| $F_{p,C}$ | = | Preload force [N]   | = | 140.000 |
| $E$       | = | Young's modulus of the steel plates [MPa]                         | = | 210.000 |
| $\alpha$  | = | Angle of load transfer [degrees]                                  | = | 30      |
| $d$       | = | Diameter of the bolt [mm]   | = | 16      |
| $\gamma$  | = | Ratio between the bolt diameter and diameter of the bolt head [-] | = | 1.6875  |
| $D_0$     | = | Available width of the connection [mm]                            | = | 120     |

In the book of Mechanical Engineering Design [57] the load transfer angle is assumed to be 30 degrees to represent the stiffness of the package at best. When substituting all parameters into [Equation 21](#), the total contraction of the plates by a preload force of 140 kN is 0.058 mm.

$$\Delta L_{\text{plates}} = 0.058\text{mm}$$

This results in a total required expansion of the spacer of 0.416 mm:

$$\Delta L_{\text{spacer}} = 0.358 + 0.058 = 0.416\text{mm}$$

To increase the volume of the spacer by temperature, the expansion in all directions must be limited to a degree of freedom in the longitudinal direction of the bolt only. This is done by implementing expansion factors in the U22 (longitudinal) direction. The amount of expansion is related to the combination of the thermal coefficient and the increase in temperature. Assumed is a thermal coefficient of 0.001. This results in a temperature increase of 11.45 degrees Celsius to obtain the correct preload force. This elevation in temperature is applied by the use of "predefined fields". These fields are located on all sides of the spacer. Other adjacent members are therefore not affected by the change in temperature. Since the total analysis consists of four steps (including preloading), the temperature after elevation remains constant at 31.45 degrees. Therefore, the increase in temperature is 11.45 degrees. In [Figure 71](#) the expansion of the spacer is shown. Since the displacement is transferred to the adjacent washers, only this connected area is representable when investigating the effective displacement. The result is that the top and bottom of the spacer displaces +0.030 and -0.470mm respectively. This results in a total expansion of 0.500mm.

$$\Delta L_{\text{spacer,FEA}} = 0.030 + 0.470 = 0.500\text{mm}$$

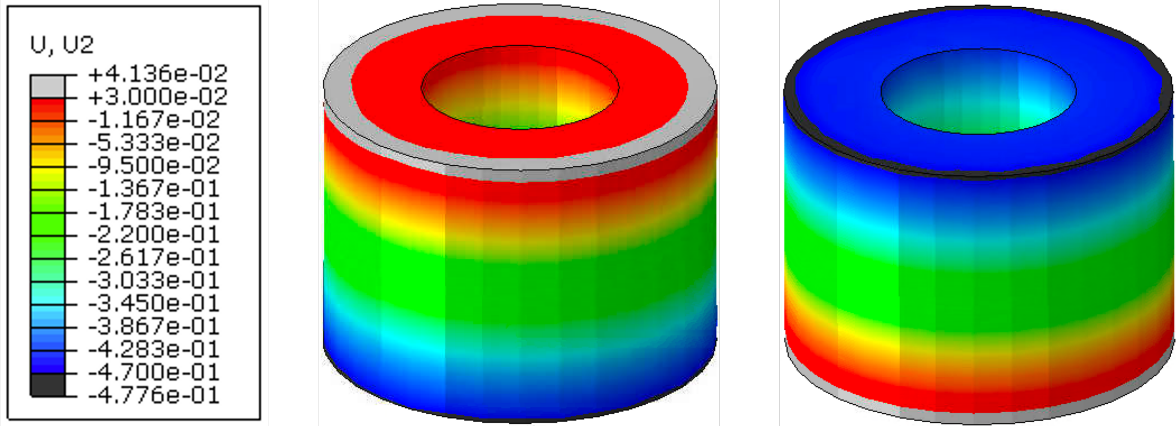


**Figure 71:** Expansion of the spacer in U2-direction (Y-direction), after the preloading load step including both top (left) and bottom (right) view of the spacer

However, according to previous calculations from Equation 20 the total elongation is expected to be 0.416mm whilst the expansion from the FEA analysis is approximately 0.500mm. This difference is due to the bending of the nut and bolt head with respect to the axis of the bolt. Since the spacer is introduced in the bolt by an eccentricity, bending occurs with respect to the longitudinal centerline of the bolt. The conclusion is that additional expansion is mandatory to accommodate the loss due to bending at both ends of the bolt.

#### 4.2.4.3 Excitation

Within this step, an increasing displacement loading is applied over a duration of eight seconds. The resistance of the model is determined similarly compared to the experiments. The maximum resistance is obtained within a range from 0 to 0.15mm at the CBG. To fulfil this requirement, the applied load is 1.0mm at the end of the load step. Since the longitudinal direction is along the x-axis, the U1 parameter is increased to 1.0mm during this loading step. Also, the loading amplitude is programmed as a “Smooth Step” similar to the preloading phase. In the next paragraph, this amplitude option is elaborated, see Paragraph 4.2.4.4.

#### 4.2.4.4 Amplitude

In ABAQUS, amplitudes are adopted into the loading step procedure to mimic loading applications. In this research, the goal of the numerical analysis is to mimic the experiment. Therefore, the loading application is preferred to be equal. When testing, the loading of the experiments has a constant increasing displacement. Therefore the displacement increases over time with a uniform distribution. However, since convergency problems occurred within the numerical analysis when assuming a linear load increment, a different approach is assumed, namely the “Smooth step”. This is a function within ABAQUS to help overcome any inertia effects. If a component with a large density is set in motion with a significant load or impact, then convergence is hard to find. This smooth step is a factorial function that is multiplied by the final load to solve convergency problems. In Figure 72, the function of the smooth step is shown. This formula is determined by Equation 22.

$$\text{Load multiplier} = A_0 + (A_1 - A_0) \cdot \xi^3 \cdot (10 - 15 \cdot \xi + 6 \cdot \xi^2) \quad (22)$$

$$\xi = \frac{t - t_0}{t_1 - t_0}$$

$A_0$  and  $A_1$  are the force multipliers at the start and end of the experiment respectively. Since the loading itself already has the preferred value, the maximum scalar value ( $A_1$ ) is 1.0. The duration of this step is equal to  $t_1$  (= eight seconds).

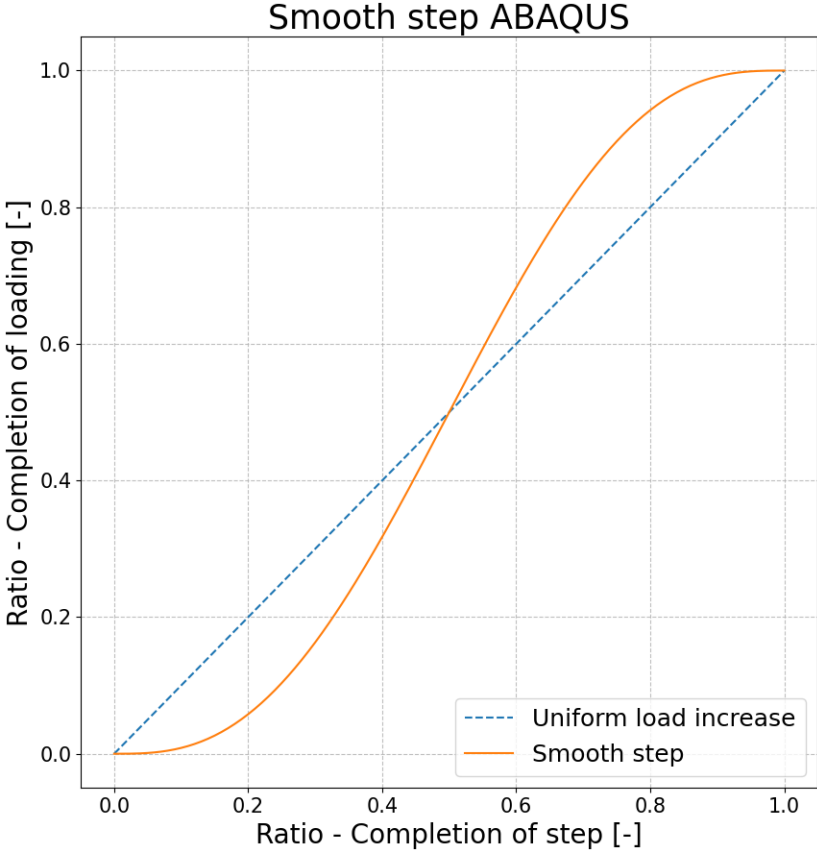


**Figure 72:** Implementation of the Smooth Step amplitude for load introduction in ABAQUS and its comparison with the tabular linear increase

In [Figure 72](#), two different graphs are shown. When applying a load by inserting a tabular consisting of a ratio from zero to one, the blue dotted line is the outcome. This graph has a linear and uniform increase in loading over time. However, the initial application of this load often introduces problems since convergency can't be found due to the inertia effects. The orange line is the smooth step function in ABAQUS. It is shown that the first couple of load steps consist of a lower load factor increase (slope) than the linear (blue) graph, thus initiating lower accelerations. Therefore, the inertia effects are lower for the case of a *Smooth step* than for the linear increase of the load over time.

#### 4.2.5 Mesh

Since the use of the Explicit version of ABAQUS is required due to the implementation of thermal expansion, the availability of meshes is limited. The shape of a mesh mostly depends on the geometry of the volumes. Within this model, simplifications are made in geometry. For example, the bolt does not contain threads or radii. The same applies to the geometry of the nut. In [Subsection 4.2.7](#), the interaction of the nut-bolt connection is elaborated since no threads are modelled.

Due to these simplifications in shape, the linear cubic mesh type, consisting of 8 nodes, is implemented. This, in combination with the Explicit method, obliges the reduced integration option. Therefore, the implemented mesh type is C3D8R. The option for reduced integration decreases the amount of integration points from the regular four to one.

The dimensions, thus the amount of meshes, influence the computational time. Therefore, the meshes outside the area of interaction are larger than meshes closer to the bolt hole. Since there is a lot of interaction at the interface with the resin, a local mesh structure is implemented. This structure has a localized mesh size of 0.5mm until the first 1mm outside the bolt hole, see [Figure 73](#).

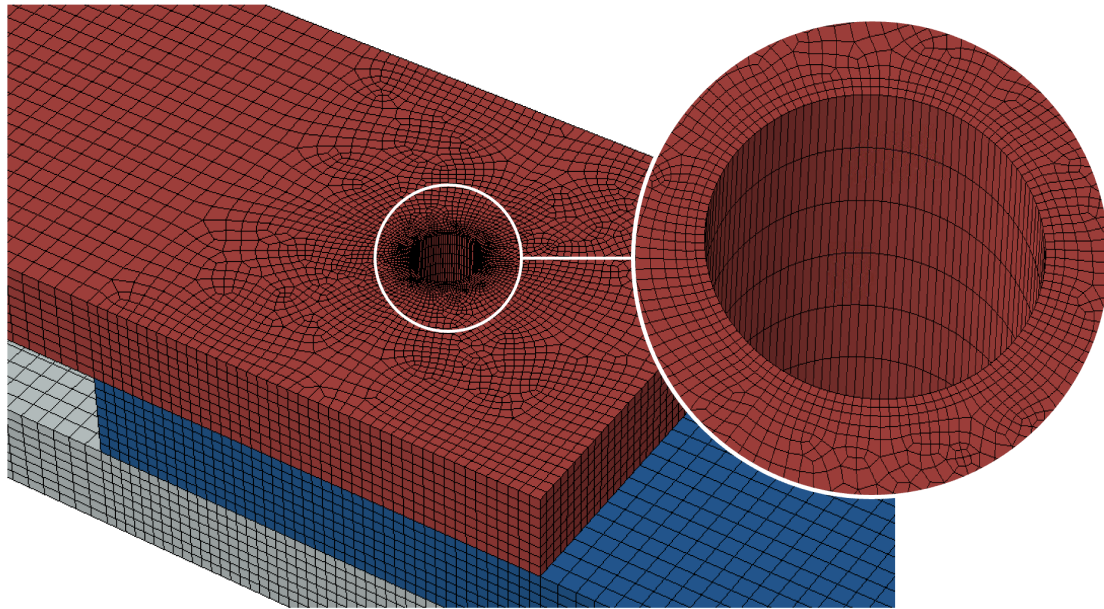


**Figure 73:** Mesh pattern of both side- and middle-plates. The closer to the bolt hole, the smaller the mesh size (up to 0.5mm)

Since the mesh sizes at the interfaces are not identical, the nodes at this interface are not connected instantly. Therefore, minimal overlapping of meshes is possible. This overlapping of meshes involves a velocity per load step. The velocity of a mesh is important since the wave speed of a material may not be exceeded. More about this is elaborated in [Subsection 4.2.6](#). If the amount of overlap does not exceed the collaborated wave speed of the material, kinetic energy is obtained from this movement. This amount of kinetic energy will be increased by the explicit solving methodology.

One of the important differences between implicit and explicit solving is that an implicit solver is unconditionally stable [53]. However, the pitfall is a less accurate option for the modelling of interactive behaviour at the shear planes compared to the explicit solver. Since the latter argument is assumed to be more important, the choice for ABAQUS/Explicit is confirmed. In the next section, the effect of the explicit solver in combination with the linear mesh is elaborated.

#### 4.2.6 Mass scaling

Due to convergency problems within the Explicit analysis after increasing the loading step and decreasing the local mesh sizes, a different solution is implemented, namely mass scaling. Scaling of the mass of an object influences the displacement capacity of the nodes. The displacement of nodes depends on the mesh and load size. When a load is too large concerning the mesh size, the deformation of a node can eventually exceed the wave speed of a material. This speed is a material property depending on two factors, Young's modulus and density. Several papers discuss the use of mass scaling and its dependent time increments [22, 3, 52]. Mass scaling is especially used in cases where the wave speed is exceeded during computation. The idea of mass scaling is reducing local densities which increases the wave speed of that particular component, see Equation 23 [1] and Equation 24. Cocchetti implies that the smallest element dimension within the model, divided by this wave speed must be larger than the time increment to prevent exceeding the wave speed [22].

$$c = \sqrt{\frac{\lambda + 2\mu}{\rho}} \quad (23)$$

$$\Delta t \leq \frac{L}{c} \quad (24)$$

Implementing these statements results in a maximum time increment ( $\Delta t$ ) of just over 1.5E-07. However, in this paper, it is noted that this approach is quite conservative. In addition to these formulas for shell elements, Cocchetti et al. also define a procedure where a volume is introduced to estimate the maximum time increment [22]. Assumed is that the smallest applied solid element has a dimension of 1 mm in all directions with a Young's modulus of 210000MPa and a Poisson ratio of 0.3. Performing all steps of this methodology results in an estimated maximum time increment of 1.32E-07.

However, such a time increment involves a significantly long computational time. Therefore, a lowered time increment is chosen. To investigate if a chosen incremental time interval is acceptable, several methodologies can be used for verification. One of them is the ratio between the kinetic and total energy. If the kinetic energy takes a high ratio of this total energy into consideration, a lower increment is preferred. In addition to this method, a comparison between the action and reaction force is made. If an increment is chosen correctly, a neglectable difference is obtained. From this procedure, the optimal time increment is assumed to be 2E-05. This decision is based on both the computational time and the reliability of the results.

#### 4.2.7 Contact interactions

In ABAQUS, the contact interaction properties can be modelled through several methods. The most used are "General contact" and "Surface-to-surface". In this model, the "Surface-to-surface" contact formulation is adopted. Within this procedure, all surfaces and their interaction must be specified. If a specific interaction is not specified, overlap of volumes will occur.

For each of these surface interactions, an interaction property is associated. Since the slip resistance at the shear planes is dependent on the friction coefficient of these planes, a normal and tangential behaviour is adopted. As normal contact, "hard contact" is assumed. For the tangential behaviour, a friction penalty is given. This penalty, or friction coefficient, is 0.52. This value is based on the obtained friction coefficient by the experiments with the used formulation according to the NEN-EN1090-2, see Table 14.

However, an important characteristic of this formulation of the friction coefficient is that a Coulomb slipping behaviour is assumed. A Coulomb friction is known as Equation 8, assuming a constant relation between the normal force ( $F_N$ ) and the slip resistance ( $F_S$ ). In Section 4.4 an elaborated view of this formulation is given.

Nevertheless, the shear planes or not the only surfaces which maintain contact with each other. As a simplification, it is assumed that all other surfaces have the same friction coefficient. Therefore all surfaces within the model that make contact over time, have the same friction coefficient of 0.52.

#### 4.2.7.1 Contact with resin

The interaction between steel surfaces is defined as described above. However, in an injected bolted connection, the resin is connected to both the bolt and plate. When assuming an interaction as described above, only the normal direction is involved in the resistance since no other interaction is defined. In the prescribed interaction above there is a consequence of an applied normal force. However, immediate shear forces are not considered. As Nijgh mentioned in his research, he assumes that the resin fails internally due to shear [50], see [Figure 74](#).



**Figure 74:** Assumed internal shear failure of resin (Nijgh [50])

Due to this observation and the obtained numerical results, additional boundary conditions and interaction properties are inserted. At first the interaction of the bolt and resin. As can be seen from [Figure 74](#), the resin almost sticks at the bolt on the top and bottom sides of the bolt. However, behind the bolt in the direction of the loading, the resin is not attached anymore which implies that the bolt and resin are not rigidly connected. To mimic this behaviour and increase the proportion of shear resistance to the total resistance against the bearing, the penalty of 0.52 is increased to 0.95 for this specific interaction.

Besides the interaction between resin and bolt, the interaction of the resin and steel plate is considered. For the numerical model, it is assumed that the resin is rigidly connected to the steel plate at the full perimeter. It was observed that if this interface is not connected, the resin "floats" in between the bolt and plate. Also for this case, [Figure 74](#) shows that the resin remains at its initial position. Therefore, it is assumed that these parts are connected rigidly. The gap only occurs behind the bolt, therefore, this interaction of the resin and the bolt is not considered to be rigidly connected.

Initially, no rigid interaction was assumed at the interface of the resin and the bolt. This reduced the resistance at 0.15mm significantly. This difference is elaborated in [Appendix G](#).

### 4.3 Results - Numerical resistance of each connection

In this section, the results of the numerical model are elaborated. This elaboration consists of the three types of connections including comparison with the experimental results. This comparison is made with the average results as shown previously by [Figure 68](#) and [Figure 69](#).

#### 4.3.1 Preloaded bolted connections (PBC)

For the connections which are preloaded only, the force-displacement graph is shown in [Figure 75](#). Within this graph, the transparent graphs are the experimental results. The maximum obtained resistance from the numerical analysis is 141kN. Whereas this resistance is almost 145kN for the experimental result. This is a decrease of 3% (see [Table 25](#)). Besides the maximum resistance, the stiffness is compared. For this determination, the same range of displacement is considered, namely from 0.003 to 0.012mm. From the numerical results, this stiffness is determined to be 7500kN/mm. Since the obtained stiffness from experiments is 7000kN/mm, the model overestimates the stiffness in this region by 7%.

**Table 25:** Numerical results of preloaded connection including comparison with obtained results from experiments

| Preloading only | Resistance | Friction coefficient [-] | Stiffness [kN/mm] |
|-----------------|------------|--------------------------|-------------------|
| Experimental    | 144.7      | 0.52                     | 7000              |
| Numerical       | 141 (-3%)  | 0.52 (0%)                | 7500 (+7%)        |

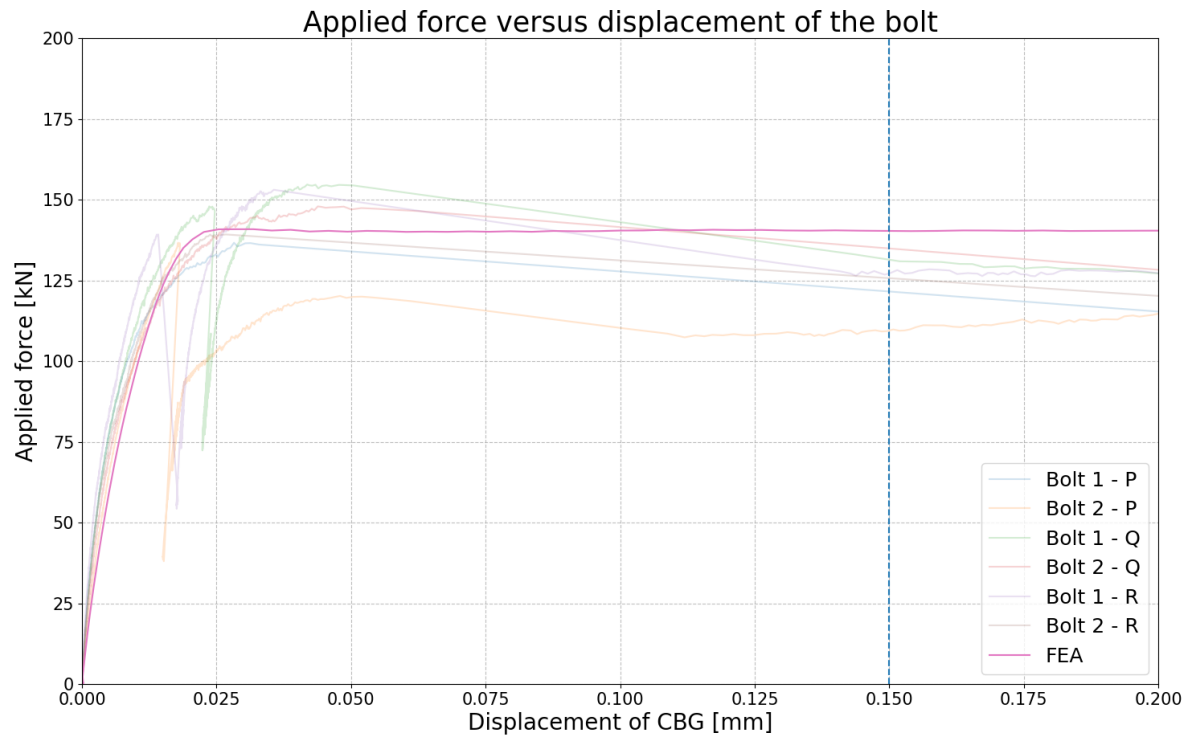


**Figure 75:** Preloading only: Numerical result of the load-displacement graph including the comparison with the experimental results

In addition to the difference in resistance and stiffness, the post-slip-behaviour shows different results. Within the experiment, the force decreases after slip, whilst within the numerical analysis this resistance remained constant. In [Appendix H](#), an elaboration is given regarding this deviation in stiffness between the numerical analysis and the obtained experimental results. Where [Section 4.4](#) elaborates the importance of the friction behaviour.

### 4.3.2 Injected bolted connections (IBC)

For the comparison of the second series, injected bolted connections (IBC), the results are shown in Table 26 and Figure 76. The maximum obtained resistance from the numerical analysis until a displacement of 0.15mm is 73.5kN. This resistance is approximately 1kN lower than the obtained resistance from experiments (74.7kN).

There is also a slight difference in stiffness between the experiment and numerical analysis. Namely an absolute difference of approximately 50kN/mm (+11%).

The difference in applied force until 0.025mm displacement is due to the hand-tightening of the bolts within the experiment.

**Table 26:** Numerical results of injected connection including comparison with obtained results from experiments

| Injection only | Resistance | Stiffness [kN/mm] |
|----------------|------------|-------------------|
| Experimental   | 74.7       | 450               |
| Numerical      | 73.5 (-2%) | 500 (+11%)        |

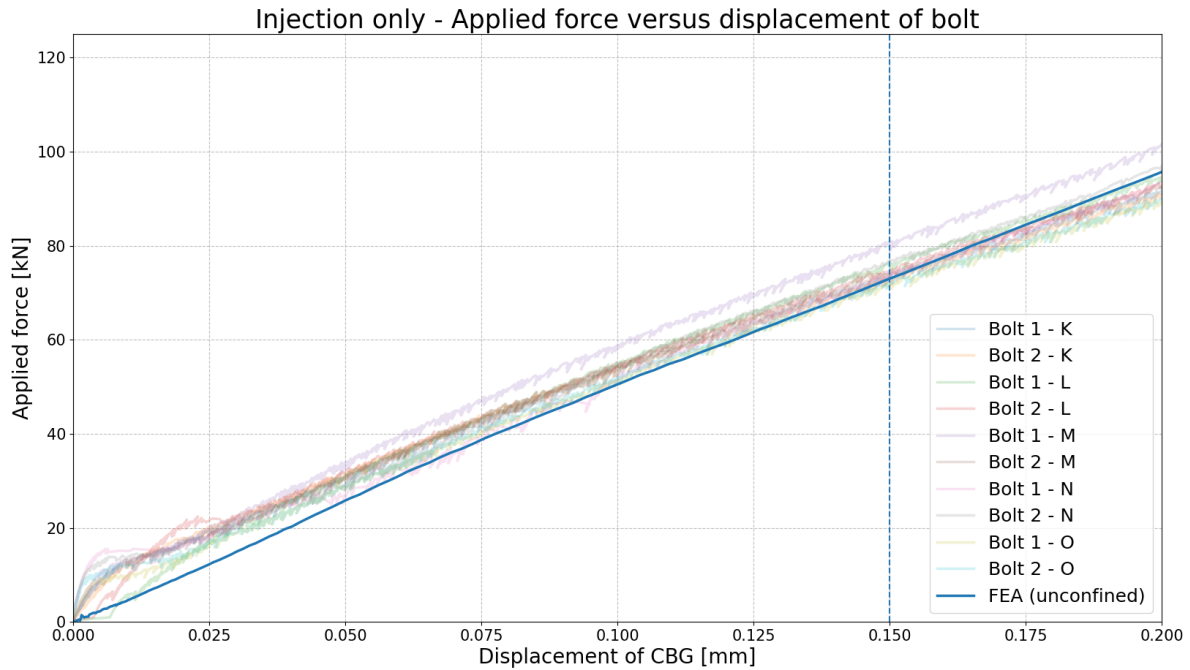


**Figure 76:** Injection only: Numerical result of the load-displacement graph including the comparison with the experimental results

### 4.3.3 Preloaded and injected bolted connections (PIBC)

In [Figure 77](#) and [Table 27](#) the results of both experiments and numerical analysis are shown. This maximum numerical resistance of a preloaded and injected bolted connection (PIBC) is 190kN. Therefore, the numerical model overestimates the average resistance by approximately +1%.

**Table 27:** Numerical results of preloaded and injected connection including comparison with obtained results from experiments

| Prel. + Inj. | Resistance [kN] | Stiffness - S1 [kN/mm] | Stiffness - S2 [kN/mm] |
|--------------|-----------------|------------------------|------------------------|
| Experimental | 187.2           | 7950                   | 150                    |
| Numerical    | 190 (+1%)       | 7950 (0%)              | 200 (+33%)             |

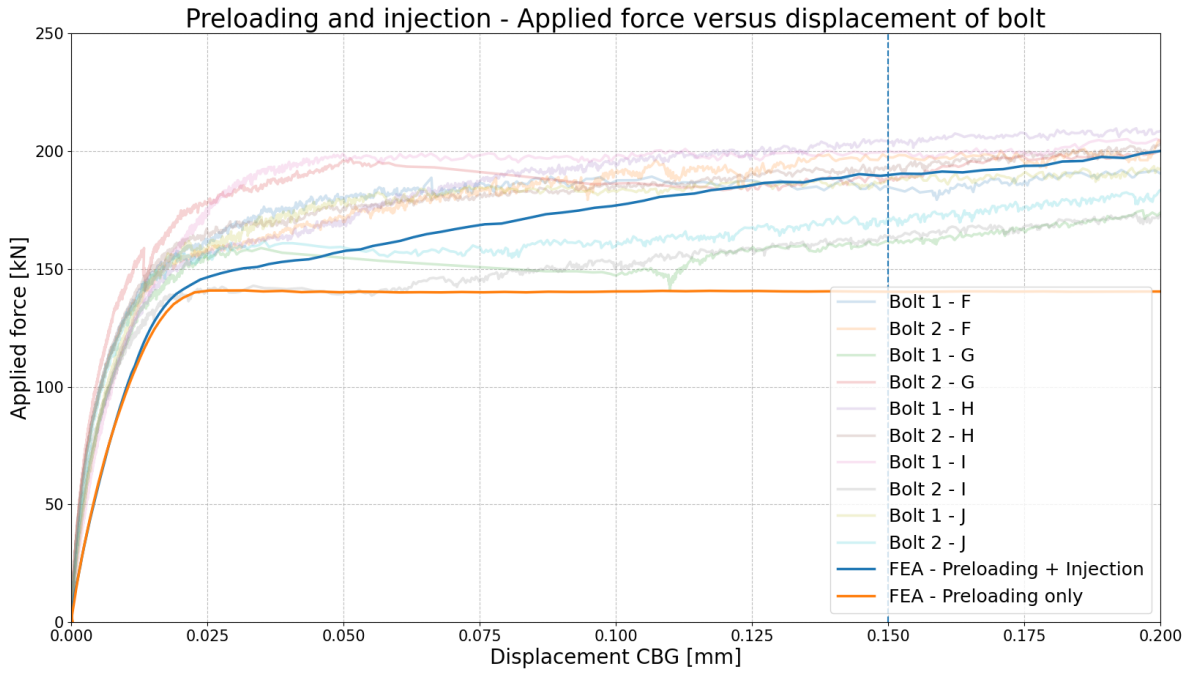


**Figure 77:** Preloading and injection: Numerical result of the load-displacement graph including the comparison with the experimental results

When looking into the stiffness of the preloaded and injected connection at the two considered slopes (Slope 1 and 2), a more significant change is observed. When considering the stiffness difference in the numerical model between a preloaded and injected and solely preloaded connection, there is a difference of 450kN/mm (+6%). This implies that for this initial phase, the injection adds a stiffness of 450kN/mm, which is similar to the obtained stiffness shown in [Table 26](#).

This similar effect was also observed from the experimental results, where the preloaded and injected connection increased stiffness compared to the connection using only preloading. This stiffness of the experiments within the implemented region is also 7950kN/mm. Similar to the obtained stiffness from the numerical model.

Nevertheless, when comparing these results with [Figure 77](#), it can be seen that the more transparent graphs are located above the finite element analysis, even if the stiffness of the numerical analysis is similar within a specific region of 0.003mm to 0.012mm. This is due to the increased stiffness before 0.003mm. In [Appendix H](#) two methods are elaborated which are thought to affect the stiffness of the numerical analysis and therefore differ from the experiment.

#### 4.3.4 Summation of individual resistances

In this section, the numerical summation of the individual components is taken into consideration. In total three different cases are elaborated. First, the potential summation according to the NEN-EN1993-1-8 is handled. Whereafter two scenarios are elaborated. These scenarios are similar to the scenarios adopted in Paragraph 3.8.7.3. This first scenario relates to the actual obtained experimental results whilst the second scenario considers customised experimental results. In the latter, the resistance of a connection does not decrease during the experiment.

##### 4.3.4.1 According to the NEN-EN1993-1-8

In Table 28, an overview is shown with the determined resistances for each serie, including the percentage difference with the individual summation of both preloading and injection. From the experiments, a decrease of 15 percent in resistance was obtained compared to the summation of these components. This was further explained in Subsection 3.8.7. From the numerical analysis, it can be seen summation is also not allowed since this difference in resistance is 11 percent. These results are obtained by the summation of the maximum resistance during a displacement period of 0.15mm.

**Table 28:** Results for obtained resistances per series including comparison of experimental and numerical results

| Type of series                    | Experiment   | Numerical analysis |
|-----------------------------------|--------------|--------------------|
| Serie 1: Preloading only          | 144.7        | 141.0              |
| Serie 2: Injection only           | 74.7         | 73.5               |
| Serie 3: Preloading and injection | 187.2 (-15%) | 190.0 (-11%)       |

#### 4.3.4.2 Scenario - summation during entire experiment

In the next subsections, two scenarios are considered. The first scenario contains **actual** experimental results. The second scenario implements **customised** results. These results are based on the statement of the NEN-EN1090-2 [15] where the resistance is determined by the maximum resistance within a certain range of displacement. Therefore, in this scenario, the resistance of each connection does not decrease during the experiment.

##### Scenario 1: Actual experimental results

In this first considered scenario, the numerical results are compared with the averaged experimental results. From this figure, it can be seen that the numerical model slightly overestimates the resistances of all individual components. However, the resistance of the injected bolted connection is underestimated until a displacement of 0.18mm. A possibility for this is due to the hand-tightening method of this connection within the experiments. Nevertheless, besides the resistance, the numerical model also overestimates the stiffness of the experiments by approximately 10%. Therefore, it does not solely depend on the tightening of the bolts. From this graph, it can be seen that for the numerical analysis, there is no displacement which allows summation of the individual components.

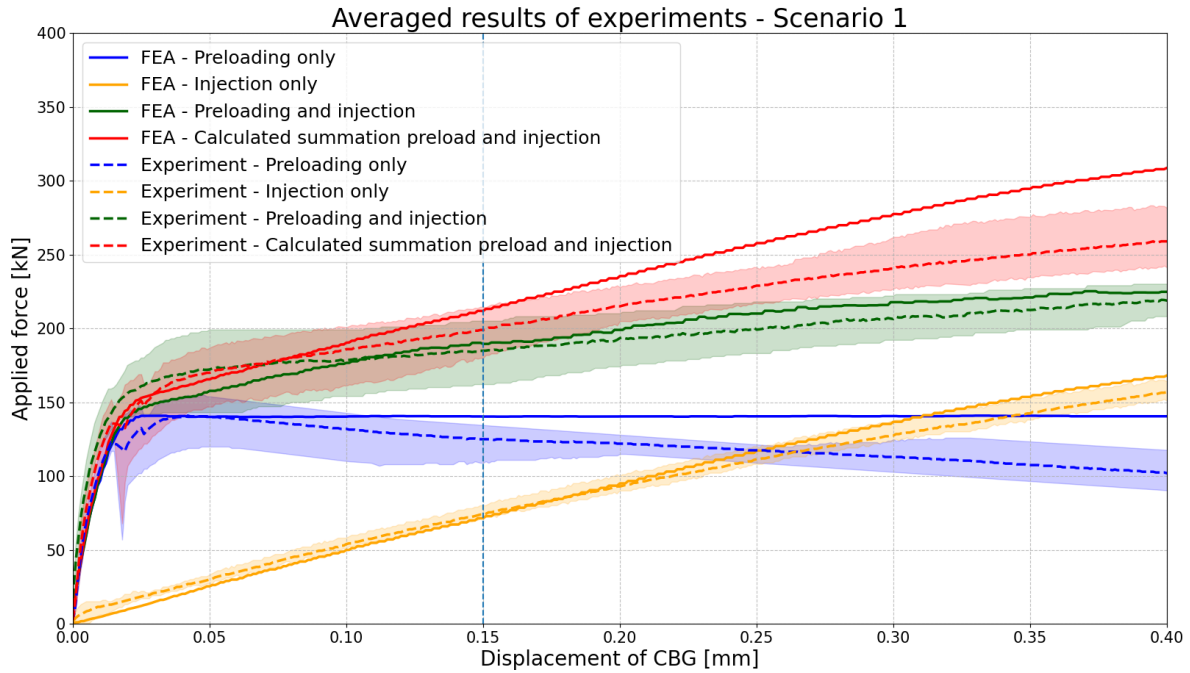


**Figure 78:** Overview of the load-displacement behaviour of different types of connections allowing a decrease in slip resistance and including averaged experimental results and numerical results. Transparent areas show the range of experimental results for each tested connection

The pitfall of the numerical model is that it underestimates the behaviour of the experiment at the transition zone from preloading to injection. The green continuous line is located below the striped green line. Both green lines represent the preloaded and injected bolted connection. Whereas the former relates to the numerical model and the latter to the averaged outcome of the experiments. However, within these experiments, significant variation within this region was obtained as well, see Figure 56. Therefore, it can be concluded that the numerical model is still located inside the area of experimental results. This area is indicated by the transparent coloured areas.

If both connections implementing preloading and injection are summed, see red line, the expected resistance is approximately 215kN. This calculated summed resistance at 0.15mm holds for both numerical and experimental results.

**Scenario 2: Customised experimental results**

The second scenario relates to the comparison with the experimental results where it is assumed that the slip-resistance does not decrease, see Figure 79. The only difference in the outcome, compared to scenario 1, are the blue and red lines representing preloading and the summation of individual values for preloading and injection. The green and orange lines do not differ.

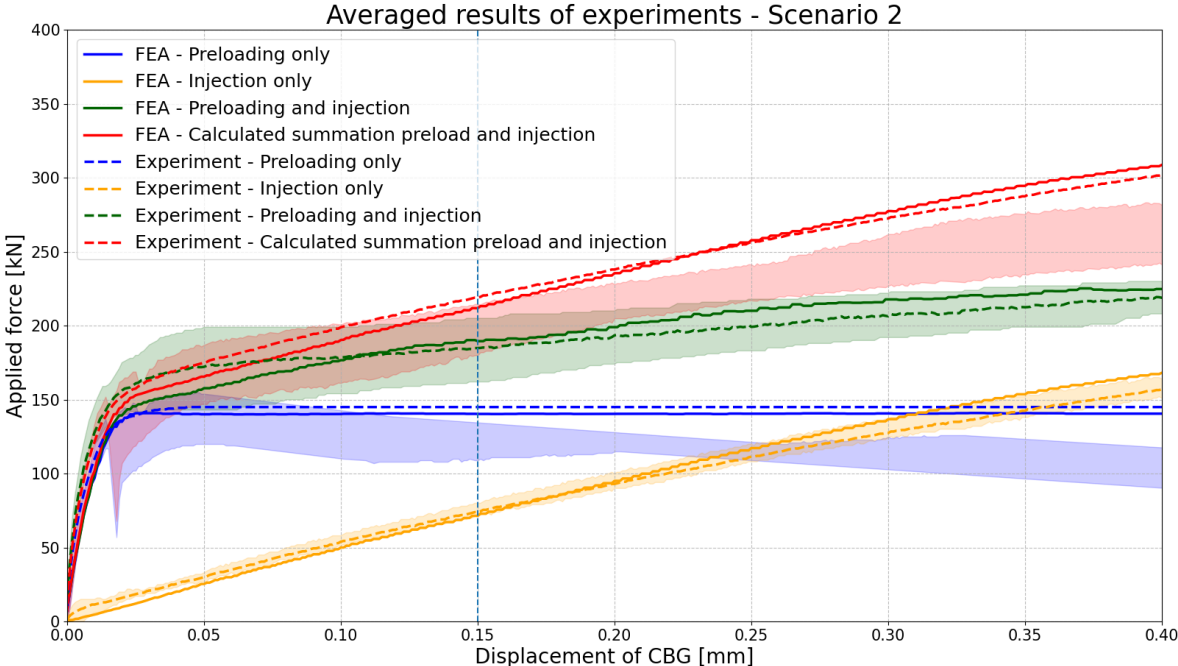


**Figure 79:** Overview of the load-displacement behaviour of different types of connections disallowing a decrease in slip resistance and including averaged experimental results and numerical results. Transparent areas show the range of experimental results for each tested connection

When looking at the difference in the preloaded connection, no significant differences are obtained. The average resistance from experiments is 144.7kN, while this resistance is 141kN for the numerical model. Both lines remain horizontal, implying that the maximum slip resistance is maintained over the entire post-slip trajectory.

Since this striped blue line (Experiment - Preloading only) increases due to the negligence of slip-resistance losses, the red striped line increases with the same amount. This results in a higher summation of individual resistance from experiments than for the numerical analysis. This is because the numerical model does not introduce a decay in slip-resistance.

## 4.4 Results - Friction coefficient

From the verification of the numerical with the experimental results, the hypothesis is drawn of a potential alternating friction behaviour. The stiffness of the experimental results shows a significant non-linear behaviour until the maximum slip resistance is reached. Comparing this with the stiffness of the numerical model, the model shows almost a linear stiffness until just before the maximum resistance. As mentioned, ABAQUS assumes a Coulomb friction (constant  $\mu$ ). To investigate any potential validity of this assumption a tribometer test is executed. Such a sliding test is used to investigate the contact behaviour of two (different) types of surfaces.

To mimic the experimented connection as much as possible, the input parameters required for the test are determined as follows. The first parameter is the normal force applied on the top specimen with an area of  $66\text{mm}^2$  ( $6 \times 11\text{mm}$ ). In the considered preloaded connection, the applied force is  $140\text{kN}$ . This force is spread over the contact surface as shown in Figure 80. Within this figure, only vertical compressive stresses are shown within the stress range of  $15$  to  $85\text{MPa}$ . The surface area containing stresses in this range is approximately  $3000\text{mm}^2$ , based on the dimensions shown in Figure 80. Assuming an equal stress distribution over this area, results in a stress of around  $45\text{MPa}$ . When taking into consideration this stress in the tribometer specimen with an area of  $66\text{mm}^2$ , the force should be almost  $3000\text{N}$ . However, the used tribometer is unfortunately limited by a normal force of  $450\text{N}$ .

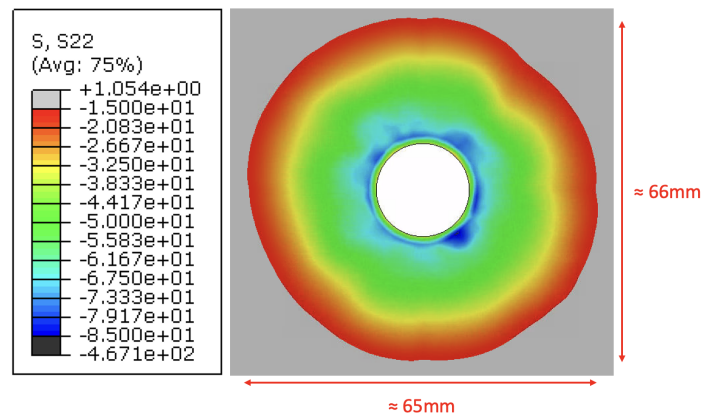


**Figure 80:** Cross-sectional view of one of the two shear planes in the numerical model showing the stresses in vertical direction S22. The visible stresses are within the compressive stress range of  $15$  to  $85\text{MPa}$

Besides the amount of normal force applied to the specimens, the amplitude and frequency are customisable. Within the used tribometer, the amplitude used for each experiment depends on the rotational angle of the screw. Therefore, unfortunately, no amplitude for each test is identical. The aimed amplitude is  $0.4\text{mm}$ , while in the experimental setup, the resistance is determined after a relative slip of  $0.15\text{mm}$ . However, when implementing this amplitude of  $0.15\text{mm}$  into the tribometer test, no reliable test results were obtained. Therefore, the amplitude is increased to  $0.4\text{mm}$  such that there is a clear difference between the micro-slip and gross-slip.

In [Table 29](#) other specifications for the experiment are shown. Where the most important parameter is the applied normal force.

**Table 29:** Test matrix for the Tribometer test

| Specimen            | Frequency [Hz] | Normal force [N] |
|---------------------|----------------|------------------|
| Specimen I          | 0.1            | 300              |
| Specimen II         | 0.1            | 300              |
| Specimen III        | 0.1            | 450              |
| Specimen IV         | 0.1            | 450              |
| Specimen V          | 0.1            | 150              |
| Specimen V - reused | 0.1            | 450              |

[Figure 81](#) indicates the damage that occurred after performing the tribometer test. On top of the bottom specimen (left), the removal of the coating due to damage is clearly visible. The top specimen (right), is pressed onto the bottom specimen with a normal force as indicated in [Table 29](#).

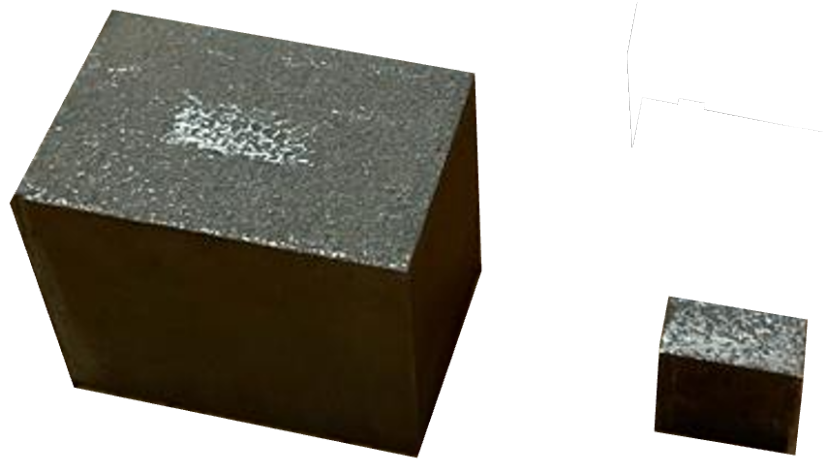


**Figure 81:** Damaged specimen (II) after performing the tribometer test

From the tests shown in [Table 29](#), [Figure 82](#) illustrates the friction force versus displacement graph of the application with 450N normal force (III, IV and V-reused). The Ethyl-Zinc-silicate interface shows a non-coulomb behaviour (example shown in [Figure 26](#)). This is identified by the peak in applied force at the end of the amplitude where the velocity is approximately zero. Therefore, one can say that for this experiment, the linear relation between the applied normal and shear force is not linear (Amonton and Coulomb's law, [Equation 8](#)). Besides the Non-Coulomb relation, a significant decay of required shear force (thus coefficient) is obtained. After almost 2 cycles, the interface is damaged in such a way that no more damage probably occurs. More or less of a steady state is created. This can be identified by the denser pattern. However, the significant difference between static and kinetic friction coefficients remains active.

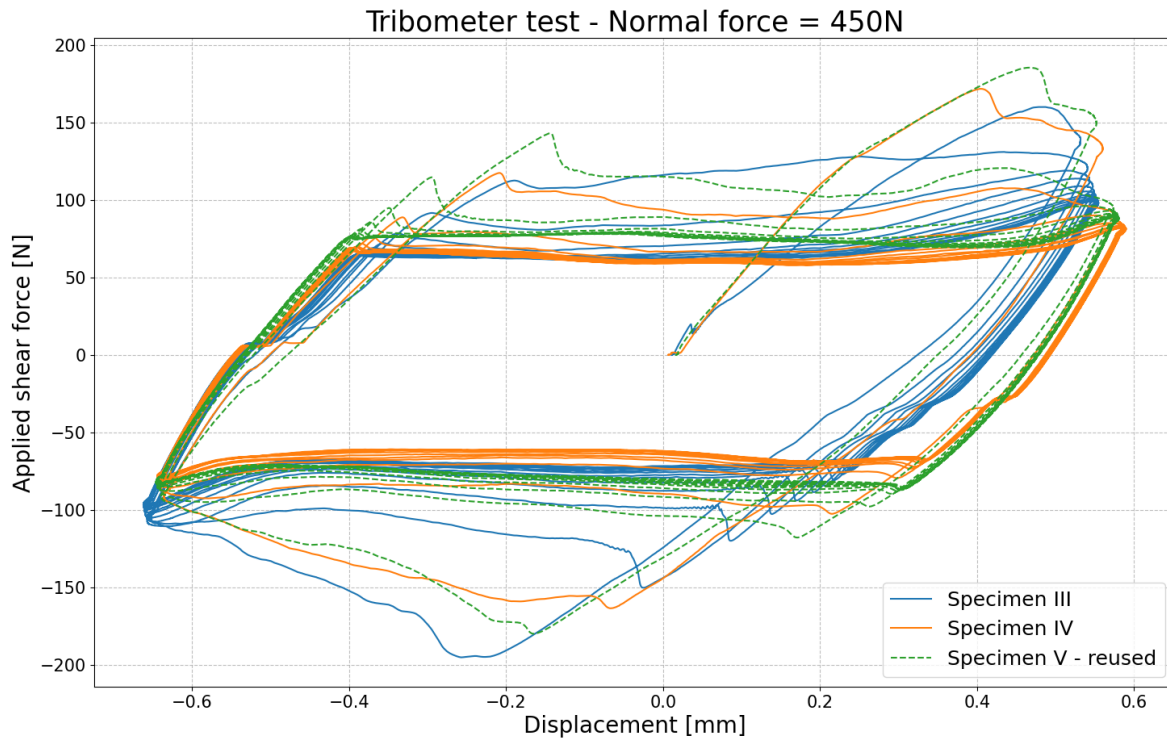


**Figure 82:** Results of the Tribometer test using two Ethyl-Zinc-Silicate coatings. The adopted frequency and amplitude are 0.1Hz and 0.6mm respectively

When comparing this result with the specimen, this effect of Non-Coulomb in combination with the significant damage, could relate to the non-linear stiffness behaviour of the preloaded connections.

When assuming that the friction coefficient is the ratio between the shear and normal force, lower coefficients are obtained in these experiments than in the experiments. This difference in percentage is up to 20%. However, since there is a high sensitivity to the friction coefficient by the degree of curing and curing of the specimens, friction coefficients are not adopted in this research. In addition, the required normal force could not be achieved within the tribometer test. It is known that the amount of stress on an interface influences the friction coefficient.

Therefore, only the relation of the interface to the Coulomb behaviour is identified.

The hysteresis of the other specimens are shown in [Figure 150](#) and [Figure 151](#), which can be found in [Appendix I](#).

# 5

## Additional research: Lowered preloading force

### 5.1 Application

The main part of this research focussed on the resistance of preload injected bolted connections according to NEN-EN1993-1-8. Within this application, the applied preload force is 110kN nominally for M16 bolts of class 10.9. This analogy relates to [Equation 1](#) where the ultimate strength is used as reference strength. However, this assumption is not always applicable to structures, especially in movable structures. Within this section, the influence of change in this preloading force is explored.

There are two considered options for preloading bolts. According to NEN6786:2021, these two options refer to the load level of the applied preload force [\[19\]](#). The first option is, as discussed, where the preload force **can** exceed the yielding limit. However, this second option relates to a preload force where the yielding limit is not exceeded. This is expressed as shown in [Equation 25](#) [\[45\]](#). A lowered preloading force is often implemented to reduce activated stresses in adjacent components. In movable structures, specific components do not contain a service life as long as the designed service life of the entire structure. Therefore, replacement is unavoidable. Some of these components are connected by preloading whereby the threaded bar is often not able to be replaced. To maintain the bar's reliability, local plastification has to be prevented. This is done by implementing a reduced preload level, such that this preloading force results in stresses below the yielding limit.

$$F_{p,C} = 0.7 \cdot f_{yb} \cdot A_s \quad (25)$$

With:

$$\begin{aligned} F_{p,C} &= \text{preloading force in bolt [N];} \\ f_{yb} &= \text{nominal yielding strength of the bolt [MPa];} \\ A_s &= \text{net section of the shaft of the bolt [mm}^2\text{].} \end{aligned}$$

In practice, these preload forces must be applied by using the combined method (torque and angle) or the torque method solely. If the bolt is of class 8.8, the installation procedure can be fulfilled by using a hydraulic torque. However, when the length of the bolt is lower than 500mm, an additional strain-measurement is required [\[45\]](#). Since settlements occur at the interface of the bolt and nut, which reduces the preload force, such measurements are mandatory. For shorter bolts, this effect can be significant [\[36\]](#). Therefore, the NEN-EN6786:2021 limits the applicability of hydraulic pretensioning for longer bolts [\[19\]](#).

## 5.2 Modified method

One can question the validity of the summation of individual resistances. This part investigates a possible applicability when using lower preloading forces. For this investigation, the same testing procedure as elaborated in the previous chapters is followed. However, the difference is that a lowered initial preloading force is applied. According to Equation 25, the preload force in the bolt is expected to be almost 100kN. This value is rounded up to 100kN. Therefore, all preloaded levels are aimed and measured to be 100kN.

In total 6 specimens are used for this part of the research. Table 30 shows the implemented testing procedure.

**Table 30:** Methodology of test series for lowered preloading force

| Test | Preloading | Injection | Nr. of connections |
|------|------------|-----------|--------------------|
| 4    | Yes ✓      | No ✗      | 6                  |
| 5    | Yes ✓      | Yes ✓     | 6                  |

## 5.3 Results - Experimental resistance of each connection

In this chapter of the report, the experimental results of the preloaded bolted connection (PBC) and preloaded and injected bolted connection (PIBC) with a reduced preload force are shown. In response to the analysed result of the abrupt slip behaviour of the previous preloaded experiments, all other bolts within the setup are now preloaded as well. By implementing this procedure, it is assumed that the arising abrupt slip minimises since bearing of those other connection are neglected by preloading.

### 5.3.1 Serie 4: Preloaded bolted connections (PBC)

The fourth series applies the lowered preloading force only. Before testing the specimens, the preloading force is applied. Since all bolts are fitted with strain gauges, the preload force in the bolt is monitored continuously. Therefore, the aimed force of 100kN as preload force is applied by this monitor. To achieve this force, a general torque is used. Since the combined method relates to a higher aimed force, this method of preloading does not apply to this current experiment.

After installation and relaxation, the initial preload forces acting in the bolt are shown in Table 31. These forces are present at the start of each test. As can be seen, the aimed force of 100kN is on average fulfilled since there is a difference of 0%. Of all bolts, the largest difference is 1%.

**Table 31:** Overview of aimed and actual initial preload force in all bolts (lowered preloading only)

|         | $F_{p,C,aim}$ [kN] | $F_{p,C,init}$ [kN] |
|---------|--------------------|---------------------|
| A1      | 100                | 98.78 (-1%)         |
| A2      | 100                | 99.54 (0%)          |
| B1      | 100                | 101.43 (+1%)        |
| B2      | 100                | 101.00 (+1%)        |
| AA1     | 100                | 99.93 (-1%)         |
| AA2     | 100                | 99.74 (0%)          |
| Average |                    | <b>100.07 (0%)</b>  |

In [Figure 83](#), an overview is shown of the load-displacement behaviour of the preloaded bolted connection using a lowered preloading force.

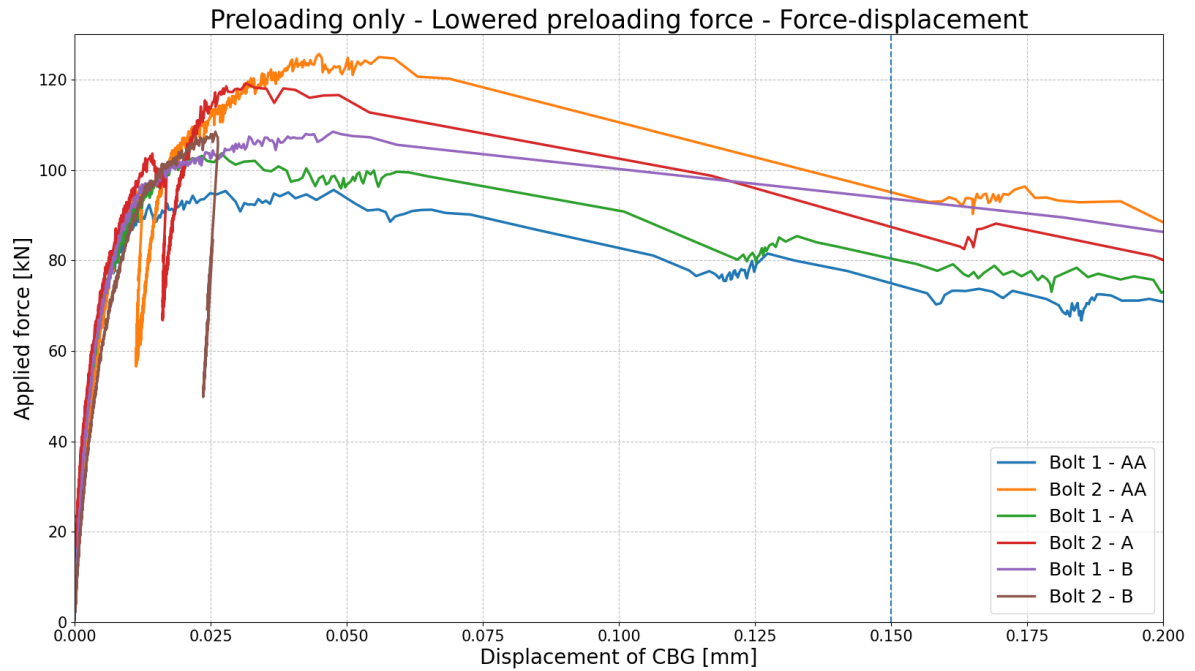


**Figure 83:** Lowered  $F_{p,C}$  - Load-displacement graph for a preloaded connection. The applied preload force  $F_{p,C}$  is 100kN average

[Table 32](#) visualises the obtained resistances from each connection as shown in [Figure 83](#). Over all tests, the average resistance of a preloaded bolted connection with an initial preload force of 100kN is 110kN. The largest difference in outcome is 14 %. Since the nominal resistance, according to NEN-EN1993-1-8, is based on nominal forces and a certain preloading method, a comparison between these outcomes is not possible. The difference between this resistance is therefore based on the increase of friction coefficient. The maximum resistance was reached at an averaged relative slip of 0.0374mm. This displacement is approximately 16% larger than the case of using a higher preload force (140kN instead of 100kN).

**Table 32:** Obtained resistances from experiments when applying a lowered preloading force only

|         | Resistance ( $F_{max}$ ) [kN] | Diff. to average [kN] | At displacement CBG of [mm] |
|---------|-------------------------------|-----------------------|-----------------------------|
| A1      | 103.67                        | -6.3 (-6%)            | 0.0270                      |
| A2      | 119.20                        | 9.2 (+8%)             | 0.0314                      |
| B1      | 108.50                        | -1.5 (-1%)            | 0.0474                      |
| B2      | 108.50                        | -1.5 (-1%)            | 0.0259                      |
| AA1     | 95.64                         | -14.6(-13%)           | 0.0476                      |
| AA2     | 125.70                        | 15.5 (+14%)           | 0.0449                      |
| Average | 110                           | N/A                   | 0.0374                      |

In [Figure 84](#), the decrease of available preload force in the bolt during the experiment is shown. Within this graph, one can identify that the experiment involving “Bolt 2-B” is interrupted before obtaining a measured displacement of 0.15mm at CBG. In addition, providing that a significantly reduced amount of abrupt slip occurs in these connections due to the preloading of all bolts in the specimens, the decrease in preload is also less abrupt.

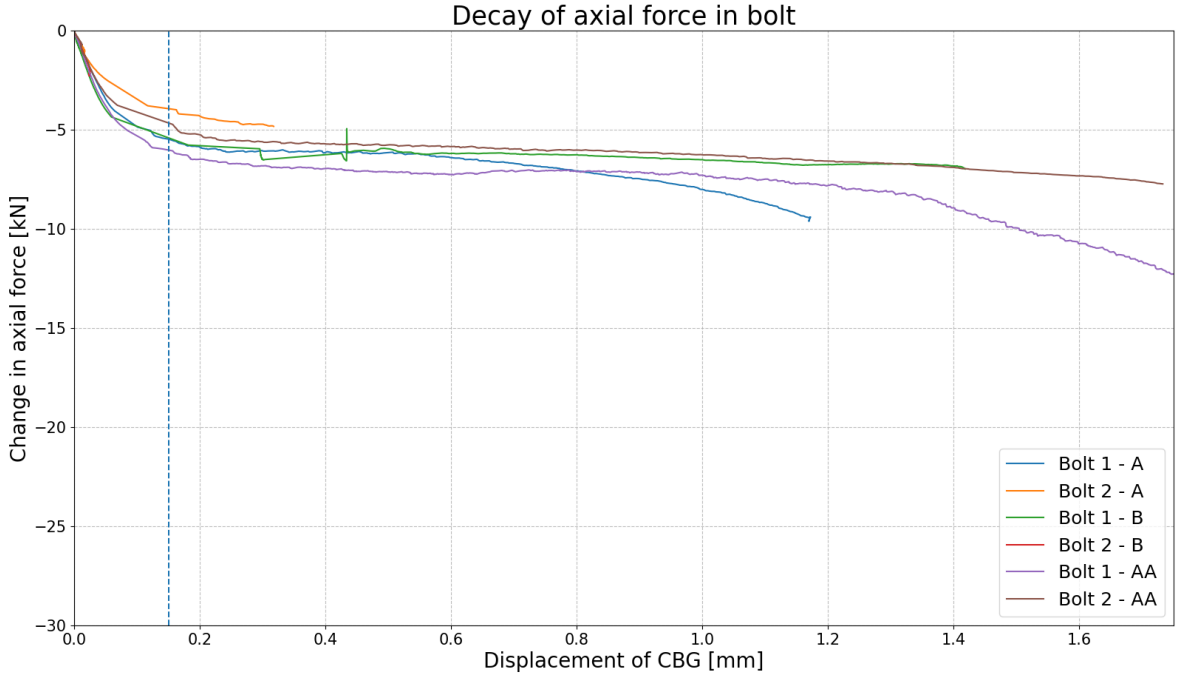


**Figure 84:** Lowered  $F_{p,C}$  - Decrease of the available preload force in each bolt during the experiment (PIBC)

As mentioned, the average displacement at CBG to obtain the maximum slip-resistance is approximately 0.03mm. At this displacement, the decrease of preload force in the bolt is between 2 and 3.5kN. This is a lower reduction than when implementing a higher initial preload force. For this last-mentioned scenario, the reduction was between 3 to 5kN.

The following figures ([Figure 85](#) and [Figure 86](#)) show the displacement of the LVDTs plotted against another relevant LVDT location. For this, two possible misalignments are considered, namely around the Y- and Z-axis (see [Figure 48](#)). From both graphs, it can be seen that there is no significant misalignment. However, in [Figure 86](#) it can be seen that within specimen A, the monitoring of the values is aborted after some displacement of 0.3mm.

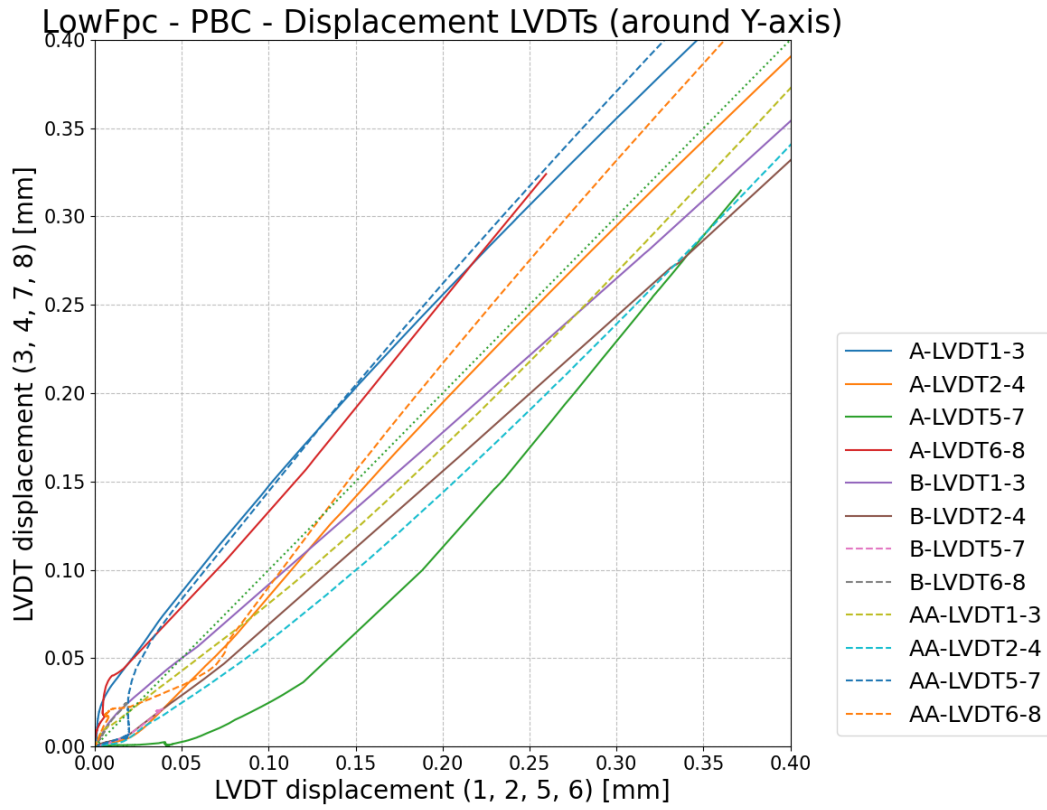


**Figure 85:** Lowered  $F_{p,C}$  - Alignment of the PBC concerning misalignment around Y-axis

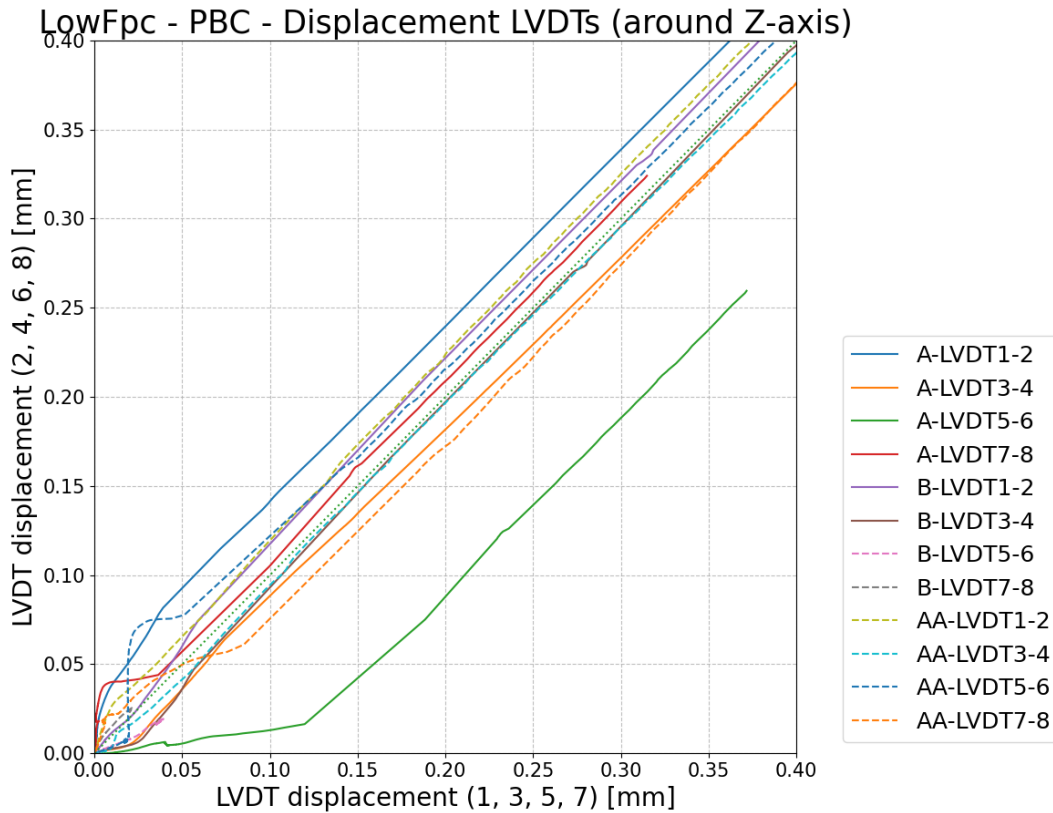


**Figure 86:** Lowered  $F_{p,C}$  - Alignment of the PBC concerning misalignment around Z-axis

### 5.3.2 Serie 5: Preloaded and injected bolted connections (PIBC)

The fifth series, using a lowered preload force, is where both preloading and injection are implemented. As preload force, again a value of 100kN is aimed for. In [Table 33](#) an overview is shown with the acting preload force at the start of the experiments. The average preload force is 99.2kN, which is a difference of 1%.

**Table 33:** Overview of aimed and actual initial preload force in all bolts for Serie (preloading only)

|         | $F_{p,C,aim}$ [kN] | $F_{p,C,init}$ [kN] |
|---------|--------------------|---------------------|
| C1      | 100                | 98.3 (-2%)          |
| C2      | 100                | 99.2 (-1%)          |
| D1      | 100                | 98.1 (-2%)          |
| D2      | 100                | 100.0 (0%)          |
| E1      | 100                | 99.5 (0%)           |
| E2      | 100                | 99.9 (0%)           |
| Average |                    | 99.2 (-1%)          |

[Figure 87](#), visualises the load-displacement behaviour of all three specimens during the experiment. The average resistance of the shown preloaded and injected bolted connection is 158.2kN. Within this figure, it can be seen that Bolt 2 - D has a significantly lower resistance (-13%) than the average. There is a significant amount of slip, including loss of force, involved in this connection which may indicate that there is a defect in the connection, such as an improper injection or lower friction coefficient. When comparing the other connections, differences are illustrated in [Figure 87](#) at the transition of the stiffness obtained from preloading and stiffness from injection. Nevertheless, after a certain displacement, the stiffness and resistance more or less converge.

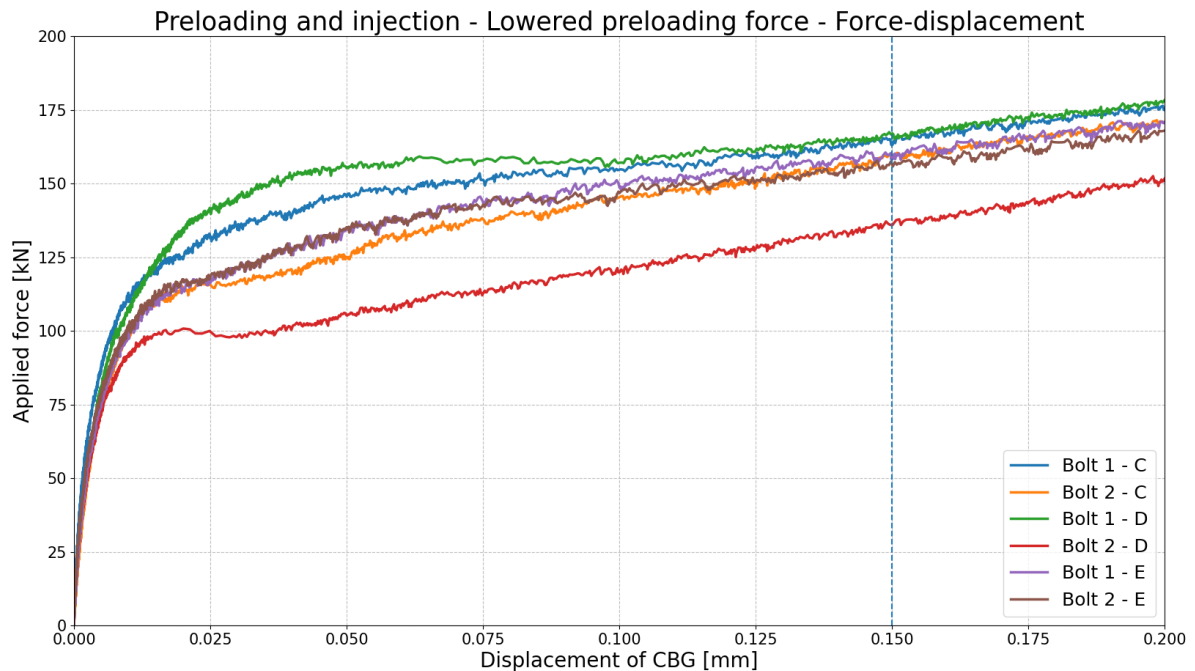


**Figure 87:** Lowered  $F_{p,C}$  - Load-displacement graph for a preloaded and injected connection. The applied preload force  $F_{p,C}$  is 100kN

From the obtained load-displacement graphs, shown in [Figure 87](#), the maximum and average resistances are summarised in [Table 34](#). The average resistance of a preloaded and injected bolted connection with an initial preload force of 100kN is 158.2kN. This resistance is 16% lower than the obtained resistance when the initial preload force is 140kN.

**Table 34:** Obtained resistances from experiments when applying both injection and preloading

|         | Resistance ( $F_{max}$ ) [kN] | Diff. to average [kN] |
|---------|-------------------------------|-----------------------|
| C1      | 165.5                         | 7.4 (+5%)             |
| C2      | 160.1                         | 1.9 (+1%)             |
| D1      | 167.5                         | 9.3 (+6%)             |
| D2      | 137.2                         | -21.0 (-13%)          |
| E1      | 161.0                         | 2.8 (+2%)             |
| E2      | 157.8                         | -0.4 (0%)             |
| Average | 158.2                         | N/A                   |

[Figure 88](#) visualises the progression of the decay in available preload force during the experiment. The maximum resistance of each experiment is obtained at a displacement of 0.15mm. At this displacement, the change in axial force is between 2 and 5kN. This decrease in preload force is a bit lower than for the experiments including an initial preload force of 140kN.

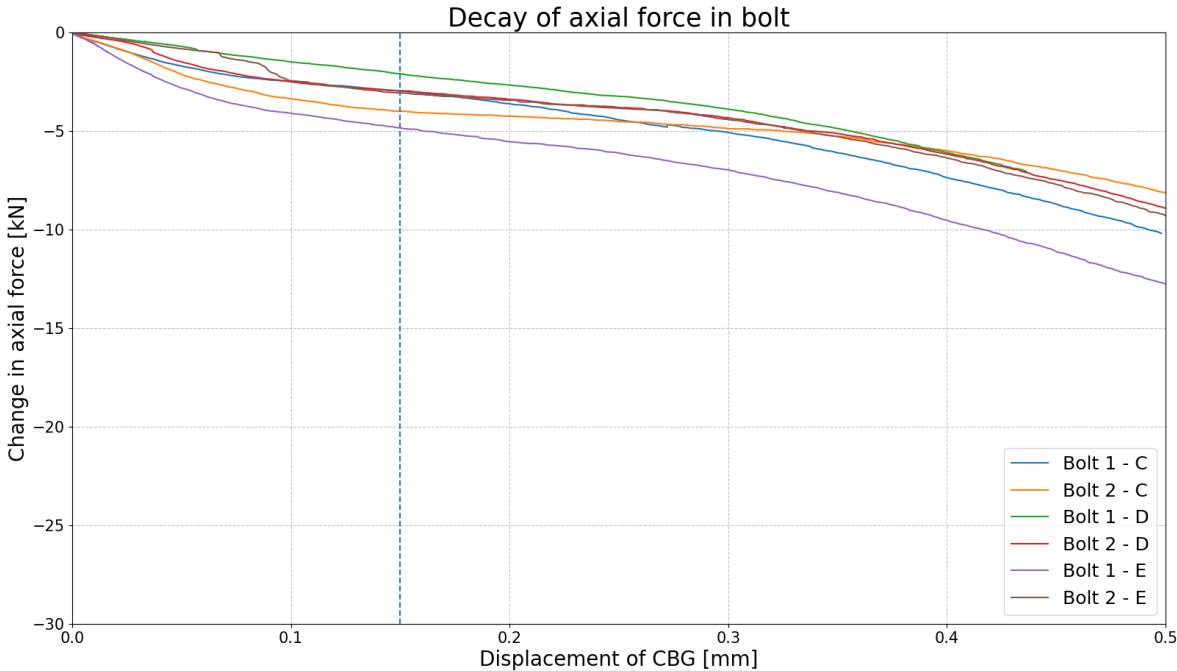


**Figure 88:** Lowered  $F_{p,C}$  - Decrease of the available preload force in each bolt during the experiment (PIBC)

Figure 89 and Figure 90 show the displacement of two related LVDTs plotted against each other. These plots give an indication of the misalignment around a certain axis as shown in Figure 48.

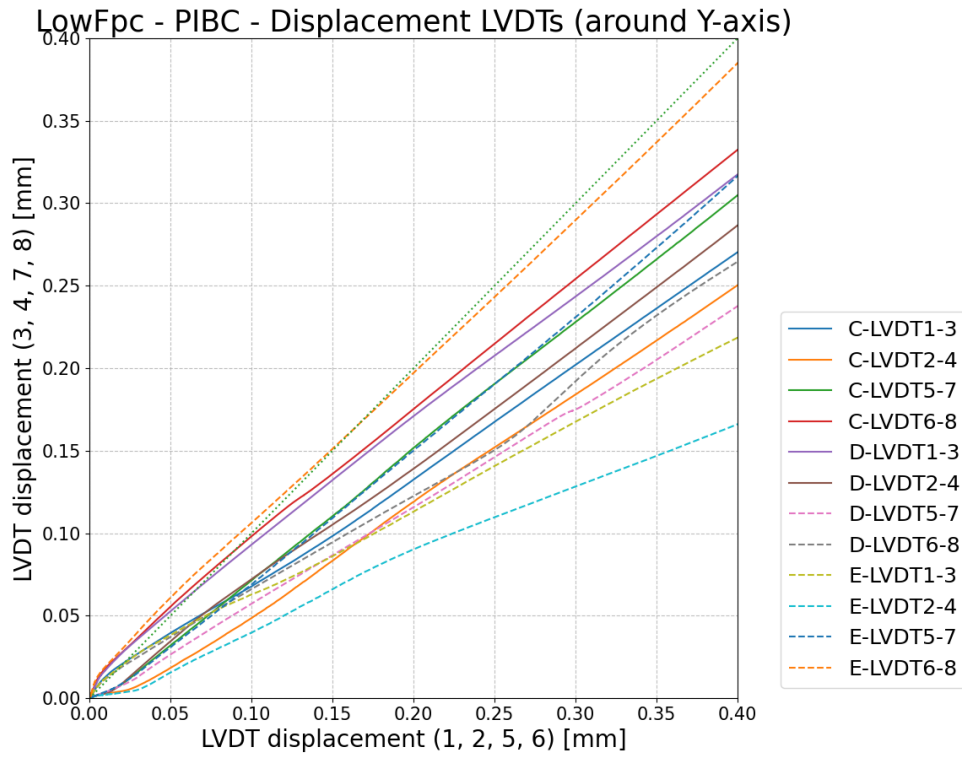


Figure 89: Lowered  $F_{p,C}$  - Alignment of the PIBC concerning misalignment around Y-axis

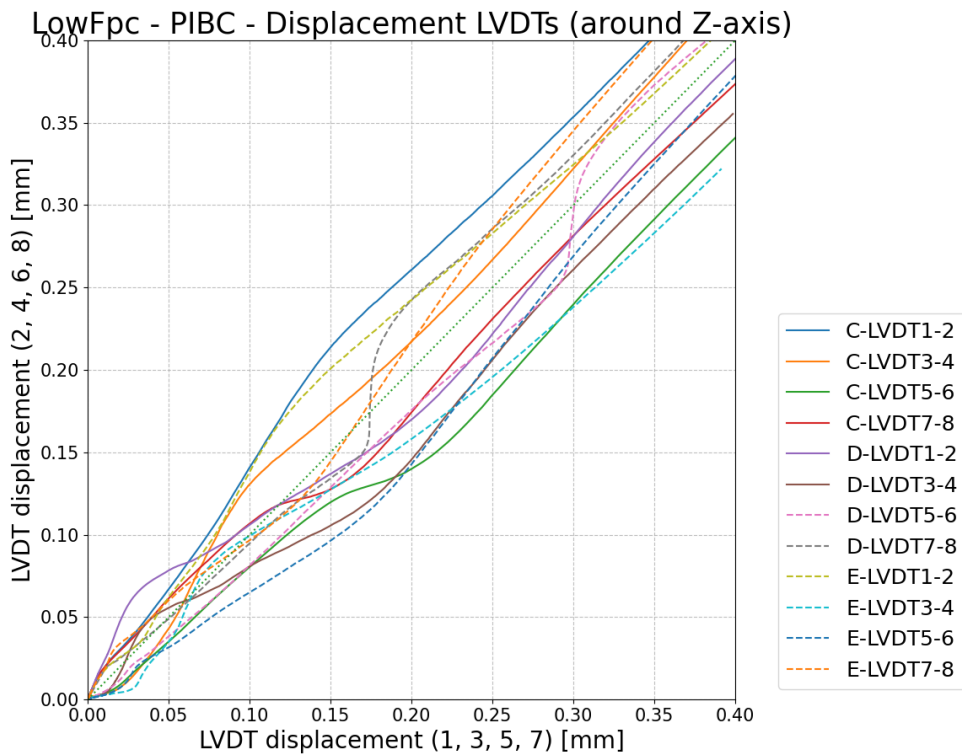


Figure 90: Lowered  $F_{p,C}$  - Alignment of the PIBC concerning misalignment around Z-axis

## 5.4 Analysis of experimental results (Lowered preloading force)

### 5.4.1 Slip-resistance of preloaded connection

Figure 83 shows the load-displacement curve for each bolt. Within this figure, the blue dotted line indicates the end of the region until 0.15mm slip at CBG. The peaks of each curve represent the maximum resistance. It can be seen that similar to the higher preloaded connections, slip occurs at approximately 0.03mm slip at CBG. Besides the similarity of the location, the behaviour after the point of slipping is similar. After slip occurs, the resistance of the connection drops significantly. Initially, four bolts (two specimens) were designed for this case. However, one additional specimen is included (specimen - AA).

Comparing this current setup with the setup of the previous experiments results in the difference that within the current tests, all bolts are preloaded. Since this experiment is displacement-controlled, no abrupt extension or contraction of the entire setup is possible. However, as this graph indicates, abrupt slip occurs. Since slip occurs, the total setup has extended which should be prevented through the displacement-controlled setup. This implies, that significant and abrupt slip in the connection is allowed by a decrease in deformation by other components in the setup. It was thought that the bearing of other connections allows this phenomenon. To investigate this option, other connections were preloaded after a neglectable amount of bearing was activated. Since these bolts are preloaded, significant abrupt slip is expected to be minimized. Nevertheless, for all specimens in this section, the abrupt slip is still visible but by smaller proportions than in the case without preloading of all other connections.

The other observation is the behaviour of bolt 2-B after reaching its potential peak. During the test, the monitored preload force in the bolt showed undefinable results whereafter the experiment was aborted and not resumed. However, no particular reason was found for this. Therefore, the additional specimen AA was added to the test matrix.

### 5.4.2 Friction coefficient

When looking into the obtained friction coefficient, the following results are derived. For this derivation of the friction coefficient, the initial preload force as shown in Table 31 is assumed.

**Table 35:** Determined friction coefficient for each bolt

|         | $F_{p,C,init}$ | $F_{max}$ | $\mu_{init}$ |
|---------|----------------|-----------|--------------|
| A1      | 98.8           | 103.7     | 0.52 (+31%)  |
| A2      | 99.5           | 119.2     | 0.60 (+50%)  |
| B1      | 101.4          | 108.5     | 0.53 (+34%)  |
| B2      | 101.0          | 108.5     | 0.54 (+34%)  |
| AA1     | 99.9           | 95.6      | 0.48 (+20%)  |
| AA2     | 99.7           | 125.7     | 0.60 (+57%)  |
| Average | 100.2          | 110       | 0.55 (+38%)  |

Over all six tests, the average friction coefficient is 0.55 (see Table 35). This value is 38% larger than the nominally assumed value of 0.4. Therefore the average resistance is also 38% larger than the expected resistance when substituting a preload force of 100kN into Equation 2 and excluding partial factors. When the initial preload force in the bolt is 140kN, the friction coefficient is determined to be 0.52. This implies that for this situation, a decrease in preload force of 29% results in an increase of the friction coefficient by 6%. This outcome is also confirmed by the research of De Vries, part of the SIROCO program [59]. Where the decrease of preload force by 20% results in an increase of friction coefficient of 5, 6 and 21 % for a grid blasted surface, alkali-zinc silicate coating and zinc sprayed metalized coating respectively. One can also say that this is expected since the coating is damaged more significantly. Adopting a higher preload force results in higher stresses at the interface of two surfaces. Such an increase in stress subsequently results in more damage when slip occurs.

### 5.4.3 Alignment of specimens

In the section of the results, the misalignment of each connection (PBC and PIBC) is shown. This misalignment relates to the local coordinate system as shown in [Figure 48](#).

In the preloaded connection, implementing an initial preload force of 100kN, there is almost no misalignment observed around both axes. Within the initial phase of the experiment, a small degree of misalignment is removed whereafter a more uniform behaviour is activated. However, both graphs A-LVDT5-7 (Y-axis) and A-LVDT5-6 (Z-axis) show a delay of the fifth LVDT with respect to LVDT six and seven. Therefore, the connection undergoes a misalignment in both directions simultaneously. After the unstable behaviour, until a displacement of 0.05mm, all pairs show more homogeneous displacement. Therefore, one can say that misalignments are resolved from this point onwards. It is therefore assumed that the misalignment has a neglectable influence on the resistance. Especially since the decrease in preload force is the lowest for this type of connection.

For the preloaded and injected bolted connection (PIBC), the misalignment around the Y-axis is not significant. However, it can be seen that all pairs are located below the linear slope of 1:1. Therefore, it is expected that during the assembly of the connections, a small deflection occurred. For the difference around the Z-axis, it is visualised in [Figure 90](#) that the relative measured displacement is less unstable than for the scenario where a larger preload force is adopted (see [Figure 59](#)). After the stabilisation of the initial imperfection, the displacement is uniform during the experiment. This is confirmed by the identical slope of each pair.

### 5.4.4 Stiffness

#### 5.4.4.1 Preloaded bolted connection (PBC)

Since the friction coefficient has been increased for a lowered applied preload force, the effect on the stiffness is investigated. To enable for comparison, the same region for the determination of the preloading force is assumed. This implies that the start and end of this stiffness region for slope 1 are 0.003 and 0.012mm slip at CBG respectively. For slope 2, these values are 0.12 and 0.21mm.

For slope 1, the same curve-fitting formula is assumed, namely:

$$F_{\text{applied}} = E0 + E1 \cdot u_{\text{CBG}} - E2 \cdot \exp(-E3 \cdot u_{\text{CBG}})$$

After the optimisation procedure, the resulting parameters from the equation above, are shown in [Table 49](#) of [Appendix H](#). The corresponding output is visualised in [Figure 91](#). The average slope of these curves is **4650kN/mm**. In the situation where the preload force is 140kN, the obtained stiffness within this region is **7000kN/mm**. This implies that within this current region, the stiffness is reduced by 34% for the configuration with the lower preload force. The average slip at which the maximum resistance of the connection is reached is at a slip of 0.0374mm. For the case using a preload force of 140kN, this location is at an average slip of 0.032mm. This difference is 16% of each other. The stiffness at a certain region between 0.003 and 0.013mm slip is 34% larger for a preload force of 140kN and the resistance only 24% higher. Therefore, it can be questioned whether this chosen region is satisfactory. However, since the friction coefficient highly depends on acting stresses and the quality state of the coating, one can also say that the accumulated damage in the case of a higher preload force significantly influences the outcome.

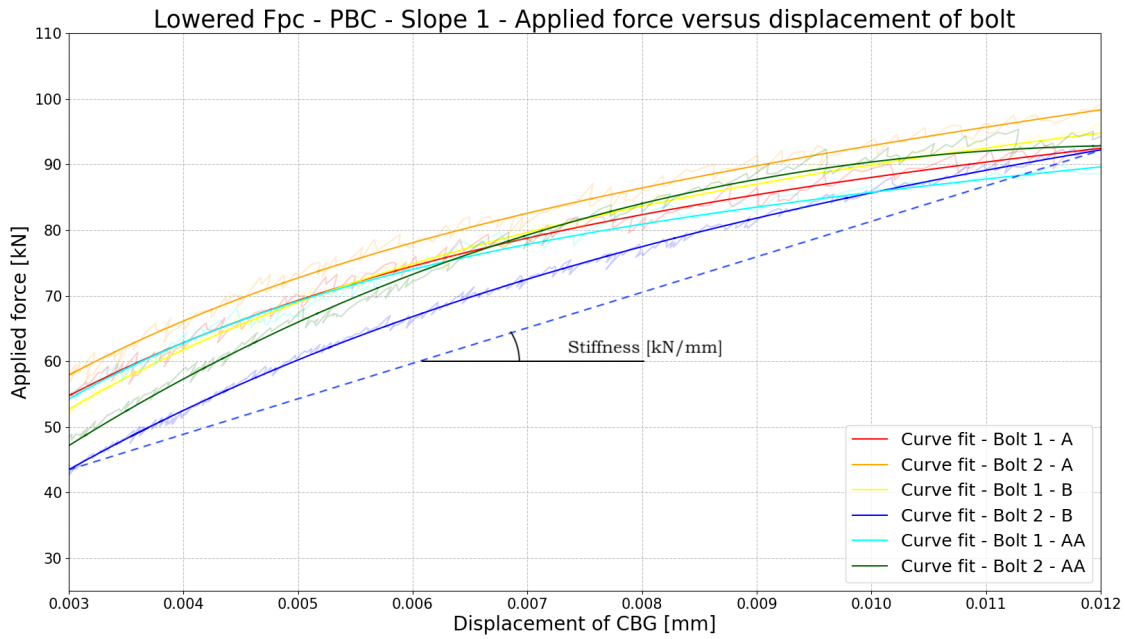


**Figure 91:** Lowered preloading - PBC - Slope 1: Curve-fit of the load-displacement curve for a preloaded connection within the range 0.003 to 0.012mm

After the maximum resistance is reached, an abrupt slip occurred. Therefore, again, this second slope is taken into consideration. To have similarity over all slopes, the same equation is assumed:

$$F_{\text{applied}} = G0E + G1E \cdot u_{\text{CBG}} - G2E \cdot \exp(-G3E \cdot u_{\text{CBG}})$$

Results after optimisation of the slope are shown in [Table 44 \(Appendix H\)](#). Substitution of these graphs results in the overview as shown in [Figure 92](#). Of these curves, the average slope is **-150kN/mm**. Compared to the average slope during abrupt slip for the scenario with a preload force of 140kN, an increase of approximately 50% is obtained. For this scenario, a slope of -100kN/mm was derived.

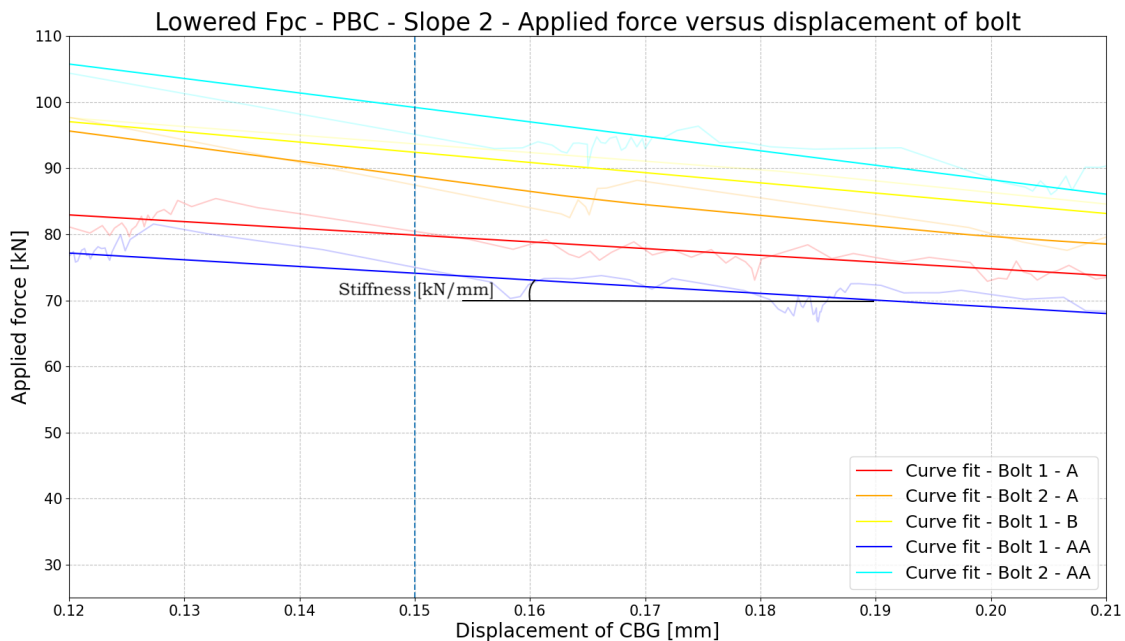


**Figure 92:** Lowered preloading - PBC - Slope 2: Curve-fit of the load-displacement curve for a preloaded connection within the range 0.12 to 0.21mm

#### 5.4.4.2 Preloaded and injected bolted connection (PIBC)

For the first slope, the same region is taken into consideration as all previous. To compute the stiffness of all experiments, each connection's output is optimised by a curve fit. For the sake of homogeneity, the same equation is used as shown below. Each curve fit is visualised in Figure 93.

$$F_{\text{applied}} = F_0 + F_1 \cdot u_{\text{CBG}} - F_2 \cdot \exp(-F_3 \cdot u_{\text{CBG}})$$

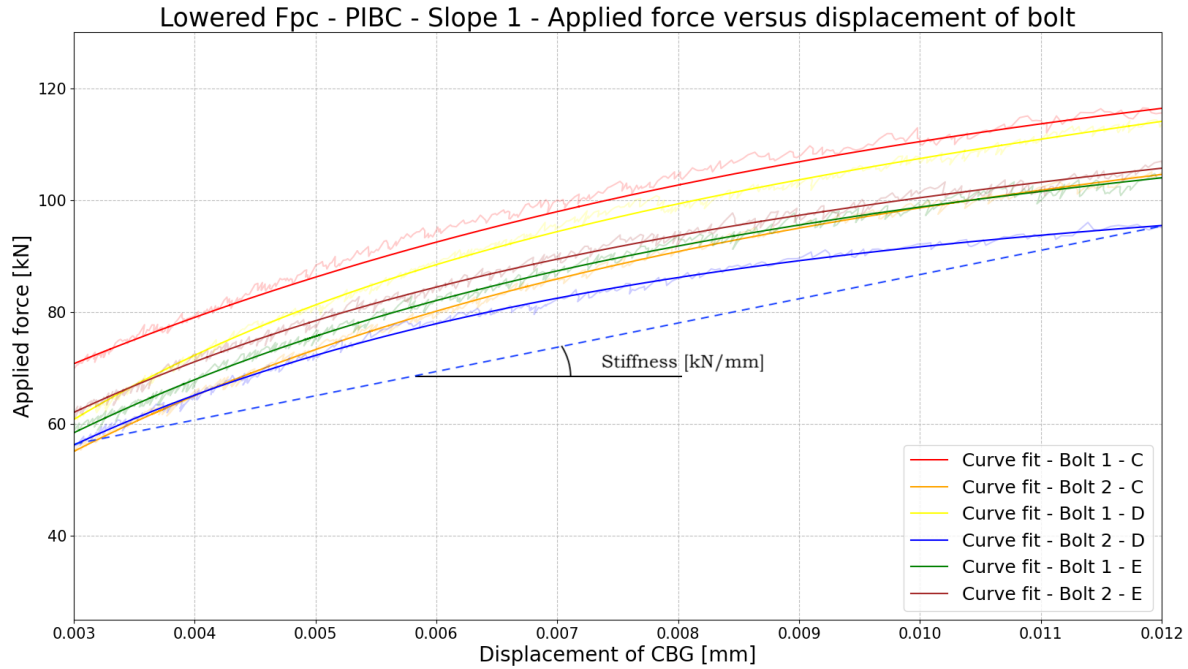


**Figure 93:** Lowered preloading - PIBC - Slope 1: Curve-fit of the load-displacement curve for a preloaded and injected connection within the range 0.003 to 0.012mm

The average stiffness of the preloaded injected bolted connection using a preload force of 100kN is **5150kN/mm**. Comparing this to the derived stiffness of the same connection implementing a preload force of 140kN, this stiffness is approximately 35% lower. This decrease in percentage is similar to the decrease in the stiffness of the preloaded bolted connections (PBC). When comparing the stiffness of 5150kN/mm with the summation of the individual stiffnesses of the lowered preloading and injection, the summed stiffness is similar to this summation. The difference is namely only 1%.

For the second slope, which relates to a displacement between 0.12 and 0.21mm, an identical equation is used as described above:

$$F_{\text{applied}} = G_0 + G_1 \cdot u_{\text{CBG}} - G_2 \cdot \exp(-G_3 \cdot u_{\text{CBG}})$$

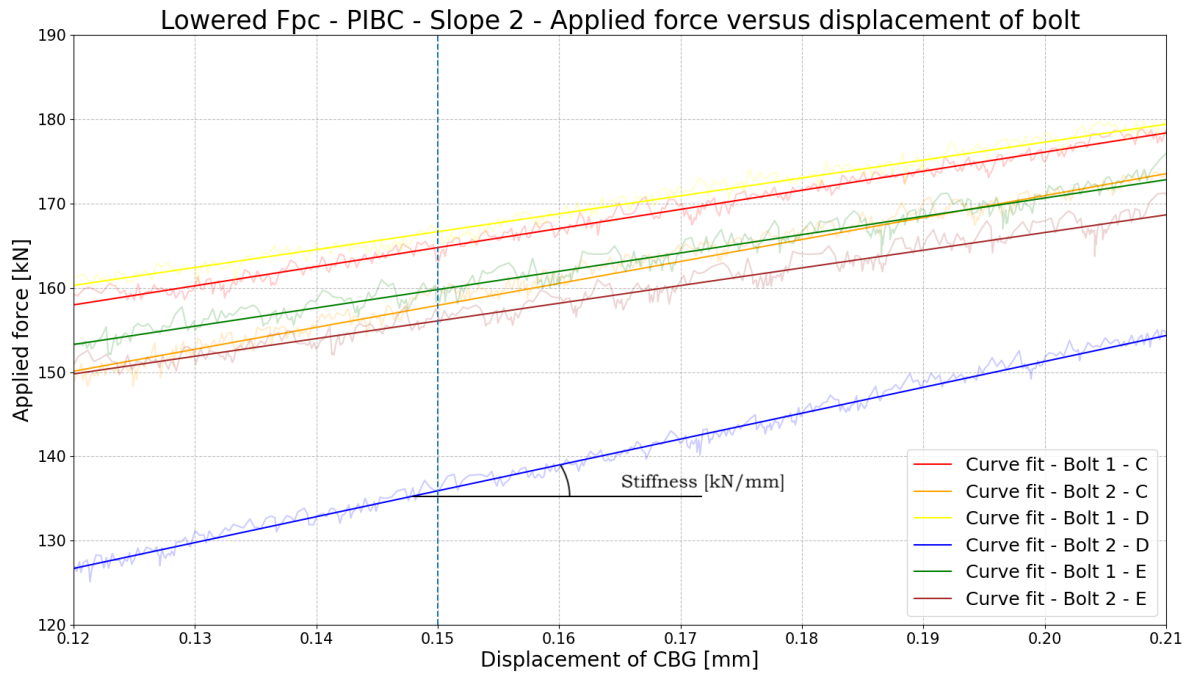


**Figure 94:** Lowered preloading - PIBC - Slope 2: Optimisation of the load-displacement curve for a preloaded and injected connection within the range 0.12 to 0.21mm

From Figure 94, the average slope of each curve is **250kN/mm**. This stiffness is significantly more than the stiffness in this region when using a higher preload force. This increase is almost 80%. It is expected that this difference is related to the amount of acting force. The average force in this region is approximately 160kN. While the acting force in this region for a connection implementing 140kN is almost 200kN. This force affects the stiffness of the resin. Since the current slope has a lower acting force, the stiffness is as expected higher.

When comparing this stiffness of 250kN/mm with the summation of the individual components, a 25% higher resistance is obtained (=200 kN/mm). For the case where a higher preloading force is used, this combined stiffness is not higher but lower, namely -33%.

#### 5.4.4.3 Comparison of stiffnesses (both $F_{p,C}=140\text{kN}$ and $F_{p,C}=100\text{kN}$ )

In Table 36, an overview is given with the calculated stiffnesses for each configuration and each slope. For the first slope, it can be seen that for both PBC and PIBC, the reduction is similar (approx. 35%). This percentage is a bit higher for the PBC in the second slope, namely 50%.

However, the most striking observation is that the stiffness of the preloaded and injected bolted connection increases by more than 67%, when reducing the preload force of 140 to 100kN. This perspective is elaborated in more detail in Subsection 5.4.5.

**Table 36:** Overview of obtained stiffnesses for each slope, each type of connection and each implemented preload force  $F_{p,C}$

|           | Slope 1   |                  | Slope 2   |                  |
|-----------|-----------|------------------|-----------|------------------|
| $F_{p,C}$ | 140kN     | 100kN (-29%)     | 140kN     | 100kN (-29%)     |
| PBC       | 7000kN/mm | 4650kN/mm (-34%) | -100kN/mm | -150kN/mm (-50%) |
| IBC       | 450kN/mm  | 450kN/mm (0%)    | 350kN/mm  | 350 kN/mm (0%)   |
| PIBC      | 7950kN/mm | 5150kN/mm (-35%) | 150kN/mm  | 250kN/mm (+67%)  |

### 5.4.5 Summation of individual resistances

In this section, the results of the experiments are substituted into [Equation 16](#) and further elaborated. This equation relates to the statement by the NEN-EN1993-1-8, that states that summation of individual resistances is allowed [\[17\]](#). In addition, the summation of each component is compared within both numerical and experimental analysis. In this part, the summation is investigated at each displacement until a displacement at CBG of 0.4mm.

#### 5.4.5.1 According to NEN-EN1993-1-8

First, the statement of the Eurocode is investigated, whether or not summation is allowed when adopting a lower preloading force. In [Table 37](#) an overview of the results is visualised including a comparison between the main experiment, implementing a preloading force of 140kN based on the tightening procedure, and the current case when this preloading force is lowered from 140kN to 100kN.

**Table 37:** Results for obtained resistances per series. Two series are compared, namely including an  $F_{p,C}$  of 140kN and 100kN for the first and second column respectively

| Type of series                               | Resistance (140kN) [kN] | Resistance (100kN) [kN] |
|--|-------------------------|-------------------------|
| Preloading only                              | 144.7                   | 110.0                   |
| Injection only                               | 74.7                    | 74.7                    |
| <i>Summation of preloading and injection</i> | <i>219.4</i>            | <i>184.7</i>            |
| Preloading and injection                     | 187.2 (-15%)            | 158.2 (-14%)            |

From this table, it can be concluded that for both cases, summation is *not allowed*. In addition, both experiments show a similar difference of approximately 15% compared to the summed values. Therefore, one can say that it is not solely the preloading force that affects this difference. As mentioned in the previous section, the stiffness of the resin is higher when subjected to a lower force. Even since the difference is compatible, the proportion of the injection component is different to both scenarios. When a preload force of 140kN is assumed, the difference between the resistance obtained from preloading only and the resistance of applying both preloading and injection is approximately 43kN. While this proportion is 48kN when the bolt is preloading by 100kN.

This absolute difference of 5kN between the two preload levels can be expected to be equal to the difference in slip resistance from both scenarios if a linear summation relationship exists between the individual resistances and the resistance of a preloaded injected bolted connection. Since the displacement after obtaining the maximum slip-resistance until 0.15mm is similar for both preload levels and the expectation that the resin contains the same stiffness, this absolute difference of 5kN is expected to be maintained. [Table 37](#) shows that the absolute difference in resistance of the two preload levels is approximately 35kN. However, at 0.15mm displacement, this resistance difference is reduced to 19kN. Therefore, it is not correct to assume that the absolute contribution of the individual resistances is similar for all implemented preload levels. This is shown in [Figure 95](#). Within this figure, four graphs are visualised showing the two different preload levels and the type of connections. In addition to this, two additional vertical lines are shown. These lines represent the average slip at which the maximum slip-resistance is obtained for a preloaded bolted connection. Since the light-blue line is located after the magenta-coloured line, the average maximum resistance is obtained after a larger slip when using a lower preload force according to the experiments. Therefore, this effect in proportion can be excluded since the resin contributes more to a lowered preloaded connection since the absolute difference decreases from 35kN to 19kN.

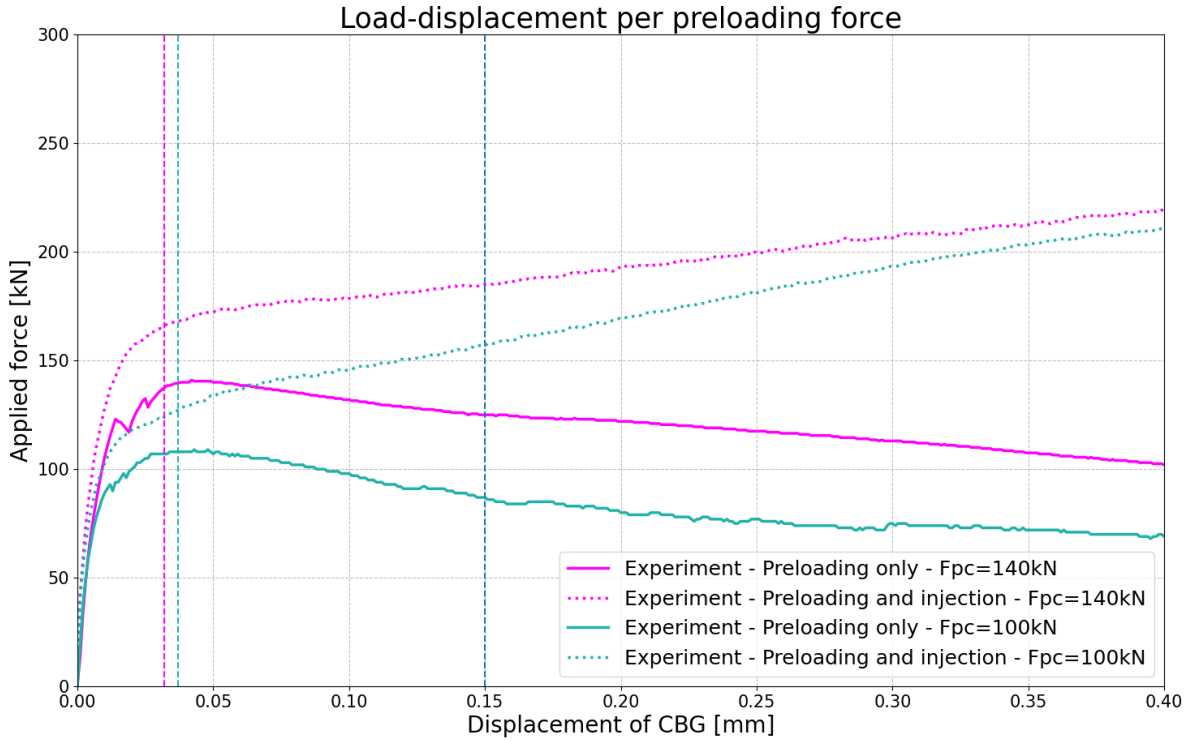


**Figure 95:** Overview of load-displacement difference between implement and  $F_{p,C}$  of 140kN (Magenta) and 100kN (Light blue) including an indication of averaged displacement at which maximum resistance for preloading only is obtained

Figure 95 also indicates that the difference in stiffness after a displacement of 0.05mm is significantly different between the two preload levels. This is also already stated in Paragraph 5.4.4.2. An overview of the determined stiffnesses within the range of 0.12 and 0.21mm displacement is shown in Table 38. One can say that after exceeding the maximum slip-resistance in a preloaded injected bolted connection, all additional applied force exceeding this resistance is taken into account by the injection. In addition, both the table and figure indicate that this contribution is not identical for all load levels. In the case of applying injection only, this stiffness is more than twice as much as for a preloaded injected connection using a preload force of 140kN in the same region.

**Table 38:** Stiffness of three different types of connections within the range of 0.12 to 0.21mm displacement at CBG (slope 2)

|   | Stiffness [kN/mm] | Ratio |
|---|-------------------|-------|
| Injection only                                      | 350               | 1     |
| Preloading + Injection ( $F_{p,C} = 100\text{kN}$ ) | 250               | 0.71  |
| Preloading + Injection ( $F_{p,C} = 140\text{kN}$ ) | 150               | 0.43  |

Even if a higher preload force is used within a preloaded connection (140kN vs 100kN), a lower stiffness is obtained in the region where bearing of the resin is activated solely (dotted lines as shown in Figure 95). After the slip-resistance is exceeded, the stiffness is higher when implementing a lower preload force than when this preload force is increased. From Figure 95 it is observed that after the maximum slip-resistance is obtained, the resistance of a preloaded bolted connection reduces in the same behaviour for different preload levels. Therefore, the absolute resistance reduces by the same proportions. From this statement, it can be concluded that the **relative** contribution of the resin to the combined resistance is higher when implementing a lower preload force.

The following parts describe two potential possibilities that affect the difference in bearing behaviour between the implemented preload levels.

The first possibility is if a higher preload force is implemented, bearing of the resin is obstructed more than when implementing a lower preload force. If the clamping force reduces the contraction of the resin, the bearing stiffness reduces. This behaviour is in line with Figure 95. In the discussion of this report, see Section 6.5, this behaviour is elaborated on.

Another option is the interaction of the preload force and shear force since the preload force of 140kN is significantly higher than the implemented preload force of 100kN which leaves less available resistance according to Equation 13. One can say that the interaction of the normal and shear component in the bolt reaches its limit. Therefore, if bearing increases (after obtaining the maximum slip resistance), the preload force drops more significantly whereby the stiffness reduces. However, in this case, it can not be determined by Figure 95 what the amount of reduction of slip-resistance is since the decrease in slip-resistance may not be that significant and therefore the contribution of the bearing resistance is unknown.

Based on the numerical analysis, it is investigated what the contribution of the individual mechanisms (preloading and injection) is on the combined resistance. In Figure 96, the contribution of the slip-resistance and bearing resistance to the obtained resistance of a preloaded and injected bolted connection for the two considered preload forces is illustrated. The small unstable behaviour of the graphs is the result of the complexity and definition of the interaction properties at the shear planes. In this figure, the bearing resistance is determined by the total resistance (blue and red graphs) subtracted by the slip-resistance (orange and purple graphs). The slip resistance is lower than presented earlier, since the acting forces in a free body cut at the shear planes are used. However, apparently, the connection gains more resistance pure at the shear planes in a preloaded and injected bolted connection. It can be seen that the contribution of bearing of the resin is similar for both preload levels. Therefore, one can say that based on this numerical model, the absolute proportion of injection is not dependent on the preload level. As Figure 95 indicates, the stiffness is, after the maximum slip-resistance is achieved, lower in case of a higher preload level. In combination with what is shown in Figure 96, this is only possible by a reduction in slip resistance. In addition, the shown bearing resistance at 0.15mm (68kN) is not equal to the resistance at 0.15mm for an injected bolted connection (74kN). Therefore, it is expected that an additional factor plays a role in the measured resistance. In Section 6.5, another possibility is elaborated on how the measured resistance differs for each type of connection.

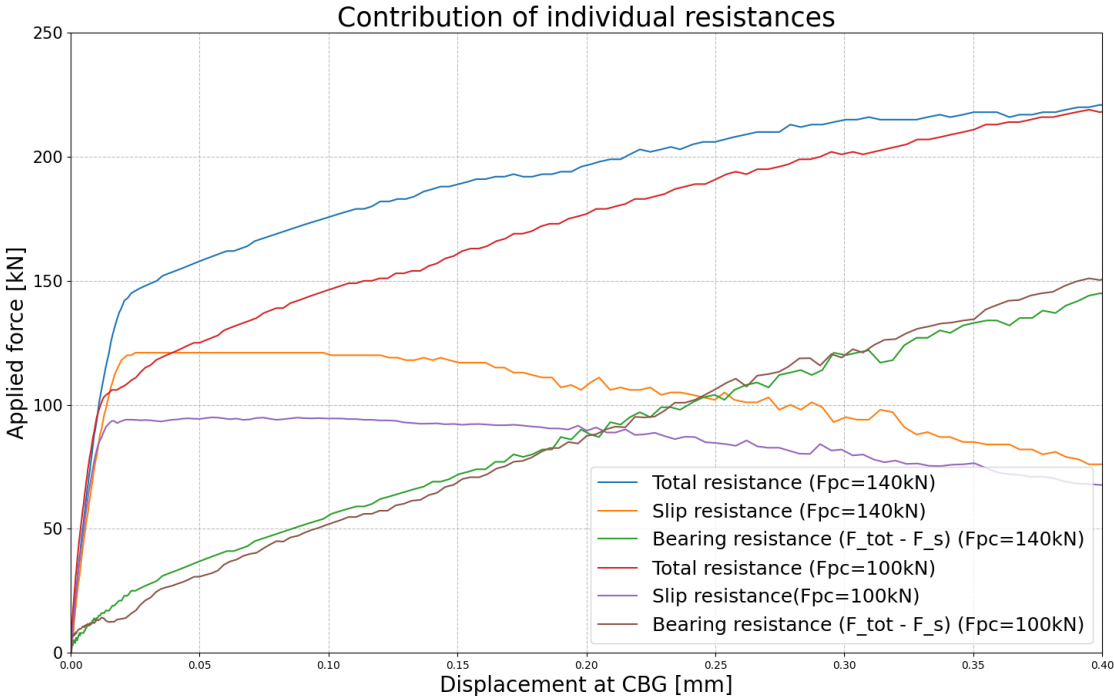


**Figure 96:** Contribution of the individual resistances to the combined resistance of a preloaded and injected bolted connection (PIBC) for two considered preload levels (140kN and 100kN). The contribution of bearing is determined by the difference between the total resistance and the slip-resistance

### 5.4.5.2 Scenario - summation during entire experiment

In the following subsections, again the statement of the Eurocode is considered along a displacement trajectory of 0.4mm. Two scenarios are considered. The first scenario implements the **actual** experimental results while the second scenario uses **customised** results. This customisation is based on one characteristic: the resistance of the connection can not decrease during the experiment.

#### Scenario 1: Actual experimental results

When comparing the experimental results using a lowered preloading force with the numerical results, the following is obtained. In [Table 39](#) and [Figure 97](#), the results and differences in the load-displacement behaviour of the considered connections are shown.

**Table 39:** Lowered Fpc: Experimental and numerical results of the obtained resistances for the three different connections including summation

|  | Resistance                            | Experiment [kN] | Numerical [kN] |
|--|---------------------------------------|-----------------|----------------|
|  | Preloading only                       | 110.2           | 105.0 (-5%)    |
|  | Injection only                        | 74.7            | 73.5 (-2%)     |
|  | Preloading + Injection                | 158.2           | 160.0 (+1%)    |
|  | Summation of preloading and injection | 184.9           | 178.5 (-3%)    |

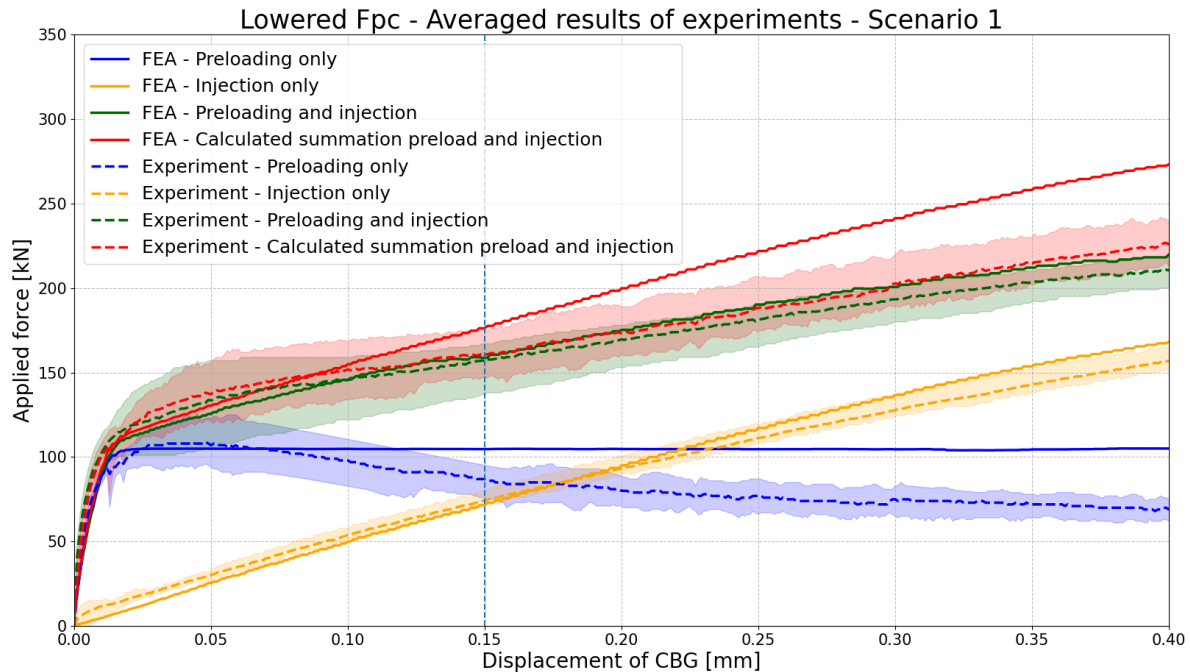


**Figure 97:** Lowered Fpc: Overview of the load-displacement behaviour of different types of connections allowing a decrease in slip resistance and including averaged experimental results and numerical results. Transparent areas show the range of experimental results for each tested connection

[Figure 97](#) visualises the three considered connections. Of these connections, the orange graphs are identical to the case where a higher preload force is shown since this connection is not related to the amount of preload force. The blue line represents the preloaded connection. Since this figure shows results that allow a decrease in resistance, the numerical and experimental graphs contain different trajectories after slip. However, the maximum slip resistance differs 5% for the preloaded bolted connection. For the connection, which is preloaded and injected, this difference is only 1%. These are shown by the green graphs. Similar to the case of the higher preload force, the green line never runs above the red line which indicates that in this scenario, summation is not allowed.

**Scenario 2: Customised experimental results**

For this second scenario, the blue and red lines, indicating the preloaded connection and the graph representing the summation of the orange and blue lines are different than for the previous scenario (see Figure 98). Since this case disallows a decay in slip resistance. This results in the upward shift of the red line shift, indicating a higher resistance. For this case, the numerical model and experiments show a better comparison. This improvement is also expected since the numerical model also neglects a decay in resistance. In addition, also for this scenario, no summation is allowed along the entire trajectory until a displacement of 0.4mm.

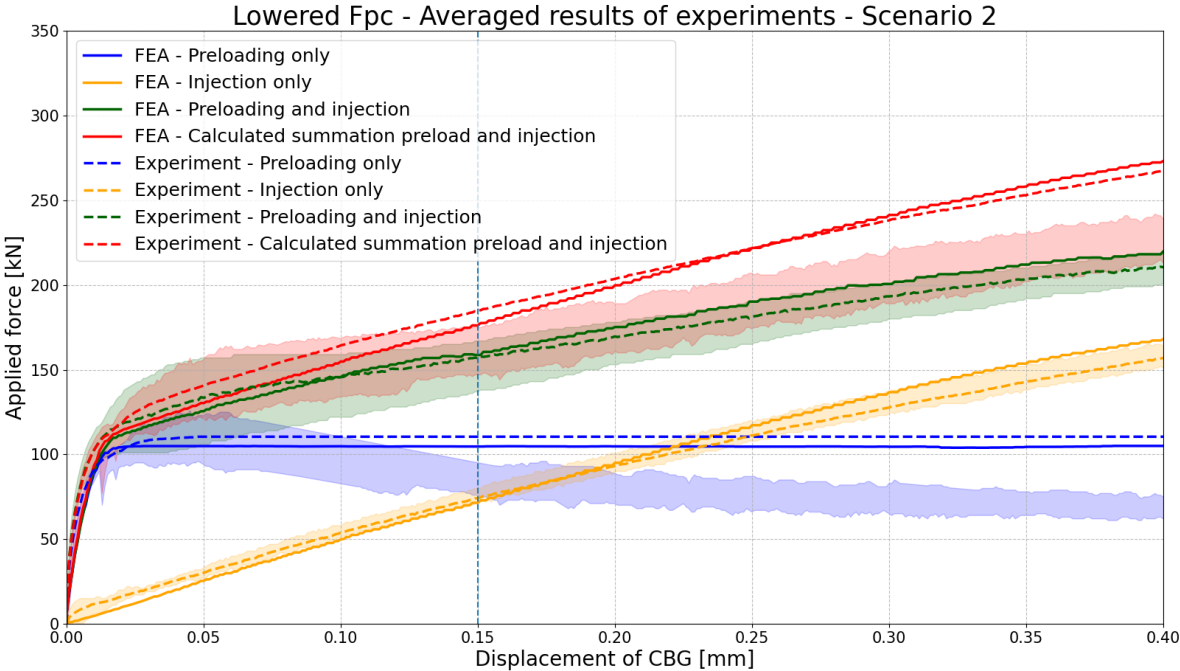


**Figure 98:** Lowered Fpc: Overview of the load-displacement behaviour of different types of connections disallowing a decrease in slip resistance and including averaged experimental results and numerical results. Transparent areas show the range of experimental results for each tested connection

For both scenarios, the numerical model is representative for the resistance of the connections. In addition, for most of the trajectory, the load-displacement behaviour of the numerical model is located in the presented area of experimental results. Since the numerical model does not include a decrease in resistance, the second scenario is comparable.

# 6

## Discussion

### 6.1 Injection of specimens

The research methodology adopted to accomplish the objectives of this research involves experimental results to investigate the feasibility of summation of individual resistances obtained from preloading and injection. Ensuring identical initial conditions, such as geometry and preload force, is required to investigate the resistances of individual connections. In the context of resin-injected connections, maintaining initial conditions relies on the material properties of the resin and its execution. The resistance of the injected bolted connection primarily depends on the resin strength. This strength is dependent on the ratio of the mixture. However, this mixture is made several times whereby each mixture is not 100% identical. To minimise the error, the volume of each mixture is increased. In this way, a small additional weight of, for instance, the hardener has less effect on the strength if the total volume of the mixture increases. Besides this, the presumed is that no significant disparities in properties will appear.

The resistance of an injected bolted connection is dependent on the bearing strength of the resin itself. In the body of this report, the assumed mixture for the resin is shown. For all injected bolted connections, this same ratio of mixture must be applied. However, an identical mixture can not be produced for each group of connections. Since the proportions are weighted on a scale, small deviations occur between each mixture and therefore affect the bearing strength and thus resistance of the connection. However, from the obtained resistances of injected bolted connections, only a small variation is observed. Therefore, one can assume that this influence is neglectable.

Besides the production of the mixture, the accuracy of injecting the bolt clearance affects the bearing resistance. The resin itself has a high viscosity and therefore requires a high pressure to be injected. Since air has to escape through a small escape channel, the pressure may be built up inside the connection. The pitfall is that air can be trapped inside the connection, which affects the behaviour of the resin when compared to a perfectly injected connection. These voids decrease the degree of confinement and therefore reduce the bearing properties of the resin. To verify if the injection of the resin is done properly and air is not trapped inside, one of the connections has been cut in the longitudinal direction as indicated in [Figure 99](#).



**Figure 99:** Cross-sectional cut of one of the injected bolted connections

It can be seen that the resin is not porous since the volume is flat and smooth. No small air bubbles are inside the resin and no trapped air is observed. Therefore, the degree of quality is assumed to be similar and satisfactory for all connections. Since all connections are installed with the same procedure. Nevertheless, since only one connection is verified, it does not automatically imply that no deviations occur throughout all injections.

## 6.2 Numerical modelling of resin

In this section of the discussion, the sensitivity of the modelled resin is elaborated. This part consists of two investigated parts, namely the effect of the height (in the direction of the bolt) and the effect of the mesh size in the thickness direction.

### 6.2.1 Decreased height of resin

In the numerical modelling process, the entire analysis consists of 3 or 4 loading steps, depending on the implementation of a preload force. In practice, the bolt is preloaded before the resin is injected to prevent damage of the resin. However, in the numerical analysis, it is not possible to allocate additional parts, such as the resin, after the initial load step and thus after preloading. Therefore, the resin is already “injected” before the preload force is applied to the bolt. In the preloaded and injected bolted connection, it was observed that due to the contraction of the clamping package, the resin undergoes significant stresses and deformations. Especially since the resin is rigidly connected to the steel plates around the entire perimeter. To prevent the introduction of unfavourable stresses and displacements, the resin is decreased in height by 5mm at each end. Such that the washer won’t compress the resin. This compression is the result of the contraction of the clamping package by the preload force.

In [Figure 100](#), the change in geometry of the resin is indicated as prescribed above. It can be seen that the resin stops at 5mm before the washer. This reshape is however only applied to the preloaded and injected bolted connection.

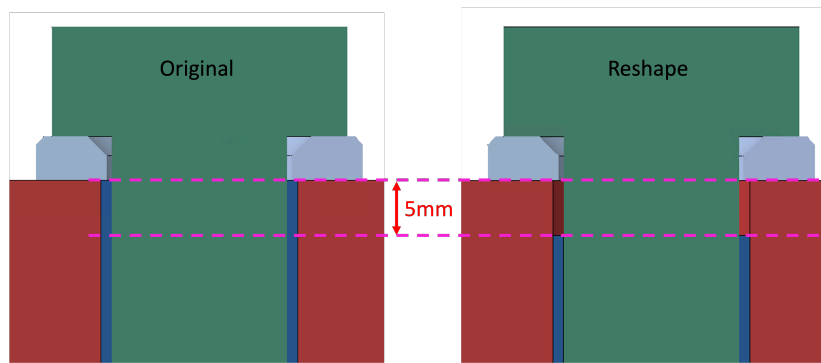


**Figure 100:** The implemented reduced height of the resin. The left figure indicates the fully injected resin that is modelled to the washer (applied to IBC). The right figure shows the reduced height of the resin to prevent additional stresses by preloading (applied to PIBC)

It can be questioned what the effect of this geometry is on the contribution of the bearing resistance of the resin to the combined resistance of a preloaded and injected bolted connection. The shorter resin namely reduces the effective length wherever the bearing resistance is derived. However, as [Figure 101](#) indicates, there is no significant difference obtained between the two modelled geometries of the resin. The blue line indicates the load-displacement behaviour when the resin is modelled up to the washer. While the orange line represents the model including reduced height of the resin.

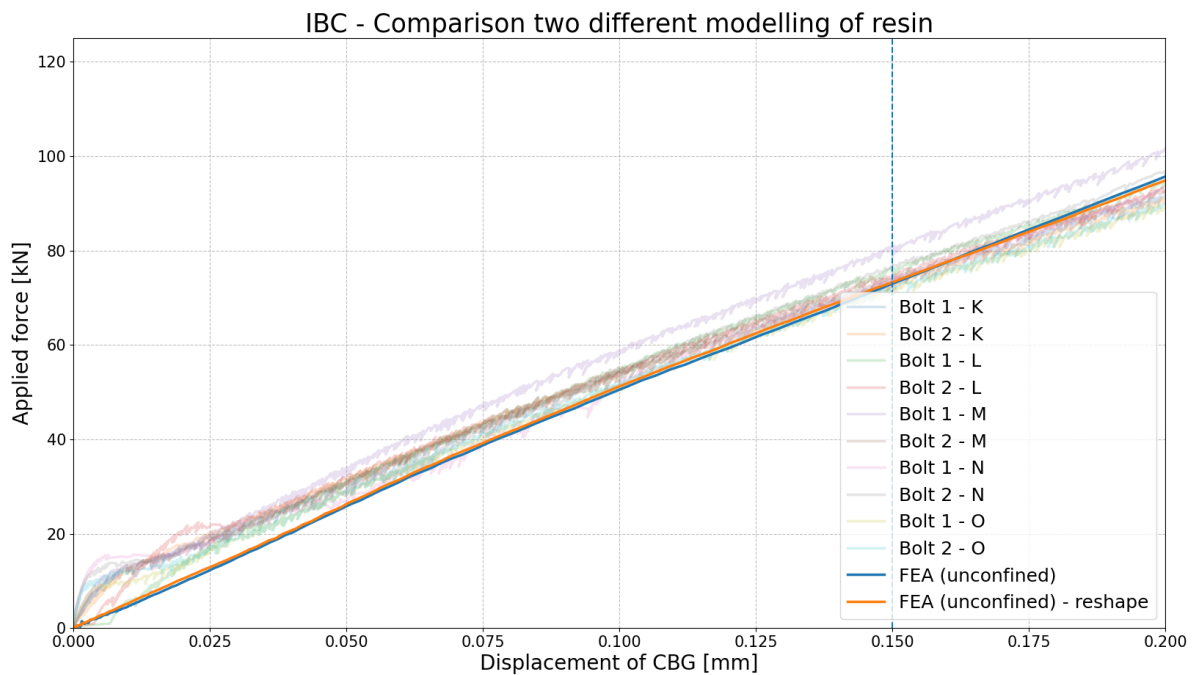


**Figure 101:** IBC - Load-displacement of the two different geometries of the resin. Fully injected and reduced height of 5mm (see [Figure 100](#))

From this figure, it can be concluded that there is no significant change that affects the obtained results of both injected (IBC) and preloaded and injected (PIBC) bolted connection when reducing the height of the resin by 5mm at each side.

### 6.2.2 Decreased mesh size of the resin

The other sensitivity relates to the mesh size of the resin in the through-thickness direction. Initially, the implemented mesh size was 0.5mm such that it was thought that this size represented a reliable resistance. This is based on both reliable output and computational time. However, this section elaborates on the effect of the assumed mesh size on the obtained bearing resistance. In [Figure 102](#), two different figures are shown. The top figure shows the decreased mesh size to 0.25mm instead of the original 0.5mm. The bottom figure visualises the decreased mesh size to 0.15mm. The implemented mesh size is applied to the entire resin. Therefore, the shown cross-sections in [Figure 102](#) are for illustrative purposes only.

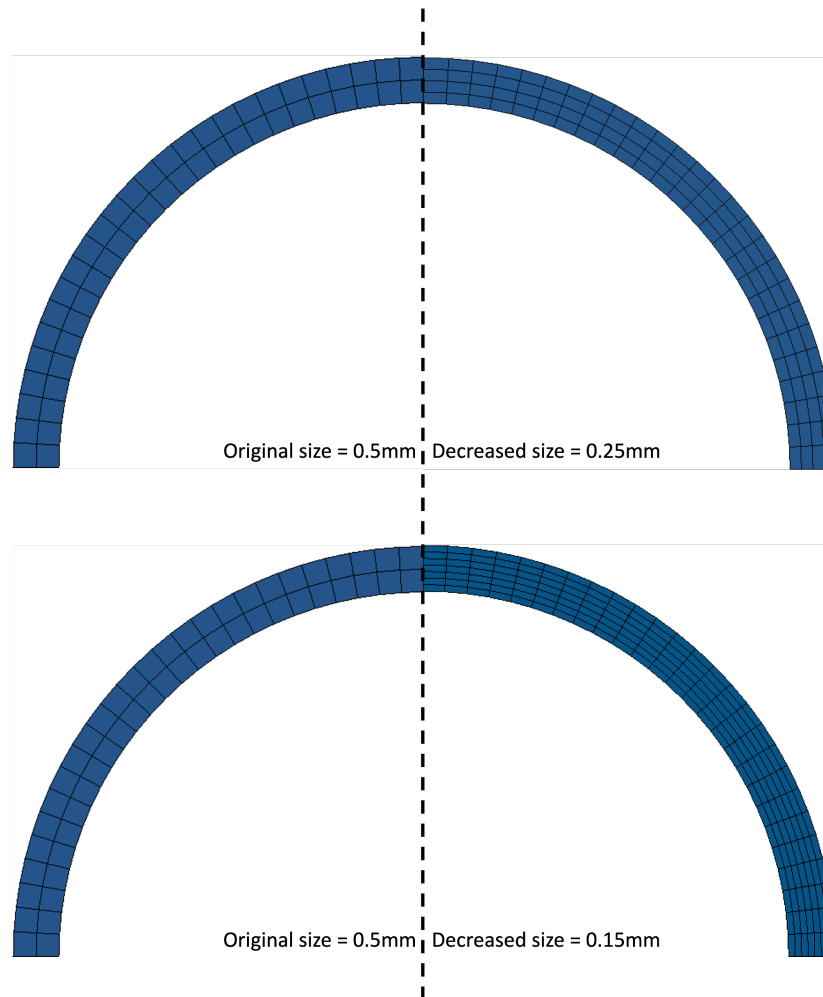


**Figure 102:** Two additional considered mesh sizes. The top indicates a mesh size of 0.25mm in the through-thickness direction and the bottom figure shows a size of 0.15mm in the through-thickness direction

In [Figure 103](#), the load-displacement graphs of the different modelled resins are shown. The blue line represents the implementation of a mesh size of the resin of 0.5mm. The orange and green lines relate to the reduced mesh sizes of 0.25m and 0.15mm.

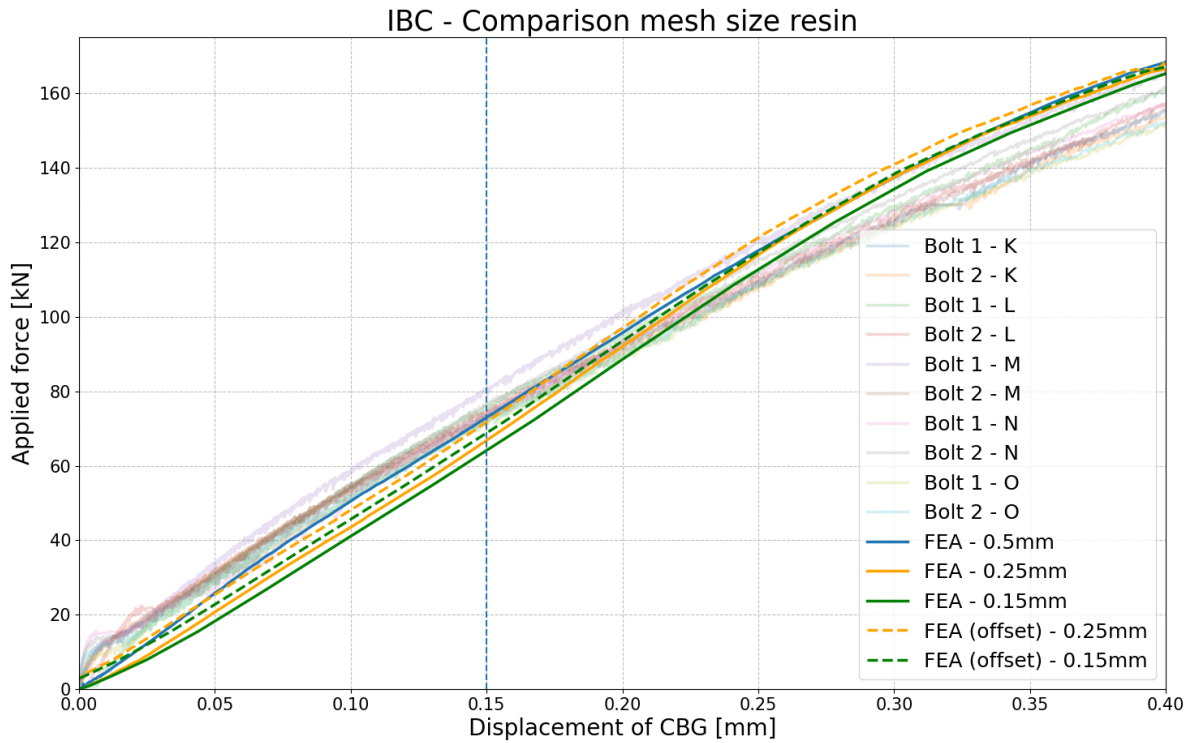


**Figure 103:** The load-displacement behaviour of three different implemented mesh sizes. Including offset of the lower mesh sizes by -0.01mm displacement at CBG

From the performed numerical analysis it is observed that at a displacement of 0.15mm at CBG, the numerical resistance reduces to 65kN and 68kN for the green and orange continuous lines respectively. Therefore, one can say that a plateau in the obtained resistance by changing the mesh size has not found yet (not fully converged). However, when looking into the trajectory of the load-displacement graph, it is observed that at the initial phase, the stiffness is significantly lower than in the case a higher mesh size is implemented. This stiffness is not expected to be the stiffness of the bearing strength of the resin. After a certain displacement of 0.05mm, the slope of the blue and both green and orange continuous lines are similar, identifying the observed stiffness of the connection. Therefore, it is expected that for smaller mesh sizes, the initial phase of the specimens initiates different behaviour. When keeping this out of consideration, the obtained graphs are shifted by a negative offset of -0.01mm (dotted lines). Therefore, the mesh size affects the load-displacement behaviour, thus resistance, of an (preloaded and) injected bolted connection. However, it is unknown what the sensitivity of the initial phase is to this load-displacement behaviour since after a displacement of 0.30mm, the behaviour is identical for all types of implemented mesh sizes. Due to the limitation in time, further investigation is mentioned in the recommendations of this report.

### 6.3 Preloading of the bolts by Combined method

In structures owned by the Dutch Ministry of Infrastructure, it is mandatory to apply the combined method as tightening method to preload bolts [61]. This is stated in the ROK, a document by Rijkswaterstaat [61]. This combined method consists of two steps where the first step describes a defined torque. The amount of torque required depends on several factors whereof the friction between the nut and bolt is one of them. The more friction occurs at the interface, the higher the required torque. According to the NEN-EN1090-2 paragraph 8.5.4. and Annex H, the required torque can be determined by experiments or two different formulas. In this research, this required torque is based on experimenting with five sets of bolt assemblies. From the obtained results, this torque ( $M_{r,test}$ ) is set at a value of 185Nm. It was thought that the to-be-applied torque (within step 1) is 75% of this determined value (=140Nm). However, this reduction of 25% is only applicable if the torque is determined by one of the two formulas ( $M_{r,1}$  or  $M_{r,2}$ ). Therefore, in this experiment, the combined method is not applied correctly since an additional reduction is considered. Within the first step of the combined method, the applied torque is too low.

During the second step of the combined method, the preload force reaches a level of preloading such that local plastification of material is initiated. This plastification ensures that additional tightening of the bolt will not result in a significant increase of the preload force in the bolt. This is also investigated by Berenbak [6]. In his research, he concludes that the chance of exceeding the preloaded force of the NEN-EN1993-1-8  $F_{p,C}$  when using the combined method is 100%. In Figure 104 a graph is shown of the preloading phase of the combined method. According to the NEN-EN1090-2, the aimed preload force in the bolt is 75% of  $F_{p,C}$ .

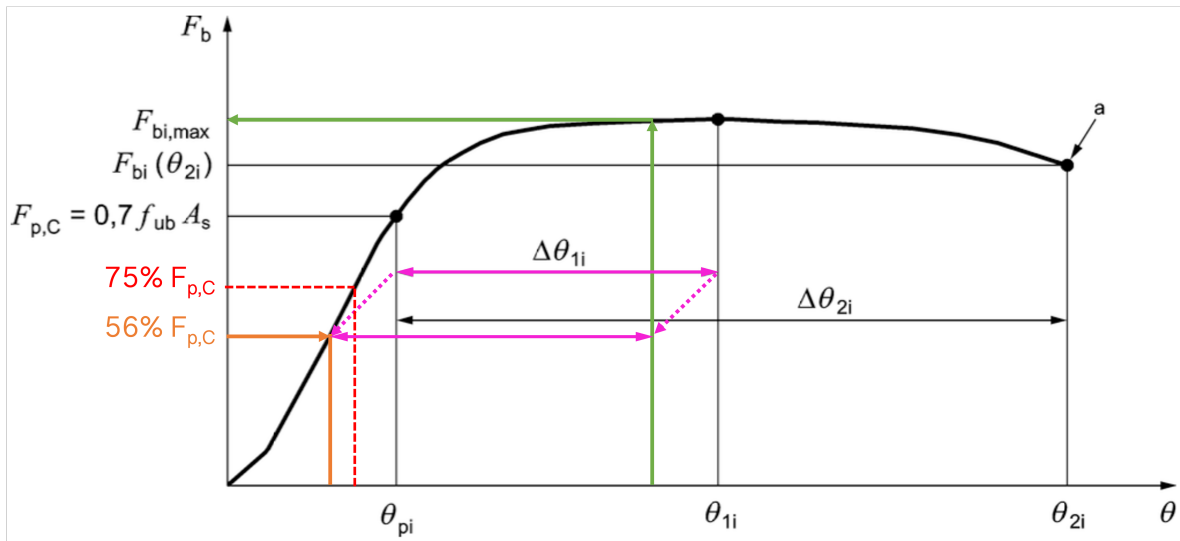


**Figure 104:** The consequence of applying a 25% less torque within the first step of the combined method to the preload force in the bolt after completion of this method. The unprocessed graph is obtained from the NEN-EN14339-2 [14]

However, in this experiment, an additional 25% reduction is incorrectly implemented whereby the aimed preload force in the bolt is 56% instead of 75% of  $F_{p,C}$ . This is indicated with the orange arrows in Figure 104. When the combined method is performed correctly, the available preload force in the bolt is expected to be higher. After completion of the first step, the bolt is rotated with an aimed angle of 120 degrees. The actual angle may differ from -15 up to +30 degrees with respect to the 120 degrees since the NEN-EN1090-2 allows such deviation in the applied angle. This stage is indicated with the horizontal magenta arrow. One can question what the effect on the preload force after completion is since a lower preload force (-25%) is acting after step one. However, from this figure, it can be concluded that the implementation of the additional reduction has a minimum effect on the preloading force. Therefore, no significant differences are expected compared to the potential outcome of the correctly performed combined method.

## 6.4 Friction coefficient

The results of the preloaded connections show that the obtained experimental resistance is 106% larger than the nominal slip-resistance. One of the reasons for this deviation is the difference in nominal and applied preloading force. Besides this difference, the friction coefficient plays a role in this significant disparity. For a surface, sprayed with an Ethyl-Zinc-Silicate (EZS) coating, the friction coefficient that can be used without performing demonstrating tests is 0.4 according to NEN-EN1090-2 [15]. Within this equation the implemented forces are the preload force at the start of the experiment (see Table 9) and the applied force at which slip occurs (see Table 10).

As mentioned in Subsection 3.8.2, the formulation of the NEN-EN1090-2 indicates the relationship between the initial preload force and the maximum applied force. However, the term “friction coefficient” is still used within the NEN-EN1090-2 even if the application is questionable. In Figure 105, an overview is given of the assumed comparison of coefficients. Where the blue dots are implemented to determine the initial friction coefficient and the yellow dots for the actual friction coefficient. It can be seen that for the calculation of the initial friction coefficient, the blue dots do not act at the same time (simultaneously). While for the yellow dots, the same point in time is used.

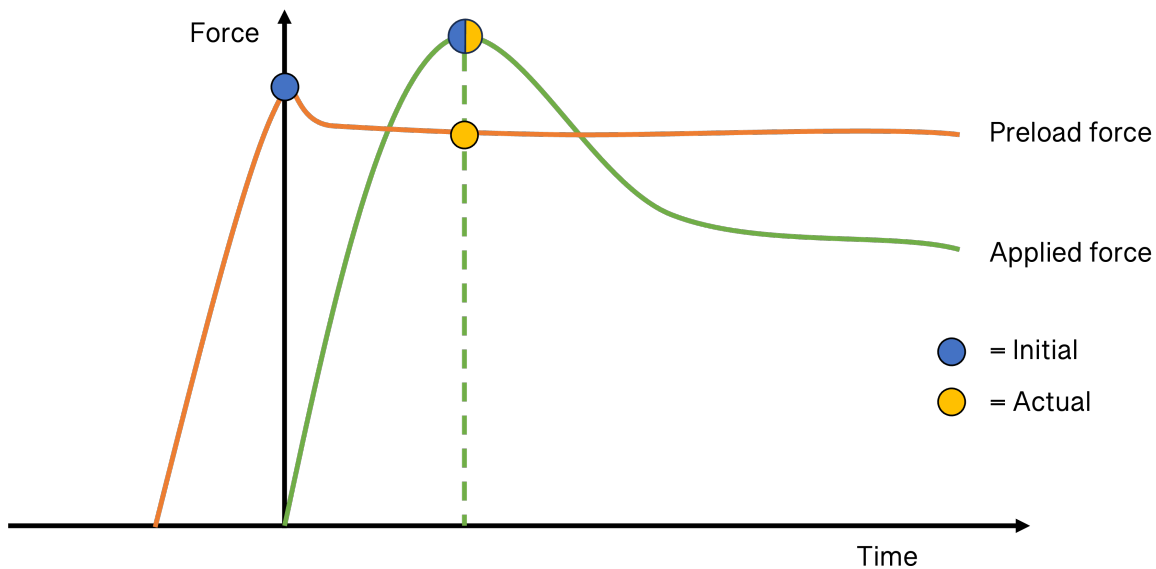


**Figure 105:** Assumption in considered preload and applied force in time between calculation of the actual and initial friction coefficient

In Section 2.5, two different methodologies were adopted to investigate the effect of the “friction coefficient”: nominal, initial and actual. The difference between these values is the substituted preload force in the bolt. In this research, the prescribed preload force by the standard is 110kN. The actual preload force after tightening according to the combined method is 140kN. While the actual preload force is expected to be a bit lower than the initial preload force. When taking into consideration the three methodologies, the following friction coefficients are observed as shown in Table 40 and Table 41.

**Table 40:** Determined friction coefficient for each bolt and difference to the nominal friction coefficient of 0.4 [15]

|         | $F_{p,C,init}$ [kN] | $F_{p,C,actual}$ [kN] | $F_{max}$ [kN] | $\mu_{init}$ [-] | $\mu_{actual}$ [-] |
|---------|---------------------|-----------------------|----------------|------------------|--------------------|
| P1      | 140.5               | 137.2                 | 136.7          | 0.49             | 0.50               |
| P2      | 137.8               | 133.2                 | 136.7*         | 0.50             | 0.51               |
| Q1      | 140.2               | 135.5                 | 154.7          | 0.55             | 0.57               |
| Q2      | 138.4               | 133.1                 | 148.0          | 0.53             | 0.56               |
| R1      | 138.7               | 135.9                 | 153.1          | 0.55             | 0.56               |
| R2      | 139.0               | 136.0                 | 139.3          | 0.50             | 0.51               |
| Average | 139.1               | 135.1                 | 144.7          | 0.52 (+30%)      | 0.54 (+34%)        |

\* = could not obtain initial resistance anymore after slip of the other connection

**Table 41:** Determined friction coefficient for each bolt and difference between two methods (based on initial and actual preload force)

|         | $F_{p,C,init}$ [kN] | $F_{p,C,actual}$ [kN] | $F_{max}$ [kN] | $\mu_{init}$ [-] | $\mu_{actual}$ [-] |
|---------|---------------------|-----------------------|----------------|------------------|--------------------|
| A1      | 98.8                | 93.3                  | 103.7          | 0.52             | 0.56               |
| A2      | 99.5                | 95.6                  | 119.2          | 0.60             | 0.62               |
| B1      | 101.4               | 97.1                  | 108.5          | 0.53             | 0.56               |
| B2      | 101.0               | 97.1                  | 108.5          | 0.54             | 0.56               |
| AA1     | 99.7                | 96.3                  | 95.6           | 0.48             | 0.50               |
| AA2     | 99.9                | 96.8                  | 125.7          | 0.63             | 0.65               |
| Average | 100.1               | 96.0                  | 110.2          | 0.55 (+37%)      | 0.57 (+44%)        |

From both tables above, it can be seen that the friction coefficient based on the initial preload force is the lowest. This is also expected since this coefficient contains the highest implemented preload force. In addition, the highest friction coefficient is obtained when considering the nominal preload force.

As indicated previously, it is thought that the equation that determines  $\mu$  is in fact not a friction coefficient. If this is not correct, then the implemented preload force must be the actual preload force. This force is related to the same time at which the maximum slip resistance is obtained.

## 6.5 Location of output versus obtained resistance

According to the NEN-EN1090-2, the experimental layout contains 8 points used to monitor the displacement. It is expected that in this way, the displacement at CBG is represented. These points are located at the centerline of each plate at the axis of the bolt. To mount these LVDTs, special components are fabricated. These components are mounted by screws as indicated in Figure 106. A tapped hole is located at the axis of the bolt and is 10mm deep. Therefore, the components can be reused and are assumed to be rigid during the entire experiment, such that reliable displacements are measured.

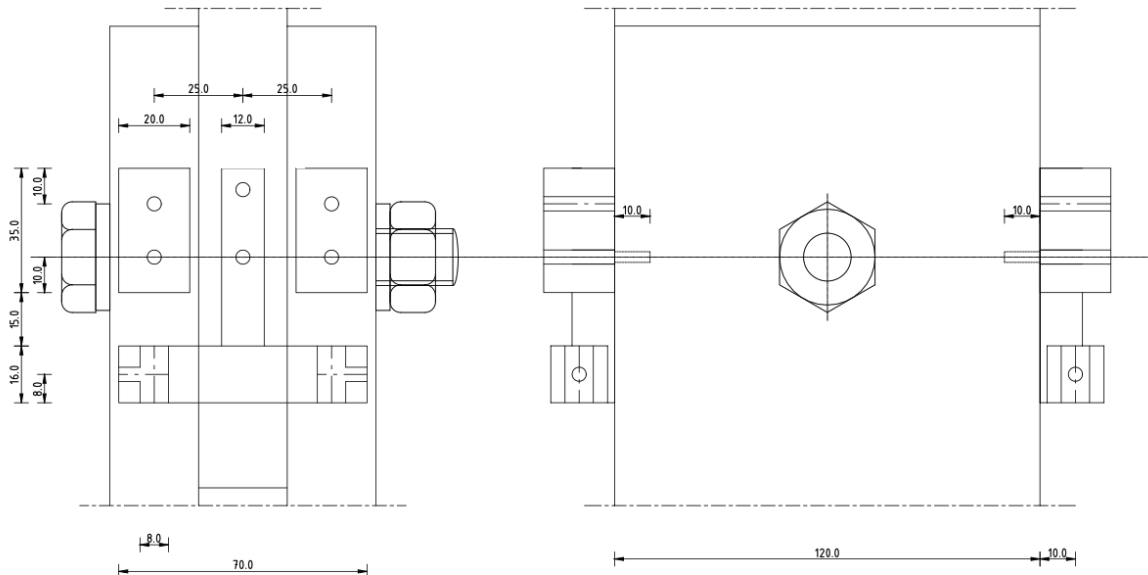


**Figure 106:** Design of the connection including components required for mounting and monitoring the displacement at CBG

However, within this research, the required components to measure this displacement are mounted to the specimens by a screw that is inserted at a maximum depth of 10mm. Therefore, one can question whether this application is in line with the design of the NEN-EN1993-1-8 shown in Figure 28 [17]. According to this methodology, the displacements at the edges of the plates are measured. However, since these monitoring instruments are attached by screws over a depth of 10mm, the actual location at which the displacement is measured might differ. This location might be located somewhere over this depth of 10mm. In addition to this, one can also argue whether such points near the edge of the plate are representable for the displacement at the bolt group. In the following parts of this discussion, both arguments are elaborated in relation to the stiffness and resistances.

### 6.5.1 Relation to the determined stiffness

First, the effect of the measuring location, somewhere along the 10mm depth, on the stiffness of the connection is considered. To investigate this effect, the displacement along the width of the plate is shown to see if a non-uniform distribution of displacement occurs. To relate this to the stiffness, two load steps are considered. The result obtained from numerical analysis indicates that for the entire interval of two load steps ( $F=45\text{kN}$  versus  $F=120\text{kN}$ ), the displacement along the width is not uniformly distributed, see Figure 107. The horizontal lines between the locations 51mm to 69mm represent the bolt hole. This part is horizontal since no nodes are located in the bolt hole.

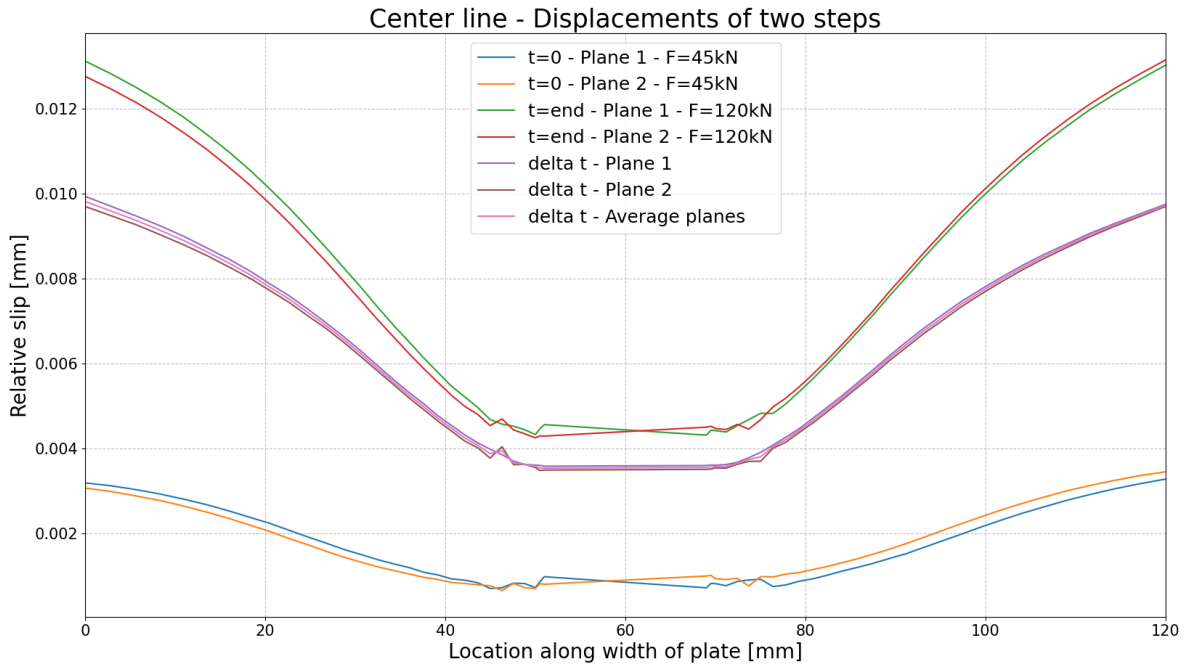


**Figure 107:** Displacement along the width of the plate at CBG for two load steps:  $F=45\text{kN}$  and  $F=120\text{kN}$  including the difference in displacement. Implemented preload force is  $140\text{kN}$

From the graphs, it can be seen that there is a difference in displacement between the edges of the plate (at 0 and 120mm) and the tip of the screw (at 10mm and 110mm). This difference already affects the stiffness of the connection since it is assumed that the edges are monitored. However, it is unknown what the behaviour of this screwed connection is with respect to displacements along the length of the screw. In addition to this statement, the absolute difference in displacement between the edge of the plate and bolt hole will increase if the exerted force on the connection increases. This is observed by the increased non-linearity for  $F=120\text{kN}$ . From this point onwards, the difference in displacement over the width of the specimen is meant by “lag-effect”.

Initially, it was thought that horizontal displacements are uniform along the width of the specimens since it is assumed that these edges represent the displacement at the center bolt group. However, this was incorrect according to the result shown in [Figure 107](#). This effect is non-uniform distribution is also considered at different widths over the height over the clamping package. Therefore, the second considered width is at the shear planes. In this case, the displacements are calculated based on nodes just above and just below the shear planes. The results are shown in [Figure 108](#).

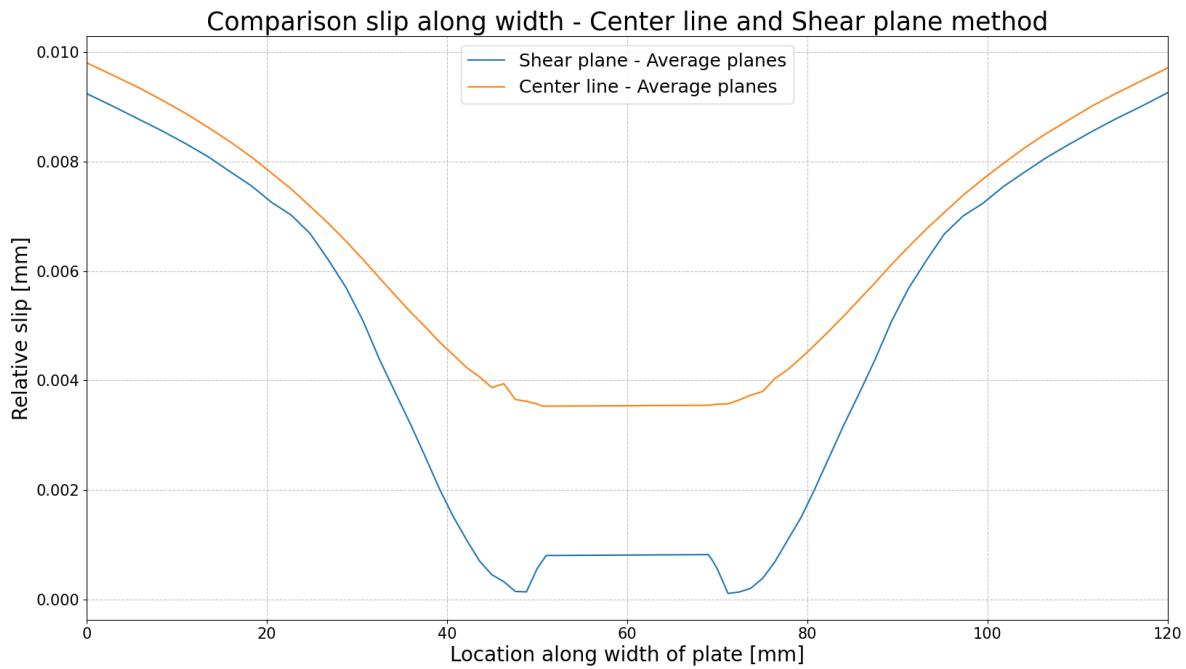


**Figure 108:** Displacement along the width of the plate at CBG and shear plane for two load steps:  $F=45\text{kN}$  and  $F=120\text{kN}$  including the difference in displacement. Implemented preload force is  $140\text{kN}$

This figure concludes that the difference in displacement between the nodes closer to the bolt hole and nodes closer to the side edges increases when getting closer to a shear plane. In the next section, the effect of the location of the measured resistances is taken into consideration.

### 6.5.2 Relation to potential summation of individual resistances

In the previous section, the acting displacements for two particular load cases are elaborated. However, it is yet unknown what this effect is for cases where a lower or even no preloading force is involved. For both experiments and numerical analyses, the summation of individual resistances over the entire measured trajectory of displacement at CBG is not allowed. It can be seen that after exceeding the slip-resistance the difference between the summation of obtained individual resistance for preloading and injection diverges from the obtained resistance of a preloaded and injected bolted connection. Within all comparisons, the displacement represents the measured displacement by the LVDTs at the edges of the plates. In the previous section, it is concluded a non-linear displacement of the width of the plates is prevailing. Since the resistance is created near/in the bolt hole, displacements in this region are important. Especially for the resin, strains have to occur inside the resin to create resistance.

Zooming in on this behaviour, the stresses and displacements along the height of the package are investigated and discussed. For this, two locations are taken into consideration to see the effect on each side of the resin. These two locations are shown in Figure 109. The outer node is located at the interface between the resin and the plate and the inner node is located at the interface of the resin and the bolt. Stresses and displacement of these locations are shown in the direction along the longitudinal axis of the bolt.

These two nodes are considered since the stresses in the resin are activated by the bearing of the resin. The amount of activated bearing resistance is dependent on the change in thickness of the resin with respect to the initial thickness (strains). This change in thickness of the resin is assumed to be equal to the difference in displacements between the two considered nodes as shown in Figure 109.

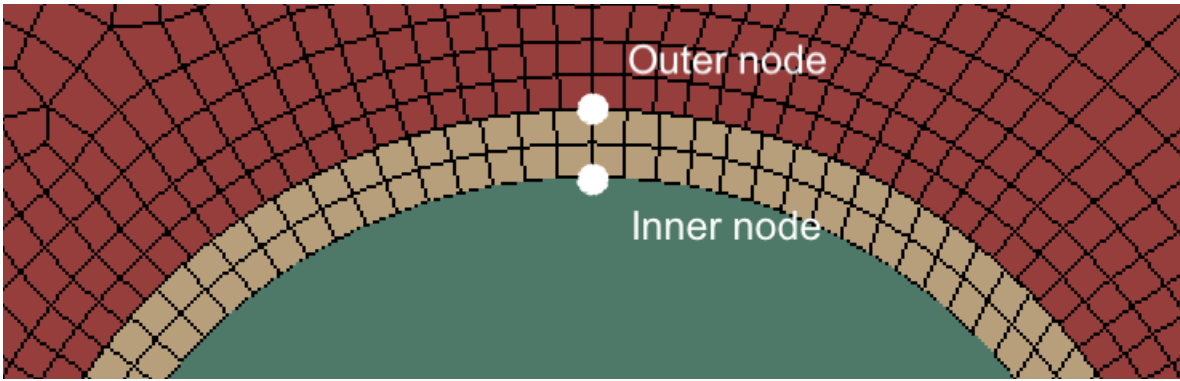


**Figure 109:** Two considered nodes at the bearing side of the connection for the investigation of the displacement and stresses along the height of the clamping package

The clamping package of the connection contains three plates of 25mm each which makes the connection double-lapped. During the application of the displacement loading, the outer plates have a bearing displacement in the opposite direction compared to the middle plate. Therefore, along the considered height, stresses are almost zero at the side-plates. The change in thickness at a relative **measured** slip of 0.15mm is visualised in [Figure 110](#). It can be seen that the signs of the values (positive or negative) between the middle- and side-plates are different.

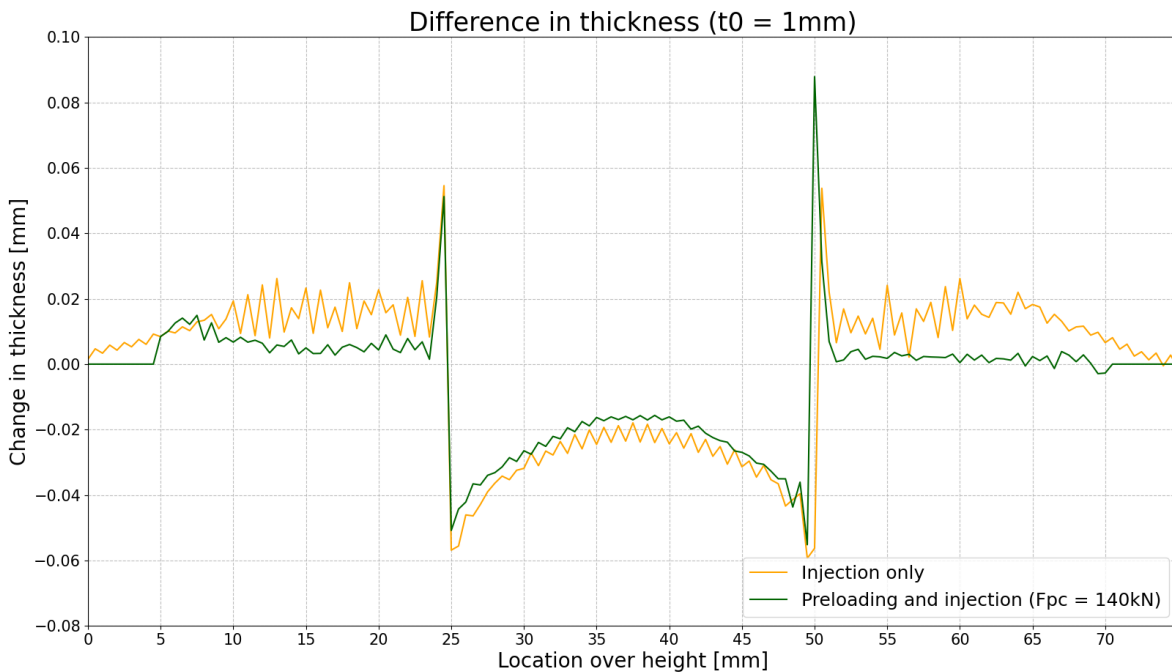


**Figure 110:** The effective difference in thickness ( $\Delta L$ ) of the resin measured at the two considered positions as shown in [Figure 109](#)

When focussing on the behaviour of the resin, the region from 25mm to 50mm is of importance. The expansion of the resin thickness is calculated by the difference in displacement of the inner and outer nodes. [Figure 110](#) shows that the closer to the shear planes, which are located at 25mm and 50mm, the larger the compression. This decrease in thickness is significantly concentrated at the shear planes rather than at the centerline of the plates. From this change in thickness, the comparison is made with the stresses that are acting along the height of these considered nodes. The results are shown in [Figure 111](#).

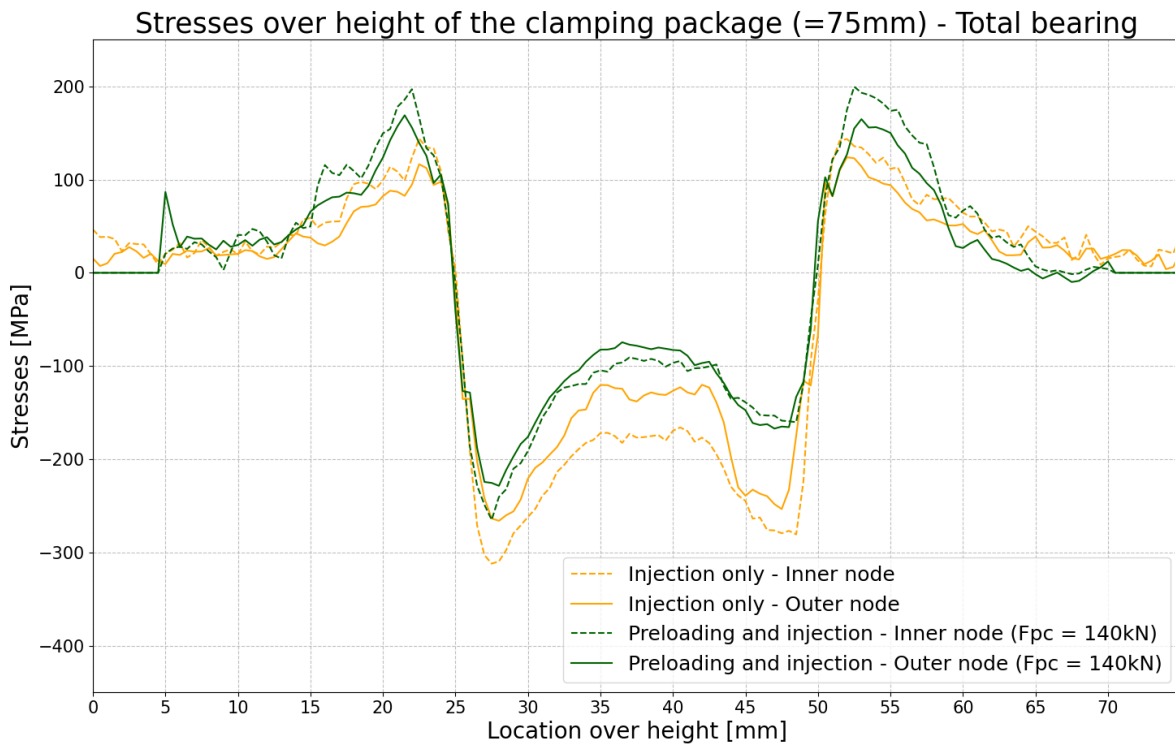


**Figure 111:** The acting stresses along the height of the clamping package measured at the two considered positions as shown in [Figure 109](#)

[Figure 111](#) indicates that significant bearing stresses of the resin are localised at the shear planes rather than distributed equally. This is also in line with Koper's results [37]. He concludes that the higher L/D-ratio decreases the degree of uniform distribution of stresses, thus increasing the local stress concentrations at the shear planes.

More importantly, from the stress distributions of both injection-only and connections using preloading and injection, it can be seen that the acting stresses in the resin of the injected-only connection are higher than for the preloaded and injected connection. Even if these stresses occur at the same **measured** displacement at the edges of the plates of 0.15mm. Therefore, it is more likely why summation of the two individual resistances (preloading and injection) is not possible. Since the stresses in the resin at the same **measured** displacement are not equal, the absolute contribution of the resin is different. This is also visualised by the obtained stiffnesses shown in [Table 38](#). This table shows that once the slip-resistance is exceeded, the higher preload force reduces the stiffness of the connection.

From these insights, it is questioned why the stresses, at the same **measured** displacement at the edges, are not similar. Therefore, additional comparison is made by adding the preload and injected bolted connection using a lowered preloaded force of 100kN. The main difference between a preloaded and non-preloaded connection is the clamping force that is initiated at the bolt(hole). In a preloaded connection, the preload force clamps a package together. This clamping force reduces when moving away from the bolt (see [Figure 80](#)). Therefore, when applying a shear force to the connection, the longitudinal stress in a fibre far away from the bolt is larger than for fibres closer to the bolt. This results in a different displacement in the longitudinal direction. [Figure 112](#) shows the displacement along the width of the plates per type of connection.

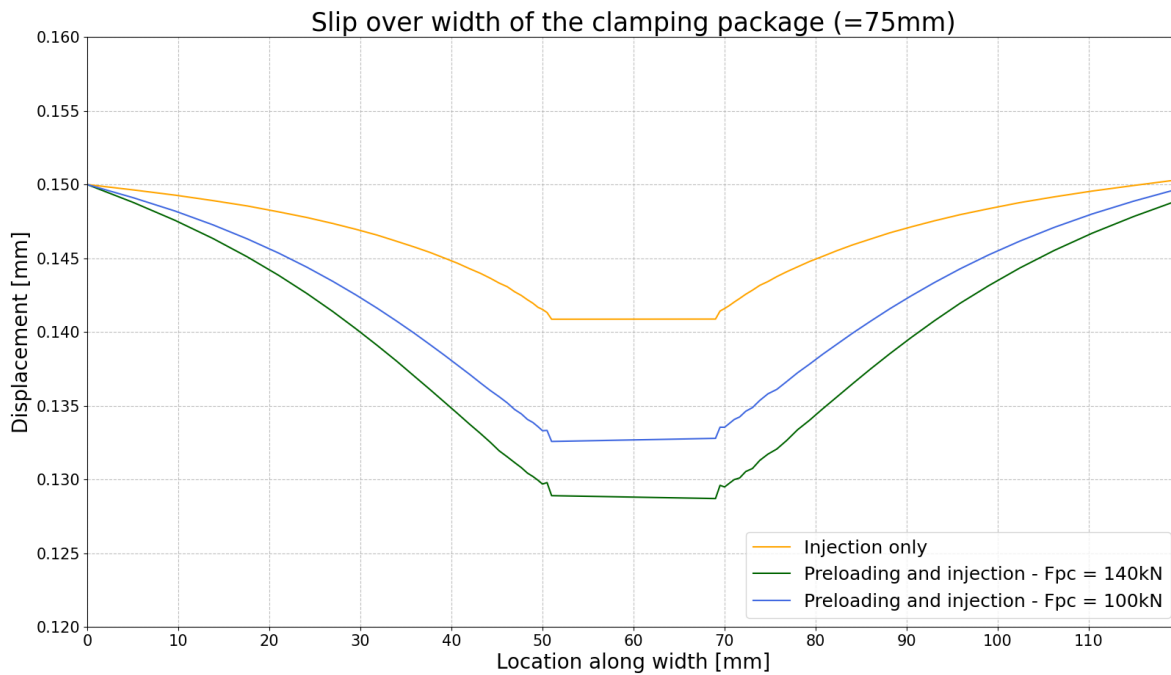


**Figure 112:** The total slip at the CBG along the entire width of the package

From this figure, [Figure 112](#), it can be seen that at the location of the bolt, the displacements are different than at the outer fibres. The bolt hole itself is located between 51 and 69mm. In other words, there is a lag of displacement between the inner and outer fibres. During an experiment, the outer fibres are measured assuming that these results are similar to the displacements at the bolt. However, in this figure, it is shown that the measured displacement at the outer fibres is not representative of the displacement at the CBG, especially for higher preloading forces. In this research, it is thus incorrectly assumed that the contribution of the resin is identical for each implementation at a **measured** displacement of 0.15mm. Therefore, comparing different connections at the same **measured** displacement is unjustified.

To conclude, within the applied methodology of measuring displacement it is assumed that displacements are uniform along the width of all specimens. However, since this is not the case, an incorrect comparison is made. A significant sensitivity emerges of the **measured** displacement on the resistance of the connection.

# 7

## Conclusion and recommendations

### 7.1 Conclusion

The aim of this research is to investigate if it is safe to assume that the resistance of a preloaded and injected bolted connection is equal to the sum of the individual obtained resistances from preloading and injection. Both experiments and numerical analyses have been performed to investigate the matter. These are executed for preloading and injection individually, and the combination of both.

The first considered resistance is the slip-resistance created by a 140kN preloaded bolt. When calculating the slip-resistance of a preloaded bolted connection according to the NEN-EN1993-1-8, a resistance of 112kN was expected, where no partial safety factor and an initial preload force of 140kN is taken into consideration. From the experiment, the obtained resistance was 144.7kN. Therefore, the NEN-EN1993-1-8 underestimates the resistance of a preloaded bolted connection. This difference in resistance is due to the increased friction coefficient. Namely, the friction coefficient is determined to be 0.52 (+30%) instead of the nominal 0.4. It should be kept in mind that this difference will increase when the implemented preload force in the nominal calculation reduces from 140kN to the nominal preload force of 110kN.

For the injected bolted connections, the Eurocode does not prescribe a particular bearing strength for the applied resin SW404+HY2404 (Rengel). The available literature states that a safe strength between 175-200MPa can be used. From experiments, the bearing strength of the resin turned out to be 187MPa when assuming uniform stress distribution and 122MPa in case the bearing strength is derived from the prescribed formula in NEN-EN1993-1-8. From these two bearing strengths, the obtained bearing resistance is 115kN (Experiment: -35%) and 74.7 kN (Experiment: 0%) respectively.

The NEN-EN1993-1-8 assumes that for preloaded and injected bolted connections, the resistance is equal to the sum of the obtained individual resistances from preloading and injection. From the calculated summation of experimented individual resistances of preloading and injection, a resistance of 219kN was expected. Nevertheless, it turned out that this resistance is only 187kN (-15%). Therefore, the summation of the individual resistances is invalid. This summation is based on the consideration of the maximum force for each individual resistance in a region until 0.15mm displacement at CBG. In addition to this, the potential summation of the individual forces at the same displacement is also considered. However, it turned out that there is no displacement that allows a safe summation for the latter procedure as well.

In the case where a lowered preload force of 100kN, instead of 140kN, a higher resistance is obtained and therefore exceeds the expected resistance of the Eurocode since the friction coefficient increases by 31%. This friction coefficient is also larger than the case of implementing a higher preloading force. With respect to a preloaded injected bolted connection, the obtained resistance from experiments is around 158kN. This resistance is -14% lower than the sum of the individual obtained resistances, which is a similar difference in percentage as for the case where a preload force of 140kN is adopted.

The model created for the numerical analysis overestimates the resistance of a preloaded and injected bolted connection with 3kN (+2%) compared to the experimental results. For the experiment where a preload force of 100kN is used, this difference is 2kN (+1%). However, these results are based on the comparison with averaged resistances obtained from experiments. In the experimental results, a variation occurs which is not identified in the numerical analysis. It was observed that the numerical analysis showed comparable behaviour with respect to this scatter along the trajectory from 0 to 0.4mm displacement at CBG.

However, in this numerical analysis, it turned out that the geometry and the amount of preload force significantly affected the experimental results. A higher stiffness was obtained in the region closer to the bolt hole rather than at the edges. Therefore, the displacements at the edges are larger than the displacement around the bolt. Assuming that the displacements at both edges represent the displacement at the center bolt group (CBG) is thus not accurate. The criterion for resistance is related to a measured displacement at CBG of 0.15mm. However, it turned out that the displacement at the bolt itself was lower. This difference increases for a higher preload force. Therefore, one can question the monitoring methodology and therefore the degree of accuracy of the obtained resistances. Furthermore, the interaction behaviour in the numerical model has a significant influence on the load-displacement behaviour. For the preloaded connection, a penalty coefficient is implemented while it is expected that an increased non-linearity model must be implemented instead of the linear relation based on the penalty coefficient. For the injected bolted connection, specific boundary conditions are implemented such that it increases resistances without increasing the Young's Modulus. However, it can still be questioned whether these boundary conditions are safe and acceptable. In addition, it was found that the contribution of the slip-resistance decreases for higher preload forces. However, this is based on the numerical model which primarily depends on the implementation of the penalty coefficient.

For a preloaded bolted connection, one specific tightening method is prescribed by Rijkswaterstaat [61]. This method consists of two steps - application of a torque and rotation - where the advantageous characteristics of each step ensure that a certain preloading force in the bolt is reached [6]. The applied torque was determined by experiments where an additional, although incorrect, reduction of the torque was assumed. This results in a significant exceedance of the preload force that is prescribed to be 110kN according to the NEN-EN1993-1-8 [17]. After completion of the (reduced) combined method, this preload force turned out to be 140kN (+27%). This confirms the power and effectiveness of the combined method that the assumed preload force of 110kN is exceeded significantly.

## 7.2 Recommendations

Based on the results obtained in this research, the following points are recommended for further investigation:

### **Different thicknesses and width of clamping package**

It was observed that the geometry of the connection, especially width and thickness affects the determined resistance of the connection. The difference in thickness affects the stress distribution, created by the preload force, at the shear planes. This change subsequently influences the **measured** displacement. In addition, thicker plates also increase shear stiffness in the plane with a length in the longitudinal direction and a width equal to the thickness of the plates. Both aspects affect the difference in displacement along the width, which subsequently influences the **measured** resistance. Besides the thickness, the width of the plates plays a role since a larger width of the plate increases the difference between **measured** and the actual displacement at CBG in case the clamping force is equal. Therefore the ratio between the preloading force and the geometry of the plates is important.

Therefore, for further research it is recommended to investigate the effect of the thickness and width of the plates, thus clamping package, on the **measured** resistance of the connection. It is proposed to investigate this relationship in more detail to explore the effects of different layouts of connections on the results.

### **Group of bolts**

Since displacements are non-uniform along the width, the resistance of a bolt group might be affected significantly. If a failure criterion is set at the same **measured** displacement for all geometries, one can question the actual resistance of a connection. For larger bolt groups, the resistance might be affected since there is an irregular displacement pattern. Therefore, it is recommended to perform research on the resistance of (larger) bolt groups.

### **Behaviour of the Ethyl-Zinc-Silicate coating**

Based on a small number of experiments, it turned out that the coating acts as a Non-Coulomb interaction. This behaviour is not in line with the currently assumed relation between the normal and shear force. In addition, it turned out that there is a significant difference between the static and kinetic shear friction coefficient. Therefore, the maximum slip-resistance reduces after this resistance has been overcome. This highlights the importance of continued research into how this affects the proportion of the slip-resistance in a preloaded and injected bolted connection.

### **Numerical: interface conditions of the resin**

To increase the numerical capacity of the injected bolted connection. Interface conditions are implemented at the connection of the resin with both steel plate (rigid) and bolt (friction). Especially, the rigid connection increased the resistance significantly with the result that it matches experimental results. However, it can be questioned if this condition is also valid for other geometries, such as larger bolt hole clearances. Therefore, it is recommended to investigate the behaviour at this interface.

### **Numerical: slipping behaviour of the coating**

As indicated, the coating behaves such that the kinetic friction coefficient is significantly lower than the static friction coefficient. In addition, there is no Coulomb behaviour, such that there is no constant factor as the relation between the applied normal force and the shear resistance. It is recommended to perform additional research on this numerical behaviour, eventually based on the results of tribometer tests.

### **Numerical: mesh size of the resin**

In the discussion, it is elaborated that the mesh size of the resin affects the load-displacement behaviour significantly within a certain range of displacement. Especially in the initial phase a different and unexplainable stiffness is observed. Therefore, further investigation of the numerical behaviour of the resin is recommended. It is also recommended to perform this investigation in combination with the applied interface conditions of the resin since it was observed that these affect the resistance significantly.

# References

- [1] *Abaqus Analysis User's Guide (6.13)*. URL: <http://130.149.89.49:2080/v6.13/books/usb/default.htm?startat=pt05ch26s01abm52.html> (visited on 08/11/2023).
- [2] Muhammad Abid, Muhammad Khalil, and Hafiz Wajid. "AN EXPERIMENTAL STUDY ON THE RELAXATION OF BOLTS". In: *IJUM Engineering Journal* 16 (May 2015). DOI: [10.31436/iijum.v16i1.539](https://doi.org/10.31436/iijum.v16i1.539).
- [3] Harm Askes, Duc C. D. Nguyen, and Andy Tyas. "Increasing the critical time step: micro-inertia, inertia penalties and mass scaling". en. In: *Computational Mechanics* 47.6 (June 2011), pp. 657–667. ISSN: 1432-0924. DOI: [10.1007/s00466-010-0568-z](https://doi.org/10.1007/s00466-010-0568-z). URL: <https://doi.org/10.1007/s00466-010-0568-z> (visited on 08/15/2023).
- [4] *ASTM D4752 Rub Test PDF — PDF — Nondestructive Testing — Copyright*. en. URL: <https://www.scribd.com/document/385294474/ASTM-D4752-Rub-Test-pdf> (visited on 08/24/2023).
- [5] *Bearing Stresses — Engineering Library*. URL: <https://engineeringlibrary.org/reference/bearing-stress-air-force-stress-manual> (visited on 09/12/2023).
- [6] J. Berenbak and F. Bijlaard. "Evaluation the tightening procedures of preloaded bolt assemblies according to prEN 1090-2: "Technical requirements for steel structures" for reaching 95% reliability as prescribed in EN 1990". en. In: *Stevin rapport 6-17-1* (2017). URL: <https://repository.tudelft.nl/islandora/object/uuid%3A07d23a74-9b6e-4a29-869c-5f7a4f30182b> (visited on 03/14/2023).
- [7] Peter J Blau. "The significance and use of the friction coefficient". en. In: *Tribology International* 34.9 (Sept. 2001), pp. 585–591. ISSN: 0301-679X. DOI: [10.1016/S0301-679X\(01\)00050-0](https://doi.org/10.1016/S0301-679X(01)00050-0). URL: <https://www.sciencedirect.com/science/article/pii/S0301679X01000500> (visited on 07/04/2023).
- [8] Peter J. Blau. "Amontons' Laws of Friction". en. In: *Encyclopedia of Tribology*. Ed. by Q. Jane Wang and Yip-Wah Chung. Boston, MA: Springer US, 2013, pp. 71–71. ISBN: 978-0-387-92897-5. DOI: [10.1007/978-0-387-92897-5\\_166](https://doi.org/10.1007/978-0-387-92897-5_166). URL: [https://doi.org/10.1007/978-0-387-92897-5\\_166](https://doi.org/10.1007/978-0-387-92897-5_166) (visited on 07/04/2023).
- [9] C. den Boer and L. P. Bouwman. "Vermoeingsonderzoek welijzeren proefstukken met injectie - voorspanbouten, voor de spoorbrug te Culemborg". en. In: *Stevin rapport 6-72-12* (1972). URL: <https://repository.tudelft.nl/islandora/object/uuid%3Ad56b561c-9279-45ca-8ee2-6025ae7c5128> (visited on 03/14/2023).
- [10] L. P. Bouwman. "De invloed van de dikteverhoudingen van hoofd-en stuikplaten op de toelaatbare stuikspanning bij verbindingen met injectiebouten". In: *Stevin rapport 6-74-11* (1974).
- [11] L. P. Bouwman and A. M. Gresnigt. "Design of bolted connections with injection bolts". en. In: *Stevin rapport 6-89-02* (1989). URL: <https://repository.tudelft.nl/islandora/object/uuid%3A2fc850c3-3a88-4c32-8a9b-5a86a5a8b2e6> (visited on 10/27/2023).
- [12] *BTMC Series Strain Gauges for Strain in Bolt...* en. URL: <https://www.althensensors.com/sensors/strain-sensors-strain-gauges/special-application-straingauges/btmc-series-strain-gauges-for-strain-in-bolt-measurement/> (visited on 09/22/2023).
- [13] Guidance BV. *Epoxy gelcoat - Epoxy gelcoat - Epoxy gelcoat - Gelcoats - Tooling & composites - catalog*. nl-NL. URL: <http://www.viba.nl/nl/catalog/tooling-composites/gelcoats/epoxy-gelcoat/epoxy-gelcoat/epoxy-gelcoat/groups/g+c+p+t+a+view> (visited on 09/06/2023).
- [14] CEN. *NEN Connect - NEN-EN 14399-2:2015 en*. 2015. URL: <https://connect.nen.nl/Standard/Detail/204283?compId=10037&collectionId=0> (visited on 09/05/2023).
- [15] CEN. *NEN Connect - NEN-EN 14399-8:2018 en*. 2018. URL: <https://connect.nen.nl/Standard/Detail/3565420?compId=10037&collectionId=0> (visited on 09/05/2023).
- [16] CEN. *NEN Connect - NEN-EN 1993-1-8:2021 Ontw. en (CONCEPT)*. 2021. URL: <https://connect.nen.nl/Standard/Detail/3644030?compId=10037&collectionId=0> (visited on 03/22/2023).

- [17] CEN. *NEN Connect - NEN-EN 1993-1-8+C2:2011 nl*. Dec. 2011. URL: <https://connect.nen.nl/Standard/PopUpHtml?RNR=164764&search=&Native=1&token=de158cf2-6b25-449e-95ef-2dca812619f7> (visited on 02/09/2023).
- [18] CEN - NB. *NEN Connect - NEN-EN 1993-1-8+C2:2011/NB:2011 nl*. 2011. URL: <https://connect.nen.nl/Standard/Detail/161665> (visited on 07/04/2023).
- [19] CEN-1. *NEN 6786-1-NEN-Connect*. 6786-1. 2021. URL: <https://connect.nen.nl/Family/Detail/73597?compId=10037&collectionId=0> (visited on 10/06/2023).
- [20] CEN-Conc. *NEN Connect - NEN-EN 1992-1-1+C2:2011 nl*. 2011. URL: <https://connect.nen.nl/Standard/PopUpHtml?RNR=159356&search=&Native=1&token=b5f2614e-082c-4103-af9d-7d0d387746bc> (visited on 09/22/2023).
- [21] CEN:4. *NEN Connect - NEN-EN 14399-4:2015 en*. URL: <https://connect.nen.nl/Standard/Detail/204280?compId=10037&collectionId=0> (visited on 11/05/2023).
- [22] Giuseppe Cocchetti, Mara Pagani, and Umberto Perego. “Selective mass scaling and critical time-step estimate for explicit dynamics analyses with solid-shell elements”. en. In: *Computers & Structures*. Special Issue IASS-IACM-2012 127 (Oct. 2013), pp. 39–52. ISSN: 0045-7949. DOI: [10.1016/j.compstruc.2012.10.021](https://doi.org/10.1016/j.compstruc.2012.10.021). URL: <https://www.sciencedirect.com/science/article/pii/S0045794912002556> (visited on 06/14/2023).
- [23] ECCS. *European Recommendations for Bolted Connections with Injection Bolts*. 1994.
- [24] *Elcometer 456 Coating Thickness Gauge - Separate — Paint Thickness Measurement*. URL: <https://www.elcometer.com/en/coatings-inspection/all-coatings-inspection/dry-film-thickness/digital/elcometer-456-separate-coating-thickness-gauge.html> (visited on 08/24/2023).
- [25] *ESDEP LECTURE NOTE [WG11]*. URL: <https://fgg-web.fgg.uni-lj.si/~pmoze/esdep/master/wg11/10320.htm> (visited on 11/05/2023).
- [26] E. S. Gadelmawla et al. “Roughness parameters”. en. In: *Journal of Materials Processing Technology* 123.1 (Apr. 2002), pp. 133–145. ISSN: 0924-0136. DOI: [10.1016/S0924-0136\(02\)00060-2](https://doi.org/10.1016/S0924-0136(02)00060-2). URL: <https://www.sciencedirect.com/science/article/pii/S0924013602000602> (visited on 07/04/2023).
- [27] A M Gresnigt, G Sedlacek, and M Paschen. “INJECTION BOLTS TO REPAIR OLD BRIDGES”. en. In: ().
- [28] A. M. (Nol) Gresnigt and J. W. B. (Jan) Stark. “- Design of bolted connections with injection bolts”. en. In: *Connections in Steel Structures III*. Ed. by Reidar BJORHOVDE, André COLSON, and Riccardo ZANDONINI. Oxford: Pergamon, Jan. 1996, pp. 77–87. ISBN: 978-0-08-042821-5. DOI: [10.1016/B978-008042821-5/50067-5](https://doi.org/10.1016/B978-008042821-5/50067-5). URL: <https://www.sciencedirect.com/science/article/pii/B9780080428215500675> (visited on 02/02/2023).
- [29] AM Gresnigt and D Beg. “Design bearing stresses for injection bolts with short and long duration high loads: 5th International conference on structural engineering, mechanics and computation SEMC, Cape Town, South Africa”. In: *International conference on structural engineering, mechanics and computation* (2013). Ed. by null s.n. null. Place: s.l. Publisher: Taylor and Francis, pp. 1317–1322. ISSN: 978-113800061-2. URL: <http://www.semc.uct.ac.za/> (visited on 03/29/2023).
- [30] AM Gresnigt, FSK Bijlaard, and D Beg. “Injection bolts in steel structures with short duration high loads: Connections VII: 7th International workshop on connections in steel structures, Timisoara, Romania”. In: *International workshop on connections in steel structures* (2012). Ed. by D Dubina and D Grecea. Place: Timisoara Publisher: University of Timisoara, pp. 423–436. ISSN: 978-92-9147-114-0. URL: <http://www.ct.upt.ro/connections/index.htm> (visited on 03/29/2023).
- [31] Zhen Guo et al. “Effect of preloading in high-strength bolts on bolted-connections exposed to fire”. en. In: *Fire Safety Journal* 90 (June 2017), pp. 112–122. ISSN: 0379-7112. DOI: [10.1016/j.firesaf.2017.04.030](https://doi.org/10.1016/j.firesaf.2017.04.030). URL: <https://www.sciencedirect.com/science/article/pii/S0379711217303181> (visited on 08/11/2023).

- [32] Hong, Won-Kee. *The investigation of the structural performance of the hybrid composite pre-cast frames with mechanical joints based on nonlinear finite element analysis*. en. Pages: 89-177. Woodhead Publishing, Jan. 2020. ISBN: 978-0-08-102721-9. DOI: [10.1016/B978-0-08-102721-9.00003-0](https://doi.org/10.1016/B978-0-08-102721-9.00003-0). URL: <https://www.sciencedirect.com/science/article/pii/B9780081027219000030> (visited on 07/31/2023).
- [33] *Interzinc 22*. URL: <https://www.international-pc.com/products/interzinc-22> (visited on 07/16/2023).
- [34] Samsiya Khaday et al. “Relationship between Friction Coefficient and Surface Roughness of Stone and Ceramic Floors”. en. In: *Coatings* 11.10 (Oct. 2021). Number: 10 Publisher: Multidisciplinary Digital Publishing Institute, p. 1254. ISSN: 2079-6412. DOI: [10.3390/coatings11101254](https://doi.org/10.3390/coatings11101254). URL: <https://www.mdpi.com/2079-6412/11/10/1254> (visited on 09/21/2023).
- [35] Kluwen, H. *Onderzoek aan verbindingen met voorspanbouten en voorspaninjectiebouten met behandelde contactvlakken onder duurbelasting t.b.v. Rijkswaterstaat — TU Delft Repositories*. Dec. 1982. URL: <https://repository.tudelft.nl/islandora/object/uuid%3Afb869ed8-f94e-47e4-968d-8de5bb5fd34a?collection=research> (visited on 03/14/2023).
- [36] M. H. Kolstein. “Het aandraaien van voorspanbouten in werktuigonderdelen”. en. In: *Stevin rapport 6-94-29* (1995). URL: <https://repository.tudelft.nl/islandora/object/uuid%3A9a1593da-776c-4fbf-aaf1-24f47ce01d83> (visited on 10/01/2023).
- [37] A. M. Koper. “Assessment of Epoxy Resins for Injected Bolted Shear Connections”. en. In: (2017). URL: <https://repository.tudelft.nl/islandora/object/uuid%3Ab9b44e86-5c62-4cac-9940-ff99e7c12429> (visited on 03/06/2023).
- [38] Leonie. *Direct Tension Indicator (DTI) — Bolt load monitoring*. en-US. URL: <https://boltSAFE.com/digital-load-cell/> (visited on 08/06/2023).
- [39] A. L. Marcelo et al. “Fatigue Properties of High Strength Bolts”. In: *Procedia Engineering*. 11th International Conference on the Mechanical Behavior of Materials (ICM11) 10 (Jan. 2011), pp. 1297–1302. ISSN: 1877-7058. DOI: [10.1016/j.proeng.2011.04.216](https://doi.org/10.1016/j.proeng.2011.04.216). URL: <https://www.sciencedirect.com/science/article/pii/S1877705811004048> (visited on 09/05/2023).
- [40] Martijn. *Stealth - Hydraulic ratchet link*. Sept. 2017. URL: <https://www.hytorc.nl/en/hydraulic-torque-wrenches/stealth/> (visited on 09/06/2023).
- [41] Robert W. Messler. *Joining of Materials and Structures: From Pragmatic Process to Enabling Technology*. en. Google-Books-ID: CRT97aa7cnMC. Butterworth-Heinemann, Aug. 2004. ISBN: 978-0-7506-7757-8.
- [42] D. M. Mulvihill et al. “Investigation of non-Coulomb friction behaviour in reciprocating sliding”. In: *Wear* 271.5 (June 2011), pp. 802–816. ISSN: 0043-1648. DOI: [10.1016/j.wear.2011.03.014](https://doi.org/10.1016/j.wear.2011.03.014). URL: <https://www.sciencedirect.com/science/article/pii/S004316481100189X> (visited on 10/18/2023).
- [43] Sayed A. Nassar and Antoine Abboud. “An Improved Stiffness Model for Bolted Joints”. en. In: *Journal of Mechanical Design* 131.12 (Dec. 2009), p. 121001. ISSN: 1050-0472, 1528-9001. DOI: [10.1115/1.4000212](https://doi.org/10.1115/1.4000212). URL: <https://asmedigitalcollection.asme.org/mechanicaldesign/article/131/12/121001/466872/An-Improved-Stiffness-Model-for-Bolted-Joints> (visited on 03/08/2023).
- [44] *NEN Connect - NEN 6788:1995 nl*. URL: <https://connect.nen.nl/Standard/Detail/17014?compId=10037&collectionId=0> (visited on 10/27/2023).
- [45] *NEN Connect - NEN-EN 1992-1-1+C2:2011/NB:2016+A1:2020 nl*. URL: <https://connect.nen.nl/Standard/Detail/3625916?compId=10037&collectionId=0> (visited on 11/05/2023).
- [46] Vervangt Nen-En. “Het vervaardigen van staal- en aluminiumconstructies - Deel 2: Technische eisen voor staalconstructies”. en. In: (Aug. 2018).
- [47] Jon Ness and Eden Prairie. “Three Ways Increasing the L/D Ratio Improves Reliability of Dynamically Loaded Bolt Joints”. en. In: ().
- [48] M. P. Nijgh. “Loss of preload in pretensioned bolts”. en. In: (2016). URL: <https://repository.tudelft.nl/islandora/object/uuid%3A4776e217-d7b7-4122-8e36-61ab7ed8c672> (visited on 03/08/2023).

- [49] M.P. Nijgh. “A multi-scale approach towards reusable steel-concrete composite floor systems”. ISBN: 9789463842075. Dissertation (TU Delft). 2021. DOI: [10.4233/uuid:983b06e7-c30b-465c-a032-2439a7e9863f](https://doi.org/10.4233/uuid:983b06e7-c30b-465c-a032-2439a7e9863f).
- [50] Martin Nijgh. “New Materials for Injected Bolted Connections: A Feasibility Study for Demountable Connections”. en. In: (2017). URL: <https://repository.tudelft.nl/islandora/object/uuid%3A089a5c6f-3c28-4c58-9b5a-34138bf2be86> (visited on 03/08/2023).
- [51] Takashi Ohara et al. “Acrylic Acid and Derivatives”. en. In: *Ullmann's Encyclopedia of Industrial Chemistry*. eprint: [https://onlinelibrary.wiley.com/doi/pdf/10.1002/14356007.a01\\_161.pub4](https://onlinelibrary.wiley.com/doi/pdf/10.1002/14356007.a01_161.pub4). John Wiley & Sons, Ltd, 2020, pp. 1–21. ISBN: 978-3-527-30673-2. DOI: [10.1002/14356007.a01\\_161.pub4](https://doi.org/10.1002/14356007.a01_161.pub4). URL: [https://onlinelibrary.wiley.com/doi/abs/10.1002/14356007.a01\\_161.pub4](https://onlinelibrary.wiley.com/doi/abs/10.1002/14356007.a01_161.pub4) (visited on 08/01/2023).
- [52] Lars Olovsson, Kjell Simonsson, and Mattias Unosson. “Selective mass scaling for explicit finite element analyses”. en. In: *International Journal for Numerical Methods in Engineering* 63.10 (July 2005), pp. 1436–1445. ISSN: 0029-5981, 1097-0207. DOI: [10.1002/nme.1293](https://doi.org/10.1002/nme.1293). URL: <https://onlinelibrary.wiley.com/doi/10.1002/nme.1293> (visited on 08/22/2023).
- [53] A. M. Prior. “Applications of implicit and explicit finite element techniques to metal forming”. en. In: *Journal of Materials Processing Technology* 45.1 (Sept. 1994), pp. 649–656. ISSN: 0924-0136. DOI: [10.1016/0924-0136\(94\)90413-8](https://doi.org/10.1016/0924-0136(94)90413-8). URL: <https://www.sciencedirect.com/science/article/pii/S0924013694904138> (visited on 06/14/2023).
- [54] *Protective coatings*. URL: <http://protective.zandleven.com/nl/Zinksilicaat-ZL-400-55> (visited on 09/23/2023).
- [55] Jason Provines et al. “ANALYSIS AND CONSTRUCTION OF THE UNITED STATES’ FIRST COMPLETELY STAINLESS STEEL BOLTED SPLICE ON A STEEL GIRDER HIGHWAY BRIDGE”. In: 2018. URL: <https://www.semanticscholar.org/paper/ANALYSIS-AND-CONSTRUCTION-OF-THE-UNITED-STATES-%E2%80%99-ON-Provines-E./b376c6c75884b98ce6ebace8c02bf8a92bf6243> (visited on 03/22/2023).
- [56] Z. Y. Qin, S. Z. Yan, and F. L. Chu. “Finite element analysis of the clamp band joint”. en. In: *Applied Mathematical Modelling* 36.1 (Jan. 2012), pp. 463–477. ISSN: 0307-904X. DOI: [10.1016/j.apm.2011.07.022](https://doi.org/10.1016/j.apm.2011.07.022). URL: <https://www.sciencedirect.com/science/article/pii/S0307904X11004021> (visited on 08/11/2023).
- [57] Md Atiqur Rahman. *Shigley's Mechanical Engineering Design*. URL: [https://www.academia.edu/42658328/Shigleys\\_Mechanical\\_Engineering\\_Design](https://www.academia.edu/42658328/Shigleys_Mechanical_Engineering_Design) (visited on 09/06/2023).
- [58] *Renovatie Suurhoffbrug*. nl. URL: <https://www.nationalestaalprijs.nl/project/renovatie-suurhoffbrug> (visited on 03/13/2023).
- [59] Directorate-General for Research and Innovation (European Commission) et al. *Execution and reliability of slip resistant connections for steel structures using CS and SS (SIROCO): final report*. eng. LU: Publications Office of the European Union, 2019. ISBN: 978-92-79-98311-5. URL: <https://data.europa.eu/doi/10.2777/554114> (visited on 04/19/2023).
- [60] Luis Resende and John B. Martin. “Formulation of Drucker-Prager Cap Model”. EN. In: *Journal of Engineering Mechanics* 111.7 (July 1985). Publisher: American Society of Civil Engineers, pp. 855–881. ISSN: 0733-9399. DOI: [10.1061/\(ASCE\)0733-9399\(1985\)111:7\(855\)](https://doi.org/10.1061/(ASCE)0733-9399(1985)111:7(855)). URL: <https://ascelibrary.org/doi/10.1061/%28ASCE%290733-9399%281985%29111%3A7%28855%29> (visited on 07/31/2023).
- [61] Rijkswaterstaat. *Standaarden RWS - Standaard*. Dec. 2021. URL: <https://standaarden.rws.nl/index.html> (visited on 03/28/2023).
- [62] Arvin R. Savkoor. “Models of Friction Based on Contact and Fracture Mechanics”. en. In: *Fundamentals of Friction: Macroscopic and Microscopic Processes*. Ed. by I. L. Singer and H. M. Pollock. NATO ASI Series. Dordrecht: Springer Netherlands, 1992, pp. 111–133. ISBN: 978-94-011-2811-7. DOI: [10.1007/978-94-011-2811-7\\_7](https://doi.org/10.1007/978-94-011-2811-7_7). URL: [https://doi.org/10.1007/978-94-011-2811-7\\_7](https://doi.org/10.1007/978-94-011-2811-7_7) (visited on 10/16/2023).

- [63] J. W. B. (Jan) Stark. “- Criteria for the use of preloaded bolts in structural joints”. en. In: *Connections in Steel Structures III*. Ed. by Reidar Bjorhovde, André Colson, and Riccardo Zandonini. Oxford: Pergamon, Jan. 1996, pp. 431–440. ISBN: 978-0-08-042821-5. DOI: [10.1016/B978-008042821-5/50099-7](https://doi.org/10.1016/B978-008042821-5/50099-7). URL: <https://www.sciencedirect.com/science/article/pii/B9780080428215500997> (visited on 02/05/2023).
- [64] Natalie Stranghöner et al. *Execution and reliability of slip resistant connections for steel structures using CS and SS (SIROCO)*. European Union, 2019. DOI: [10.2777/554114](https://doi.org/10.2777/554114).
- [65] Natalie Stranghöner et al. “Optimization of the test procedure for slip factor tests according to EN 1090-2”. en. In: *Steel Construction* 10.4 (2017), pp. 267–281. ISSN: 1867-0539. DOI: [10.1002/stco.201710040](https://doi.org/10.1002/stco.201710040). URL: <https://onlinelibrary.wiley.com/doi/abs/10.1002/stco.201710040> (visited on 03/07/2023).
- [66] *TCB Standard - High Strength Structural Preloaded Bolts — Tension Control Bolts*. URL: <https://www.tcbolts.com/en/products/tcb-standard> (visited on 08/06/2023).
- [67] Dieter Ungermann and Lisa Kröger. “Load-deformation behavior of injection bolts for maintenance of steel structures under dynamic loads”. en. In: *ce/papers* 6.3-4 (2023), pp. 1190–1195. ISSN: 2509-7075. DOI: [10.1002/cepa.2232](https://doi.org/10.1002/cepa.2232). URL: <https://onlinelibrary.wiley.com/doi/abs/10.1002/cepa.2232> (visited on 09/14/2023).
- [68] Siamak Valinasab. “Standard Test Method for Measuring MEK Resistance of Ethyl Silicate (Inorganic) Zinc-Rich Primers by Solvent Rub”. In: (). URL: [https://www.academia.edu/14277390/Standard\\_Test\\_Method\\_for\\_Measuring\\_MEK\\_Resistance\\_of\\_Ethyl\\_Silicate\\_Inorganic\\_Zinc\\_Rich\\_Primers\\_by\\_Solvent\\_Rub](https://www.academia.edu/14277390/Standard_Test_Method_for_Measuring_MEK_Resistance_of_Ethyl_Silicate_Inorganic_Zinc_Rich_Primers_by_Solvent_Rub) (visited on 08/04/2023).
- [69] Vries, P. de and Berger, S. *Influence of surface treatment and type of coating system on the slip factor and on the corrosion protection in case of carbon steel*. en. Mar. 2018.
- [70] Jiaming Wang et al. “Experimental and numerical investigation of mortar and ITZ parameters in meso-scale models of concrete”. en. In: *Theoretical and Applied Fracture Mechanics* 109 (Oct. 2020), p. 102722. ISSN: 0167-8442. DOI: [10.1016/j.tafmec.2020.102722](https://doi.org/10.1016/j.tafmec.2020.102722). URL: <https://www.sciencedirect.com/science/article/pii/S0167844220302986> (visited on 07/31/2023).
- [71] Haohui Xin, Martin Nijgh, and Milan Veljkovic. “Computational homogenization simulation on steel reinforced resin used in the injected bolted connections”. en. In: *Composite Structures* 210 (Feb. 2019), pp. 942–957. ISSN: 0263-8223. DOI: [10.1016/j.compstruct.2018.11.069](https://doi.org/10.1016/j.compstruct.2018.11.069). URL: <https://www.sciencedirect.com/science/article/pii/S0263822318336274> (visited on 07/31/2023).



## Measuring coating

Within the procedure of applying a coating on the shear planes of the specimen, the initially applied coating was rejected. This section elaborates the results of quality control why this coating was rejected.

In [Figure 113](#) the averaged measured thicknesses per shear plane is shown. This averaging is done by determining the mean value of the coating thickness for each plane as shown in [Figure 39](#). Within [Figure 113](#), identifies two different types of coatings, namely the middle and cover plates in blue and green respectively. The horizontal distribution relates to the thickness measured at the uncoated positions. This thickness relates to the grit-blasted steel surface. On the vertical axis, the average applied coating thickness per plane is shown. As mentioned, these values are determined by the difference between coated and uncoated thicknesses. Where all data should be positioned around the 60  $\mu\text{m}$  since this was the requested thickness.

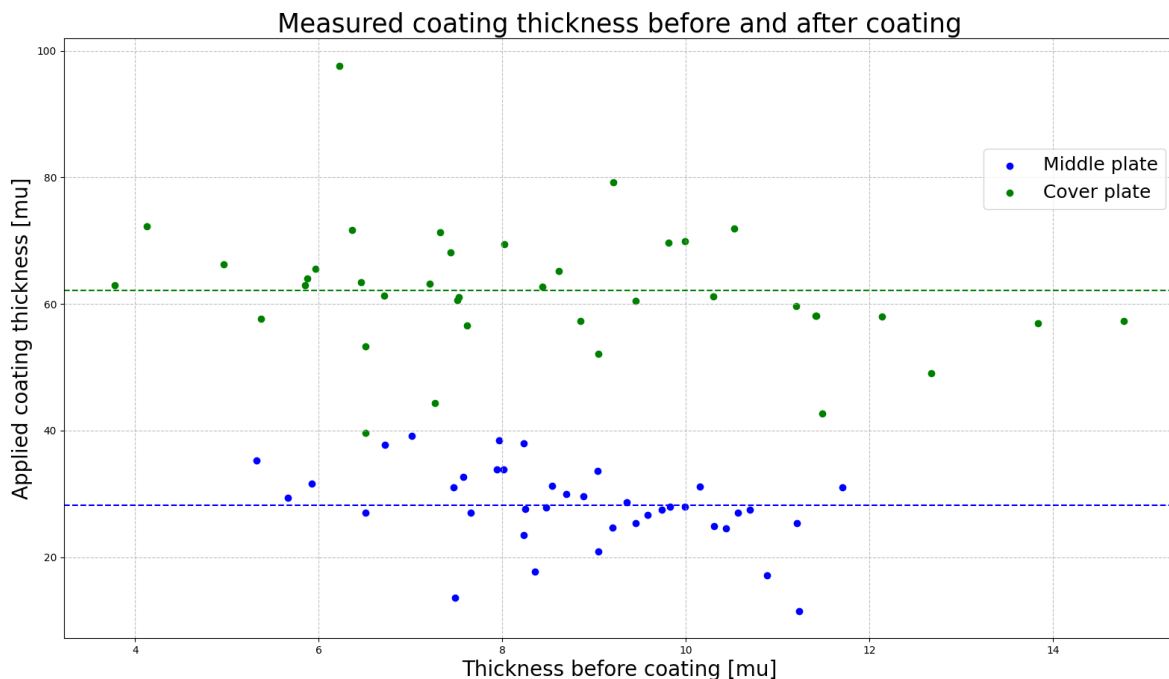


**Figure 113:** Difference in measured thickness between coated and uncoated surface areas

When looking into the different thicknesses visualised in [Figure 114](#), it can be concluded that all initial values are comparable between the middle and cover plates. This is also expected since all plates underwent the same sand-blasting procedure. However, after the steel is coated, a significant difference in thickness is observed between the two types of plates. From this graph, the clear difference between the cover and middle plates can be identified easily. The main plate has an average thickness of approximately  $30\mu\text{m}$ , whereas the cover plates have a mean coating thickness of more than  $60\mu\text{m}$ . Discrepancies in applied coating thickness may introduce side effects which must be considered when comparing results.

[Figure 113](#) shows the results for each shear plane. However, each plane consists of four monitored locations. In [Figure 114](#) an overview is shown of the number of measured thicknesses at each location. Similar to [Figure 113](#), a clear variation is observed. Within this graph, distinguishment is made between the middle and cover plates and the type of surface. From this figure, it can be concluded that the uncoated surfaces do not differ over the type of plates. However, after coating, one can see that a clear division occurs between the types of plates. The average coating thickness of the middle plates is just below  $40$  microns, while this thickness is approximately  $65$  microns for the cover plates. Those values should have been approximately  $60\mu\text{m}$ .

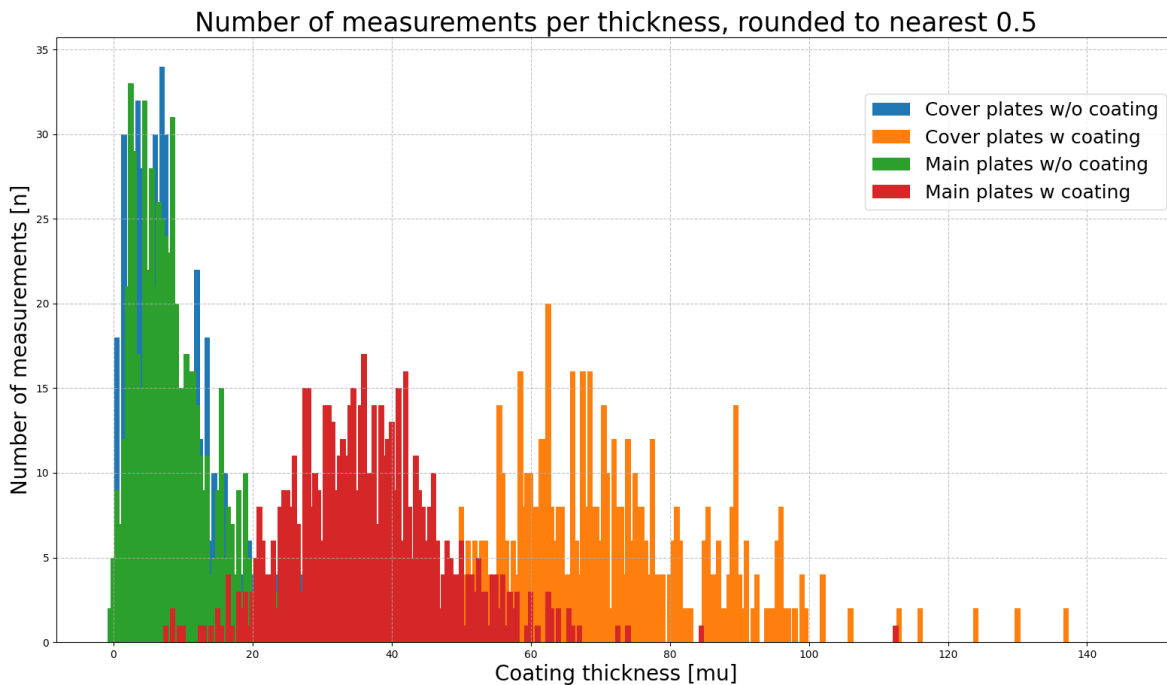


**Figure 114:** Distribution of different measured coating thicknesses for the initial coating

In addition to this conclusion, it turned out that the applied coating was not cured correctly. After application of the primer, the layer must be cured by resting under a high relative humidity [54]. If this curing procedure is not performed correctly, poor adhesion and drying of the coating occurs. To investigate the quality of adhesion and drying, the MEK-test is executed. [Figure 115](#) shows the results of the MEK-test for two different coatings. [Figure 115a](#) visualises the damaged coating for the initially applied coating. Whereas [Figure 115b](#) shows the results of the final and accepted coating.



(a) Degradation of the initially applied primer after 21 rubs



(b) Two types of degradation of the final applied primer after 50 rubs. Left and right path relates to the dry and moist cotton buds respectively

**Figure 115:** Different outcomes after the MEK-test: (a) initial coating (b) final coating

Figure 115a indicates the degradation of the initially applied coating after already 21 rubs. Since the plain became visible, the test was disrupted. Due to these substandard results, the plates were recoated since the results must remain reliable and applicable. Figure 115b indicates that the coating is still in a reasonable state and thus accepted.

# B

## Installation and calibration of strain gauges

### B.1 Installation

In general, long holes with small diameters are created implementation one of the two methods.

- Spark machining, also known as electrical discharge machining;
- Drilling

Spark machining can, subsequently, also be executed by two methods, namely wire cutting and die-sinking. However, due to the expected conical shape of the hole after completion, spark machining was not preferred. Drilling steel is in general more straightforward. Nevertheless, the hardness of material affects the applicability of drilling. Since the bolt's class is 10.9, the material is significantly harder than general S235 or S355 steel. Therefore, general drills can not be used. Therefore, special drills are procured for this research to make sure that holes can be drilled more easily. During the execution of drilling itself, there is an introduction of heat into the bolt due to the required amount of energy. To minimize negative effects, cooling fluids are used during the process. These fluids, along with the steel grease may adhere to the inner surface after completion, potentially affect the strain gauge measurements. Ensuring acceptable and reliable measurements requires the bolt hole to be cleaned by the following steps:

1. Using air pressure to remove initial grease and cooling fluids;
2. Rinsing of bolt hole with acetone;
3. Removing grease with a brush/toothpick;
4. Again rinsing with acetone;
5. Removing moisture with a compressor.

Of these steps, the last is of importance. Particularly in the context of the CN-adhesive. If moisture is not removed adequately from the bolthole, the strain gauges may get stuck during installation.

### B.1.1 Influential parameters

To monitor the voltage that runs through the circuit, each individual bolt must be connected to an amplifier. This connection is created by four cables which are soldered to the wire ends of the strain gauges, see [Appendix B](#). Since this soldering and the length of the cables affect the resistance, all bolts are calibrated individually. Therefore, all bolts are assigned to one specific channel.

The cable, which connects the strain gauge to the amplifier, represents resistances in the circuit. However, these resistances may vary, not only by production and installation but also by temperature and humidity. The increase of resistance due to temperature is dependent on the material of the cable. Therefore, additional measurements are taken into consideration to minimize such errors. First of all, to monitor the variation in voltages, a Wheatstone-Bridge principle is used. This application is often used when having an interest in the minimum difference in resistance that occurs. Impacts, such as temperature increase the error since materials have different thermal coefficients. Therefore the additional application is a three-way connection to the strain gauge. A three-way connection is an additional internal circuit which reduces the error produced by temperature significantly, see [Figure 116](#).

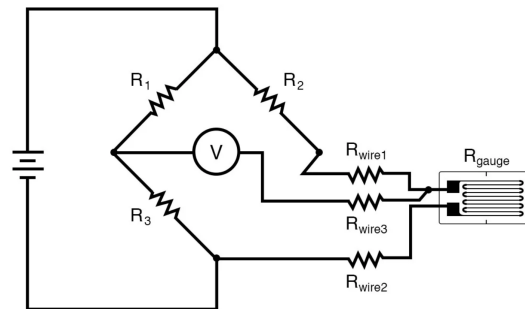


**Figure 116:** Quarter bridge with a 3-wire configuration (3 lead wires)

Such a circuit, as presented above, helps to minimize the error in results. A note is that all three lead wires are required to have a similar length, equal material properties and cross-sectional area. Only then, the error is minimized. These errors that initially may be created from, for instance, temperature are small. However, the increase in resistance ( $\Delta R$ ) compared to the initial resistance ( $R$ ) is not neglectable. The result is that even small influential factors may affect results tremendously. It is assumed that applying the quarter bridge with three lead wires to the setup gives an accurate and reliable outcome.

## B.2 Calibration

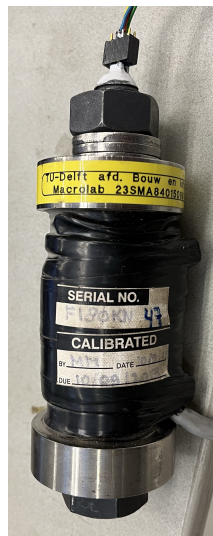
In [Subsection 3.5.2](#), the calibration procedure of the bolts is elaborated. In this section, it is mentioned that this calibration is performed in the testing rig by an elongation of the bolt. However, this is not performed by the first four bolts is executed by a load cell, see [Figure 117a](#). This application of preloading has a pitfall, namely the load introduction at the threads. When increasing the axial force stepwise to 110kN, the nut is pushed outwards, see [Figure 117b](#). Increasing the axial force in the bolt is achieved by rotating the nut. During the application of the torque the nut is still pushed outwards whereby wear and tear of the threads occurs. This increases the frictional force at the interface of the nut which is unfavourable. In addition, this damage to the threads influences the procedure of the combined method. Therefore the load cell methodology is redefined to calibration of the bolts inside the testing rig by a tensile test principle. Such a test is similar to the tensile test performed as explained in [Section 3.4](#). However, the maximum allowable exerted force is still 110kN.

In Table 42 output of the calibration procedure of one bolt is given. As mentioned before, one entire procedure consists of two single calibrations whereby the final conversion factor is averaged of the two calibrations. For example, for the bolt above, the first assessment resulted in a rounded factor of 12.219. The second attempt also has an outcome of 12.219. The absolute difference between these two is recognizable from the fourth decimal onwards. One can say that for this bolt, the difference is neglectable. However, still, all individual bolts have been calibrated twice since defects can not be detected visually and the location of the bolts (might) affect the conversion factor.

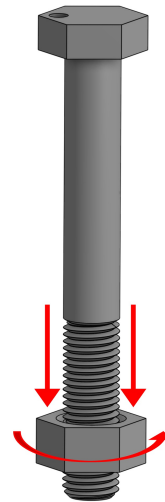
Within Table 42, several parameters are given per calibration. The input column relates to the difference in voltage that runs through the circuit compared to an unloaded condition. The second column, named value, visualises the acting normal force in the bolt, which is equal to the force applied by the testing rig. Division of these two parameters is the calibration factor of that load step. According to the table above, the calibration factor is equal during the entire procedure. However, this is the final outcome instead of the calibration of the step. In the last column, the error is given which is the absolute difference between the calibration factor of that single step and the factor after completion of one entire procedure.

**Table 42:** Results for the calibration procedure of one bolt

| Calibration 1 |              |            |               |              | Calibration 2 |              |            |               |              |
|---------------|--------------|------------|---------------|--------------|---------------|--------------|------------|---------------|--------------|
| <i>Input</i>  | <i>Value</i> | <i>Cal</i> | <i>Offset</i> | <i>Error</i> | <i>Input</i>  | <i>Value</i> | <i>Cal</i> | <i>Offset</i> | <i>Error</i> |
| 0.071         | 0.423078     | 12.21925   | -0.42405      | 0.020438     | 0.121         | 0.070293     | 12.21986   | -1.1834       | 0.224912     |
| 0.87          | 10.2514      | 12.21925   | -0.42405      | 0.044707     | 0.917         | 10.0056      | 12.21986   | -1.1834       | 0.01661      |
| 1.686         | 20.3057      | 12.21925   | -0.42405      | 0.128104     | 1.78          | 20.6311      | 12.21986   | -1.1834       | 0.063155     |
| 2.473         | 29.9546      | 12.21925   | -0.42405      | 0.160458     | 2.883         | 34.1937      | 12.21986   | -1.1834       | 0.147255     |
| 3.282         | 39.8795      | 12.21925   | -0.42405      | 0.199989     | 3.532         | 42.1429      | 12.21986   | -1.1834       | 0.165769     |
| 4.101         | 49.8186      | 12.21925   | -0.42405      | 0.131528     | 4.183         | 50.1292      | 12.21986   | -1.1834       | 0.196943     |
| 4.912         | 59.7434      | 12.21925   | -0.42405      | 0.14652      | 5.08          | 61.0795      | 12.21986   | -1.1834       | 0.186033     |
| 5.741         | 69.8444      | 12.21925   | -0.42405      | 0.117766     | 5.873         | 70.7279      | 12.21986   | -1.1834       | 0.144088     |
| 6.658         | 80.9923      | 12.21925   | -0.42405      | 0.060619     | 6.659         | 80.2451      | 12.21986   | -1.1834       | 0.056482     |
| 7.465         | 90.7698      | 12.21925   | -0.42405      | 0.022812     | 7.603         | 91.6829      | 12.21986   | -1.1834       | 0.041261     |
| 8.3           | 100.861      | 12.21925   | -0.42405      | 0.134681     | 8.298         | 100.078      | 12.21986   | -1.1834       | 0.13896      |
| 9.125         | 110.823      | 12.21925   | -0.42405      | 0.253558     | 9.118         | 109.955      | 12.21986   | -1.1834       | 0.282241     |
| 0.078         | -0.02915     | 12.21925   | -0.42405      | 0.558202     | 0.121         | 0.039462     | 12.21986   | -1.1834       | 0.255743     |



(a) Implementation of the load cell for four bolts



(b) Unfavourable loading of the calibration process. Both rotating and pushing of the nut

**Figure 117:** Initial setup for calibration and the accompanying load introduction

# C

## Experimental results - Load displacement

### C.1 Serie 1 - Preloaded bolted connection (PBCs)

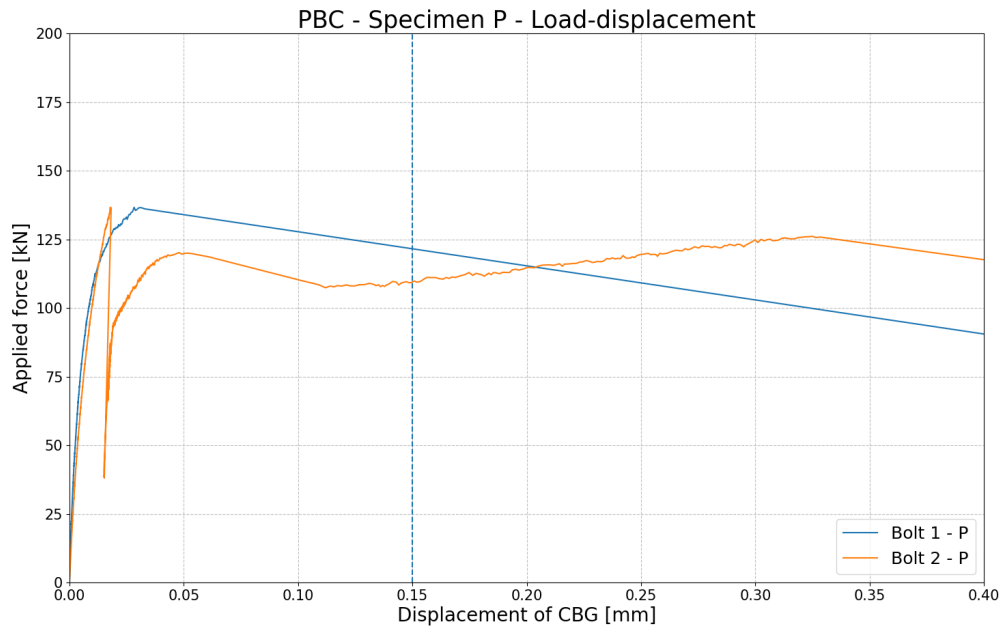


**Figure 118:** PBC - Load-displacement graph of specimen P

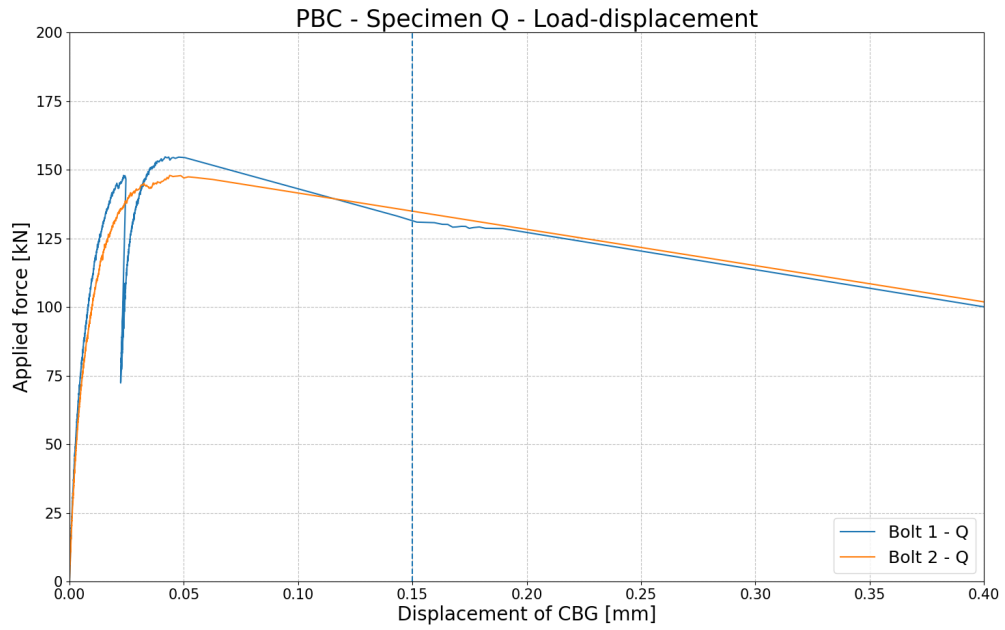


**Figure 119:** PBC - Load-displacement graph of specimen Q

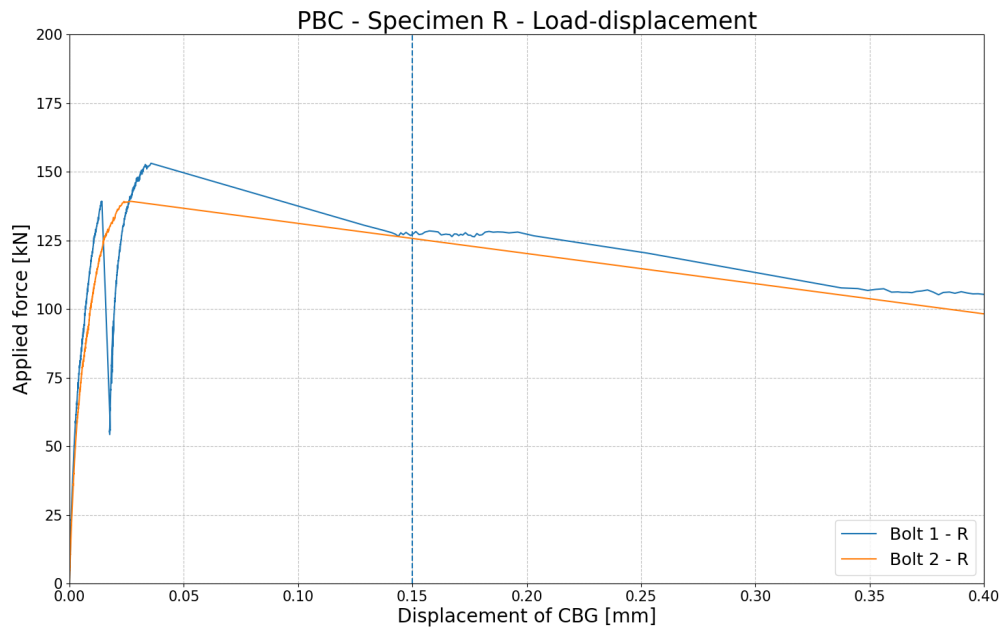


**Figure 120:** PBC - Load-displacement graph of specimen R

C.2 Serie 2 - Injected bolted connection (IBCs)

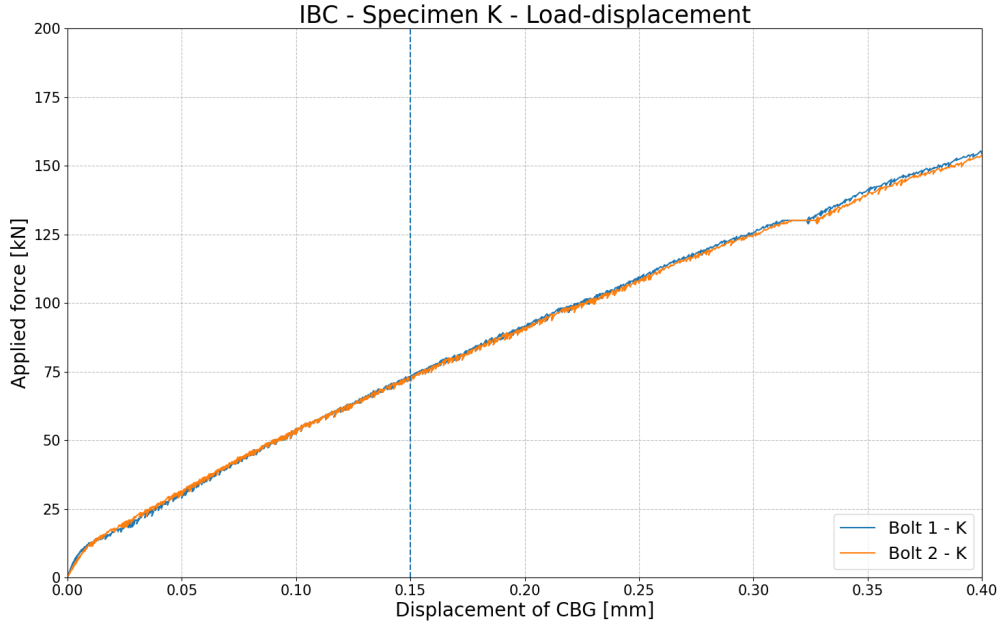


Figure 121: IBC - Load-displacement graph of specimen K

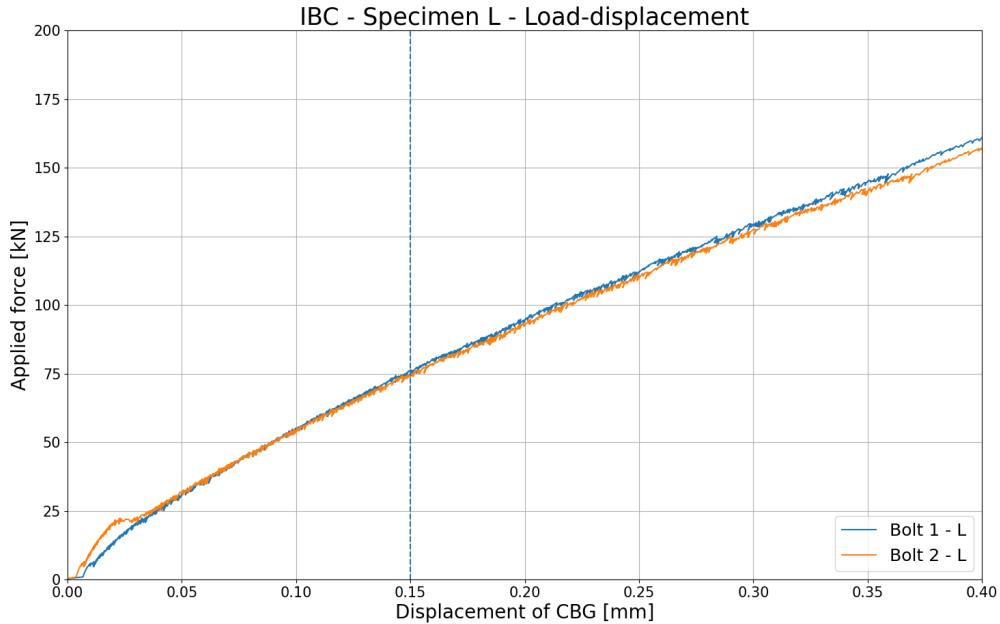


Figure 122: IBC - Load-displacement graph of specimen L

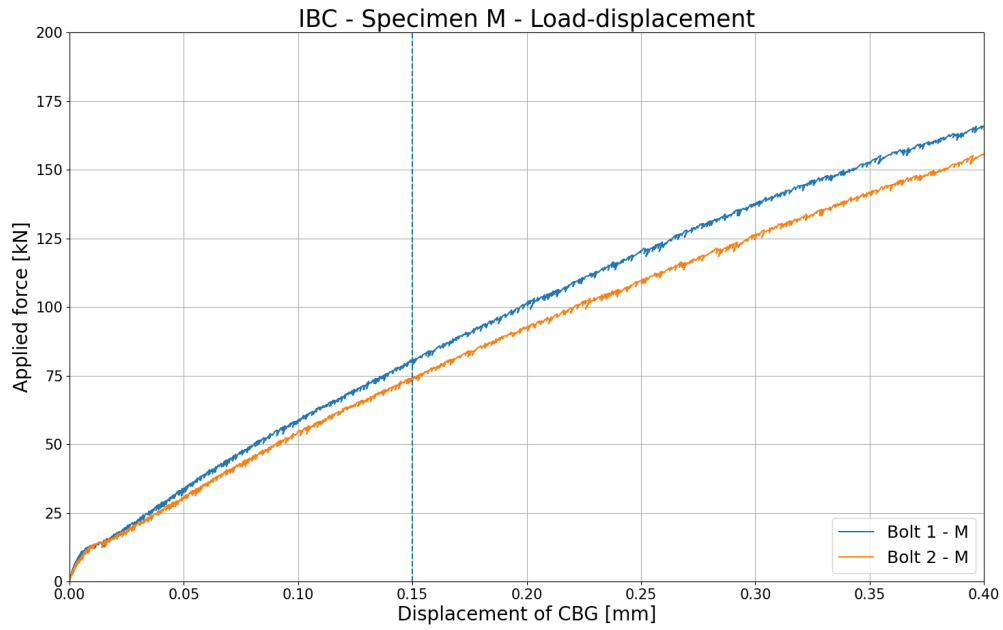


Figure 123: IBC - Load-displacement graph of specimen M

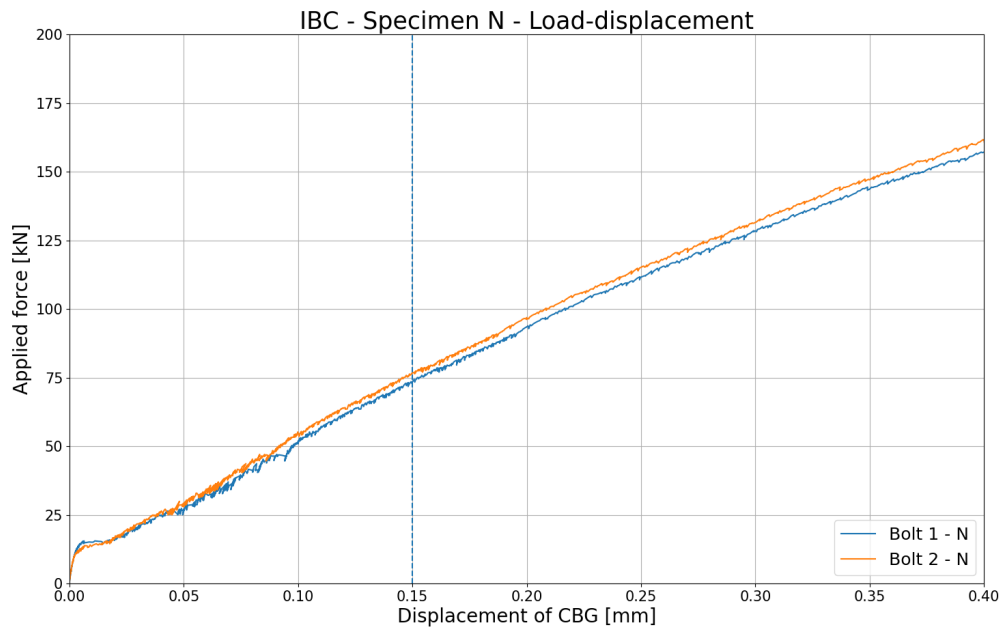


Figure 124: IBC - Load-displacement graph of specimen N

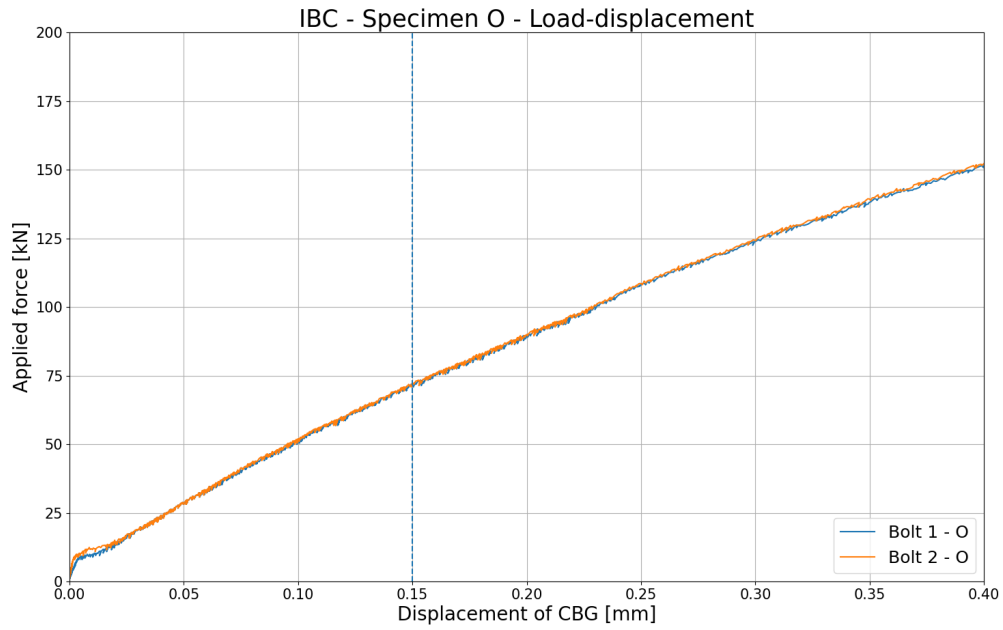


Figure 125: IBC - Load-displacement graph of specimen O

### C.3 Serie 3 - Preloaded and injected bolted connection (PIBCs)

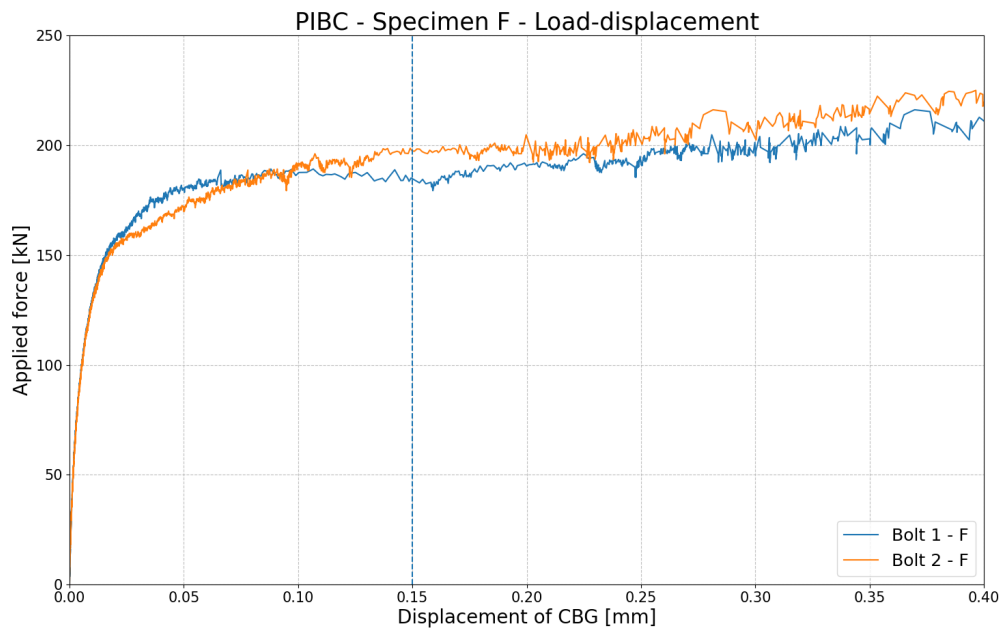
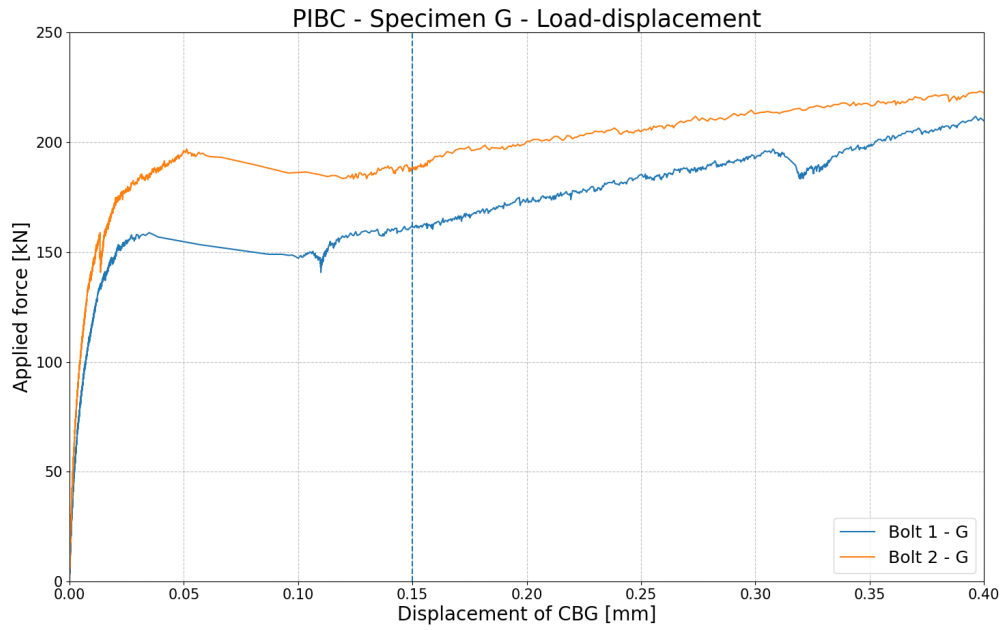
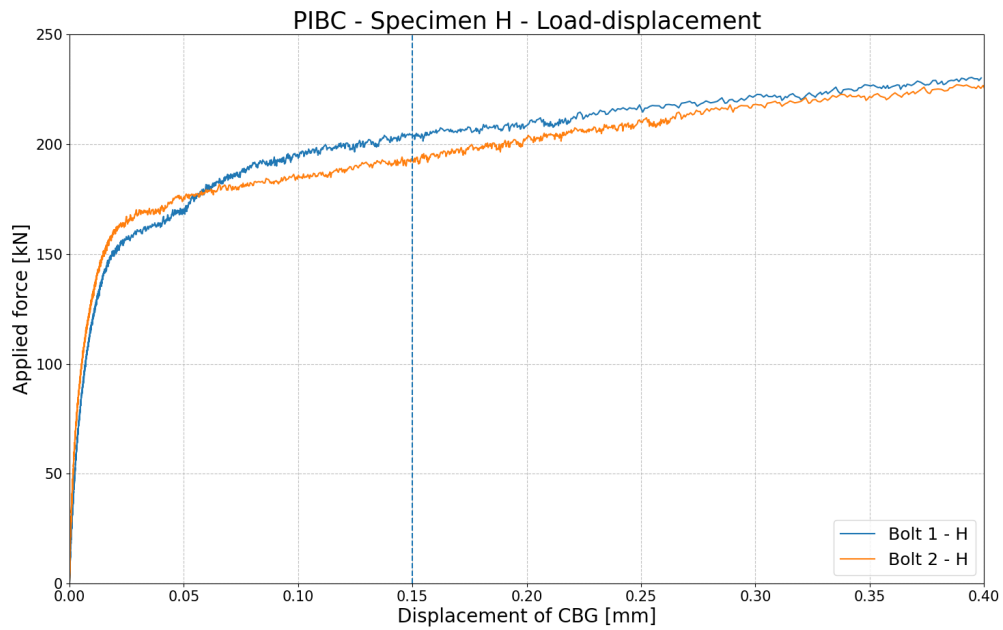


Figure 126: PIBC - Load-displacement graph of specimen F



**Figure 127:** PIBC - Load-displacement graph of specimen G



**Figure 128:** PIBC - Load-displacement graph of specimen H

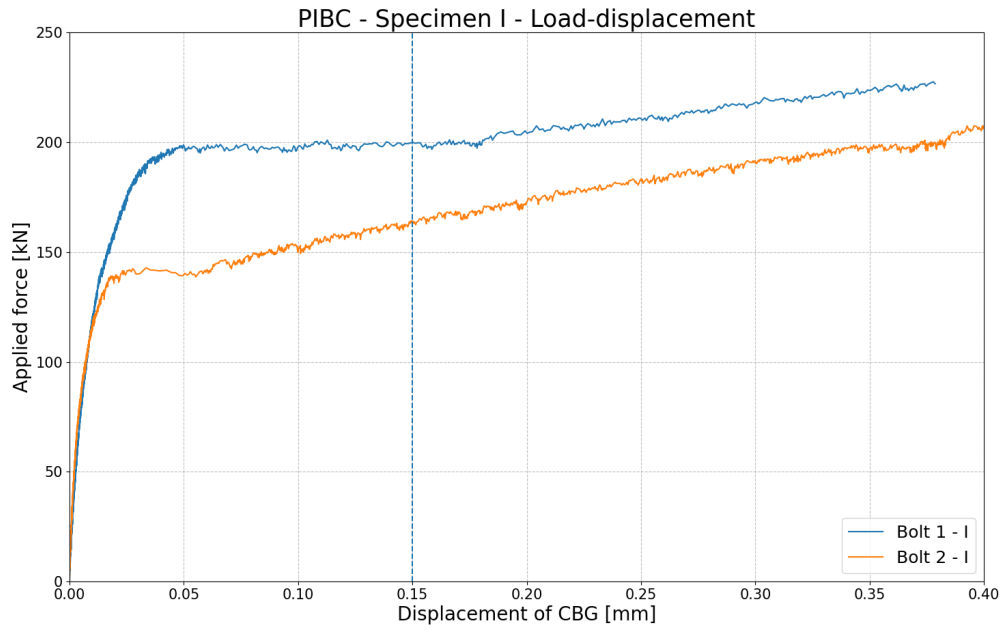


**Figure 129:** PIBC - Load-displacement graph of specimen I

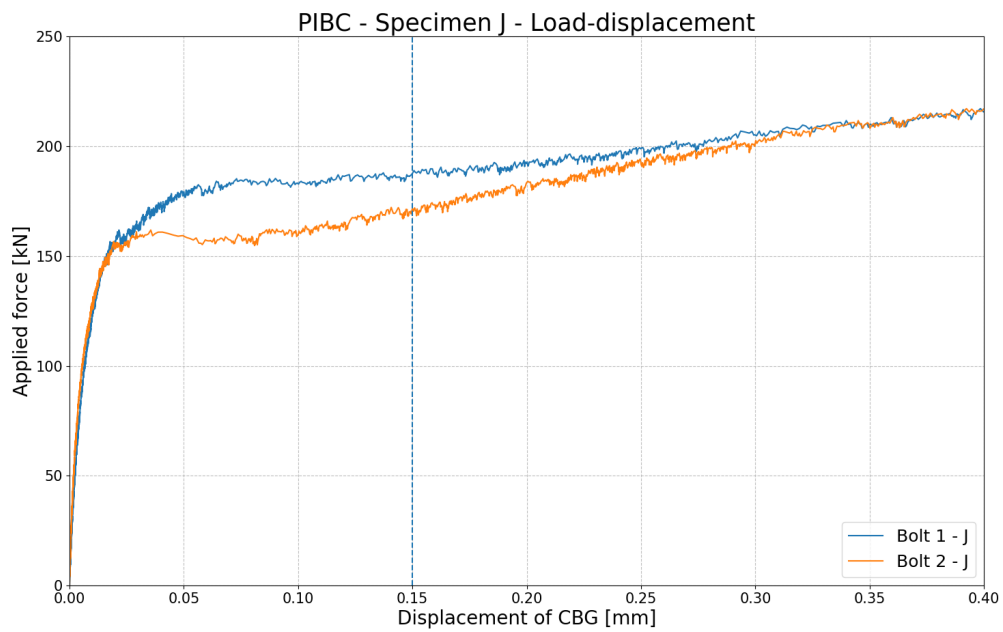


**Figure 130:** PIBC - Load-displacement graph of specimen J

### C.4 Serie 4 - Lowered $F_{p,C}$ - Preloaded bolted connection (PBCs)

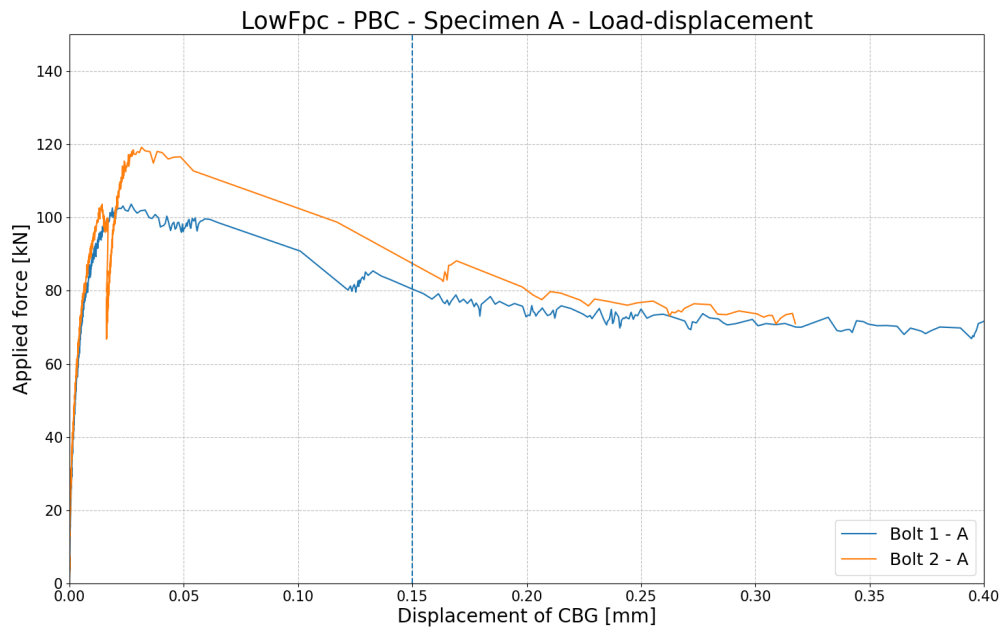


Figure 131: Lowered  $F_{p,C}$  - PBC - Load-displacement graph of specimen A

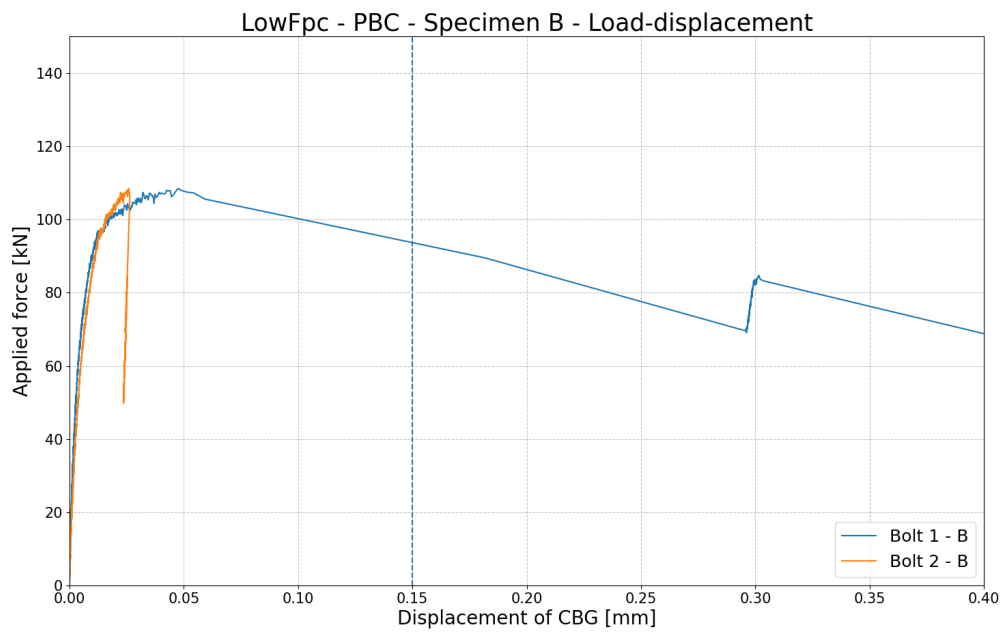
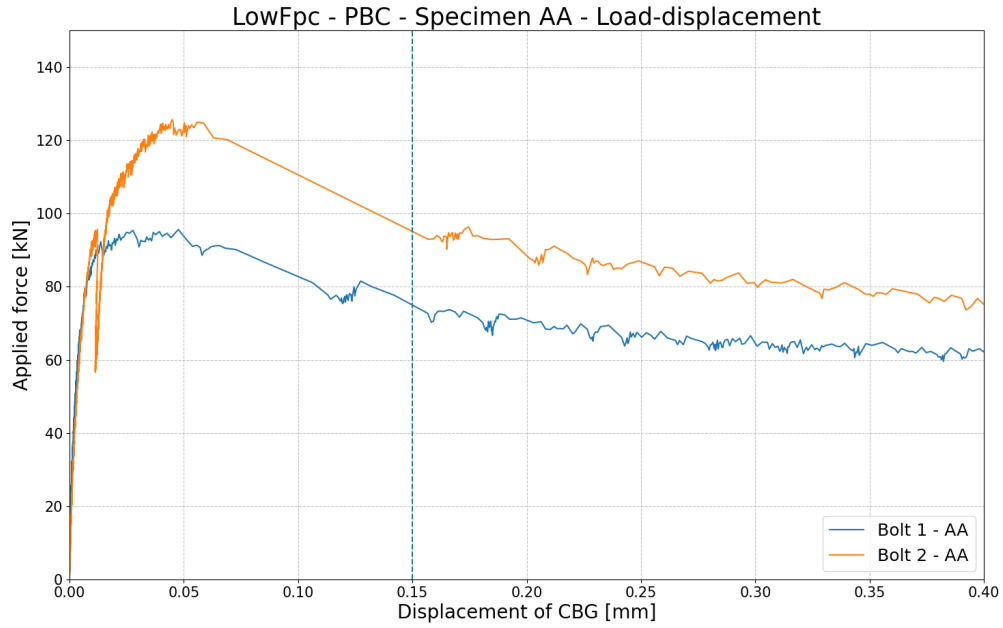
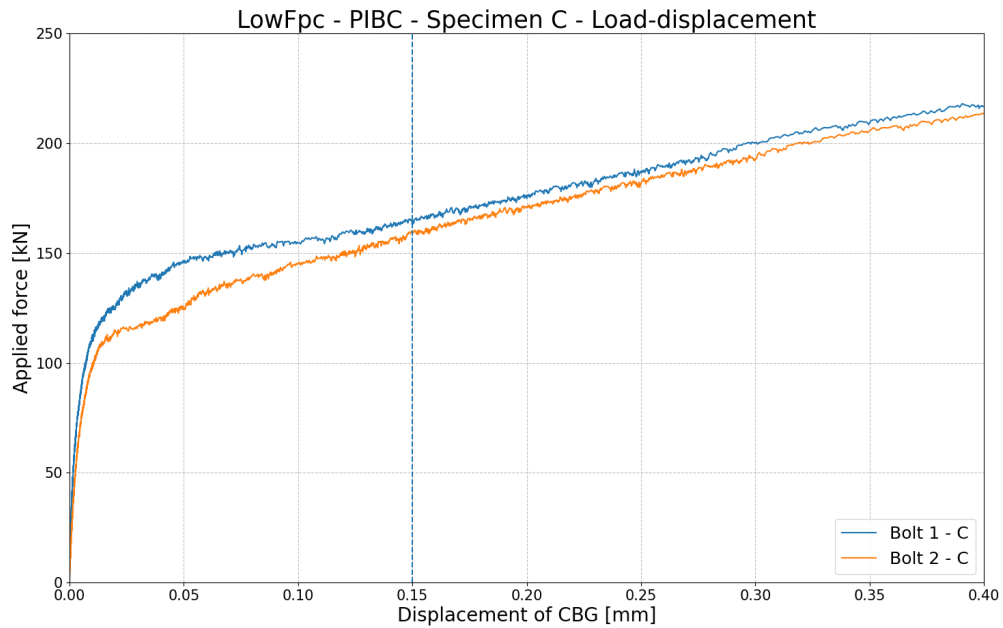


Figure 132: Lowered  $F_{p,C}$  - PBC - Load-displacement graph of specimen B



**Figure 133:** Lowered  $F_{p,C}$  - PBC - Load-displacement graph of specimen AA

### C.5 Serie 5 - Lowered $F_{p,C}$ - Preloaded and injected bolted connection (PIBCs)



**Figure 134:** Lowered  $F_{p,C}$  - PIBC - Load-displacement graph of specimen C

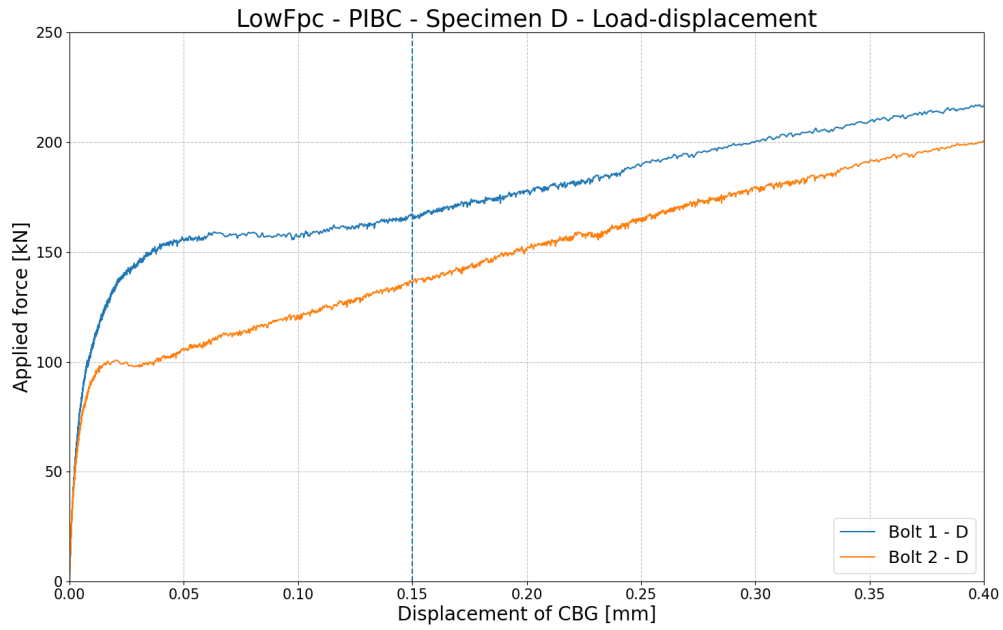


Figure 135: Lowered  $F_{p,C}$  - PIBC - Load-displacement graph of specimen D

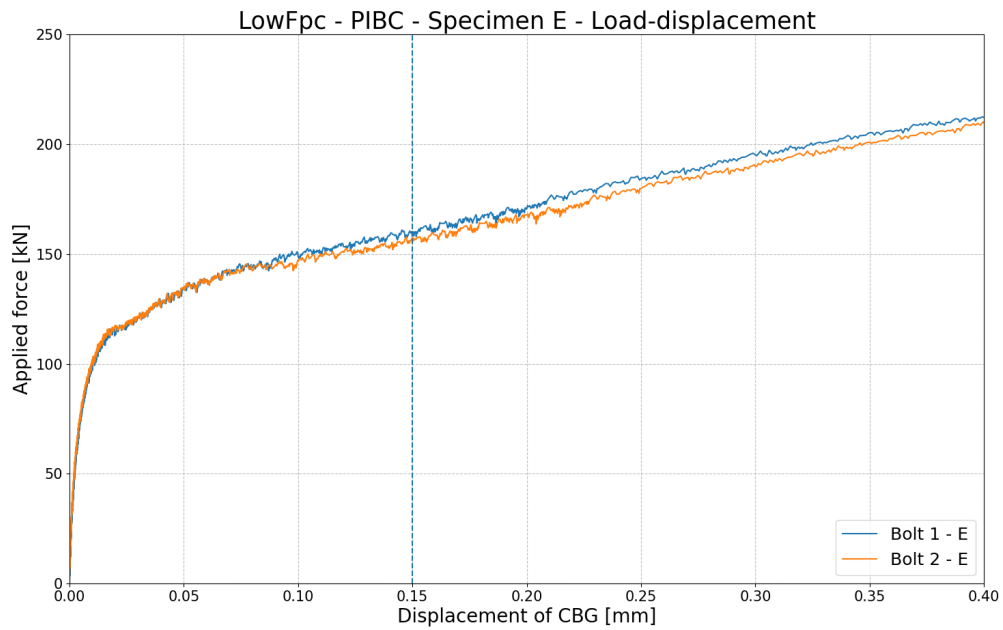


Figure 136: Lowered  $F_{p,C}$  - PIBC - Load-displacement graph of specimen E

# D

## Experimental results - Change in axial force

## D.1 Serie 1 - Preloaded bolted connection (PBCs)

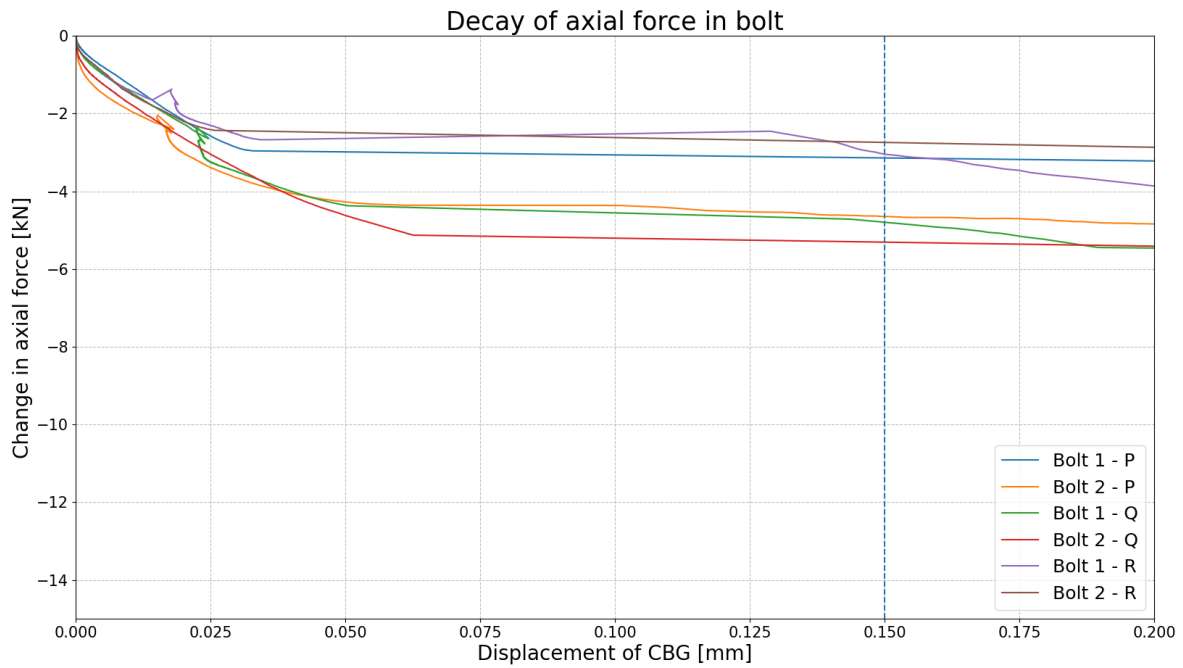


Figure 137: PBC - Decay of preload force until  $U_{CBG}=0.2\text{mm}$

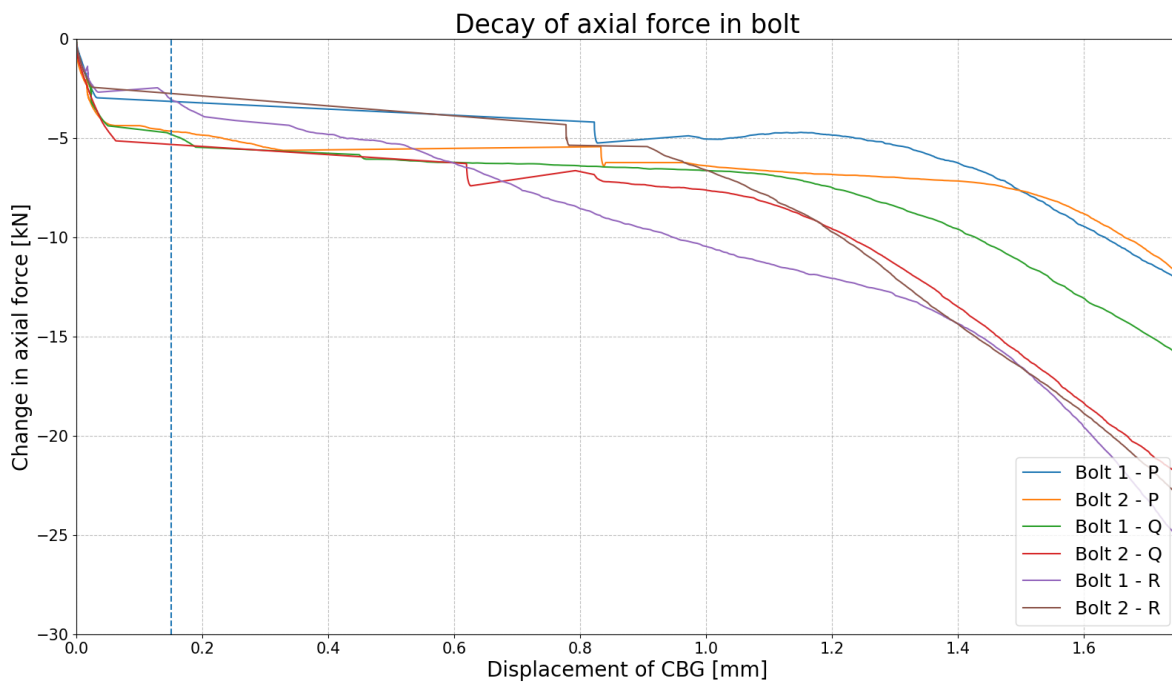


Figure 138: PBC - Decay of preload force until  $U_{CBG}=1.75\text{mm}$

## D.2 Serie 2 - Injected bolted connection (IBCs)

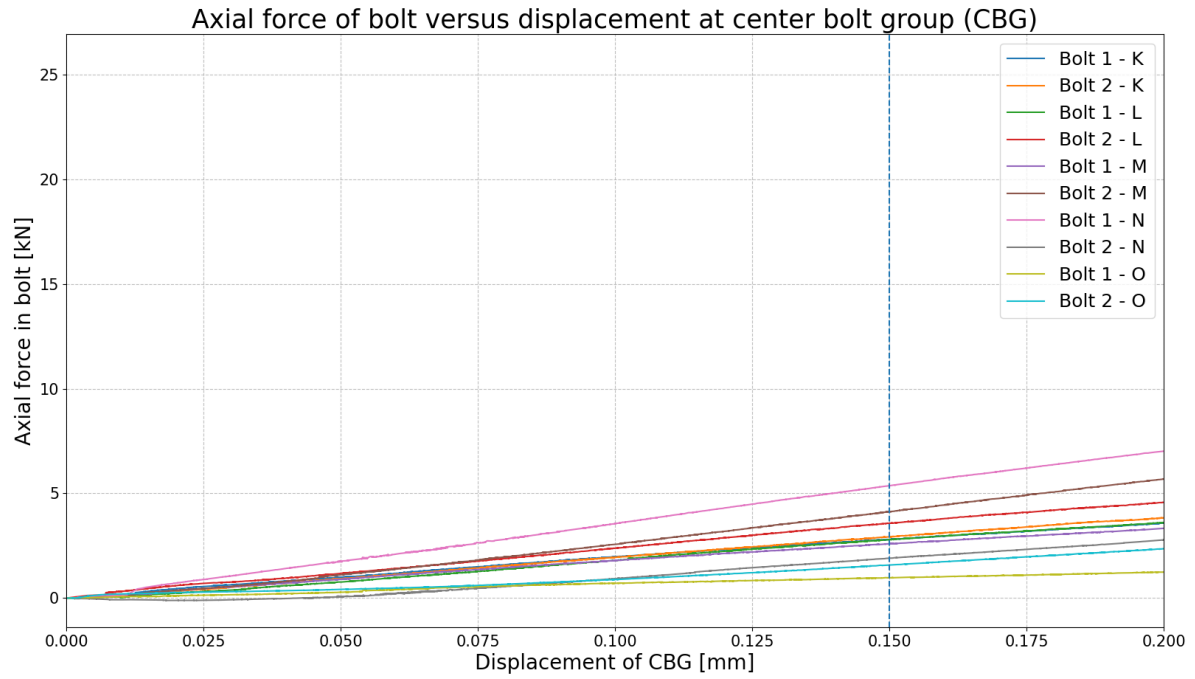


Figure 139: IBC - Increase in axial force until  $U_{CBG}=0.2\text{mm}$

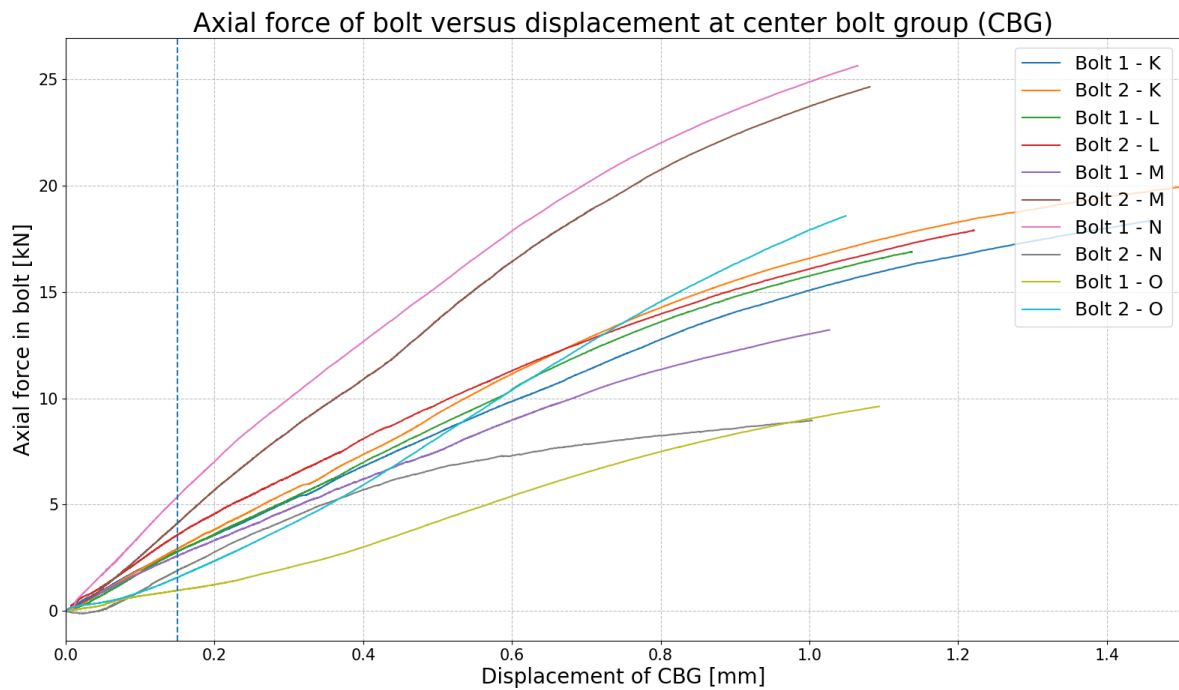
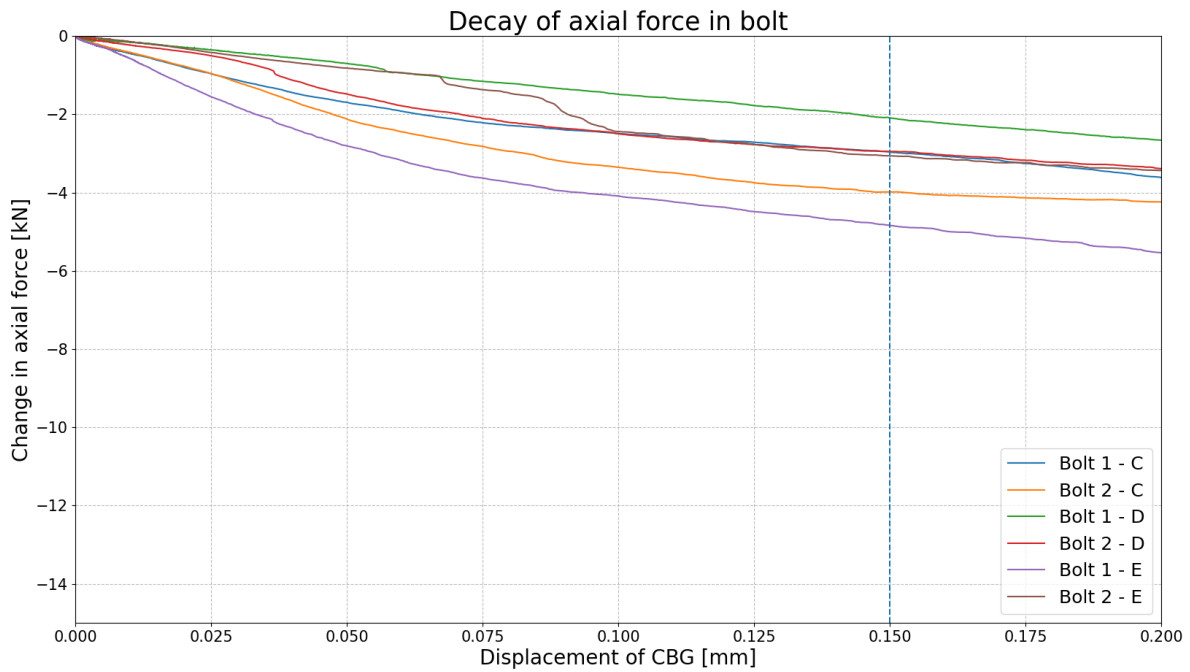
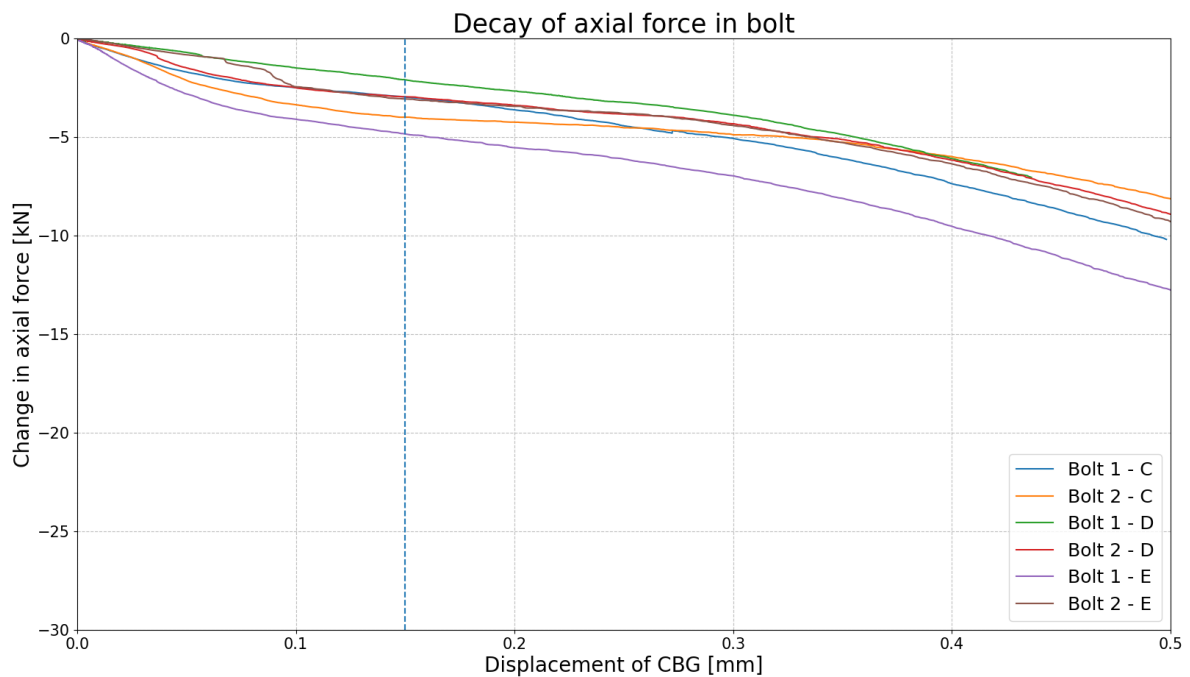


Figure 140: IBC - Increase in axial force until  $U_{CBG}=1.5\text{mm}$

### D.3 Serie 3 - Preloaded and injected bolted connection (PIBCs)



**Figure 141:** PIBC - Decay of preload force until  $U_{CBG}=0.2\text{mm}$



**Figure 142:** PIBC - Decay of preload force until  $U_{CBG}=0.5\text{mm}$

#### D.4 Serie 4 - Lowered $F_{p,C}$ - Preloaded bolted connection (PBCs)

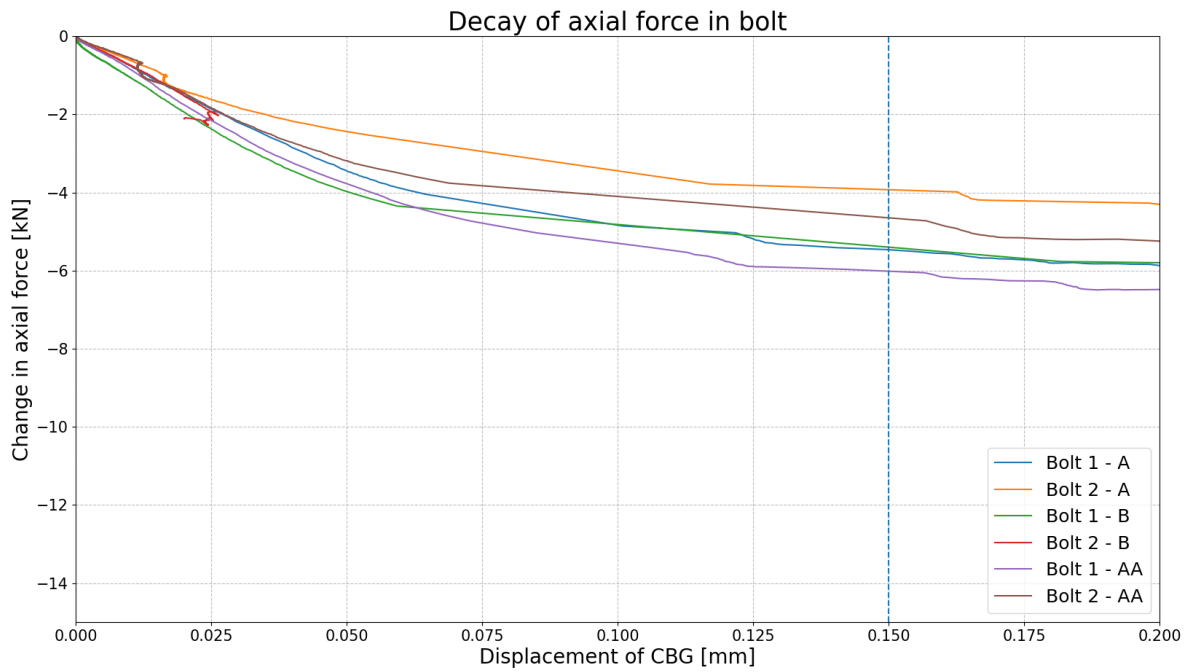


**Figure 143:** Lowered  $F_{p,C}$  - PBC - Decay of preload force until  $U_{CBG}=0.15\text{mm}$

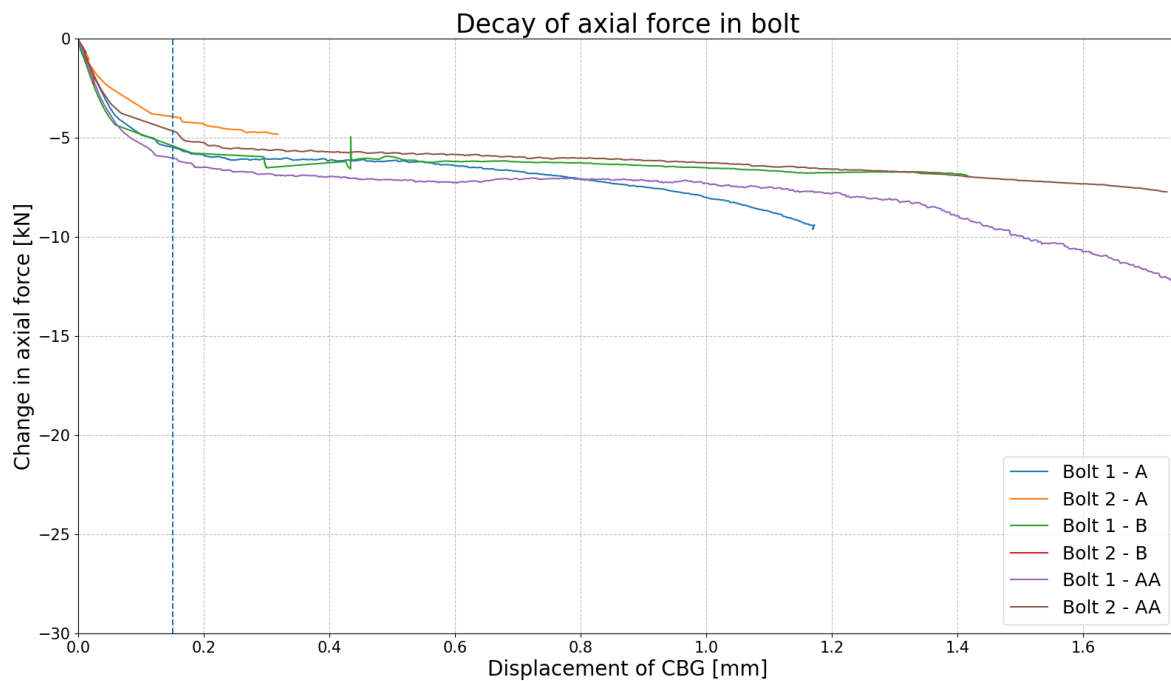


**Figure 144:** Lowered  $F_{p,C}$  - PBC - Decay of preload force until  $U_{CBG}=1.75\text{mm}$

## D.5 Serie 5 - Lowered $F_{p,C}$ - Preloaded and injected bolted connection (PIBCs)

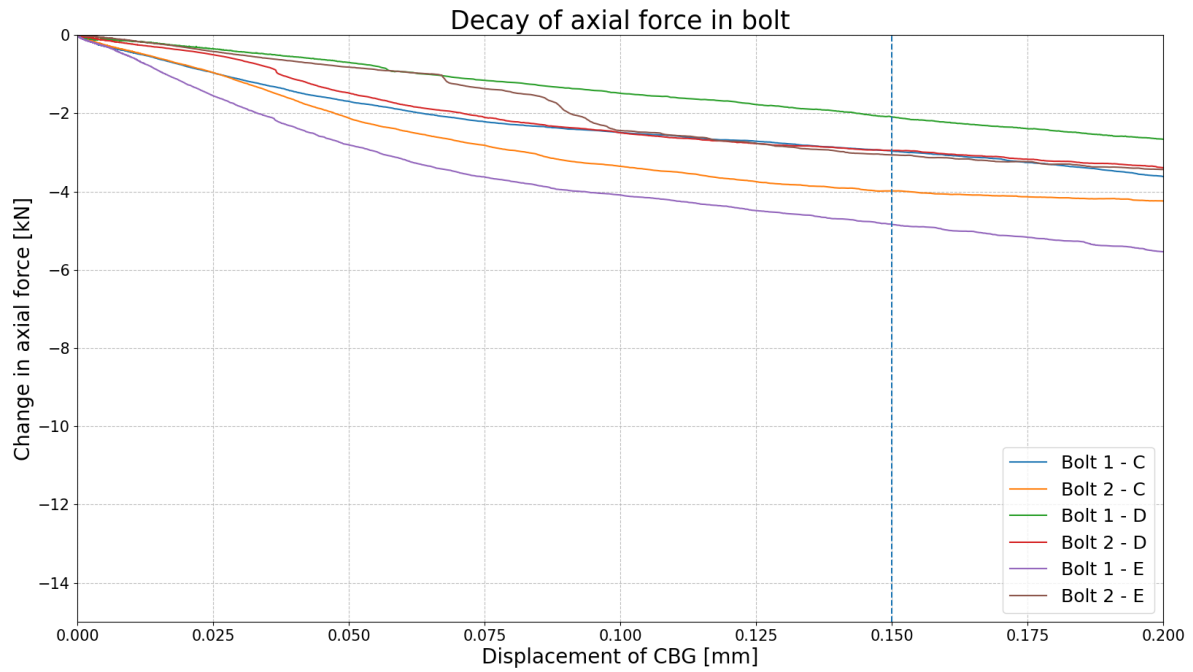


Figure 145: Lowered  $F_{p,C}$  - PIBC - Decay of preload force until  $U_{CBG}=0.2\text{mm}$

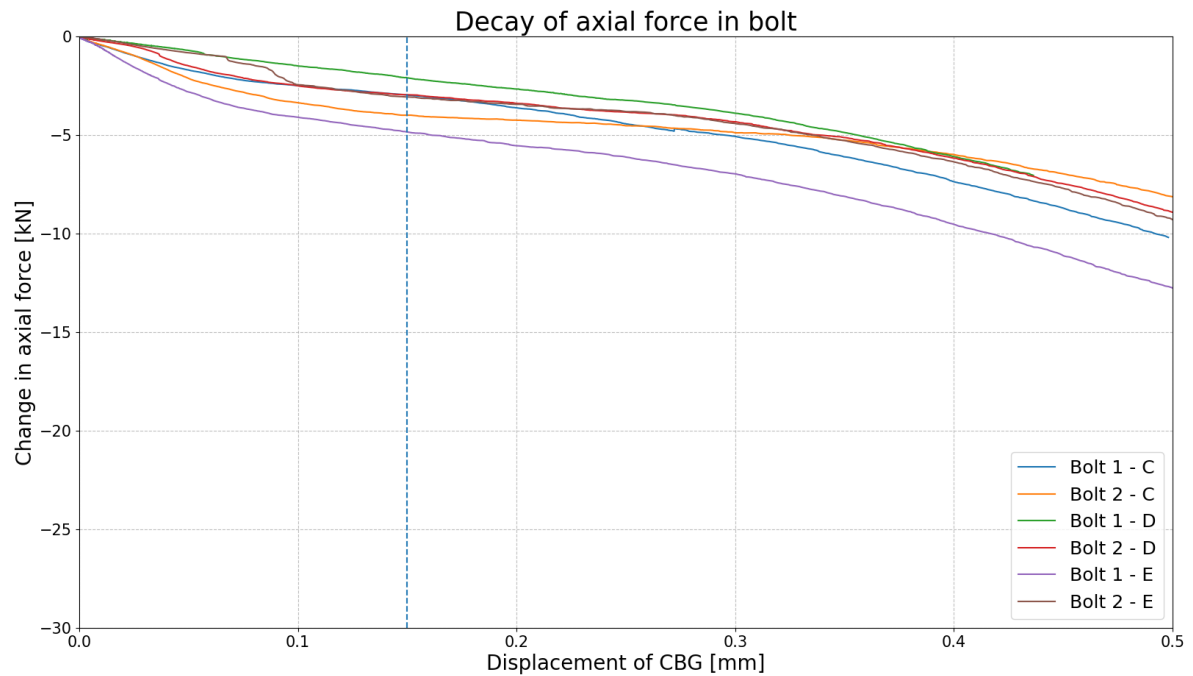


Figure 146: Lowered  $F_{p,C}$  - PIBC - Decay of preload force until  $U_{CBG}=0.5\text{mm}$

# E

## Stiffness parameters

**Table 43:** Preloading only - Slope 1 - Optimisation parameters of each bolt to determine the trajectory

|    | <b>A0</b> | <b>A1</b> | <b>A2</b> | <b>A3</b> | $R^2$ - value |
|----|-----------|-----------|-----------|-----------|---------------|
| P1 | 110.5     | 925.3     | 107.8     | 214.5     | 0.9996        |
| P2 | 91.1      | 2814.8    | 90.0      | 161.6     | 0.9999        |
| Q1 | 109.3     | 1752.5    | 107.25    | 194.1     | 0.9994        |
| Q2 | 128.4     | 461.8     | 125.4     | 142.8     | 0.9989        |
| R1 | 61.9      | 5768.3    | 60.1      | 448.1     | 0.9993        |
| R2 | 91.9      | 2169.9    | 89.2      | 225.6     | 0.9982        |

**Table 44:** Preloading only - Slope 2 - Optimisation parameters of each bolt to determine the trajectory

|    | <b>D0A</b> | <b>D1A</b> | <b>D2A</b> | <b>D3A</b> | $R^2$ - value |
|----|------------|------------|------------|------------|---------------|
| P1 | 141        | -125       | 141        | 156        | 0.999         |
| P2 | 97         | 86         | 96         | 1727000    | 0.998         |
| Q1 | 154        | -142       | 154        | 30504      | 0.996         |
| Q2 | 154        | -132       | 154        | 375891     | 0.999         |
| R1 | 147        | -116       | 146        | 33649      | 0.984         |
| R2 | 143        | -112       | 143        | 183        | 0.999         |

**Table 45:** Injection only - Slope 1 - Optimisation parameters of each bolt to determine the trajectory

|    | <b>B0</b> | <b>B1</b> | <b>B2</b> | $R^2$ - value |
|----|-----------|-----------|-----------|---------------|
| K1 | 5.011     | 536.709   | 541.875   | 0.999         |
| K2 | 5.442     | 539.505   | 590.272   | 0.999         |
| L1 | 0.819     | 623.424   | 812.770   | 0.999         |
| L2 | 5.070     | 554.271   | 599.226   | 0.997         |
| M1 | 5.084     | 595.201   | 613.209   | 0.999         |
| M2 | 4.928     | 540.296   | 527.951   | 0.999         |
| N1 | 6.878     | 439.199   | 6.442     | 0.994         |
| N2 | 6.161     | 492.435   | 189.168   | 0.997         |
| O1 | 3.586     | 522.250   | 475.768   | 0.999         |
| O2 | 4.656     | 506.795   | 407.614   | 0.998         |

**Table 46:** Injection only - Slope 2 - Optimisation parameters of each bolt to determine the trajectory

|    | <b>D0B</b> | <b>D1B</b> | <b>D2B</b> | $R^2$ - value |
|----|------------|------------|------------|---------------|
| K1 | 5.011      | 536.709    | 541.875    | 0.999         |
| K2 | 5.442      | 539.505    | 590.272    | 0.999         |
| L1 | 0.819      | 623.424    | 812.770    | 0.999         |
| L2 | 5.070      | 554.271    | 599.226    | 0.997         |
| M1 | 5.084      | 595.201    | 613.209    | 0.999         |
| M2 | 4.928      | 540.296    | 527.951    | 0.999         |
| N1 | 6.878      | 439.199    | 6.442      | 0.994         |
| N2 | 6.161      | 492.435    | 189.168    | 0.997         |
| O1 | 3.586      | 522.250    | 475.768    | 0.999         |
| O2 | 4.656      | 506.795    | 407.614    | 0.998         |

**Table 47:** Preloading and injection - Slope 1 - Optimisation parameters of each bolt to determine the trajectory

|           | <b>C0</b> | <b>C1</b> | <b>C2</b> | <b>C3</b> | $R^2$ - value |
|-----------|-----------|-----------|-----------|-----------|---------------|
| <i>F1</i> | 94.326    | 3785.841  | 85.679    | 335.72    | 0.999         |
| <i>F2</i> | 101.097   | 3150.895  | 91.311    | 298.559   | 0.999         |
| <i>G1</i> | 77.545    | 4390.781  | 69.993    | 299.575   | 0.999         |
| <i>G2</i> | 113.832   | 3532.611  | 106.042   | 279.889   | 0.998         |
| <i>H1</i> | 106       | 2651.948  | 100.866   | 205.714   | 0.999         |
| <i>H2</i> | 88.315    | 4396.994  | 82.625    | 367.791   | 0.999         |
| <i>I1</i> | 75.029    | 5070.824  | 74.968    | 237.469   | 0.999         |
| <i>I2</i> | 86.677    | 3193.901  | 81.837    | 313.997   | 0.998         |
| <i>J1</i> | 105.211   | 3065.484  | 102.983   | 208.404   | 0.999         |
| <i>J2</i> | 98.216    | 3377.173  | 93.158    | 300.207   | 0.999         |

**Table 48:** Preloading and injection - Slope 2 - Optimisation parameters of each bolt to determine the trajectory

|           | <b>D0</b> | <b>D1</b> | <b>D2</b> | <b>D3</b> | $R^2$ - value |
|-----------|-----------|-----------|-----------|-----------|---------------|
| <i>F1</i> | 169.543   | 101.561   | 169       | 179.61    | 0.985         |
| <i>F2</i> | 221.995   | -110.681  | 221.414   | 21.263    | 0.970         |
| <i>G1</i> | 128.364   | 221.285   | 127.444   | 120.072   | 0.991         |
| <i>G2</i> | 160.533   | 194.753   | 159.608   | 43.469    | 0.994         |
| <i>H1</i> | 191       | 89.082    | 190.268   | 34.987    | 0.991         |
| <i>H2</i> | 167.846   | 168.934   | 166.91    | 64.124    | 0.991         |
| <i>I1</i> | 187.237   | 80.568    | 186.689   | 227.996   | 0.991         |
| <i>I2</i> | 134.346   | 191.843   | 133.798   | 66.171    | 0.989         |
| <i>J1</i> | 174.963   | 81.883    | 174.802   | 212.331   | 0.991         |
| <i>J2</i> | 138.488   | 214.395   | 138.328   | 104.073   | 0.984         |

**Table 49:** Lowered Fpc - Preloading only - Slope 1 - Optimisation parameters of each bolt to determine the trajectory

|     | <b>E0</b> | <b>E1</b> | <b>E2</b> | <b>E3</b> | $R^2$ - value |
|-----|-----------|-----------|-----------|-----------|---------------|
| A1  | 77.78     | 1405.99   | 63.42     | 281.73    | 0.9957        |
| A2  | 73.35     | 2184.12   | 57.95     | 322.85    | 0.9962        |
| B1  | 80.47     | 1425.32   | 72.46     | 272.11    | 0.9981        |
| B2  | 80.82     | 1548.33   | 75.68     | 196.52    | 0.9988        |
| AA1 | 72.30     | 1510.92   | 69.46     | 374.80    | 0.9927        |
| AA2 | 384.39    | -11120.44 | 377.83    | 72.61     | 0.9941        |

**Table 50:** Lowered Fpc - Preloading only - Slope 2 - Optimisation parameters of each bolt to determine the trajectory

|     | <b>G0E</b> | <b>G1E</b> | <b>G2E</b> | <b>G3E</b> | $R^2$ - value |
|-----|------------|------------|------------|------------|---------------|
| A1  | 101.08     | -101.98    | 5.90       | 0.0026     | 0.806         |
| A2  | 128.23     | -336.28    | -2.03      | -11.11     | 0.9882        |
| B1  | 112.80     | -154.36    | -2.55      | 0.00016    | 0.9982        |
| B2  | N/A        | N/A        | N/A        | N/A        | N/A           |
| AA1 | 89.37      | -101.73    | 88.10      | 153.51     | 0.9528        |
| AA2 | 132.04     | -218.83    | 130.76     | 879        | 0.9678        |

**Table 51:** Lowered Fpc - Preloading and injection - Slope 1 - Optimisation parameters of each bolt to determine the trajectory

|    | <b>F0</b> | <b>F1</b> | <b>F2</b> | <b>F3</b> | $R^2$ - value |
|----|-----------|-----------|-----------|-----------|---------------|
| C1 | 129.47    | 259.59    | 91.81     | 144.85    | 0.9947        |
| C2 | 94.11     | 1359.36   | 84.01     | 222.68    | 0.9988        |
| D1 | 85.38     | 2537.09   | 85.54     | 325.96    | 0.9985        |
| D2 | 92.48     | 591.85    | 79.87     | 247.52    | 0.9984        |
| E1 | 95.22     | 1145.39   | 80.85     | 232.72    | 0.9975        |
| E2 | 90.21     | 1559.26   | 71.36     | 259.17    | 0.9969        |

**Table 52:** Lowered Fpc - Preloading and injection - Slope 2 - Optimisation parameters of each bolt to determine the trajectory

|    | <b>G0</b> | <b>G1</b> | <b>G2</b> | <b>G3</b> | $R^2$ - value |
|----|-----------|-----------|-----------|-----------|---------------|
| C1 | 130.78    | 226.67    | -1100     | 500       | 0.9898        |
| C2 | 118.85    | 260.54    | -1100     | 500       | 0.9874        |
| D1 | 134.79    | 212.53    | -1100     | 500       | 0.9838        |
| D2 | 89.86     | 307.08    | -1100     | 500       | 0.9924        |
| E1 | 127.21    | 217.30    | -1100     | 500       | 0.9696        |
| E2 | 124.62    | 209.75    | -1100     | 500       | 0.9745        |

# F

## ABAQUS - Material properties

**Table 53:** Implemented material properties for the bolt, washer and nut in ABAQUS

| <b>Bolt - 10.9</b> |                |
|--------------------|----------------|
| Density            | 7.85E-09       |
| <i>Elastic</i>     |                |
| Young's Modulus    | 210000         |
| Poisson's ratio    | 0.3            |
| <i>Plastic</i>     |                |
| Yield stress       | Plastic strain |
| 900                | 0              |
| 1232               | 0.2            |

**Table 54:** Implemented material properties for the plates

| <b>Plates - S355</b> |                |
|----------------------|----------------|
| Density              | 7.85E-09       |
| <i>Elastic</i>       |                |
| Young's Modulus      | 210000         |
| Poisson's ratio      | 0.3            |
| <i>Plastic</i>       |                |
| Yield stress         | Plastic strain |
| 355                  | 0              |
| 490                  | 0.2            |

**Table 55:** Implemented material properties for the spacer (including thermal expansion coefficient)

| <b>Spacer - S355</b>    |                |
|-------------------------|----------------|
| Density                 | 7.85E-09       |
| <b><i>Elastic</i></b>   |                |
| Young's Modulus         | 210000         |
| Poisson's ratio         | 0.3            |
| <b><i>Plastic</i></b>   |                |
| Yield stress            | Plastic strain |
| 355                     | 0              |
| 490                     | 0.2            |
| <b><i>Expansion</i></b> |                |
| $\alpha_{11}$           | 0              |
| $\alpha_{22}$           | 0.001          |
| $\alpha_{33}$           | 0              |

**Table 56:** Implemented material properties for the resin (SW404+HY2404)

| <b>Resin (Associative flow)</b>        |            |
|--|------------|
| Density                                | 1.80E-06   |
| <b><i>Elastic</i></b>                  |            |
| Young's Modulus                        | 5640       |
| Poisson's ratio                        | 0.315      |
| <b><i>Drucker Prager</i></b>           |            |
| Angle of friction                      | 10.33      |
| FlowStress Ratio                       | 0.93       |
| Dilation Angle                         | 10.33      |
| <b><i>Drucker Prager Hardening</i></b> |            |
| 80                                     | 0          |
| 85                                     | 0.00120146 |
| 90                                     | 0.00257954 |
| 95                                     | 0.00409868 |
| 100                                    | 0.00571089 |
| 105                                    | 0.00774785 |
| 110                                    | 0.0102398  |
| 115                                    | 0.0133859  |
| 120                                    | 0.0185948  |
| 125                                    | 0.0351337  |
| 130                                    | 0.0732029  |
| 135                                    | 0.106261   |
| 140                                    | 0.156484   |



## ABAQUS - Effect of interface conditions IBC

In the initial phase of the numerical analysis, the interface conditions associated to the resin were related to the normal and tangential behaviour. Where the tangential behaviour was penalised with respect to the normal force. However, from this model, it turned out that the resistance of the resin was significantly lower than the obtained stiffness of the experiments. The experimental results were approximately five times larger than the obtained resistance from the numerical results. This is visualised in [Figure 147](#).

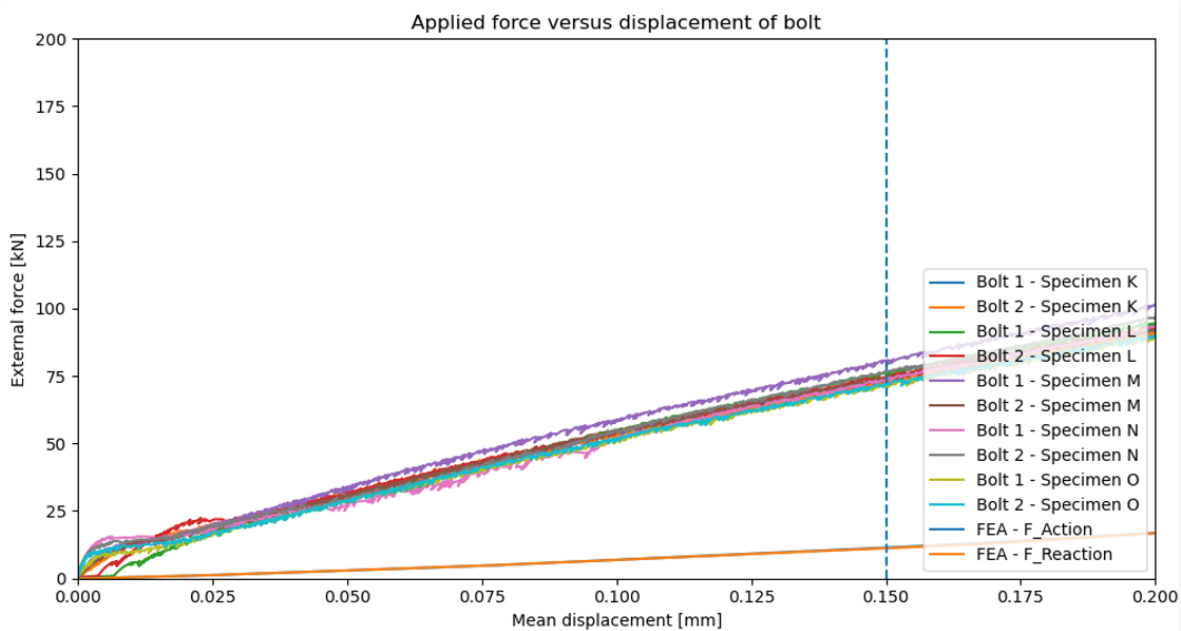


**Figure 147:** IBC: Numerical results before including rigid interaction at the interface of the resin with the steel plates

By adding the conditions at the interfaces of the resin with the bolt and the resin with the steel plates, the resistance immediately increases to the situation as shown in the body of this report (see [Figure 51](#)).

# H

## ABAQUS - Stiffness

In [Chapter 4](#), the numerical model constructed for verification of the experiments is elaborated. Within this chapter, several aspects, including stiffness, are taken into consideration. As mentioned, the stiffness of the models that require a preload does not satisfy the obtained stiffness of the model. To solve this, two main possibilities are taken into consideration:

1. Modelling interaction properties;
2. Location of output

These two aspects are considered since, after verification, a significant difference occurs with small changes. However, the final result does not adopt these observations since more verification of these solutions is required.

The main focus is laid on the stiffness behaviour until the maximum slip resistance is reached. In the main body of this report, the stiffness within a certain region is taken into consideration. However, in this part of the appendix, this entire initial slope is used for comparison.

### H.1 Modelling interaction properties

In ABAQUS, there are several modules which can be used for computing interactions and their properties. In this case, it is chosen to work with the “Surface-to-Surface contact”. However, another option is to apply the “General contact”. The main difference is the assignment of possible contacts. However, each of these subsequently requires an interaction property. Some of these frictional interaction properties are dependent on parameters such as: “Penalty”, “Sliprate”, “Exponential decay” etc. In this case, the basic command “Penalty” is used. This option assumes Coulomb friction behaviour. Such that the acknowledged penalty is the coefficient ratio between the normal and shear force. However, to verify the effect of possible Non-Coulomb behaviour multiple interaction properties are attempted. All of these attempts are shown in Figure 148.

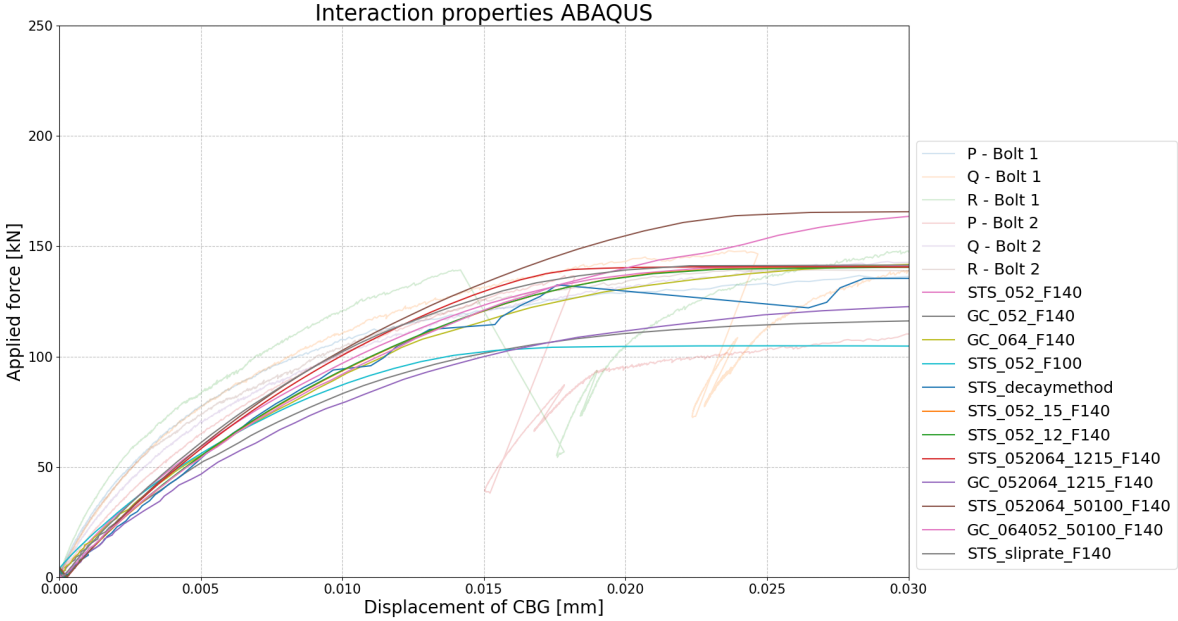


**Figure 148:** Overview of the load-displacement behaviour of a preloaded bolted connection. Transparent graphs indicate obtained results from experiments whereas the other represents numerical results assuming different interaction properties

From this figure, several methodologies adopted can be seen. The legend identifies the type of solver that is used, namely “Surface-to-Surface contact” (STS) or “General contact” (GC). After that, the properties of the interaction is shown. Where 052 stands for the applied penalty of 0.52. In addition, stress components can be assigned. For example, 052-5 stands for a penalty of 0.52 at a stress level of 15MPa. Keeping in mind that some parameters are realistic and some aren’t. Both are taken into consideration to investigate the effect on the behaviour.

However, since this graph identifies only a few options that contain a resistance as expected, namely approximately 140kN, no significant difference in slope between those options is obtained. More important is that, especially until a displacement of 0.005mm, all interactions have more or less a similar stiffness. While this stiffness in the experiments is significantly larger. Nevertheless, one can question the applicability of the penalty method for such applications.

## H.2 Location of output

Besides the investigation of the effect of interaction properties on the stiffness, also the location that determines this stiffness is considered. In the discussion of this report, see [Chapter 6](#), the stiffness difference over the width is elaborated. It is mentioned that a wider plate increases the relative displacement difference with respect to the bolt hole. However, the width of the plate was chosen such that no bearing behaviour is expected to be involved due to its transverse stiffness. In addition, this width is 20% larger than the width in accordance with the standard layout of the experimented specimens. Therefore, if this width is reduced, the effect of change in displacement increases.

The NEN-EN1090-2 refers to monitored displacements based on the centerlines of each plate. Therefore, three different locations that could represent the behaviour of the connection are considered. All three locations are located at the centerline of the bolt(group):

1. At the edge of the plate (Acc. to NEN-EN1993-1-8);
2. 3mm inside the plates;
3. 30mm inside the plates.

If these locations are considered in combination with the orange graph of [Figure 108](#), then the difference in load-displacement behaviour for a preload and injected connection implementing a preload force of 140kN results in the output as shown in [Figure 149](#)

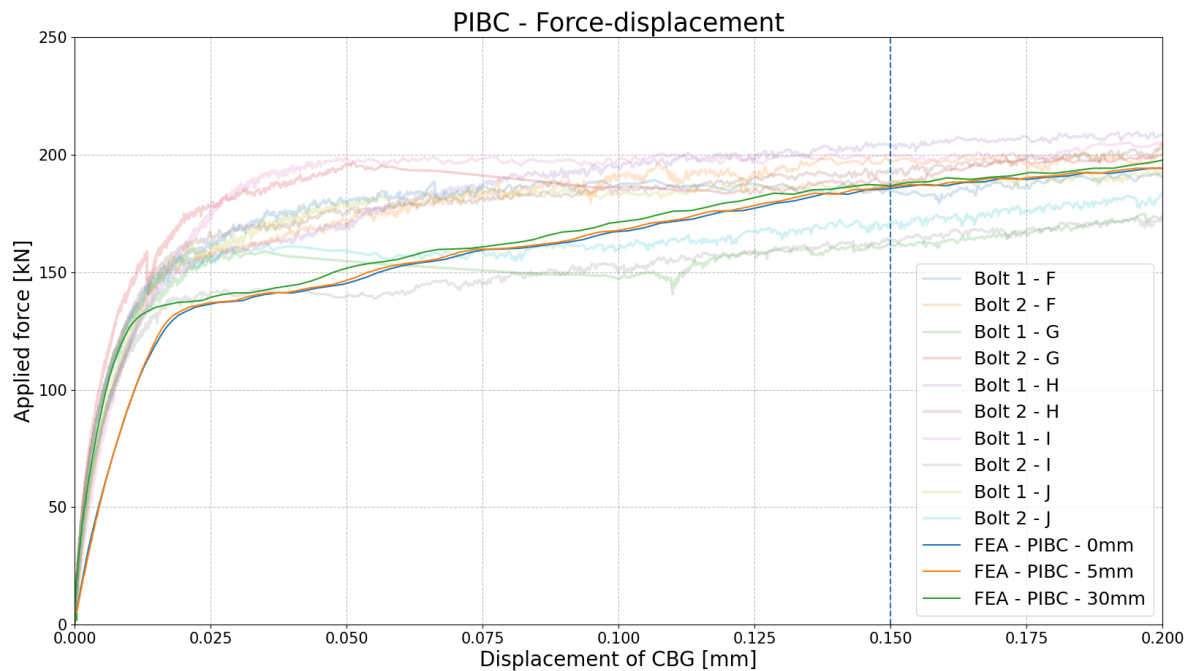


**Figure 149:** Load displacement graphs based on three output locations

From this, it can be seen that for this initial phase, until the maximum slip-resistance is reached, stiffness increases significantly. This increase is identical to the decrease in displacement with respect to the edges as shown in [Figure 108](#) since the stiffness is calculated by the ratio of the exerted force in the total cross-section divided by the displacement of this node. Therefore, the calculated stiffness is not an actual stiffness.

# I

## Results Tribometer

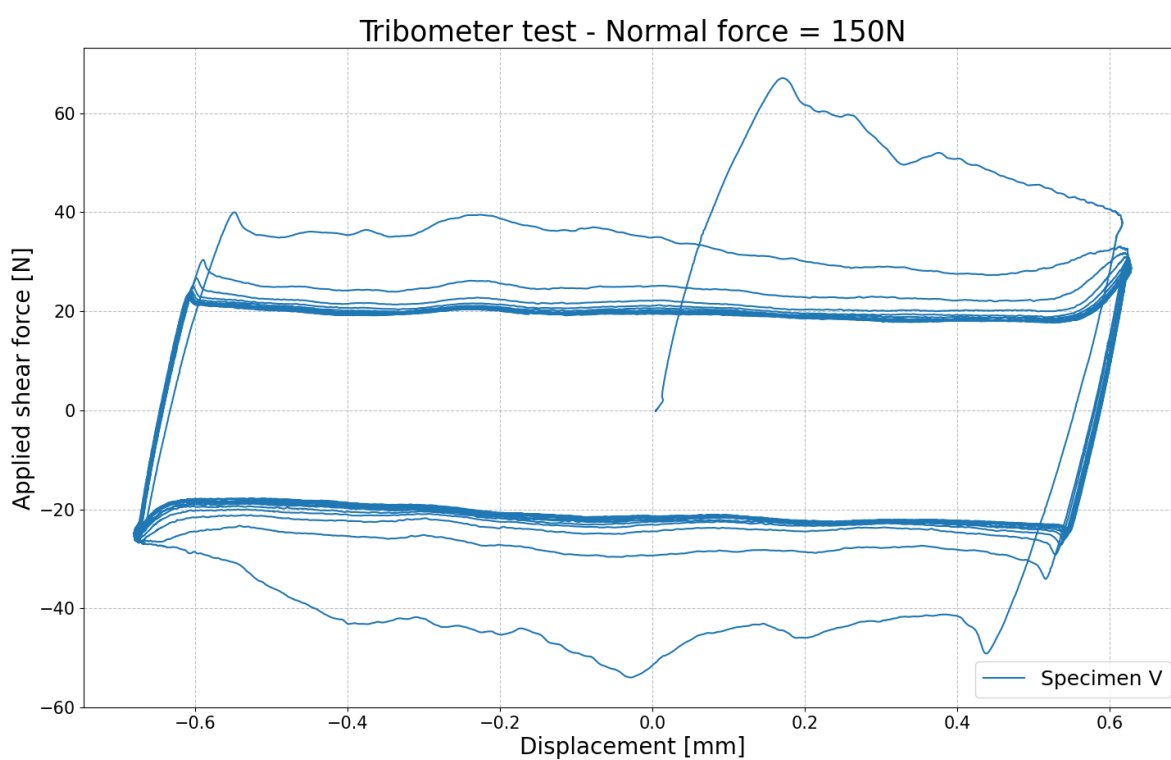


**Figure 150:** Results of the Tribometer test, where the frequency is 0.1Hz and amplitude is 0.6mm

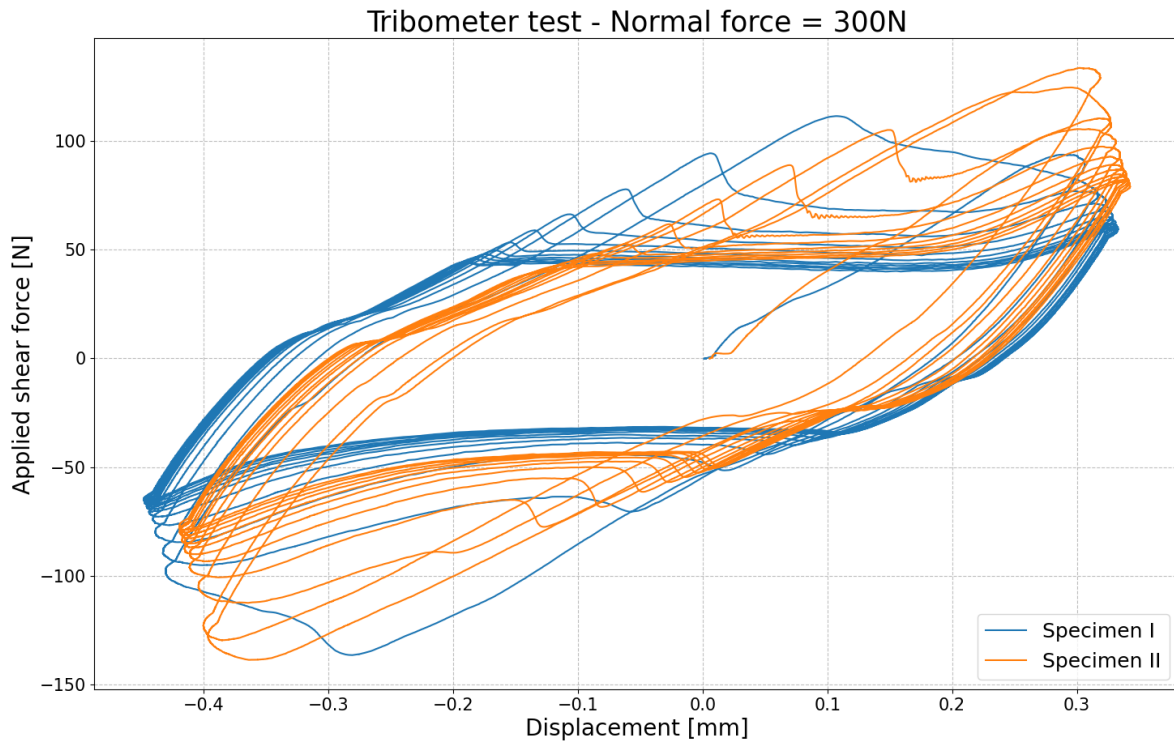


**Figure 151:** Results of the Tribometer test, where the frequency is 0.1Hz and amplitude is 0.35mm

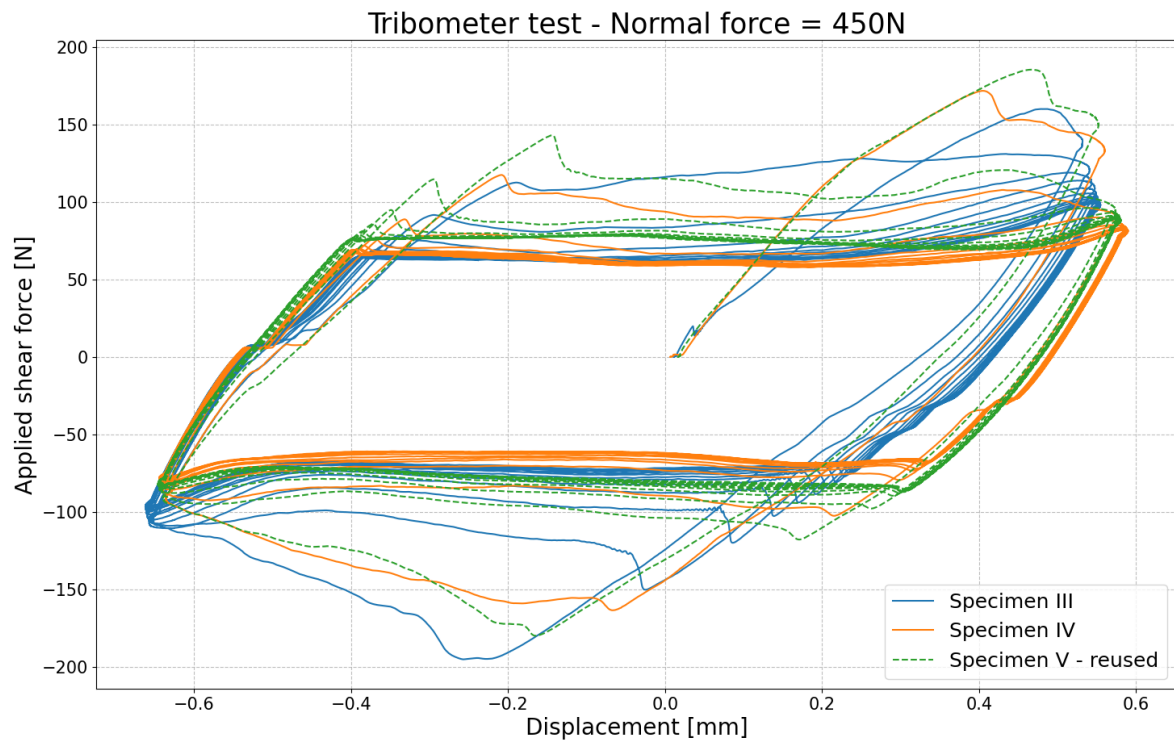


**Figure 152:** Results of the Tribometer test, where the frequency is 0.1Hz and amplitude is 0.6mm